



**Synthesis and characterization of coordination polymers based on
coinage metal ions and thio-derivatives of guanosine and uridine**

Pablo Rojas Martinez

A thesis submitted for the degree of

Doctor of Philosophy in Chemistry

School of Natural and Environmental Sciences

Newcastle University

March 2022

Abstract

This work focuses on the search for new materials with useful optical and electronic properties based on nucleic acid-based components for possible use in nanotechnology.

Towards this, two coordination polymers have been prepared using 6-thioguanosine, as a ligand, and univalent coinage metal ions of Ag(I) and Cu(I). [Ag(I)-6-thioguanosine]_n was structurally characterized using mass spectroscopy, UV-Vis, FTIR, CD, SEM and AFM. This material has shown to have a polymeric one-dimensional chain structure with Ag(I) ions coordinating two sulfur atoms. In addition, these chains form long polymeric strands when individually associate in parallel and also, they form helices with a left-handed orientation. Additionally, the optical properties of the material showed luminescence emission suggesting that [Ag(I)-6-thioguanosine]_n possess chiro-optical properties.

A similar material was obtained in the reaction of Cu(I) ions to give the corresponding coordination polymer, [Cu(I)-6-thioguanosine]_n as confirmed by characterization by mass spectroscopy, UV-Vis, FTIR, CD, SEM and AFM characterization. These showed the formation of a one-dimensional coordination polymer with Cu(I) ions bringing three sulfur atoms in form of fibres, that can associate one on top of another to form longer polymer chains. In this case, the material was fluorescence and electrically conductive after an oxidative doping process.

Both systems formed metallo-supramolecular hydrogels when prepared at high concentrations, from 15 to 60 mM. They both were analyzed structurally by rheology, UV-Vis and CD confirming the formation of polymeric strands. In addition, these compounds were analyzed under AFM and they showed the formation of large one-dimensional fibres that entangled by self-assembling to form the characteristic fibrillar

network of a hydrogel. Also, both systems showed luminescence emission that combined with their chiral features showed CPL emission properties. Only [Cu(I)-6-thioguanosine]_n displayed electrical conductivity without doping and this confirmed its nanowire behavior.

As a promising application for these materials, a prototype of a nanowire-based gas sensor was prepared to detect ozone and VOCs. Firstly, [Cu(I)-6-thioguanosine]_n was used as a potential gas sensor but it was discarded due to the poor stability and degradation shown to sense ozone and a time-dependent response for VOCs. Instead, a nanocomposite based on [Au(I)-6-thioguanosine]_n and Multi-Walled Carbon Nanotubes (MWCTNs) was prepared and characterized structurally by AFM, Raman spectroscopy and SEM. A sensor based on [Au(I)-6-thioguanosine]_n/MWCNTs was also built and this showed a stable response and high sensitivity for VOCs, especially for ethanol.

Finally, two coordination polymers were prepared using a thio-modified nucleoside prepared synthetically, 4-thiouridine. [Ag(I)-4-thiouridine]_n and [Au(I)-4-thiouridine]_n complexes were structurally characterized using mass spectrometry, UV-Vis, FTIR, CD, SEM and AFM. In the case of [Ag(I)-4-thiouridine]_n, the system formed a hydrogel with a structure based on coordination polymer similar to that formed with 6-thioguanosine. These are individual one-dimensional chains that self-assemble intertwining forming a supramolecular network. For [Au(I)-4-thiouridine]_n, the structural analysis concluded with the formation of aggregates and it suggested the formation of Au(I) thiolate polymers that interact through aurophilic interactions. In addition, the optical properties of both Ag(I) and Au(I) systems showed higher luminescence emissions compared to the 4-thiouridine isolated confirming chiro-optics features of coinage-metal thiolate coordination polymers.

To my grandfather Luis

Acknowledgements

Firstly, I would like to thank very much to my two supervisors Prof. Andrew Houlton and Dr. Benjamin Horrocks for choosing me as the most suitable candidate to do the PhD with you at Newcastle University. Over the past four years I have received your unconditional guidance and support in the lab and I am very grateful for it. You have been very respectful to me but what I value most is the patience you have had with me during the completion of the doctorate. It was easy to integrate coming from a foreign country and it has been thanks to your understanding and help at all times. I will never be able to repay you for the opportunity you have given me to study abroad. Sincerely, thanks a million.

I would like to thank Dr. El-Zubir for the countless times I went to your office to ask for help. You never refused despite how bothered I was, and I thank you very much. We spent, perhaps, too much time in front of the AFM screen, but the conversation with you aroused in me a lot of interest in things far from science. I am very grateful for everything you have taught me, and I wish you and your whole family the best because you deserve it.

Gema I would like to thank you for all the help and support in 'Spanish' that you have given me. I really appreciate all the time you have spent in the lab helping me or showing me around the city. I hope I have been able to compensate you with mutual support during the long weeks in Newcastle. I have learned a lot about English culture, and I owe a lot to you. Thank you very much for all this and I hope that in the future we will coincide to do interesting things.

I would like to thank all the people who were part of the Chem Nanolab corridor and who are now doctors, Milene, Shams, Patrick, Rachel, Glenn, Sam and especially to Liam Mistry for the great help given at the beginning of my days in Newcastle

University, it has been a pleasure working with you. Of course, I could not forget the lab partners with whom I have spent the most time, the future doctors and dear friends Cheney and David. I really appreciate the time that we have spent in the lab, in the office or outside together and I will not be able to forget so many moments that made me enjoy my stay in Newcastle. I hope you have the future you want, and I will continue to insist that you come to Granada to visit me. Honestly, I wish you the best. In addition to the rest of the people who belong or belonged to the Chem Nanolab corridor, Dr. Fulton, Dr. Pike, Dr. Tuite, Liam MacGarry, Marcello and MChem students, Andrew and James, I would like to thank them for the magnificent treatment they had with me. It has been a pleasure working with you.

I would also like to remember other people who have helped me during my period in Newcastle, Cristina, Manuel Moneris, Manuel Abelairas, Tom from the stores and many other people from the university and the city that helped me to establish myself in a totally unknown city for me.

Of course, my PhD would not have been possible without INDEED group thanks to European funding. It has been an incredible experience to share with all of you this time. I cannot believe I have been to the places where we have been, sharing our research at conferences that seemed unreachable. These events have given me enormous satisfaction and has awakened an interest in science and its influence on society that I was unaware of until now. Many thanks to Natalia and PhD students of the group for the time we have spent together.

None of this would have been possible if I had not met you a while ago Migue. I will be eternally grateful for the opportunity you gave me to apply for this PhD. Thanks for your support and help from Spain, it is being a pleasure to share knowledge and scientific concerns with you. For all the people who aroused real interest in chemistry at the

Universidad de Granada, especially Prof. Antonio Parody. Also, thanks to my undergraduate colleagues and in particular to Victor for waiting for me every Christmas before going on holidays.

To my friends in Spain, Luis Angel y Jesus for the great friendship that unites us and the support that you sent from Spain. I am very grateful and happy for your successes. To all other companions that I left along the way, thanks for everything.

To my family thanks for making me the way I am. There are no words to express my deep gratitude I have for you; you have been a huge support during all my academic career. Since I took the first flight to Newcastle, I saw you far away, but I felt you close. I will not be able to give you back everything you have offered me during all these years, I hope that this work compensates something, this work is for you, you can consider it as yours. Thanks Mila, thanks Juan, thanks Irene.

And finally, to my precious Lourdes. It has been several years apart, but I hope that from now on we can share more time together. You have been very important throughout this process and I want to especially thank you for the love and help you have always given me. In addition, I thank you for all the experiences we have shared as well as your eternal patience with me. I hope that in the future I can return everything you have given me. For a future together, Lourdes.

All these words have been the ones I wanted to write the most. I feel very lucky to have had all these people during my PhD in Newcastle. All of them have made me a better scientist and a better person. Thank you all.

Table of Contents

Chapter 1. Introduction	1
Chapter 2. Experimental Techniques	42
Chapter 3. Preparation and characterization of a coordination polymer designed from 6-thioguanosine and Ag(I)	62
Chapter 4. Preparation and characterization of a coordination polymer designed from 6-thioguanosine and Cu(I).....	86
Chapter 5. Preparation and characterization of coordination polymers hydrogels designed from 6-thioguanosine with Ag(I) and Cu(I) coinage metal ions	110
Chapter 6. A nanowire-based gas sensor	151
Chapter 7. Synthesis of 4-thiouridine. Preparation and characterization of coordination polymer designed from 4-thiouridine with Ag(I), Au(I) and Cu(I) coinage metal ions	185
Chapter 8. Conclusions & Outlook.....	225
Appendix	232

Abbreviations

A	Absorbance
CNTs	Carbon Nanotubes
cm ⁻¹	Centimetres raised to minus one
°	Degrees
°C	Degrees Celsius
DNA	Deoxyribonucleic acid
DMSO	Dimethyl sulfoxide
E	Electric field
eV	Electron volts
eq	Equivalent
F I	Fluorescence Intensity
G-quartets	Guanine-quartets
HSAB	Hard-soft acid-base
h	Hours
I	Intensity
kHz	Kilo-hertz
L	Ligand
LMWG	Low molecular-weight gelators
B	Magnetic field
m/z	Mass/Charge
MΩ	Mega-ohms
T _m	Melting Temperature
M	Metal
MBE	Platinum microband electrodes
μL	Micro-litres
μm	Micro-meters

mA	Milli-amps
mdeg	Milli-degree
mg	Milli-grams
mL	Milli-litres
mm	Milli-meters
mM	Milli-molar
mmol	Milli-mole
mS	Milli-siemens
mW	Milli-watts
min	Minutes
M	Molar
θ	Molar ellipticity
nA	Nano-amps
nm	Nano-meter
Nm^{-1}	Newtons/meters
N	Normality
ppm	Parts per million
RNA	Ribonucleic acid
s	Seconds
TLC	Thin Layer Chromatography
tRNA	Transfer RNA
T	Transmittance
VOCs	Volatile Organic Compounds
V	Volts
W	Watts
λ	Wavelength

List of Figures

Figure 1.1: Nanomaterials that take advantage of the structural characteristics of DNA

Figure 1.2: Scheme of the hydrogen bond between thymine-adenine and cytosine-guanine bases. b) Representation of a DNA double-helix structure

Figure 1.3: Scheme of Hoogsteen-type pairing of adenine-thymine and guanine-cytosine⁺ base pairs

Figure 1.4: Scheme for the different DNA conformations represented as balls and ribbons

Figure 1.5: Scheme of the four steps of DNA synthesis by phosphoramidite method in an automatic synthesizer

Figure 1.6: Nanostructures build with DNA

Figure 1.7: DNA origami formation

Figure 1.8: Macromolecular DNA structures

Figure 1.9: A controlled three-dimensional architecture based on the interactions between complementary strands of DNA forming a superlattice of nanoparticles in specific places

Figure 1.10: Model of a metal templating on DNA to prepare nanowires and a combination of DNA Origami and metal templating on DNA

Figure 1.11: Interaction of a DNA double helix molecule with a metal ion and the subsequent hydrogen bond substitution by a metal coordination between nucleic acids

Figure 1.12: Scheme of a) adenosine, b) thymidine, c) guanosine, d) cytidine and e) uridine with their preferred sites of metal interactions

Figure 1.13: Example of functionalization of materials following metal mediate base pairs strategy

Figure 1.14: Scheme examples of metal mediated base pairs structures

Figure 1.15: Cu(II) mediated hydroxypyridone nucleobases forming a DNA duplex

Figure 1.16: Scheme of a coordination polymer formation

Figure 1.17: Examples of coordination polymers frameworks

Figure 1.18: Examples of thio-derivatives nucleosides

Figure 1.19: Structure models of metal sulfides

Figure 1.20: Coordination polymers based on the interaction between a metal ion and a thio-modified nucleobase

Figure 1.21: A fragment of a coordination polymer crystal based on Co(II) and 6-thioguanine

Figure 1.22: Coordination polymers based on Cu(I) thiolates

Figure 1.23: One-dimensional scheme for a Ag(I) thiolate coordination polymer based on mercaptopropionic acid as a ligand

Figure 1.24: Crystal structure of a helical thiolate coordination polymer based on Au(I) and thiophenolate

Figure 1.25: Scheme of a hydrogel structure

Figure 1.26: Scheme of a supramolecular gel formation

Figure 2.1: Electromagnetic radiation a) linearly and b) circularly polarized

Figure 2.2: Jablonski diagram

Figure 2.3: Scheme of the interaction between primary electrons with sample surface atoms

Figure 2.4: Schematic diagram of SEM

Figure 2.5: Scheme of an AFM operation procedure and components to measure

Figure 2.6: Picture of a MBE used to measure electrical properties

Figure 3.1: Schematic one-dimensional Ag coordination polymers through the c axis

Figure 3.2: Schematic two-dimensional Ag coordination polymer structures

Figure 3.3: Scheme of 6-thioguanosine Ag(I) complex preparation

Figure 3.4: UV-Vis spectrum for a basic solution of 6-thioguanosine and for compound **1**

Figure 3.5: FTIR spectrum for 6-thioguanosine as a solid powder and a dried solution of **1**

Figure 3.6: CD spectrum for a basic solution of 6-thioguanosine at 10 mM and **1** at 1 mM

Figure 3.7: SEM image for dried sample of **1**

Figure 3.8: AFM image for **1** at 0.01 mM concentration in water and dried on mica

Figure 3.9: AFM images from dried solution of **1** at 0.01 mM concentration in water

Figure 3.10: AFM image from dried solution of **1** at 0.01 mM concentration in water

Figure 3.11: Proposed scheme models for the one-dimensional coordination polymer **1** structure

Figure 3.12: Luminescence spectrum for a basic solution of 6-thioguanosine at 1 mM and for **1** at 1 mM at 350 nm excitation

Figure 3.13: Two-terminal I-V characteristic of two samples, blue line corresponding to electrode background and orange line to **1** solution dried on the electrode

Figure 4.1: Schematic examples of one-dimensional Cu(I) thiolate coordination polymer

Figure 4.2: Schematic examples of two-dimensional Cu(I) thiolate coordination polymer

Figure 4.3: Scheme of 6-thioguanosine Cu(I) complex preparation

Figure 4.4: UV-Vis spectrum for a basic solution of 6-thioguanosine and **1**

Figure 4.5: FTIR spectrum for 6-thioguanosine as a solid and a dried solution of **1**

Figure 4.6: CD spectrum for a basic solution of 6-thioguanosine at 10 mM and **1** at 1 mM

Figure 4.7: SEM image for a dried solution of **1**

Figure 4.8: AFM image for **1** at 0.1 mM concentration in water and dried on mica

Figure 4.9: AFM image for a dried solution of **1** at 0.001 mM in water and dried on mica

Figure 4.10: Proposed scheme models for the one-dimensional coordination polymer **1** structure

Figure 4.11: Luminescence spectra for a basic solution of 6-thioguanosine at 1 mM at 330 nm excitation and for **1** at 1 mM at 440 nm excitation

Figure 4.12: Two-terminal I-V characteristic of three samples

Figure 5.1: Scheme of the preparation of metallogels

Figure 5.2: Nucleoside representation of a) guanosine and b) uridine

Figure 5.3: Hydrogen bonds interactions between guanine molecules to form G-quartets formed in presence of metal ions

Figure 5.4: Examples of LMWG derived from nucleosides

Figure 5.5: Structural schemes of metallogels based on coinage metals thiolate coordination polymer

Figure 5.6: Scheme for the reaction between Ag(I) salt and 6-thioguanosine

Figure 5.7: Rheological results for Ag(I) complex at 15 mM and 30 mM

Figure 5.8: UV-Vis spectra for a basic solution of 6-thioguanosine and **1** at 30 mM

Figure 5.9: CD spectra for a basic solution of 6-thioguanosine at 10 mM and **1** at four different concentrations.

Figure 5.10: Proposed scheme models for the coordination polymer **1** hydrogel structure

Figure 5.11: Luminescence spectra for a basic solution of 6-thioguanosine at 30 mM at 350 nm excitation and for **1** at 10 mM and 30 mM at 430 nm excitation

Figure 5.12: CPL experiment showing g_{lum} values between 400 and 800 nm for **1** at 30 mM and 10 mM

Figure 5.13: Scheme for the reaction between Cu(I) salt and 6-thioguanosine

Figure 5.14: Rheological results for Cu(I) complex at 30 mM and 60 mM

Figure 5.15: UV-Vis spectra for a basic solution of 6-thioguanosine and **2** at 30 mM

Figure 5.16: Melting temperature experiments for a 30 mM **2** at 250 nm

Figure 5.17: CD spectra for a basic solution of 6-thioguanosine at 10 mM and **2** complexes at five different concentrations

Figure 5.18: Proposed scheme models for the coordination polymer **2** hydrogel structure

Figure 5.19: Luminescence spectra for a basic solution of 6-thioguanosine at 1 mM at 350 nm excitation and for **2** complexes at 10 mM and 30 mM at 470 nm excitation

Figure 5.20: CPL experiment showing g_{lum} values for **2** hydrogels at a) 60 mM and at b) 20 mM

Figure 5.21: Two-terminal I-V characteristic of three samples

Figure 6.1: Interdigitated Pt on glass microelectrodes (DRP-G-IDEPT10)

Figure 6.2: Schematic of the ozone rig

Figure 6.3: Schematic of the VOC sensing test rig

Figure 6.4: AFM image on air of polymer strands of drop-cast

Figure 6.5: AFM images a) bare MWCNTs, b) Au(I)-6-thioguanosine/MWCNTs composite and c) Cu(I)-6-thioguanosine/MWCNTs composite

Figure 6.6: SEM images a) bare MWCNTs b) Au(I)-6-thioguanosine/MWCNTs composite and c) Cu(I)-6-thioguanosine/MWCNTs composite

Figure 6.7: Raman spectra of bare MWCNTs an Au(I)-6-thioguanosine/MWCNTs

Figure 6.8: Two-terminal I-V characteristics of three samples with different rations Au(I)-6-thioguanosine/MWCNTs and bare MWCNTs control

Figure 6.9: Schematic diagram showing two MCNTs before and after be coating with coordination polymer

Figure 6.10: Two-terminal I-V characteristic for a typical pure Cu(I)-6-thioguanosine device

Figure 6.11: Data for the response of the resistance of a Cu(I)-6-thioguanosine to 23.5 ppm ozone at a volume flow rate of 100 mL/min

Figure 6.12: Typical raw data showing the reversibility of the current response of Cu(I)-6-thioguanosine to chloroform vapour

Figure 6.13: Data for the response of the dc current at fixed bias of 1V for a Cu(I)-6-thioguanosine to three VOCs

Figure 6.14: 90% response time for Cu(I)-6-thioguanosine to ethanol vapour as a function of the partial pressure of ethanol at the sensor

Figure 6.15: Long term exposure raw current data for Cu(I)-6-thioguanosine for (a) chloroform at 16.6 kPa and (b) ethanol at 43.8 kPa

Figure 6.16: Typical raw data showing the reversibility of the current response of a control device based on MWCNTs alone to ethanol, chloroform and acetone

Figure 6.17: Raw data showing response of Au(I)-6-thioguanosine/MWCNTs (20%) to ethanol, chloroform and acetone. It is clear that there is much larger change in the film resistance during ethanol exposure

Figure 6.18: Fractional change in resistance, S , upon exposure to ethanol at various partial pressure and for difference compositions of the sensing material

Figure 6.19: Fractional change in resistance, S , in response to VOCs at various fractions of their saturated vapour pressure and different compositions of the sensing material

Figure 6.20: t_{90} values for various compositions Au(I)-6-thioguanosine/MWCNTs for each analyte studied

Figure 7.1: Three-dimensional model structure for a) uridine and b) 4-thiouridine

Figure 7.2: Scheme of crystal structures based on 4-thiouracil and metal ions

Figure 7.3: Scheme of a crystal structure based on 2-thiouracil and Ag(I) ions

Figure 7.4: Scheme of a) the crystal structure based on 2-thiouracil and Au(I) ions

Figure 7.5: Scheme of some of crystal structures based on Au(I) ions and thiouracil derivatives

Figure 7.6: Scheme of crystal structures based on Cu(I) ions and thiouracil derivatives

Figure 7.7: Reaction scheme of uridine protection

Figure 7.8: Reaction scheme for the thiolation in C4

Figure 7.9: Reaction scheme for the deprotection of 4-thiouridine

Figure 7.10: Scheme of the mechanism for the protection of alcohol groups in uridine

Figure 7.11: Scheme of the mechanism for the thiolation in position 4 of acetyl-protected uridine by Lawesson's reagent

Figure 7.12: Scheme of the mechanism for the deprotection of acetyl-protected 4-thiouridine to obtain a yellow solid, 4-thiouridine

Figure 7.13: Scheme of 4-thiouridine Ag(I) complex preparation

Figure 7.14: UV-Vis spectrum for 4-thiouridine and **1**

Figure 7.15: FTIR spectra for 4-thiouridine and **1**

Figure 7.16: CD spectra for 4-thiouridine and **1**

Figure 7.17: SEM image for Ag(I) product at 200 μm

Figure 7.18: AFM image for **1** at 0.1 mM concentration in water and dried on mica

Figure 7.19: AFM images for **1** at 0.01 mM concentration in water and dried on mica

Figure 7.20: AFM images for **1** at 0.01 mM concentration in water and dried on mica

Figure 7.21: Proposed scheme models for the one-dimensional coordination polymer **1** structure

Figure 7.22: Luminescence spectra for an aqueous solution of 4-thiouridine at 60 mM and **1** at 100 mM at 380 nm excitation

Figure 7.23: Scheme of Au(I)-4-thiouridine complex preparation

Figure 7.24: UV-Vis spectra for 4-thiouridine and **2**

Figure 7.25: CD spectra for 4-thiouridine and **2**

Figure 7.26: AFM image for **2** at 0.1 mM concentration in water and dried on mica

Figure 7.27: AFM image for **2** at 0.1 mM concentration in water and dried on mica

Figure 7.28: Proposed scheme model for the one-dimensional coordination polymer **2** structure

Figure 7.29: Emission spectra of 4-thiouridine with excitation at 380 nm and **2** with excitation at 450 nm and 550 nm

Figure 8.1: Side view of a model of a one-dimensional coordination polymer for Ag(I) thiolate, and for Cu(I) thiolate

Chapter 1. Introduction

Table of Contents

1.1. Nanotechnology	3
1.2. Introduction to nucleic acids	4
1.3. DNA nanotechnology and Origami	8
1.4. DNA functionalization	11
1.4.1. Nanoparticles	11
1.4.2. Metal templating	12
1.4.3. Metallo-base pairs DNA.....	13
1.5. DNA based coordination polymer approach.....	18
1.5.1. Interaction between metals and thio-modified nucleosides	22
1.5.2. Coinage metal thiolate coordination polymers.....	26
1.5.2.1. Cu(I)	26
1.5.2.2. Ag(I).....	27
1.5.2.3. Au(I).....	28
1.5.3. Hydrogels	30
1.6. Conclusions.....	32
1.7. References	33

1.1. Nanotechnology

Since the mid-20th the interest in the synthesis of materials in the nanometer scale range has increased due to the possibilities for their new properties and performances compared to more traditional materials, with applications in fields such as energy storage, environmental processing, electronics and medicine.¹⁻³ There are two approaches for the preparation of nanomaterials, top-down and bottom-up and their difference lies in the starting material used for the synthesis. While the first uses bulk material, such as silicon wafer and processes this to ever smaller features, the second approach looks to build up to the nanoscale from sub-nanoscale molecules to form complex assemblies.⁴ This approach takes inspiration from biology with, for example, the synthesis of biopolymers such as DNA and proteins from their respective building blocks, nucleosides and amino acids.^{5,6} Apart from their biological functions, there is a great interest in the preparation of a new class of nanomaterials using these biomolecular building blocks that can be assembled into predictable and desirable structures.⁷ In this regard DNA can be prepared in a tetrahedron form to encapsulate proteins (Figure 1.1a),⁸ or to crystallize them within a DNA mesh (Figure 1.1b),⁹ in addition to DNA Origami technique that will be explained in depth later. However, the intrinsic, opto-electronic properties of these biopolymers are rather limited and, as a consequence, methods have been explored and developed for the incorporation of technological useful properties, conductivity or luminescence¹⁰ to them. Different routes have been established to introduce functions on these biomolecules, for example electrical,¹¹ optical¹² or magnetic properties,¹³ and the method of specific interaction of transition metals with them is the preferred.¹⁴ Of particular relevance to the work in this thesis are the methods that seek to utilize, or adapt, the transition metal ion bonding features of DNA, whilst maintaining its molecular structure.¹⁵ The work presented in this thesis explores the use of modified nucleosides as a means to

introduce new physical properties into DNA-like materials based on coordination polymers.

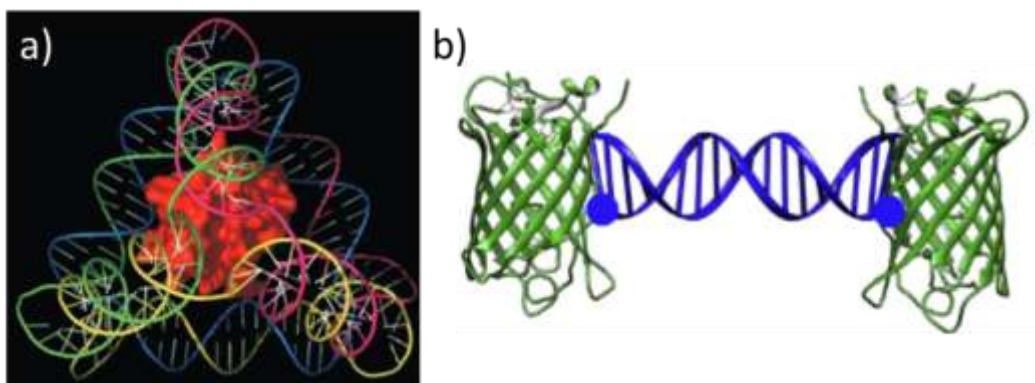


Figure 1.1. Nanomaterials that take advantage of the structural characteristics of DNA, a) a model to DNA encapsulating proteins⁸ and the crystallization of proteins (blue circles indicate specific amino acids attachment position for DNA strands) (b).⁹

1.2. Introduction to Nucleic Acids

Deoxyribonucleic acid, DNA, has the capacity to store and transfer the genetic information in the sequence of a linear polymer containing four nucleobases, adenine (A), thymine (T), cytosine (C) and guanine (G) (Figure 1.2a). These nucleobases are divided into two groups, purines (A and G) and pyrimidines (T and C).¹⁶ Nucleotides are formed by a nucleobase, a ribose ring and a phosphate group and they are covalently linked by phosphodiester bonds through 3' and 5' carbon of the sugar forming a one-dimensional strand (Figure 1.2b).¹⁶

The structure of duplex DNA is based on the recognition between nucleobase pairs A-T and G-C through specific hydrogen bonds (Figure 1.2a,b).¹⁷ These electrostatic connections are supplemented by hydrophobic stacking interactions to produce the well-known Watson-Crick's helix.¹⁸ In DNA's structure, the geometry and arrangement of nucleobases follow the Watson-Crick model which represents the optimum stability

of the structure with the maximum number of hydrogen bonds possible formed.¹⁹ Thus, the interaction of two complementary polymeric strands by their nucleosides leads to the formation of a double helix which is responsible for the production of other biomolecules with specific functions within the cell.²⁰ Later on, it was found that nucleotides A and G could form additional hydrogen bonds through their N7 atoms, known as Hoogsteen-type base pairing (Figure 1.3).²¹

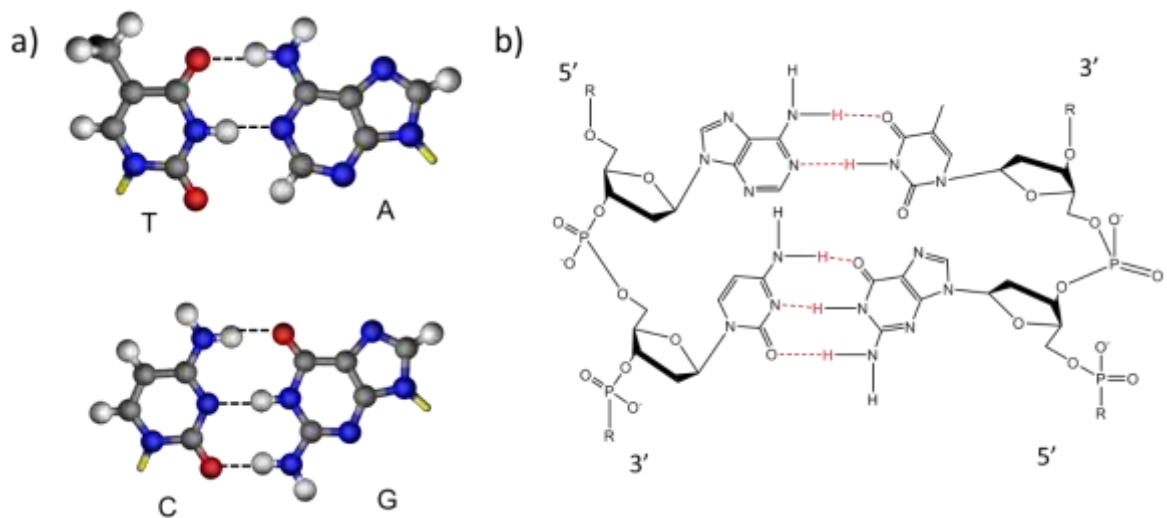


Figure 1.2. a) Scheme of the hydrogen bond between thymine-adenine and cytosine-guanine bases. b) Representation of a DNA double-helix structure. It is built by two strands of nucleotides linked by specific hydrogen bonds in opposite directions, 5' to 3' versus 3' to 5'.

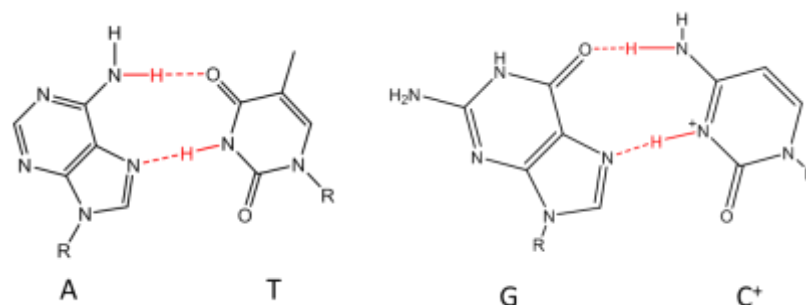


Figure 1.3. Scheme of Hoogsteen-type pairing of adenine-thymine and guanine-cytosine⁺ base pairs (R= deoxyribose ring).

The more common form of duplex DNA is the so-called 'B-form' where the two strands of polymers are entangling in a right-handed anti-parallel way with approximately ten base pairs per turn and 20 Å of diameter of the helix (Figure 1.4b).²² Other conformations of duplex DNA are known such as 'A' and 'Z' forms. A-form consists in right-handed double helix with similar diameter as B-form and with eleven base pairs per turn, also the base tilt is more pronounced in A-form. The structural changes between A and B-forms lie in a closer distance between nucleotides for A-form and also their position is not located inside the helical axis like B-form does, because of this A-form DNA exhibits thicker helices (Figure 1.4a).²³ The differences of B-forms with the Z-form DNA are more radical. Z-form exhibits a left-handed double helix with twelve base pairs per turn and 18 Å of diameter, so the structure is thinner and longer. Also, the order of the helix is following a zig-zag sequence (Figure 1.4c). Specifically, this type of DNA is common for G and C residues because G adopts a syn- and C anti-conformation.²⁴

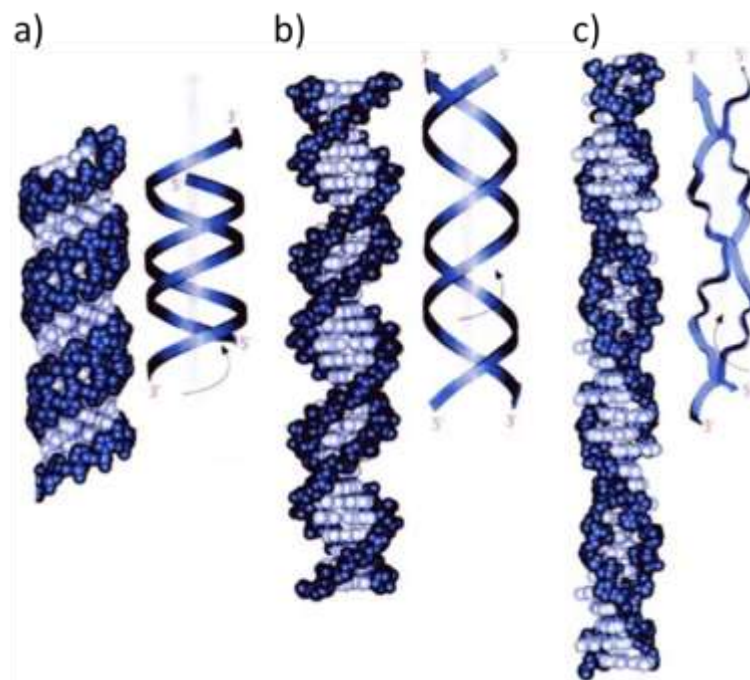


Figure 1.4. Scheme for the different DNA conformations represented as balls and ribbons. a) A-DNA form, b) B-DNA form and c) Z-DNA form.²⁵

To prepare DNA there are various synthetic routes. The use of enzymes provides a fast and low-cost method, and it is the main method to prepare long strands of DNA, about hundreds of nucleotides, using a template extracted from animal cells although it has the inconvenience of the uncontrolled ordering of nucleotides of the template.²⁶ Chemical methods includes array-based oligo synthesis²⁷ and the solid-phase technique, a well-established process used regularly in industry.²⁸ The solid-phase synthesis is based on a cycle where nucleotides are added one by one to the final sequence through a reaction between a reactive nucleoside added to a solid-supported growing chain. The synthesis consists in four steps and it is normally carried out in an automated DNA synthesizer (Figure 1.5).

The process begins with the coupling of the first protected deoxy-nucleoside at the 3' end to the solid support through an ester bond; the protecting group, DMT (4,4'-dimethoxytrityl), is attached to the C5'. Then, deprotection of the DMT group using trichloroacetic or dichloroacetic acids in dichloromethane occurs. The second nucleobase is added as a reactive nucleoside-phosphoramidite which is activated when mixed with tetrazole and it is attached to the 5' end of the deoxy-nucleoside bonded to the support, generating a phosphite triester. The next step is called 'capping' because the addition of acetic anhydride and N-methylimidazole dissolved in THF/pyridine ensures that the chains that have not reacted with phosphoramidite during the previous stage are blocked. The addition of iodine in water and THF/pyridine after the capping causes oxidation of the unstable phosphite triester intermediate to phosphate triester. The resulting molecule is comparable to DNA polymer and therefore, this process can be repeated the number of times necessary for the desired length of the oligonucleotide. The direction of the synthesis is 3' to 5'. Besides, at the end of the cycle it is possible to liberate the oligonucleotide from the support with the addition of ammonia; nucleobases and phosphate protecting groups are removed by

an ammonia solution and heat. The yield of each step normally exceeds 98% which is good for oligonucleotides between 2 to 60 nucleobases although the number of impurities increases with different lengths of product obtained for longer oligonucleotides. Because of that, HPLC techniques are used at the end of the synthesis.

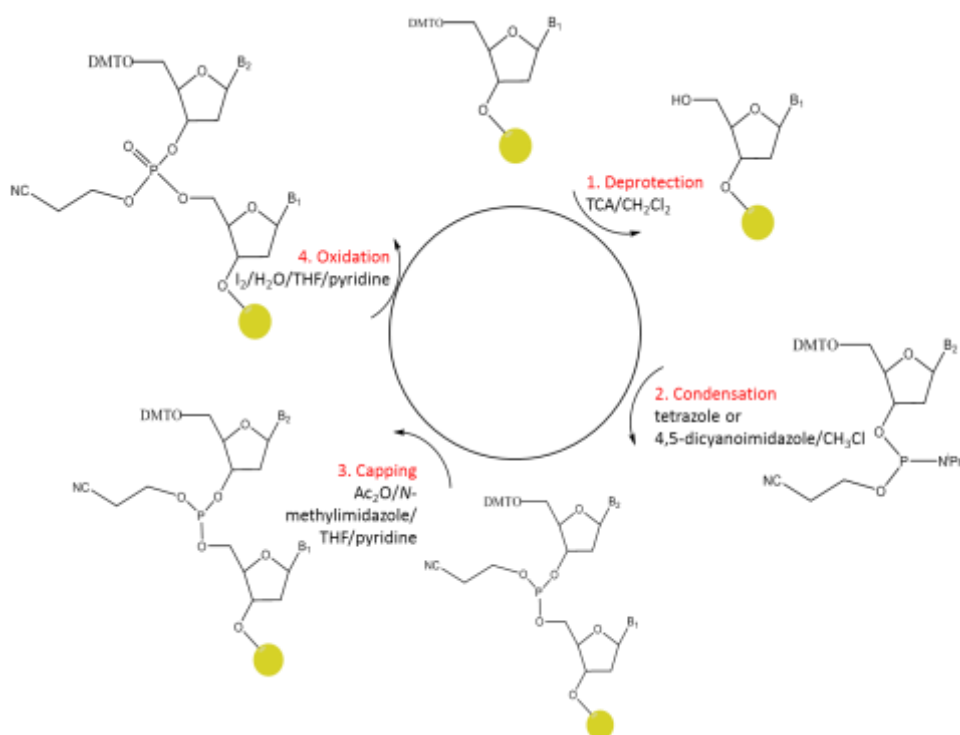


Figure 1.5. Scheme of the four steps of DNA synthesis by phosphoramidite method in an automatic synthesizer.

1.3. DNA nanotechnology and Origami

As we have seen, apart from biological properties, DNA stands out because of self-assembly properties of its components leading to the formation of a variety of organized architectures via complementary hydrogen bond formation.²⁹ This biomolecule is crucial for the development of nanotechnology, a science field with aim of generate materials controlling structure and composition at the nanoscale.³⁰ The use

of DNA in nanotechnology is due to the fact that its size and morphology can be designed with nanometric precision by programming its sequence of bases.^{31,32}

So, the famous double helix DNA structure has been studied for over 30 years for its use in nanotechnology. The first interesting study was developed by Seeman group in 1998 and it suggests the use of DNA as a construction material for nanometer-sized objects (Figure 1.6a).³³ Specifically, the complex structures exposed here are based on catenates made of cyclic single DNA polymers (Figure 1.6b).³⁴ Eight years later Rothemund group exposed a revolutionary new technique called 'DNA origami' (Figure 1.7).³⁵ In this case, a long single continuous strand of DNA, with more than thousand nucleotides, is systematically folded using a large number of smaller complementary DNA strands, between 10 to 40 nucleotides, and consequently it forms into the desired shape, allowing the assembling the same initial long strand of DNA, into squares, rectangles, stars and many other two-dimensional shapes.³⁶

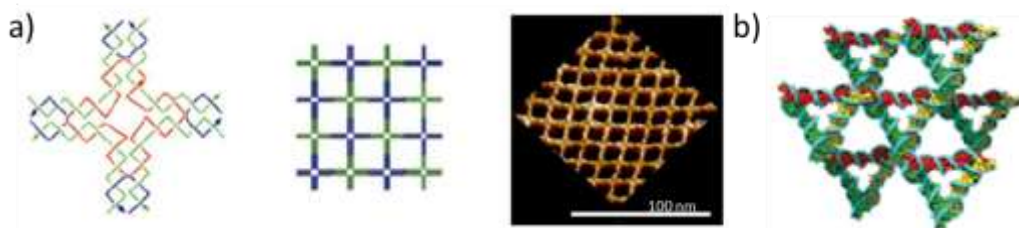


Figure 1.6. Nanostructures build with DNA, a) two-dimensional tiles assembled lattices and b) illustrated the formation of a three-dimensional rhombohedral structure.³⁷

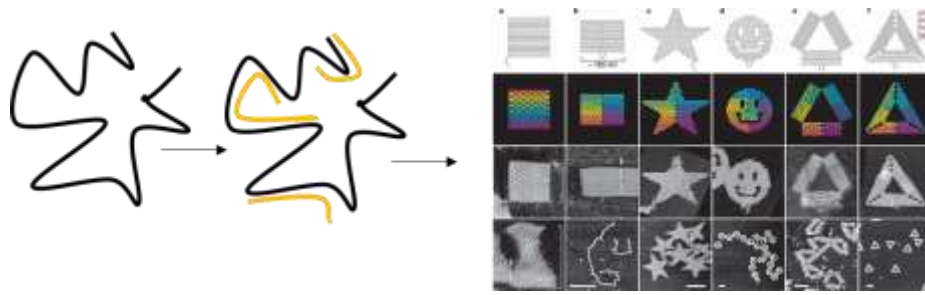


Figure 1.7. DNA origami formation. Black lines represent a single DNA strand that interacts with complementary shorter strands (yellow lines) folding until they form DNA origami shapes.³⁵

From 2008 until now, the development of three-dimensional lattices (Figure 1.8a), three-dimensional DNA Origami (Figure 1.8b) or single crystals among other nanostructures have been developed ending into two well defined fields, nanoparticle-templated DNA bonds or hybridization-based DNA bonds.³⁷ The difference between these two lies in the preparation of such nanomaterials, while the first is based on many crossed unions between molecules like in DNA Origami, the second uses nanoparticles as templates to build, for example, colloidal nanoparticle crystals.³⁸ All of these techniques confirm that DNA is a really useful building-block for nanoscale materials because the controllable length scale, morphology and self-assembling properties that allows bottom-up fabrication with nanometric precision through programming of sequence.

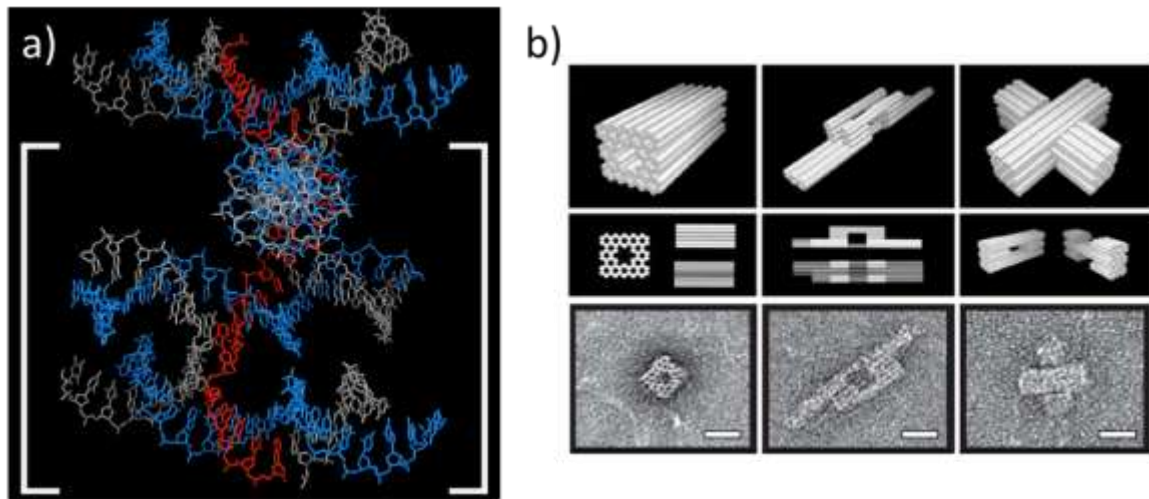


Figure 1.8. Macromolecular DNA structures, a) three-dimensional lattices³⁹ and b) three-dimensional DNA origami (scale bars are 20 nm).³⁷

1.4. DNA functionalization

DNA has showed how promising are their structural properties for its use in nanotechnology, developing new entities that give to the biomolecule a new perspective to investigate.^{40,41} Having this in mind, DNA has been exposed to modification in order to improve their properties and applications. Some examples have illustrated basic alteration on DNA, attaching, by covalent bond, fluorescence markers to DNA ends in order to change its solubility properties^{42,43} or the modification of original nucleobases to study stabilities of the double helix.^{44,45}

1.4.1. Nanoparticles

A simple attempt to modify or integrate DNA with components is the functionalization of DNA with nanoparticles. This method allows to create superlattices (Figure 1.9) by the programmability of DNA assembly with nanoparticles, forming two or three-dimensional architectures.^{46,47} The metal nanoparticles used are Au,⁴⁸ Ag, Al⁴⁹ or Fe

among other and mainly these materials have medical applications, such as in cancer therapies or to detect specific human cells.⁵⁰

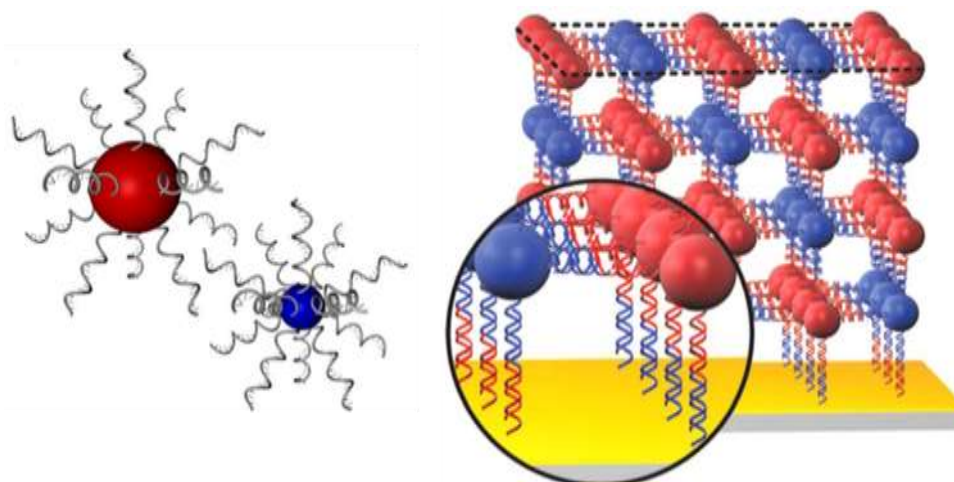


Figure 1.9. A controlled three-dimensional architecture based on the interactions between complementary strands of DNA forming a superlattice of nanoparticles in specific places.^{46,47}

1.4.2. Metal templating

However, some studies have demonstrated that for some applications the components of DNA are rather limited for suitable electronic properties.^{51,52} To address this, studies have been carried out to modify or integrate DNA with synthetic molecules that can give function to the DNA scaffolds.³⁰ The metal templating on DNA was proposed as a possible method to induce electrical properties on DNA structure (Figure 1.10a).^{53,54} The main characteristic of these investigations is the use of DNA molecule as a template to control the morphology of larger materials throughout a bottom up preparation. In this regard, the negative charged phosphate backbone and specific nucleobase locations are essentials for interactions with metal ions derived from Ag,⁵³ Cu⁵⁵ or Pt,⁵⁶ which are subsequently reduced to metal.⁵⁷ After metal deposition onto DNA, a one-dimensional wire, nanowire, is formed and it exhibits electrical conducting

properties (Figure 1.10a).^{58,59} In general, the issue of DNA-templated technique is the uncontrolled growth of metal particles size which causes heterogeneous ordering of such particles on the template and then an imprecise electrical carrying.⁶⁰ To avoid that, a combination of a suitable chemical modification on DNA strand folded into an origami structure, following the DNA-templated approach, has been investigated bringing a more controlled way of metallic growth (Figure 1.10b).⁶¹ This is because metal particles will recognize and link to specific positions on the DNA strands.

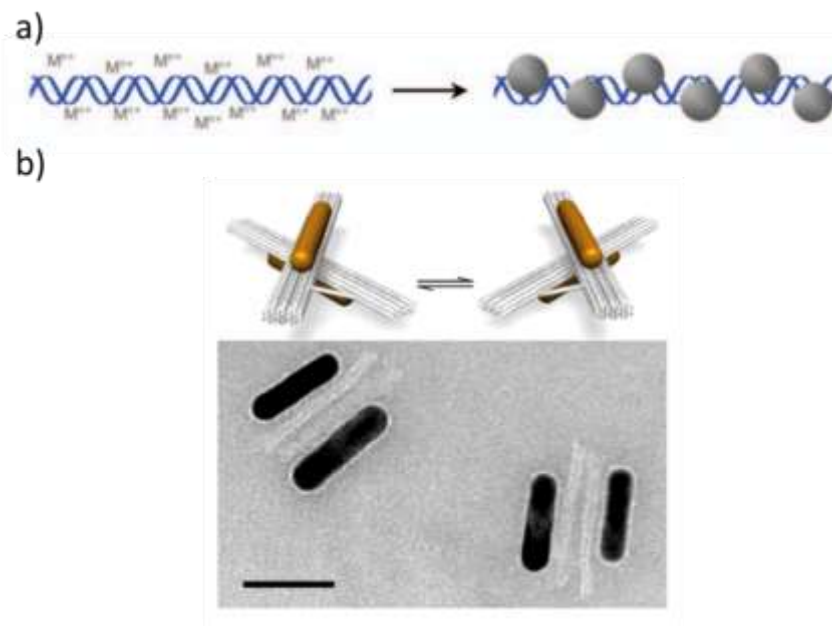


Figure 1.10. Model of a metal templating on DNA to prepare nanowires (grey balls indicate metal (0)) (a)⁶² and a combination of DNA Origami and metal templating on DNA (b) (yellow bars are meta or metal nanoparticles; scale bar is 50 nm).⁶³

1.4.3. Metallo-base pairs DNA

To obtain functionalized material a la carte, a related method has focused on the affinity of transition metal ions to DNA and the subsequently replacement of hydrogen bonds by coordination bonds within DNA structures; this approach is called metallo-base pairs DNA (M-DNA)⁶⁴ and it indicates the formation of metal-modified base pairs

(Figure 1.11).^{65,66} The use of DNA as a polydentate ligand with extremely rich coordination chemistry, as exemplified by the 'Cisplatin' drug,⁶⁷ allows the attaching of transition metal ions to their strands and thereby incorporate luminescence, electrical or magnetic properties to its structure.^{59,68,69} Specifically, the interest of using nucleosides as ligands arises from their large number of donor sites available for metal bonding (Figure 1.12).

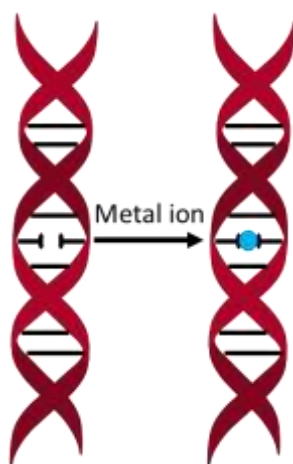


Figure 1.11. Interaction of a DNA double helix molecule with a metal ion and the subsequent hydrogen bond substitution by a metal coordination between complementary base pairs.

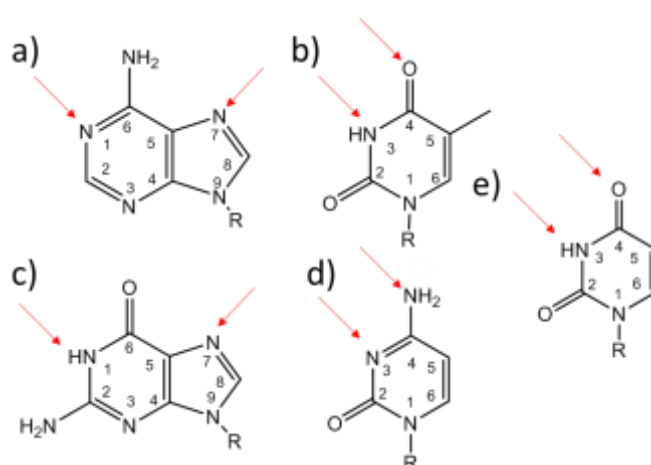


Figure 1.12. Scheme of a) adenosine, b) thymidine, c) guanosine, d) cytosine and e) uridine with their preferred sites of metal interactions. Red arrows indicate donor sites available for metal bonding. (R= ribose ring).

The M-DNA system is of interest due to the versatility of metal ions functionalization of DNA and it can be sub-classified into different approaches, the formation of non-canonical base pairs by the exchange of hydrogen bonds in natural nucleobases or artificial ligands to coordination bonds with metal ions^{70,71} and the reversible bonding of metal ions to part of the DNA not involved in base pairing.⁷² In addition, M-DNA improves a controllable deposition of metal ions by DNA strands⁷³ and contributes to maintain the persistent distortion of crosslinking of DNA duplexes by metal ions that form kinetically inert complexes.^{34,74,75}

Mainly, M-DNA approach has focused on the development of metal-modified base pairs where there is a substitution between hydrogen bonds and metal coordination bonds without altering the Watson-Crick bonding scheme, retaining and stabilizing the double-helical structure of the oligonucleotide. Besides, it has been showed that the formation of a M-DNA system makes use of the programmability of the sequence of DNA to introduce a concrete number of metal ions in specific locations.^{65,76-78} These systems are designed to be incorporated into nanodevices as conductive films, bringing electronics applications because of the optimistic vision of the molecular wire nature of M-DNA (Figure 1.13).⁷⁹

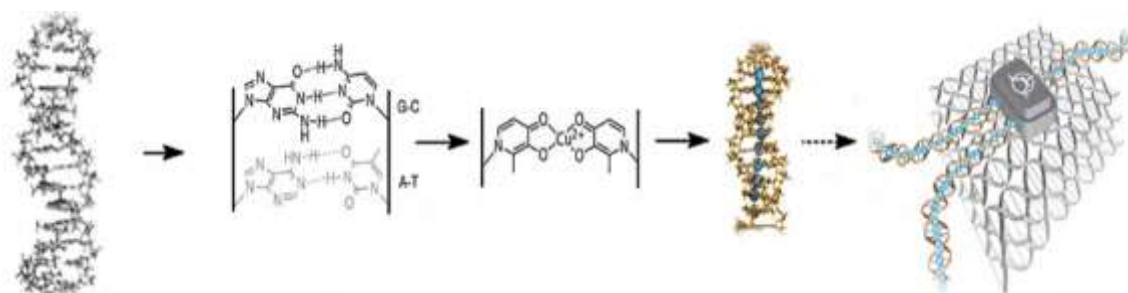


Figure 1.13. Example of functionalization of materials following metal modified or mediated base pairs strategy. Metal ions are introduced into modified DNA strands (nucleosides) forming materials that can be integrated into electrical nanodevices.⁷³

Some of the approaches to the design of metal-base pairing DNA systems were carried out with Hg(II) (Figure 1.14a)⁸⁰ or Zn(II) (Figure 1.14b)⁸¹ and more recently Ag(I) (Figure 1.14c),⁷⁶ Ni(II)⁸² or Cu(II).⁸³ Besides, the interaction between DNA and transition metals has been widely studied with other metal ions like Co(II), Mn(II), Cd(II), Au(I) or Cu(I) and (II),⁸⁴⁻⁸⁶ which confirms different ways of coordination of these metals to DNA.⁸⁷ In particular, Hg(II) and Ag(I) are able to form a thermodynamically stable bond with the double helix without structure modification or phosphate interaction with ΔG^0 values between -2.7 and -1.7 KJ/mol respectively.⁸⁷

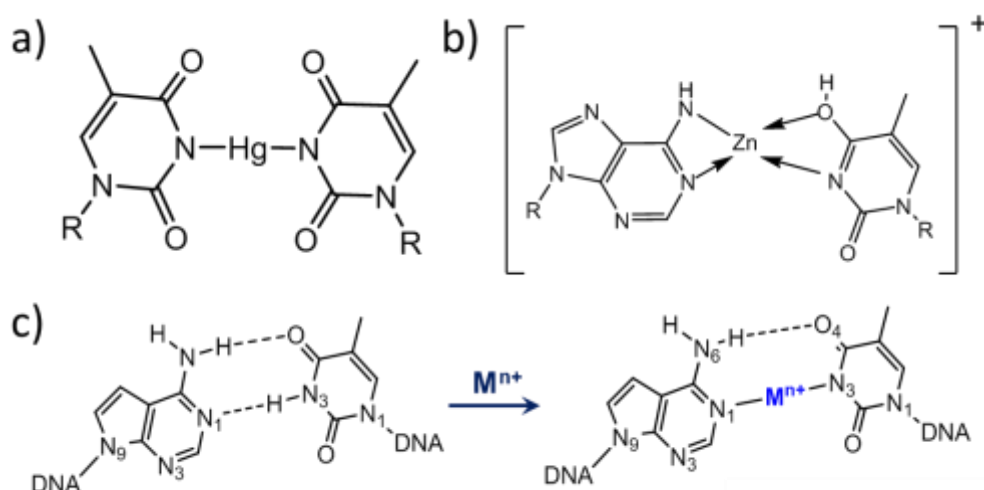


Figure 1.14. Scheme examples of metallo-base pairs DNA structures a) Hg(II) coordinating two thymidines, b) Zn(II) mediating between an adenine and a thymidine following a Hoogsteen type pairing and c) bonding of a metal cation, Ag(I), to the position N1 of 7-deazadenine by hydrogen bonding substitution. (R= deoxyribose ring).

These systems highlight in some applications. The use of M-DNA as sensors is based on the recognition of specific transition metal ions by nucleobases or larger oligonucleotide sequences.^{88,89} Although another application of M-DNA systems is

their use as molecular wires, the capacity of M-DNA to have magnetic or electrical properties is controversial, it is not clear that these systems show electrical charge transfer capacities.⁹⁰ It is usual to find big differences in electro-magnetic results depending on the sequence or metal ion used and M-DNA preparation.⁹⁰ Whereas the duplex prepared with Cu(II) and hydroxypyridone (Figure 1.15) showed magnetic properties,⁹¹ the sequence becomes crucial to determine such properties.⁹² In this regard, other metals ions, Zn(II) or Ni(II), have been also investigated with discrepant results.^{93,94}

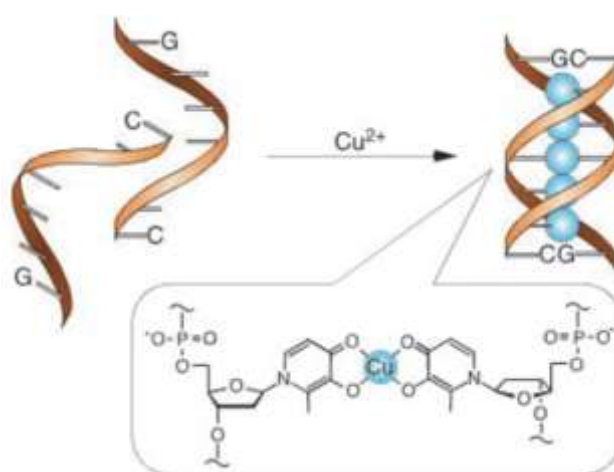


Figure 1.15. Cu(II) mediated hydroxypyridone nucleobases forming a DNA duplex.⁹¹

Although it has been shown that DNA owns semiconductive properties under certain conditions^{95,96} other studies have shown that DNA possess weak electronic properties suitable to be incorporated into electronic devices.⁹⁹ This is due to different factors such as the length of DNA strands or certain chemical modifications in nucleotides.^{95,96,99} In some cases, the fact that DNA acts as an insulator encouraged researchers to investigate its interaction with transition metals, leading to the formation of molecules with interesting electrical properties for use in nanotechnology, such as

nanowires or biosensors.¹⁰ Although, metal templating on DNA showed electrical conductivity properties, metallo-base pairs DNA has not obtained conclusive results.⁹⁸

A crucial issue for metallo-base pairs DNA compounds is that the addition of metal ions to DNA scaffolds do not produce inherent conductivity.⁹⁸ Some studies have analyzed the reasons for such behavior concluding that they are mainly due to the electronic structure of M-DNA. The filled valence band in the metal ion and an empty conduction band in the ligand with a considerable band gap between them, appear to be crucial factors to determinate if such materials conduct electricity.⁹⁸ To overcome the lack in electrical properties on M-DNA, the product usually needs an extra modification along the chain, mainly focus on the reduction of metal ions to their metallic form.^{99,100}

1.5. DNA based coordination polymer approach

The strategy followed through this thesis is the use of the coordination polymer approach as a means to incorporate new properties into DNA-based materials. The use of DNA components as a ligand, specifically nucleosides that form it, opens the possibility to link metals directly to them with established patterns.¹⁰¹ The use of transition metals will provide new properties to the system such as electronic functionality, magnetism or redox properties.¹⁰²⁻¹⁰⁴ In addition, as some of the research shows,^{53,105} this approach allows to build supramolecular structures in different frameworks.

Coordination polymers are defined as hybrid compounds based on a metal ion and an organic or inorganic ligand, forming as a result one or two-dimensional complexes (Figure 1.16 and 1.17).¹⁰⁶ In addition, these compounds can form three-dimensional compounds, described as metal-organic frameworks (MOFs).¹⁰⁷ In general, the bonding between metal ions and ligands is driven by electron donor-acceptor properties as it is considered in the hard-soft acids and bases theory.¹⁰⁸ Following such

theory, metal ions are treated as Lewis acids and ligands as Lewis bases.¹⁰⁹ Depending on the composition of coordination polymers, they can be divided into acid-acid, base-base or acid-base categories.¹¹⁰ They exhibit promising properties that can be applied in different fields such as in sensing or optical devices, catalysis, luminescence, magnetic or conductivity¹¹¹ depending on metal ions and bridging ligands used in their preparation.¹¹²

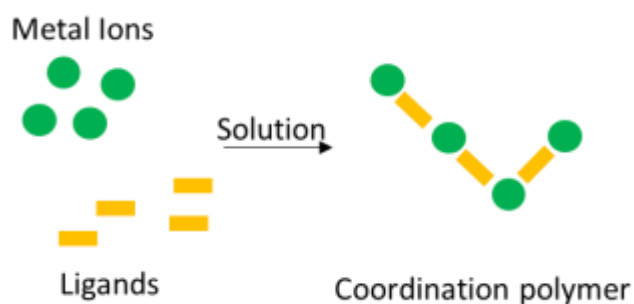


Figure 1.16. Scheme of a coordination polymer formation. The specific interaction between metal ions and organic or inorganic ligands lead to the formation of a coordination polymer.

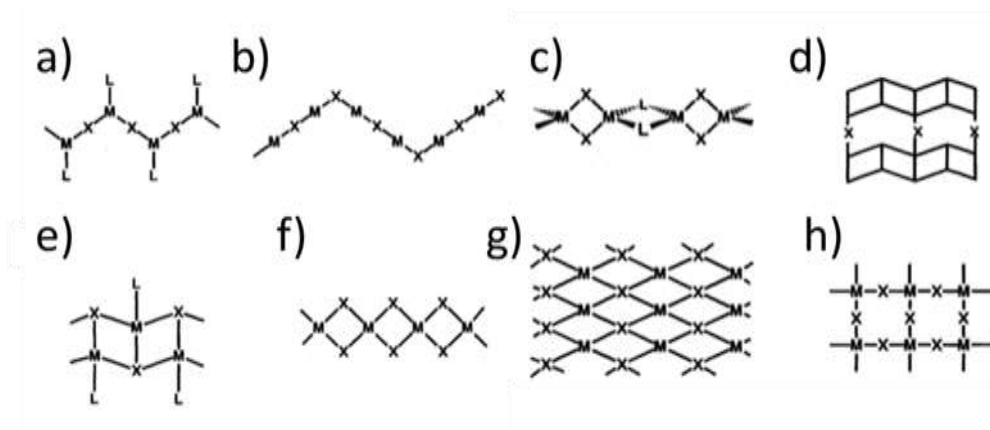


Figure 1.17. Examples of coordination polymers frameworks, a) and b) indicates a linear-zigzag coordination polymer, c) and f) a structure in rhomboid form of coordination polymers, d) a double ribbon structure, e) ribbon structure, g) a double chain coordination polymer structure and h) a layered structure. M represents metal ion, X the organic ligand and L the organic groups of the metal compound.¹¹³

The use of coordination polymers as optical devices arises from their chiro-optics properties and specifically, the interest lies in the preparation of homochiral helices.¹¹⁴⁻¹¹⁷ Due to their luminescence properties, coordination polymers based on aromatic ligands and transition metals are compounds with high photoluminescence properties. These complexes have demonstrated their potential use as light-emitting diodes (LEDs),¹¹⁸ such is the case of Tb(III).¹¹⁹ Magnetism properties of coordination polymers are also used as magnetic switches,¹²⁰ or molecule-base magnets.^{121,122}

The interest of electrical conductivity properties of coordination polymers has been increased recently due to their application in nanotechnology and specifically, as new materials for gas sensing or electrochromic films.¹²³ The use of coordination polymer in batteries, fuel cells, molecular wires or capacitors has demonstrated how abundant and tunable are potential applications of such materials.¹²⁴ Apart from the use in optoelectronics devices,¹²⁵ coordination polymer can be used for other applications. Energy production, gas separation and non-linear optics have been also demonstrated that coordination polymers are versatile compounds with a rich field of applications.^{124,126}

Apart from many biological applications, such as drug delivery or tissue imaging, biocompatible components of coordination polymers are preferred due to their sustainable characteristic.¹²⁷ In that sense, coordination polymers based on nucleobase or nucleobase derivatives ligands are components with a reduced environmental impact.¹²³ Nucleobases also highlight in their high possibilities of metal bonding sites, showing a wide range of structures as well as self-assembling properties.¹²⁷ Specifically, the idea here is to develop efficient methodologies in the preparation and characterization of coordination polymers based on modified nucleobase derivatives.

Nucleoside derivatives are an important range of compounds with biological functions, and specifically, thio-nucleosides.¹²⁸ There are many soft-mutated nucleosides with a sulfur group found on modified RNA oligonucleotides, e.g. 2-thiocytidine, 5-methyl-2-thiouridine, 5-methylaminomethyl-2-thiouridine, 2-methylthio-N6-adenosine, 6-thioguanosine and 4-thiouridine (Figure 1.18).¹²⁹ In addition to their biological purposes, many thio-modificated nucleosides have been incorporated into DNA and RNA with the idea of bringing new functions to these biomolecules and explore potential applications due to its photosensitivity and photo-crosslink properties in RNAs or proteins.^{130,131} Some studies have showed their presence on DNA oligonucleotides without appreciable change in the stability of the strand¹³²⁻¹³⁴ except 2'-deoxy-6-thioguanosine that decrease thermodynamic stability of DNA double-helix.^{135,136} Focusing on 4-thiouridine and 6-thioguanosine, studies have investigated the effect of its occupancy on a oligomeric RNA double strands. In the case of 4-thiouridine, RNA undergoes thermodynamic stabilization, around 2 kcal/mol, of base pairs when 4-thiouridine is bonded to guanosine by hydrogen bonds.¹³⁷ In the opposite, for 6-thioguanosine, there is a decrease in thermodynamic stability for RNA oligonucleotides of the order of 11 kcal/mol.¹³¹

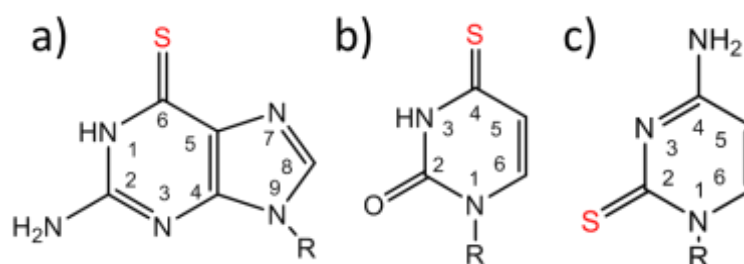


Figure 1.18. Examples of thio-derivatives nucleosides, a) 6-thioguanine, b) 4-thiouridine and c) 2-thiocytidine. (R= ribose ring).

1.5.1. Interaction between metals and thio-modified nucleosides

Although many ways of nucleosides modification have been examined, the use of thio-derivatives of nucleosides have probed its capacity to coordinate metals forming coordination polymers.^{136,138} The capacity of sulfur to bridge metal ions is well-known¹³⁹ and it allows a direct connection between metals along the polymer. Therefore, the bottom-up synthesis of coordination polymers using modified nucleobases with thiol derivatives and transition metals will lead to the formation of a metal-sulfur polymer that can be introduced inside DNA.¹⁴⁰ The specificity of the interaction is based on the hard and soft acids and bases Lewis theory, HSAB theory, since sulfur is a soft base, large and polarizable, with high affinity to soft acids like transition metals.¹⁴¹ As highlighted in previous section, the coordination chemistry of nucleosides owns a high versatility as ligands, with a large number of donor sites available for metal bonding (Figure 1.12).¹⁴² To avoid this, the modification of nucleobases with thiol derivatives will evade natural bonding sites and will bond the metals in particular places. Using this approach, it will be possible to obtain appropriate coordination geometry for the desired architecture avoiding some problems seen in others DNA functionalization approaches like the uncontrolled introduction of metal ions into DNA.^{55,143}

It has been demonstrated the capacity of a thio-modified nucleoside, 4-thiouridine inserted in a DNA oligomeric chain, to coordinate strongly divalent metals ions, Cd(II), in specific bonding places.¹⁴⁴ There are other examples of particular interest where oligonucleotides with thio-modified nucleotides in DNA or RNA are linked specifically to metals, e. g. the possibility of self-assembling metal-colloidal, Au or Ag-nanoparticles, through complementary oligonucleotides to produce three-dimensional hybrid compounds or superlattices with potential electrical or optical applications, such as quantum dots or plasmonic materials suitable for circuitry.¹⁴⁵⁻¹⁴⁷ The

complementary strands of oligonucleotides are controlling precisely the position of each nanoparticle and they influence the distance and interactions between them.¹⁴⁸ This aspect is crucial for the optoelectronic properties that these compounds will display on their applications like the surface plasmon resonance-based sensors.¹⁴⁹ Furthermore, a similar method to M-DNA has been used to coordinate metals like Pd(II), Ni(II), Pt(II) to thio- modified oligonucleotides.¹⁵⁰ The incorporation of transition metal to these oligonucleotides has been used due to chemical or physical properties that these metal display such as optical or magnetic.¹⁵⁰

The main idea of the interaction between sulfur atoms of modified nucleosides and metal ions is the interesting semiconducting properties that these compounds display, similar to metal sulfides (Figure 1.19).¹⁵¹⁻¹⁵³ It is possible to find them in nature as minerals, pyrite or galena, and artificially by synthesis, so its preparation can be programmed for specific applications. Metal sulfides are composed by a S^{2-} anion and a metal cation forming a variety of stoichiometries and therefore, crystalline structures.¹⁵⁴ Structurally, they can form one-, two- or three-dimensional configurations.¹⁵⁵ Usually metal sulfides are known material due to its wide range of application as nano-electronic devices, sensors, batteries or LEDs due to their inherent magnetic, electrical, thermoelectric, photoelectric or photocatalytic properties, among others.^{156,157} Synthetic metal sulfides such as ZnS or Cu_2S have display optoelectronics properties very useful in semiconducting industry featuring luminescence or photochemistry.¹⁵⁹ In addition, they have been used as photocatalysts, p-type semiconductors, nanogenerators or solar cells.^{158,159}

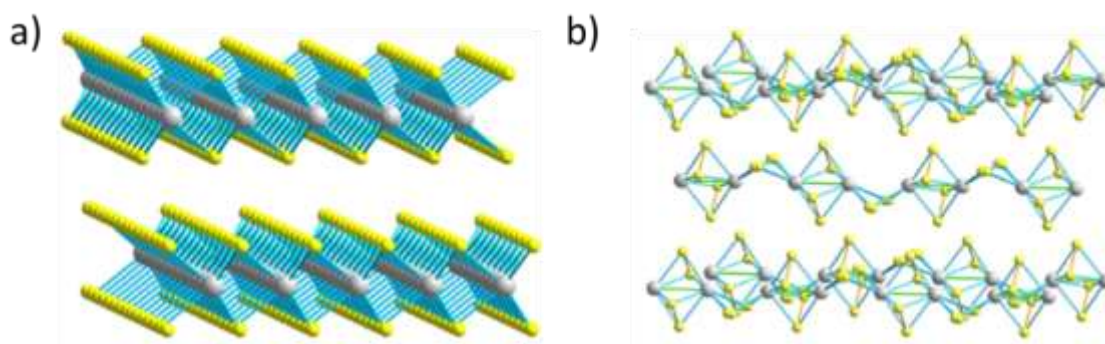


Figure 1.19. Structure models of metal sulfides, MoS₂ (a) and VS₄ (b) (grey balls are metal ions and yellow balls sulfur atoms).¹⁶⁰

The use of thio-derivatives of nucleobases as single molecules have been used in the reaction with transition metals and as result coordination polymers have been obtained. The interaction between 6-thioguanine and Cd(II) forms a coordination polymer where metal ions are bonding to S(C6) and N7 of the ligand (Figure 1.20a) and the polymer displays potential conductivity properties which makes this coordination polymer ideal as molecular wires for nano-electronics applications.¹⁶¹ The extension of the study to other transition metals include the use of Ni(II), Co(II) and Co(III). Two one-dimensional coordination polymers have been prepared with Ni(II) using two similar ligands 6-mercaptapurine and 6-thioguaninate. The structural characteristics of these compounds are the formation of polymeric chains where Ni(II) ions are attaching two ligands by four sulfur atoms and two nitrogen atoms at position 7 of the thiolate (Figure 1.20b).¹⁰⁵ This compound exhibits electrical conductivity in accordance to computational studies and it suggests potential nanotechnological applications being integrated as semiconductor in electronic chips.¹²⁴ The interaction between Co(II) and 6-thioguanine have led to the formation of a one-dimensional coordination polymer with metal ions coordinating two ligands by four sulfur atoms and two nitrogen atoms in position 7 of 6-thioguanosine (Figure 1.21).¹⁶¹ This polymer has

exhibited antiferromagnetic and semiconductor behavior which are essential characteristic to be integrated into electronics devices.¹⁶¹ Also, the reaction between Cu(II) and a modified uracil nucleobase has produced a one-dimensional coordination polymer with temperature dependent magnetic properties and semiconductor behavior.¹⁶² All of these coordination polymers have demonstrated that they can be formed using DNA derivatives and therefore, it suggests the possibility to prepare complexes architectures by interactions of coordination polymers with specific DNA sequences.¹⁶² The research presented in this work extends the study of the formation of coordination polymers to coinage metal ions.

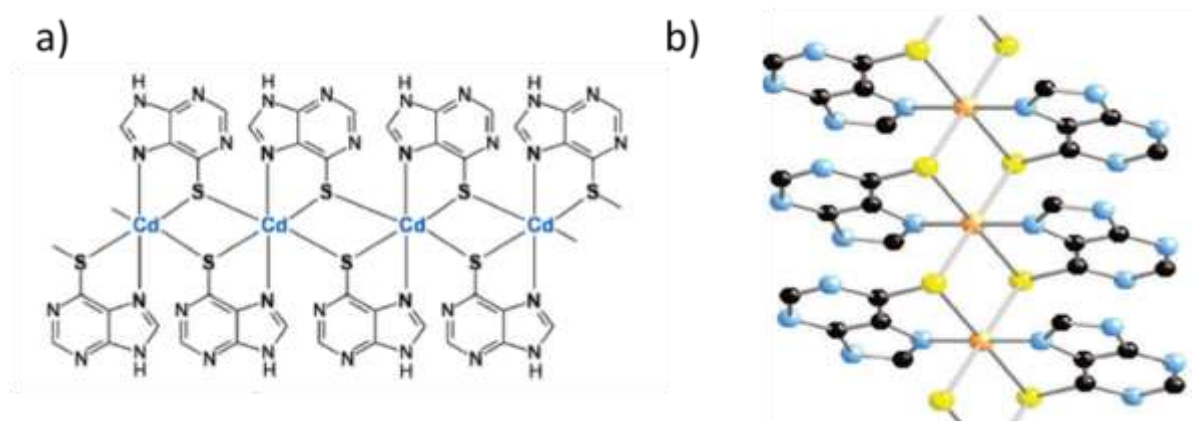


Figure 1.20. Coordination polymers based on the interaction between a metal ion and a thio-modified nucleobase, a) illustrates the crystal structure of a coordination polymer based on Cd(II) and 6-mercaptapurine¹⁶³ and b) Crystal structure of a thiolate coordination polymer based on Ni(II) ions and 6-thioguanine (Ni(II) ions are represented as light brown balls, sulfur atoms as yellow balls and nitrogen atoms as blue balls).¹²⁴

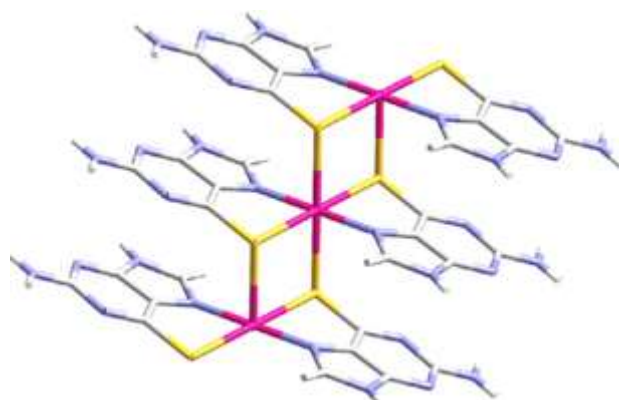


Figure 1.21. A fragment of a coordination polymer crystal based on Co(II) (pink bars) and 6-thioguanine (sulfur atoms in yellow).¹⁶¹

1.5.2. Coinage metal thiolate coordination polymers

1.5.2.1 Cu(I)

Coordination polymers based on coinage metals(I) ions and thiolates ligands have exhibit interesting properties for their use in nano-electronic devices. Due to its promising properties such as electronic and magnetic in the nanoscale field, Cu(I) is a perfect candidate to be integrated into coordination polymers.¹⁶⁴ In general, coordination polymers based on Cu(I) ions and thiolate ligands have exhibited luminescence and electrical properties (Figure 1.22a).^{165,166} There are examples that illustrated this behavior; a complex based on Cu(I) and a aliphatic thiolate has exhibited optical properties due to charge transfer between the metal and ligand,¹⁶⁷ and a coordination polymer based on Cu(I) and methanethiol has been called nanowire due to its conductivity properties at room temperature (Figure 1.22b).¹⁶⁸ Other one-dimensional Cu(I) thiolate polymers based on thiophenol groups have been used as field effect transistors due to their charge mobility properties.¹⁶⁹ The self-interaction between 6-mercaptapurine and Cu(I) lead to the formation of a coordination polymer

where sulfur group is attaching Cu(I) ions along the length of the strand,¹⁷⁰ although this material did not exhibit any semi-conducting properties.^{163,171}

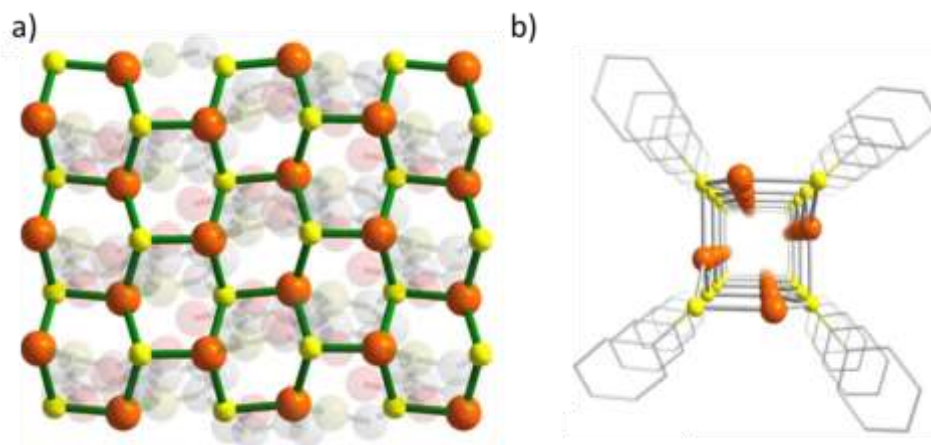


Figure 1.22. Coordination polymers based on Cu(I) thiolates, (a) shows a two-dimensional layered structure for the complex Cu(I) 6-mercaptonicotinate¹⁶⁶ and (b) shows a one-dimensional coordination polymer from a central view of $[\text{Cu}(\text{SPh})]_n$, both highlight Cu(I)-sulfur bonds (Cu(I) ions are orange balls and sulfur atoms yellow balls).¹⁶⁸

1.5.2.2. Ag(I)

The interaction of Ag(I) with sulfur atoms lead to the formation of Ag(I) thiolates with a variety of structures, clusters, nanoparticles or coordination polymers with particular interactions between Ag(I) ions.^{172,173} The polymeric nature of Ag(I) thiolates has sparked interest due to the promising optical properties that they exhibit such as photoluminescence, photothermal or thermochromic effects.^{174,175} Also, the versatility of these compounds to form polymeric structures in one-, two- and three-dimensions, depending on the ligand, has provides to Ag(I) thiolates a structural advantage to utilize them in specific applications like sensing.¹⁷⁶ Some examples illustrated this, lamellar structure of a coordination polymer based on Ag(I) and mercaptopropionic acid has

exhibited tunable optical and photoluminescence properties depending on temperature, that open possibilities to use such polymer in bio-imaging and optoelectronics. (Figure 1.23)¹⁷⁷ Numerous Ag(I) thiolate clusters have also showed adaptable emission properties depending on the anion used in their preparation which suggests that such compounds are useful in applications as fluorophores.¹⁷⁸ In addition, coordination polymers based on aromatic ligands and Ag(I), possess potential use as light-emitting diodes (LEDs).¹⁷⁹

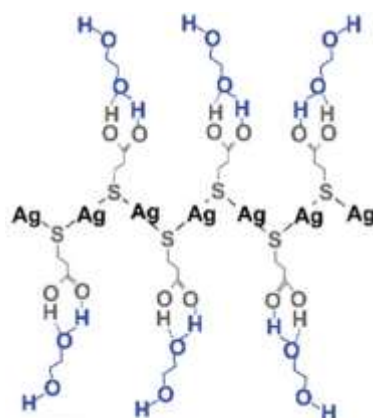


Figure 1.23. One-dimensional scheme for an Ag(I) thiolate coordination polymer based on mercaptopropionic acid as a ligand.¹⁷⁷

1.5.2.3. Au(I)

The linear coordination of Au(I) ions with sulfur atoms of a ligand forms a coordination polymer with interesting properties similar to metal sulfides compounds and exhibit photoluminescence and electrical conductivity.^{140,180} In these coordination polymers, Au(I) atoms usually exhibit a particular characteristic, the presence of aurophilic interactions due to relativistic effects which improves the stability of Au(I) thiolate coordination polymers.¹⁸¹ A one dimensional Au(I) thiolate coordination polymer based on a thiophenol ligand has exhibited phosphorescence properties due to charge transfer between metal and ligand and a long lifetime of excited states (Figure 1.24).¹⁸²

A lamellar two-dimensional coordination polymer based on Au(I) and a thiophenol derivative ligand has showed photoluminescence properties but also thermochromism so it suggests that this polymer could be used sensing application.^{180,183} Another coordination polymer based on a transition metal and a thio-derivative nucleoside has been reported, the interaction between Au(I) and 6-thioguanosine. The description of the structure of this compound is similar to above compound where the Au(I) ions are self-coordinating two sulfur atoms forming a one-dimensional coordination polymer with Au(I)-sulfur backbone. This material has showed characteristic properties of semiconductor compounds such as luminescence or conductance under oxidative doping conditions. In addition, it has been demonstrated that the coordination polymer motifs can be integrated to oligonucleotides. So then, it has confirmed the possibility of functionalized DNA through the coordination polymer route.¹⁴⁰

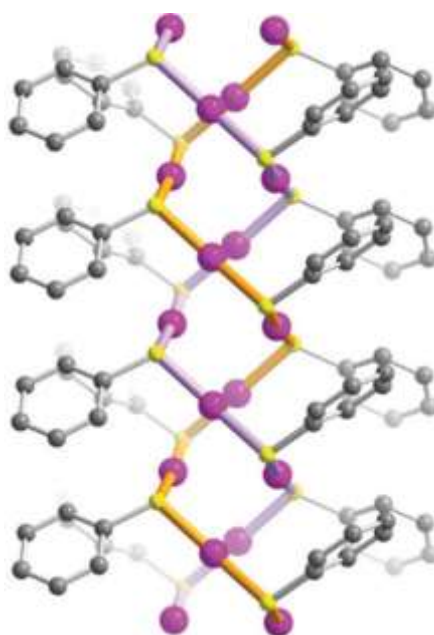


Figure 1.24. Crystal structure of a helical thiolate coordination polymer based on Au(I) and thiophenolate (Au(I) ions are purple balls and sulfur atoms are yellow balls).¹⁸²

1.5.3. Hydrogels

Apart from opto-electronics properties, coinage metals can also display interesting properties as hydrogels when they interact with thiolate compounds. This is the case of an Au(I) glutathione supramolecular hydrogel that will be analyzed in chapter 5.¹⁸⁴

In general, a hydrogel is a three-dimensional network formed by microscopic blocks that crosslink, chemical or physically, to sustain the structure, holding water molecules within it.¹⁸⁵ Physically hydrogels are neither liquid nor solid although they have features of both, diffusion but not flowing, similar to human tissues. Because of that and their biocompatibility, they have found application in medical fields such as drug delivery or tissue engineering.^{186,187}

Although there are several gels classifications depending on the type of solvent or state of the gel, in this introduction we will always refer to hydrogels as gels prepared under water solvent. Xerogel form is described as dry gel at room temperature and its preparation will be showed in chapter 5.¹⁸⁸

There are two types of hydrogels and they both differ in the way that the gel is built. Those in which the hydrogel network is maintained by covalent crosslink of its molecules is called chemical gels (Figure 1.25a). Conversely, when the hydrogel structure is held by non-covalent crosslink of their components it is called a physical gel (Figure 1.25b).¹⁸⁹ Common non-covalent interactions include hydrogen bonds, π - π base stacking, hydrophobic effects or metallophilic interactions.¹⁸⁹ The interactions within the hydrogels are crucial to evaluate the resistance capacity of the network to maintain its structure after a force applied to them and it can be tested under rheology. Therefore, in chemical gels once the network is broken there are no possibilities of recovering its original shape.¹⁸⁷ In opposite, physical gels possess self-healing

reversible properties after undergoing under a specific strain so, although the hydrogel can suffer an alteration in its structure it is not losing its internal ordering.¹⁹¹

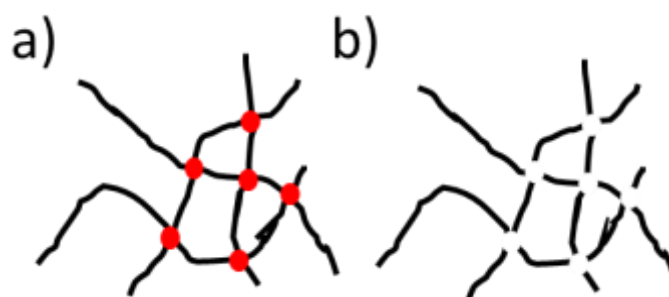


Figure 1.25. Scheme of a hydrogel structure differentiating between a) chemical gels with covalent bonds in its structure indicate by red dots and b) physical gels without covalent bond in its network. Black lines are polymers that forms the gel.

As part of physical gels, we can find supramolecular gels. They are defined as a network composed by a variety of building block linked through non-covalent interactions. Specifically, these building blocks are molecules or complexes with molecular weight less than 3000 Da, they are considered low molecular weight gelators.¹⁹² These supramolecular gels are based on the self-assembly interactions between the components of hydrogels allowing reversibility properties due to the soft nature these non-covalent interactions.¹⁸⁶

Generally, the formation of supramolecular gels networks starts with a one-dimensional polymer formed by building block molecules (Figure 1.26). These polymers can assemble by non-covalent interactions to form complexes structures like fibres or bundles of aggregates. Finally, they can form laminar or fibrillar three-dimensional structures by the entanglement of such nano-fibres.^{193,194} Besides, reversible properties of supramolecular gels provide the capacity to control the morphology of the networks altering the preparation and molecules used^{192,195} which

open a wide window of applications for these compounds in opto-electronic, lubricants or three-dimensional printing.¹⁹⁵⁻¹⁹⁸

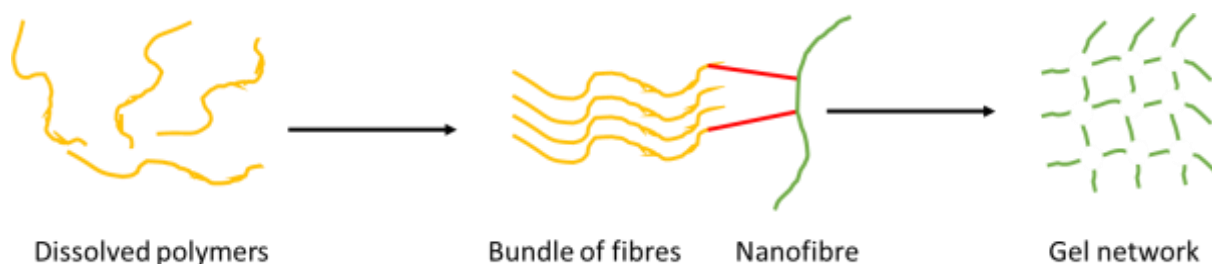


Figure 1.26. Scheme of a supramolecular gel formation. Firstly, polymers (yellow lines) are dissolved in a water medium until they interact through non-covalent interactions forming nanofibers (green lines). These nanofibers self-assemble bundling together to form the gel network.

To build supramolecular hydrogels is essential to find molecules with recognition capacity to allow interaction between them and therefore self-assemble into extended three-dimensional networks. In that sense, nucleobases, nucleosides and nucleic acids have been used because of their capacity to form specific hydrogen bonds or π -stacking between the bases.^{199,200} The interaction between a thio-derivative nucleobase, 6-thioguanosine, with coinage metals have resulted in the formation of a hydrogel that will be examined in chapter 5.

1.6. Conclusions

The increase of interest in nanoelectronics in industry has led to search for materials with specific properties, this chapter has presented a possible combination between DNA and coordination polymers as promising molecules for nanotechnological applications. Although different approaches have been used to functionalize DNA, the preparation of coordination polymers with coinage metals and thio-derivatives

nucleosides provides particular properties to the complex, similar to metal sulfides compounds well-known semiconductor materials. In addition, certain coordination polymers form hydrogels which provides to the final complex with interesting structural properties.

Therefore, this thesis will focus on the preparation of coordination polymers based on coinage metals, Ag(I) and Cu(I) fundamentally, with a sulfur derivative from guanosine, 6-thioguanosine. Besides, the scope of the study will expand with the preparation of coordination polymers based on Ag(I) and Cu(I) and the preparation of a nanowire-based gas sensor based on these materials will be evaluated. Finally, the reaction of a thio-modified nucleobase, 4-thiouridine, with coinage metal(I) ions will be evaluated.

1.7. References

- 1- Junk, A., Riess, F., *Am. J. of Phys.* 2006, **74**, 825.
- 2- Baig, N., Kammakam, I., Falath, W., *Mater. Adv.* 2021, **2**, 1821-1871.
- 3- Narain, R., (ed.) 2020, *Polymer Science and Nanotechnology, Fundamentals and Applications*, ch. 18, 435-453, Elsevier.
- 4- Liu, Y., Mai, S., Li, N., Yiu, C., Mao, J., Pashley, D., Tay, F., *Acta Biomaterialia* 2011, **7**, 1742-1751.
- 5- Rose, A., *Nutrients* 2019, **11**, 2623.
- 6- Neidle, S., (ed.) 2008, *Principles of Nucleic Acid Structure*, ch. 2, 20-37, Academic Press.
- 7- Seeman, N., Sleiman, H., *Nat. Rev. Mat.* 2018, **3**, 17068.
- 8- Erben, C., Goodman, R., Tuberfield, A., *Angew. Chem. Int. Ed.* 2006, **45**, 7414-7417.
- 9- Winegar, P., Hayes, O., McMillan, J., Figg, A., Focia, P., Mirkin, C., *Chem* 2020, **6**, 1007-1017.
- 10- Salah, K., Ansari, A., Alrokayan, S., *J. of Biomedicine and Biotechnology* 2010, **2010**, 715295.
- 11- Liu, S., Clever, G., Takezawa, Y., Kaneko, M., Tanaka, K., Guo, X., Shionoya, M., *Angew. Chem.* 2011, **123**, 9048-9052.
- 12- Barrois, S., Wagenknecht, H., *Beilstein J. Org. Chem.* 2012, **8**, 905-914.
- 13- Tanaka, K., Shionoya, M., *Coord. Chem. Rev.* 2007, **251**, 2732-2742.
- 14- Samanta, P., Pati, S., *Chem. A Eur. J.* 2014, **20**, 1760-1764.

- 15- Metcalfe, C., Thomas, J., *Chem. Soc. Rev.* 2003, **32**, 215-224.
- 16- Alberts, B., Johnson, A., Lewis, J., Raff, M., Roberts, K., Walter, P., 2002, *Molecular Biology of the Cell*, 4th ed, Garland Science, New York.
- 17- Travers, A., Muskhelishvili, G., *The FEBS Journal* 2015, **282**, 2279-2295.
- 18- Watson, J., Crick, F., *Nature* 1953, **171**, 737-738.
- 19- Sinden, R., Pearson, C., Potaman, V., Ussery, D., *Adv. in Genome Biology* 1998, **5**, 1-141.
- 20- Minchin, S., Lodge, J., *Essays in Biochemistry* 2019, **63**, 433-456.
- 21- Takahashi, S., Sugimoto, N., *Acc. Chem. Res.* 2021, **54**, 2110-2120.
- 22- Wing, R., Drew, H., Takano, T., Broka, C., Tanaka, S., Itakura, K., Dickerson, R., *Nature* 1980, **287**, 755-758.
- 23- Arnott, S., *Trends in Biochemical Sciences* 2006, **31**, 349-354.
- 24- Rich, A., *Nature Structural & Molecular Biology* 2003, **10**, 247-249.
- 25- Nelson, D., Cox, M., 2008, *Lehninger Principles of Biochemistry*, 5th ed., ch. 8, Freeman, New York.
- 26- Hao, M., Qiao, J., Qi, H., *Genes* 2020, **11**, 116.
- 27- Wan, W., Li, L., Xu, Q., Wang, Z., Yao, Y., Wang, R., Zhang, J., Liu, H., Gao, X., Hong, J., *Nucleic Acids Research* 2014, **42**, e102.
- 28- Hughes, R., Ellington, A., *Cold Spring Harb. Perspect. Biol.* 2017, **9**, a023812.
- 29- Nummelin, S., Kommeri, J., Kostianen, M., Linko, V., *Adv. Mat.* 2018, **30**, 1870175.
- 30- Aldaye, F., Palmer, A., Sleiman, H., *Science* 2008, **321**, 1795-1799.
- 31- Dietz, H., Douglas, S., Shih, W., *Science* 2009, **325**, 725-730.
- 32- Castro, C., Kilchherr, F., Kim, D., Shiao, E., Wauer, T., Wortmann, P., Bathe, M., Dietz, H., *Nat. Meth.* 2011, **8**, 221-229.
- 33- Seeman, N., *Angew. Chem. Int. Ed.* 1998, **37**, 3220-3238.
- 34- Clever, G., Kaul, C., Carell, T., *Angew. Chem. Int. Ed.* 2007, **46**, 6226-6236.
- 35- Rothmund, P., *Nature* 2006, **440**, 297-302.
- 36- Nangreave, J., Han, D., Liu, Y., Yan, H., *Current Opinion in Chemical Biology* 2010, **14**, 608-615.
- 37- Jones, M., Seeman, N., Mirkin, C., *Science* 2015, **347**, 1260901.
- 38- Park, S., Lytton, A., Lee, B., Weigand, S., Schatz, G., Mirkin, C., *Nature* 2008, **451**, 553-556.
- 39- Simmons, C., Zhan, F., Biktoft, J., Qi, X., Han, D., Liu, Y., Sha, R., Abdallah, H., Hernandez, C., Ohayon, Y., Seeman, N., Yan, H., *J. Am. Chem. Soc.* 2016, **138**, 10047-10054.
- 40- Heckel, A., Famulok, M., *Biochimie* 2008, **90**, 1096-1107.

- 41- Aldaye, F., Lo, P., Karam, P., McLaughlin, C., Cosa, G., Sleiman, H., *Nat. Nanotech.* 2009, **4**, 349-352.
- 42- Niemeyer, C., *Angew. Chem. Int. Ed.* 2001, **40**, 4128-4158.
- 43- Nguyen, T., Brewer, A., Stulz, E., *Angew. Chem. Int. Ed.* 2009, **48**, 1974-1977.
- 44- Seelan, F., He, Y., *J. Org. Chem.* 2003, **68**, 367-377.
- 45- Brenner, S., *Acc. Chem. Res.* 2004, **37**, 784-797.
- 46- Macfarlane, R., Lee, B., Jones, M., Harris, N., Schatz, G., Mirkin, C., *Science* 2011, **334**, 204-208.
- 47- Senesi, A., Eichelsdoerfer, D., Macfarlane, R., Jones, M., Auyeung, E., Lee, B., Mirkin, C., *Angew. Chem. Int. Ed.* 2013, **52**, 6624-6628.
- 48- Kuzuya, A., Ohya, Y., *Polymer Journal* 2012, **44**, 452-460.
- 49- Varshavskii, M., Ikonnikov, E., Tolstyko, E., Belykh, R., Sokolov, P., Bakulev, V., Rolich, V., Lopatko, K., *Journal of Nanomaterials* 2016, **2016**, 3237250.
- 50- Nicolson, F., Ali, A., Kircher, M, Pal, S., *Adv. Sci.* 2020, **7**, 2001669.
- 51- Balleste, R., Castillo, O., Sanz, P., Olea, D., Gomez, J., Zamora, F., *EurJIC* 2009, **2009**, 2885-2896.
- 52- Liu, S., Clever, G., Takezawa, Y., Kaneko, M., Tanaka, K., Xuefeng, G., Shionoya, M., *Angew. Chem. Int. Ed.* 2011, **50**, 8886-8890.
- 53- Braun, E., Eichen, Y., Sivan, U., Ben, G., *Nature* 1998, **391**, 775-778.
- 54- Keren, K., Berman, R., Braun, E., *Nano Letters* 2004, **4**, 323-326.
- 55- Watson, S., Wright, N., Horrocks, B. R., Houlton, A., *Langmuir* 2010, **26**, 2068-2075.
- 56- Mertig, M., Ciacchi, L., Seidel, R., Pompe, W., De Vita, A., *Nano Letters* 2002, **2**, 841-844.
- 57- Mohamed, H., Watson, S., Horrocks, B. R., Houlton, A., *Nanoscale* 2012, **4**, 5936-5945.
- 58- Pate, J., Zamora, F., Watson, S., Wright, N., Horrocks, B. R., Houlton, A., *J. Mater. Chem. C* 2014, **2**, 9265-9273.
- 59- Watson, S., Pike, A., Pate, J., Houlton, A., Horrocks, B. R., *Nanoscale* 2014, **6**, 4027-4037.
- 60- Helmi, S., Ziegler, C., Kauert, D., Seidel, R., *Nano Letters* 2014, **14**, 6693-6698.
- 61- Bayrak, T., Jagtap, N., Erbe, A., *Int. J. Mol. Sci.* 2018, **19**, 3019.
- 62- Ma, N., Sargent, E., Kelley, S., *J. Mater. Chem.* 2008, **18**, 954-964.
- 63- Kuzyk, A., Jungmann, R., Acuna, G., Liu, N., *ACS Photonics* 2018, **5**, 1151-1163.
- 64- Lippert, B., *JBIC J. Biol. Inorg. Chem.* 2022, **27**, 215-219.
- 65- Takezawa, Y., Shionoya, M., *Acc. Chem. Res.* 2012, **45**, 2066-2076.
- 66- Zhou, W., Saran, R., Liu, J., *Chem. Rev.* 2017, **117**, 8272-8325.

- 67- Alderden, R., Hall, M., Hambley, T., *J. Chem. Educ.* 2006, **83**, 728.
- 68- Watson, S., Mohamed, H., Horrocks, B. R., Houlton, A., *Nanoscale* 2013, **5**, 5349-5359.
- 69- Yuan, Z., Chen, Y., Li, H., Chang, H., *Chem. Commun.* 2014, **50**, 9800-9815.
- 70- Wettig, S., Wood, D., Lee, J., *Journal of Inorganic Biochemistry* 2003, **94**, 94-99.
- 71- Atwood, J., (ed.), 2017, *Comprehensive Supramolecular Chemistry II*, 259-263, Elsevier.
- 72- Egli, M., *Chemistry & Biology* 2002, **9**, 277-286.
- 73- Clever, G., Shionoya, M., *Coord. Chem. Rev.* 2010, **254**, 2391-2402.
- 74- Ono, A., Torigoe, H., Tanaka, Y., Okamoto, I., *Chem. Soc. Rev.* 2011, **40**, 5855-5866.
- 75- Kondo, J., Sagawara, T., Saneyoshi, H., Ono, A., *Chem. Commun.* 2017, **53**, 11747-11750.
- 76- Santamaria, N., Mendez, J., Salas, J., Galindo, M., *Angew. Chem. Int. Ed.* 2016, **55**, 6170-6174.
- 77- Megger, D., Fonseca, C., Hoffmann, J., Brutschy, B., Bickelhaupt, M., Muller, J., *Chem. A Eur. J.* 2011, **17**, 6533-6544.
- 78- Kentaro, T., Shionoya, M., *Chemistry Letters* 2006, **35**, 694-699.
- 79- Kondo, J., Tada, Y., Dairaku, T., Hattori, Y., Saneyoshi, H., Ono, A., Tanaka, Y., *Nat. Chem.* 2017, **9**, 956-960.
- 80- Katz, S., *Biochim. Biophys. Acta* 1963, **68**, 240-253.
- 81- Lee, J., Latimer, L., Reid, R., *Biochem. Cell Biol.* 1993, **71**, 162-168.
- 82- Switzer, C., Shin, D., *Chem. Commun.* 2005, 1342-1344.
- 83- Zhang, L., Meggers, E., *J. Am. Chem. Soc.* 2005, **127**, 74-75.
- 84- Eichhorn, G., Shin, Y., *J. Am. Chem. Soc.* 1968, **90**, 7323-7328.
- 85- Pages, B., Ang, D., Wright, E., Aldrich, J., *Dalton Trans.* 2015, **44**, 3505-3526.
- 86- Farrell, N., 1989, *Transition Metal Complexes as Drugs and Chemotherapeutic Agents*, ch. 1, Kluwer Academic.
- 87- Izatt, R., Christensen, J., Rytting, H., *Chem. Rev.* 1971, **71**, 439-481.
- 88- Liu, X., Wu, Z., Zhang, Q., Zhao, W., Zong, C., Gai, H., *Anal. Chem.* 2016, **88**, 2119-2124.
- 89- Taherpour, S., Golubev, O., Lonnberg, T., *Inorg. Chim. Acta* 2016, **452**, 43-49.
- 90- Jash, B., Muller, J., *Chem. A Eur. J.* 2017, **23**, 17166-17178.
- 91- Tanaka, K., Tengeiji, A., Kato, T., Toyama, N., Shionoya, M., *Science* 2003, **299**, 1212-1213.
- 92- Gong, H., Li, X., *Analyst* 2011, **136**, 2242-2246.

- 93- Aich, P., Labiuk, S., Tari, L., Delbaere, L., Roesler, W., Falk, K., Steer, R., Lee, J., *J. of Mol. Biol.* 1999, **294**, 477-485.
- 94- Liu, B., Bard, A., Li, C., Kraatz, H., *J. Phys. Chem. B* 2005, **109**, 5193-5198.
- 95- Endres, R., Cox, D., Singh, R., *Rev. Mod. Phys.* 2004, **76**, 195-214.
- 96- Kumar, N., Wilkinson, E., Kumar, S., Bailey, L., Vilan, A., Zhang, Z., Qi, D., Tadich, A., Tuite, E., Pike, A., Tucker, J., Nijhuis, C., *J. Am. Chem. Soc.* 2021, **143**, 20309-20319.
- 97- Müller, J., *Nature* 2006, **444**, 698.
- 98- Mistry, L., El-Zubir, O., Dura, G., Clegg, W., Waddell, P., Pope, T., Hofer, W., Wright, N., Horrocks, B. R., Houlton, A., *Chem. Sci.* 2019, **10**, 3186-3195.
- 99- Linares, F., Garcia, E., Lopez, F., Domingo, M., Orte, A., Rodriguez, A., Galindo, M., *Chem. Sci.* 2019, **10**, 1126-1137.
- 100- Pandian, S., Yuan, C., Lin, C., Wang, W., Chang, C., *Advances in Physics: X* 2017, **2**, 22-34.
- 101- Lippert, B., *Coord. Chem. Rev.* 2000, **200-202**, 487-516.
- 102- Abd, A., Strohm, E., *Polymer* 2012, **53**, 4879-4921.
- 103- Xie, J., Wang, L., Anderson, J., *Chem. Sci.* 2020, **11**, 8350-8372.
- 104- Garcia, A., Zabala, A., Ramirez, G., Delgado, J., Fernandez, B., Cepeda, J., Rodriguez, A., *CrystEngComm* 2020, **22**, 5086-8095.
- 105- Amo, P., Castillo, O., Alexander, S., Welte, L., de Pablo, P., Rodriguez, I., Gomez, J., Zamora, F., *Inorg. Chem.* 2009, **48**, 7931-7936.
- 106- Dalai, S., *Journal of Physical Science* 2011, **15**, 223-230.
- 107- Batten, S., Champness, N., Chen, X., Garcia, J., Kitagawa, S., Ohrstrom, L., O'Keefe, M., Paik, M., Reedijk, J., *CrystEngComm* 2012, **14**, 3001-3004.
- 108- LoPachin, R., Gavin, T., DeCaprio, A., Barber, D., *Chem. Res. Toxicol.* 2012, **25** (2), 239-251.
- 109- Chattaraj, P., Lee, H., Parr, R., *J. Am. Chem. Soc.* 1991, **113**, 1855-1856.
- 110- Du, M., Li, C., Liu, C., Fang, S., *Coord. Chem. Rev.* 2013, **257**, 1282-1305.
- 111- Chen, C., Suslick, K., *Coord. Chem. Rev.* 1993, **128**, 293-322.
- 112- Janiak, C., *Dalton Trans.* 2003, 2781-2804.
- 113- Kitagawa, S., Kondo, M., *Bull. Chem. Soc. Jpn.* 1998, **71**, 1739-1753.
- 114- Zhang, J., Zhou, Y., Yao, Y., Chen, Z., Gao, T., Li, H., Yan, P., *J. Mater. Chem. C.* 2020, **8**, 6788-6796.
- 115- Saalfrank, R., Maid, H., Hampel, F., Peters, K., *EurJIC* 1999, **1999**, 1859-1867.
- 116- Wu, B., Zhang, W., Yu, S., Wu, X., *J. Chem. Soc., Dalton Trans.* 1997, 1795-1796.
- 117- Andres, R., Gruselle, M., Malezieux, B., Verdaguer, M., Vaissermann, J., *Inorg. Chem.* 1999, **38**, 4637-4646.

- 118- Dong, Y., Jin, G., Smith, M., Huang, R., Tang, B., Loye, H., *Inorg. Chem.* 2002, **41**, 4909-4914.
- 119- Seward, C., Hu, N., Wang, S., *J. Chem. Soc., Dalton Trans.* 2001, 134-137.
- 120- Real, J., Gaspar, A., Niel, V., Muñoz, C., *Coord. Chem. Rev.* 2003, **236**, 121-141.
- 121- Mathoniere, C., Nuttall, C., Carling, S., Day, P., *Inorg. Chem.* 1996, **35**, 1201-1206.
- 122- Kahn, O., *Adv. in Inorg. Chem.* 1995, **43**, 179-259.
- 123- Carne, A., Carbonell, C., Imaz, I., MasPOCH, D., *Chem. Soc. Rev.* 2011, **40**, 291-305.
- 124- Givaja, G., Amo, P., Gomez, C., Zamora, F., *Chem. Soc. Rev.* 2012, **41**, 115-147.
- 125- Kelly, M., 1995, *Low-Dimensional Semiconductors*, Clarendon, Oxford.
- 126- Batten, S., Murray, K., *Coord. Chem. Rev.* 2003, **246**, 103-130.
- 127- Amo, P., Zamora, F., *Coord. Chem. Rev.* 2014, **276**, 34-58.
- 128- Yokoyama, M., *Synthesis* 2000, **12**, 1637-1655.
- 129- Ajitkumar, P., Cherayil, J., *Microbiol. Rev.* 1988, **52**, 103-113.
- 130- Gaynor, J., Bentley, J., Cosstick, R., *Nat. Protoc.* 2007, **2**, 3122-3125.
- 131- Gladysz, M., Andralojc, W., Czapik, T., Gdaniec, Z., Kierzek, R., *Scientific Reports* 2019, **9**, 4385.
- 132- Christopherson, M., Broom, A., *Nucleic Acids Research* 1991, **19**, 5719-5724.
- 133- Xu, Y., Zheng, Q., Swann, P., *Tetrahedron* 1992, **48** (9), 1729-1740.
- 134- Onizuka, K., Taniguchi, Y., Sasaki, S., *Nucleos., Nucleot. & Nucleic Acids* 2009, **28**, 752-760.
- 135- Christopherson, M., Broom, A., *Nucleos., Nucleot. & Nucleic Acids* 1994, **13**, 351-368.
- 136- Lunn, S., Hribesh, S., Whitfield, C., Hall, M., Houlton, A., Bronowska, A., Tuite, E., Pike, A., *ChemBioChem* 2018, **19**, 1115-1118.
- 137- Testa, S., Disney, M., Turner, D., Kierzek, R., *Biochemistry* 1999, **38**, 16655-16662.
- 138- Held, H., Roychowdhury, A., Brenner, S., *Nucleos., Nucleot. & Nucleic Acids* 2003, **22**, 391-404.
- 139- Oudar, J., *Materials Science and Engineering* 1980, **42**, 101-109.
- 140- Al-Mahamad, L., El-Zubir, O., Smith, D., Horrocks, B. R., Houlton, A., *Nat. Commun.* 2017, **8**, 720.
- 141- Heitner, H., Lippard, S., Sunshine, H., *J. Am. Chem. Soc.* 1972, **94**, 8936-8937.
- 142- Hadjiliadis, N., Sletten, E., (ed.), 2009, *Metal Complex-DNA Interactions*, ch. 4, 95-132, Blackwell.

- 143- Mohamed, A., Watson, S., Horrocks, B. R., Houlton, A., *J. Mater. Chem. C* 2015, **3**, 438-446.
- 144- Kowalik, T., Varnagy, K., Swiatek, J., Jon, A., Sovago, I., Sochacka, E., Malkiewicz, A., Spychata, J., Koztowski, H., *J. of Inorg. Biochem.* 1997, **65**, 257-262.
- 145- Mirkin, C., Letsinger, R., Mucic, R., Storhoff, J., *Nature* 1996, **382**, 607-609.
- 146- Sun, D., Gang, O., *J. Am. Chem. Soc.* 2011, **133**, 5252-5254.
- 147- Young, K., Ross, M., Blaber, M., Rycenga, M., Jones, M., Zhang, C., Senesi, A., Lee, B., Schatz, G., Mirkin, C., *Adv. Mat.* 2014, **26**, 653-659.
- 148- Macfarlane, R., Jones, M., Lee, B., Auyeung, E., Mirkin, C., *Science* 2013, **341**, 1222-1225.
- 149- Radha, B., Senesi, A., O'Brien, M., Wang, M., Auyeung, E., Lee, B., Mirkin, C., *Nano Letters* 2014, **14**, 2162-2167.
- 150- Takezawa, Y., Tanaka, K., Yori, M., Tashiro, S., Shiro, M., Shionoya, M., *J. Org. Chem.* 2008, **73**, 6092-6098.
- 151- Kamakura, Y., Tanaka, D., *Chemistry Letters* 2021, **50**, 523-533.
- 152- Paca, A., Ajibade, P., *Int. J. Mol. Sci.* 2021, **22**, 12294.
- 153- Toe, C., Zhou, S., Gunawan, M., Lu, X., Ng, Y., Amal, R., *J. Mater. Chem. A* 2021, **9**, 20277-20319.
- 154- Weber, T., Prins, R., Santen, R., (ed.), 1998, *Transition Metal Sulphides*, Springer, Dordrecht.
- 155- Chandrasekaran, S., Yao, L., Deng, L., Bowen, C., Zhang, Y., Chen, S., Lin, Z., Peng, F., Zhang, P., *Chem. Soc. Rev.* 2019, **48**, 4178-4280.
- 156- Li, T., Lee, Y., Teng, H., *J. Mater. Chem.* 2011, **21**, 5089-5098.
- 157- Lai, C., Lu, M., Chen, L., *J. Mater. Chem.* 2012, **22**, 19-30.
- 158- Lu, M., Lu, M., Chung, Y., Chen, M., Wang, Z., Chen, L., *J. Phys. Chem. C* 2009, **113**, 12878-12882.
- 159- Lai, C., Huang, K., Chen, J., Lee, C., Hwang, B., Chen, L., *J. Mater. Chem.* 2010, **20**, 6638-6645.
- 160- Xu, X., Liu, W., Kim, Y., Cho, J., *Nanotoday* 2014, **9**, 604-630.
- 161- Amo, P., Alexandre, S., Hribesh, S., Galindo, M., Castillo, O., Gomez, C., Pike, A., Soler, J., Houlton, A., Zamora, F., *Inorg. Chem.* 2013, **52**, 5290-5299.
- 162- Amo, P., Castillo, O., Gomez, C., Hassanein, K., Verma, S., Kumar, J., Zamora, F., *Inorg. Chem.* 2013, **52**, 11428-11437.
- 163- Amo, P., Rodriguez, I., Castillo, O., Olea, D., Guijarro, A., Alexandre, S., Gomez, J., Zamora, F., *Inorg. Chem.* 2006, **45**, 7642-7650.
- 164- Hassanein, K., Cappuccino, C., Amo, P., Lopez, J., Maini, L., Bandini, E., Ventura, B., *Dalton Trans.* 2020, **49**, 10545-10553.
- 165- Veselska, O., Podbevsek, D., Ledoux, G., Fateeva, A., Demessence, A., *Chem. Commun.* 2017, **53**, 12225-12228.

- 166- Pathak, A., Shen, J., Usman, M., Wei, L., Mendiratta, S., Chan, Y., Sainbileg, B., Ngue, C., Chen, R., Hayashi, M., Luo, T., Chen, F., Chen, K., Tseng, T., Chen, L., Lu, K., *Nat. Commun.* 2019, **10**, 1721.
- 167- Fujisawa, K., Imai, S., Kitajima, N., Moro-oka, Y., *Inorg. Chem.* 1998, **37**, 168-169.
- 168- Veselska, O., Demessence, A., *Coord. Chem. Rev.* 2018, **355**, 240-270.
- 169- Che, C., Li, C., Chui, S., Roy, V., Low, K., *Chem. A Eur. J.*, 2008, **14**, 2965-2975.
- 170- Dubler, E., Gyr, E., *Inorg. Chem.* 1988, **27**, 1466-1473.
- 171- Zamora, F., Amo, P., Sanz, P., Castillo, O., *Inorg. Chimica Acta* 2009, **362**, 691-706.
- 172- Jin, R., Zeng, C., Zhou, M., Chen, Y., *Chem. Rev.* 2016, **116**, 10346-10413.
- 173- Krebs, B., Henkel, G., *Angew. Chem. Int. Ed.* 1991, **30**, 769-788.
- 174- Yam, V., Au, V., Leung, S., *Chem. Rev.* 2015, **115**, 7589-7728.
- 175- Veselska, O., Dessal, C., Melizi, S., Guillou, N., Podbevsek, D., Ledoux, G., Elkaim, E., Fateeva, A., Demessence, A., *Inorg. Chem.* 2019, **58**, 99-105.
- 176- Wang, Q., Dong, S., Tao, D., Li, Z., Jian, Y., *Coord. Chem. Rev.* 2021, **432**, 213717.
- 177- Wang, J., Graf, R., Riedinger, A., *J. Mater. Chem. C* 2021, **9**, 11079-11084.
- 178- Shen, Y., Jin, J., Duan, G., Yu, P., Xie, Y., Lu, X., *Chem. A Eur. J.* 2021, **27**, 1122-1126.
- 179- Ren, T. Lin, C., Amalberti, P., Macikenas, D., Protasiewicz, J., Baum, J., Gibson, T., *Inorg. Chem. Commun.* 1998, **1**, 23-26.
- 180- Veselska, O., Okhrimenko, L., Guillou, N., Podbevsek, D., Ledoux, G., Dujardin, C., Monge, M., Chevrier, D., Yang, R., Zhang, P., Fateeva, A., Demessence, A., *J. Mater. Chem. C* 2017, **5**, 9843-9848.
- 181- Pyyko, P., *Angew. Chem. Int. Ed.* 2004, **43**, 4412-4456.
- 182- Lavenn, C., Okhrimenko, L., Guillou, N., Monge, M., Ledoux, G., Dujardin, C., Chiriac, R., Fateeva, A., Demessence, A., *J. Mater. Chem. C* 2015, **3**, 4115-4125.
- 183- Lavenn, C., Guillou, N., Monge, M., Podbevsek, D., Ledoux, G., Fateeva, A., Demessence, A., *Chem. Commun.* 2016, **52**, 9063-9066.
- 184- Odriozola, I., Loinaz, I., Pomposo, J., Grande, H., *J. Mater. Chem.* 2007, **17**, 4843-4845.
- 185- Wichterle, O., Lim, D., *Nature* 1960, **185**, 117-118.
- 186- Peters, G., Davis, J., *Chem. Soc. Rev.* 2016, **45**, 3188-3206.
- 187- Ye, J., Fu, S., Zhou, S., Li, M., Li, K., Sun, W., Zhai, Y., *Eur. Polymer J.* 2020, **139**, 110024.
- 188- Livage, J., Henry, M., Sanchez, C., *Progress in Solid State Chemistry* 1988, **18**, 259-341.

- 189- Weiss, R., Terech, P., (ed.), 2006, *Molecular Gels: Materials with self-assembled fibrillar network*, 6th ed., Springer.
- 190- Bhattacharyya, T., Saha, P., Dash, J., *ACS Omega* 2018, **3**, 2230-2241.
- 191- Maity, G., *Journal of Physical Science* 2007, **11**, 156-171.
- 192- Bacani, R., Trindade, F., Politi, M., Triboni, R., (ed.), 2020, *Nano Design for Smart Gels*, ch. 3, 35-69, Elsevier.
- 193- Casuso, P., Carrasco, P., Loinaz, I., Cabañero, G., Grande, H., Odriozola, I., *Soft Matter* 2011, **7**, 3627-3633.
- 194- Demirci, U., Khademhosseini, A., (ed.), 2016, *Gels Handbook*, ch. 9, 219-250.
- 195- Chivers, P., Smith, D., *Nat. Rev. Mat.* 2019, **4**, 463-478.
- 196- Zhong, R., Tan, Q., Wang, S., Zhang, H., Zhang, F., Xiao, M., Man, T., Qi, X., Li, L., Zhang, W., Pei, H., *Adv. Mat.* 2018, **30**, 1706887.
- 197- Sangeetha, N., Maitra, U., *Chem. Soc. Rev.* 2005, **34**, 821-836.
- 198- Terech, P., Weiss, R., *Chem. Rev.* 1997, **97**, 3133-3160.
- 199- Sivakova, S., Rowan, S., *Chem. Soc. Rev.* 2005, **34**, 9-21.
- 200- Araki, K., Yoshikawa, I., *Top. Curr. Chem.* 2005, **256**, 133-165.

Chapter 2. Experimental Techniques

Table of Contents

2.1. Characterization Techniques.....	44
2.1.1. Mass spectroscopy, MALDI-ToF	44
2.1.2. UV-Vis absorption spectroscopy	45
2.1.3. Fourier transform infrared (FTIR) spectroscopy	46
2.1.4. Circular Dichroism spectroscopy (CD).....	47
2.1.5. Luminescence emission spectroscopy	49
2.1.6. Circular polarized luminescence spectroscopy (CPL)	51
2.1.7. Scanning electron microscopy (SEM).....	53
2.1.8. Atomic force microscopy (AFM)	55
2.1.9. Electrical measurements	57
2.1.10. Rheology	58
2.1.11. Nuclear magnetic resonance (NMR)	60
2.2. References	60

2.1. Characterization Techniques

After the preparation of the reaction products, a wide range of techniques were used to characterize them. To obtain structural information of the material prepared, few spectroscopies give important insight in this regard. The techniques used were mass spectroscopy, Uv-Vis absorption spectroscopy, infrared spectroscopy (FTIR), circular dichroism and nuclear magnetic resonance. In addition, the morphology of the samples was analyzed under microscopic techniques, scanning electron microscopy and atomic force microscopy. To measure inherent properties of the materials prepared, luminescence spectroscopy, circular polarized luminescence and conductivity measurements were also performed.

In the following section every technique will be explained and substantiated essentially and the reason for its use will be indicated.

2.1.1. Mass spectroscopy, MALDI-ToF

Matrix-assisted laser desorption/ionization mass spectrometry (MALDI-MS) together with the time-of-flight (ToF) mass analyzer provided information about the elemental composition and isotopic relation of the molecules under study.¹ Specifically, MALDI-ToF has better sensitivity, faster response and high accuracy for molecular weight data than usual ESI mass spectroscopies, and makes it exceptional for the high-resolution detection of the structures of heavy biomolecules or biopolymers of around 500000 Daltons.

Basically, mass spectrometry consists in an ion source that hit the sample forming sample ions. Then, they suffer an acceleration under an electrostatic field, a mass analyzer divides such ions depending on their mass/charge ratio and a detector gives the spectrum indicating ions formed and their quantities. As a characteristic of a MALDI-ToF-MS is the fact that the process of ionization of the sample is initiated by

photons and then the analyzer separates the ions depending on the time they reach the detector (based on the mass/charge relation). It allows to identify different molecules weight associated to the preparation.²

The preparation of the sample commit to dissolve it into an organic matrix in order to decrease sample fragmentation and also to obtain higher intensities.

2.1.2. UV-Vis absorption spectroscopy

The UV-Vis light absorption is characteristic of every molecule and it can be used efficiently for its identification, quantification and characterization through transitions between electronic energy levels.³ Sulfur derivatives from nucleosides absorb UV-Vis light in the range between 200-800 nm due to the nitrogen bases, purines and pyrimidines, and the main component of its absorption are π - π^* electronic transitions.⁴ Also, other groups in nucleoside derivatives such as thiol/thione are responsible for n- π^* transitions, although its contribution to the absorption of the molecule is small.⁵ The interactions of these thio-nucleobases with metals modify the electronic configuration of the original thio-nucleobase and then a change in the spectra is expected.

The UV-Vis technique consists in two separated cuvettes, one for the sample and another for the solvent used in the experiment, exposed to a double equivalent radiation source previously adapted by a monochromator. Then the intensities of each transmitted beams are compared in the detector, amplified and recorded in a spectrum.³

The absorption intensity is based on the Beer-Lambert law (Equation 1), where A is the absorbance, I_0 and I are intensities of the incident and transmitted light respectively, ϵ is the molar extinction coefficient, l the path length of the cuvette and c the concentration.⁶

$$A = \log_{10} \frac{I_0}{I} = \varepsilon \cdot l \cdot c \quad (\text{Eq. 1})$$

Based on this technique, melting temperature experiment consists in the change of intensity of absorbance at a fixed wavelength for a range of temperatures. As a result, a melting curve is obtained and the midpoint of it is called melting temperature (T_m). Generally, this technique is used to measure the denaturalization of DNA strands because of the difference in light absorption of nucleobases in a double helix or in single strands, T_m indicates when the 50% of molecules are forming double helix and 50 % of nucleobases are unstacked. Depending on DNA conformation, the light absorption changes; light absorption decreases for a double helix because the nucleobases are oriented towards the inside of the structure and the opposite for nucleobases that are not stacking, producing a hipo-/hiper-chromicity effect. Therefore, it is possible to determine changes in the structure following intensity changes in absorbance.⁷

2.1.3. Fourier transform infrared (FTIR) spectroscopy

In the infrared area of energy of the electromagnetic spectra, 5000-400 cm^{-1} , are present most of the vibrations of the molecules. These vibrations are represented in the infrared spectrum with energy bands that correspond to energy absorption of different chemical bonds that forms each molecule. Because of that, the study of the spectra produced a detailed information about the structure of the molecules. Our target to study in the molecules will be mainly the carbon-sulfur groups.³

Then, a characterization based on FTIR is related to molecular vibration frequencies. These depends on the mass of atomic groups involved in the interactions and bond force constant according to the equation 2, where c is the speed of light, k the force constant and μ the reduced mass.

$$\bar{\nu} = \frac{1}{2\pi c} \sqrt{\frac{k}{\mu}} \quad (\text{Eq. 2})$$

Associated to high wavenumber vibrations are stretching modes of groups formed by light atoms because deformation or bending modes have low force constant.

For our measurements a Fourier transform infrared spectroscopy (FTIR) has been used. This technique consists in a source of infrared light, a Nernst filament heated electrically until 1000-1800°C, that is divided in two beams, one beam is reflected into a fixed mirror (at 90° from the source) and the other beam to a movable mirror (at 180° from the source) and finally they are recombined and interfered. The solid sample, in the direction of the recombined beam, absorbs the light and the detector record the spectra. The movable mirror allows to change the pathlength and it is reflected in the interferogram. The application of the Fourier transformation (FFT) operation on it changes the time-dependent signal to a spectrum that plots intensity (transmittance or absorbance) against wavenumber.⁸

FTIR spectra was recorded using an attenuated total reflection (ATR) accessory. It allows to measure directly from a solid sample deposited on a crystal because the infrared beam passed through it and the beam is reflected in the sample, it is based on internal reflection. The main advantages of FTIR-ATR technique are the fast speed of the measurement and the high resolution of the spectrum.⁸

2.1.4. Circular Dichroism spectroscopy (CD)

The light is composed by electric and magnetic fields oscillating at right angles to each other and perpendicular to the direction of light propagation (Figure 2.1a). The light can be described as a transverse wave whose polarization is defined by the direction of its electric field. Specifically, a circular polarization of the light happens when the

electric field is constant but traces helices over the direction of propagation, then the electric field vectors form a circle with a particular angle (Figure 2.1b).³

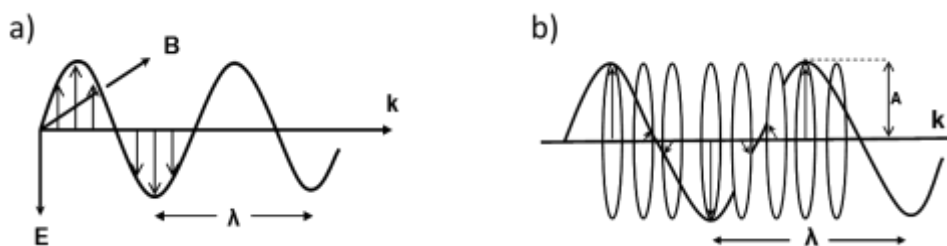


Figure 2.1. Electromagnetic radiation a) linearly and b) circularly polarized (the arrows represent electric field radiation vector). (B is the magnetic field; E is the electric field; A is the amplitude; λ is the wavelength; k is the direction of propagation).

Chiral molecules have different absorption coefficient for right or left circular polarized light at any wavelength. A circular dichroism spectrum is a representation of the difference between absorption coefficient for the right and left circular polarized light versus wavelength. Obviously, for long polymeric structures the intensity of the circular dichroism signal will be large because of the cooperativity of polymeric units.

Circular dichroism is based on the Equation 3:

$$\Delta A = (\epsilon_L - \epsilon_R) \cdot c \cdot l \quad (\text{Eq. 3})$$

ΔA is the difference between absorbance for left and right circularly polarized light, c is the molar concentration and l the pathlength of the cuvette. The unit of CD signal is the degree of ellipticity, θ .

The chirality of nucleosides is due to the ribose that take part in their structure. Although many molecules are not chiral, its interaction with the nucleosides modify its

circular dichroism signal and so the circular dichroism become a useful tool to study such interaction. It is not possible to get any precise information about the structure of the molecule, but it is acceptable the information that this technique displays in order to know approximately the conformation and arrangements of the molecule by comparison with reference molecules.⁷

The circular dichroism spectrometer consists in a light source directed to a polarizer that produces a linear polarized light. After that, a quarter phase plate will produce the circular polarized light that will pass through the sample, it will absorb the light and after that a detector will sense the transmitted light. The spectra represent CD signal versus wavelength.

2.1.5. Luminescence emission spectroscopy

Emission spectroscopy is well-described in the Jablonski diagram. Figure 2.2 shows different processes, absorption, fluorescence and phosphorescence. Luminescence spectroscopy is defined as the study of the emission of radiation, after an absorption, from a higher electronic energy level (S_1 , S_2 , T_1) to a lower electronic energy level (S_0) and it includes fluorescence and phosphorescence processes.³

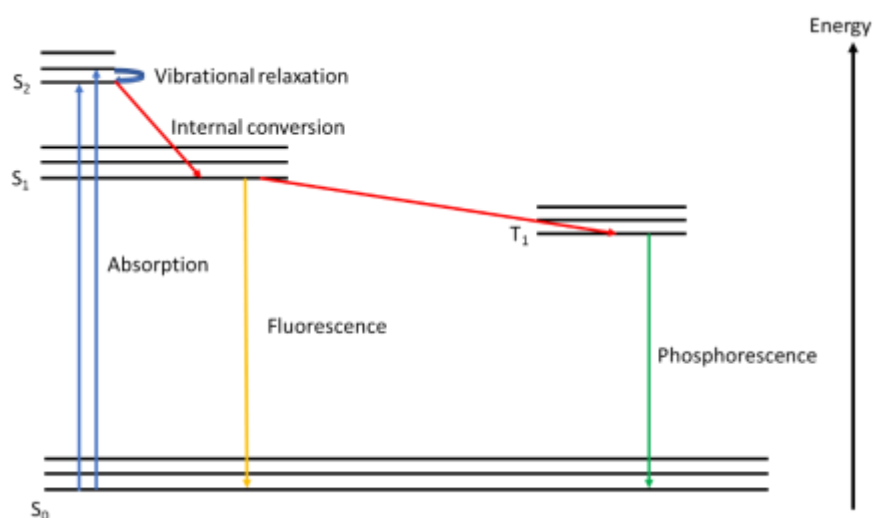


Figure 2.2. Jablonski diagram. This scheme shows different emission processes between the electronic energy level (S₂ and S₁ to S₀). Also, it indicates non-radiative relaxation processes such as vibrational relaxation between vibrational levels of an electronic energy level and internal conversion between two excited electronic energy levels.

After the absorption, a fluorescence process is defined as the emission of the electromagnetic radiation from an excited electronic state to the ground electronic state in approximately 10⁻⁸ s. The energy of the light emitted is lower than the absorption and it could be due to different processes, the molecule loses some of its energy in internal vibrational relaxations; the emission might not go directly to the ground electronic state; very quick internal non-radiative conversion between excited electronic energy levels.⁹

Phosphorescence is another emission process where after the absorption of energy, the electrons cross from the first electronic excited state (S₁) to a triplet state (T₁) and then emit radiation to the lower energy level (S₀) in around 10⁻³s. The fact that a

non-radiative process occurs before the phosphorescence emission, makes its energy emission lower than in the case of fluorescence process.⁹

The emission process is always preceded by an absorption. The energy transitions promoted by the absorption of light for the sulfur derivative nucleosides are mainly due to the nitrogen bases that forms the nucleosides, π - π^* or n - π^* transitions but not the only ones. The interaction of the metal(I) with the sulfur also promotes different distribution of electronic charge in the molecule and therefore different absorption/emission is observed.⁷

Luminescence spectroscopy measure the lifetime, intensity and polarization of the emission processes explained above, so then, changes in the spectrum will indicate changes in the internal structure of the products compared with original reagents. Also, it will be possible to establish potential luminescence properties of the prepared product.

The instrument to measure luminescence properties consists on an energy source, filter and directed to the sample with a particular wavelength. A detector located at 90° from the sample holder allows to measure the light emitted by the sample, avoiding any absorption. Finally, the signal is amplified and recorded on a spectrum of luminescence intensity versus wavelength.⁹

2.1.6. Circular polarized luminescence (CPL)

Related to circular dichroism spectroscopy, circular polarized luminescence (CPL) measures chiral properties of an emission.¹⁰ Similar to spectroscopic techniques, CPL contributes to elucidate structural properties of the molecules providing important insight about excited states. CD and CPL are then complementary techniques based on optical activity, but with some differences as well, CPL is more sensible and selective than CD due to the nature of the emission process which is related to the

excited state of a chiral group.¹¹ Consequently it is possible to elucidate stereochemical structure as well as three-dimensional insight on materials with chiral groups in excited states.¹²

Circular polarized luminescence is based on the difference between the left and right emission of a chiral molecule and such magnitude and the degree of polarization is represented by the emission dissymmetry factor (g_{lum}) (Equation 4):

$$g_{lum} = \frac{2\Delta I}{I} \quad (\text{Eq. 4})$$

ΔI indicates the difference between the left and right emission and I indicates the sum of left and right emission. If g_{lum} is +2 indicates a left CPL emission and it is -2 indicates a right CPL emission.¹⁰ Higher values of g_{lum} are usually associated to lanthanides, Eu(III) ≈ 1.3 ,¹³ and not to organic molecules although attempts have been made on them with the idea of modulate their excited states.¹⁴ Such modulations are usually related to self-assembly processes or modification of their chemical environment.¹⁵

CPL instrumentation consists in an excitation source, a laser that is directed to a monochromator (410 nm). The light hit the sample and at 90° degrees the emission passes through a photo elastic modulator (quarter-wave plate), a linear polarizer and a scanning monochromator. This signal goes to the detector and the amplifier transforms it into a legible signal for the computer. Finally, a CPL versus wavelength and g_{lum} versus wavelength graphs are produced.¹⁰

The well-known chirality of ribose ring connected to possible luminescence properties of the material prepared makes this technique useful to determine the internal electronic structures and examine the chiral properties of excited states of the product prepared.

2.1.7. Scanning electron microscopy (SEM)

Scanning electron microscopy is a technique that provides images of the sample surface by electron-surface interactions. The resolution of the images is always greater than 10 nm, but it is possible to reach 1 nm depending on the characteristics of the instrument.

This technique consists in the penetration of an electron beam in the sample, the range of the energy of the beam is between 0.2 and 40 KeV. After that three processes can happen; some of the electrons in the surface of the sample absorbs the energy of the beam and secondary electrons are expelled by the outer shell of the atoms, then a detector traps those electrons and forms the image of the sample surface, surface features are mainly detected with these electrons (Figure 2.3a); the beam produces backscattered electrons when electrons are reflected after hit atoms of the sample without interactions, these electrons are detected by a back scatter detector (Figure 2.3b); when the beam interact with inner shell electrons producing secondary electrons, a X-ray emission is produced when a higher energy electron fill the shell releasing energy (Figure 2.3c). Specifically, the secondary electron imaging was used for our experiments where the electron beam hit the sample in a particular area to make the picture of the surface.¹⁶

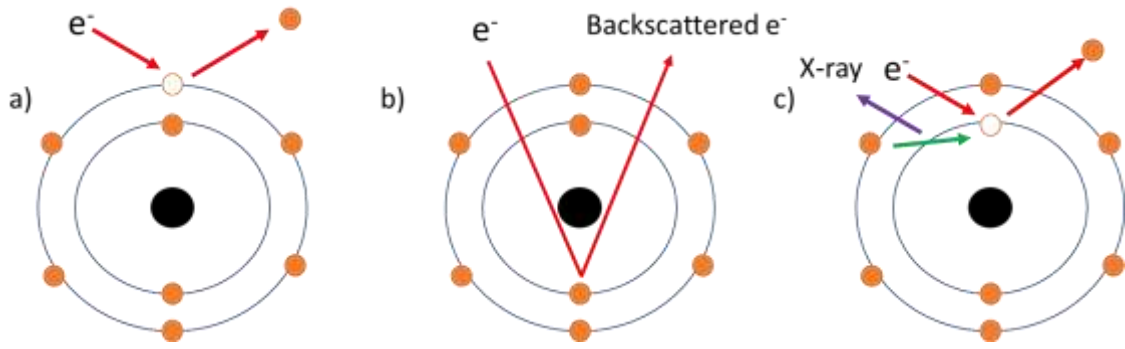


Figure 2.3. Scheme of the interaction between primary electrons with sample surface atoms. a) indicates the impact of primary electron with outer shell electrons from surface atoms emitting secondary electrons; b) indicates the deviation of the electron due to repulsion inside the atom and the emission of backscattered electrons; c) indicates the collision of primary electrons with inner shell electrons and the emission of secondary electrons and x-ray radiation due to the movement of an electron to the inner shell.

SEM instrument consists in an electron gun, source of electrons, that produces a high-speed electron beam that is directed towards the sample by a series of lenses, condenser and objective, in order to make the beam as small as possible to improve the resolution. After the collision of the beam with the sample, there are few processes but, in our case, the secondary electrons are the only detected (Figure 2.4). All the instrument is cover by a vacuum column to avoid the deflection of the electron beam.¹⁶

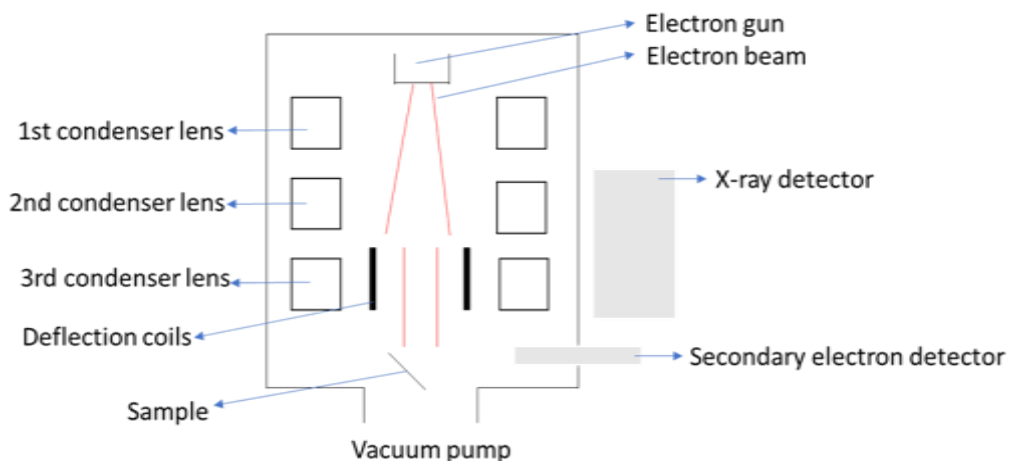


Figure 2.4. Schematic diagram of SEM.

2.1.8. Atomic force microscopy (AFM)

To have an insight of the morphology of the sample the Atomic Force Microscopy (AFM) technique produces one, two or three-dimensional images of the sample surface in the order or nanometer scale at high resolution.

Basically, AFM examines the topography of the surface of a sample with a tip, producing a two-dimensional image at high resolution. AFM follows a similar procedure as scanning probe microscopies. These are the scanning near field optical microscope, or the scanning probe microscopies.

The fundamentals of the technique, based on scanning principles, can be divided in contact or non-contact modes between the sample and the tip. These two types of AFM differ, in the first case the tip is in physical contact with the sample and in the second case the tip oscillates around the sample surface. These operation modes contrast in resolution and in the damage to the sample. All the experiments showed in here were done using a tapping mode which allow to have high resolution when the tip is not in a continuous contact with the sample.¹⁷ In tapping mode the tip is vibrating

during the scan since the contact with the sample surface is intermittent to avoid the maximum damage to the sample.

The instrument consists on a sample holder, in our case magnetic, where the sample is deposited on a mica wafer attached to a magnetic disc. Above the sample is the tip, made of silicon or silicon nitride usually and with a radius of curvature of few nanometers approximately, attached to the cantilever as a probe and an incident laser beam. The cantilever is propped by a holder with a piezoelectric piece that acts as an elevator to adjust the distance between the sample surface and the tip. Once the tip 'feel' the surface of the sample a deflection in the cantilever (in accordance to Hooke's law) change the laser beam and it is reflected in the detector (photodiode). Hooke's law is defined in equation 5, where x represents the lateral and vertical deflection of the cantilever between the tip and the surface of the sample due to the force, f , and k is the cantilever spring constant. Therefore, the absolute force is measured after determination of k . Because the stiffness of the cantilever is known, the change in height of the tip is directly related to the force by equation 5.

$$f = -kx \quad (\text{Eq. 5})$$

The detector turns physical changes in the cantilever into an electrical signal (Figure 2.5).¹⁷ The signals on the deflections are processed by a software obtaining a topographical image of the sample surface.

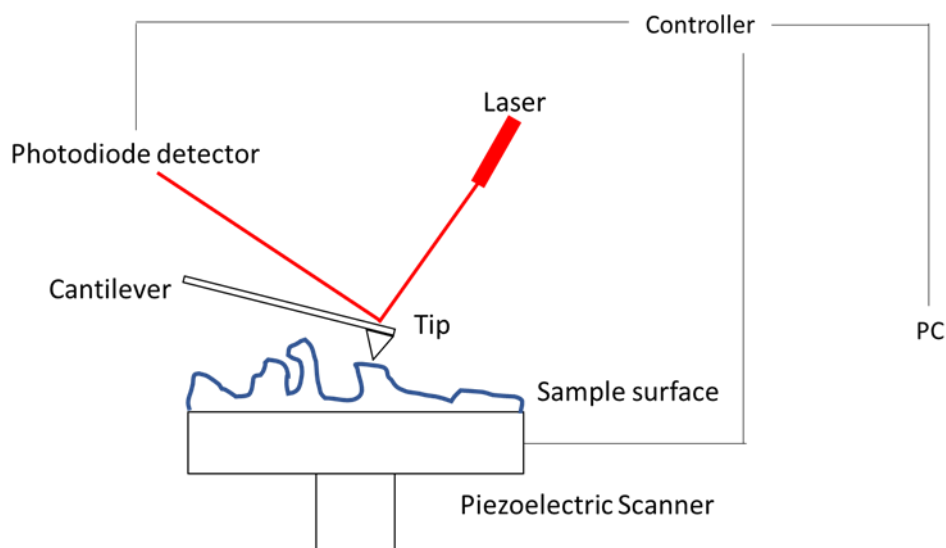


Figure 2.5. Scheme of an AFM operation procedure and components to measure.

Then, the operation principle is based on a change in the position of the cantilever produced by changes in the surface of the sample when the tip is scanning, and it is monitored with a laser light that reflect any difference respecting the original position of the cantilever on the detector.¹⁷

2.1.9. Electrical measurements

All the electrical measurement where tested on a mechanical probe station. This instrument allows to measure conductivity properties of semiconductor devices. Basically, a pair of tips apply a voltage through the material and a resulting current is measured.

To measure current-voltage properties of the material, it should be deposited onto a non-insulated area of the platinum microband electrodes. Such electrodes are tested in the response of the device to an external stimulus, electrical in this case.

The probe station is in a close chamber with nitrogen atmosphere and consists in a thermal chuck where the sample is deposited. The chuck is mounted on a stage which

allows the movement of the chuck inside the chamber. Next to the chuck, in a planar surface, are located the manipulators, they contain the probe tips, coated with platinum, that need to be connected, with high precision, to the platinum electrodes. This connection between the probe station and the electrodes is magnified by an optical microscope (Figure 2.6). The probe station is connected to a computer with the necessary software and it changes the current parameters according to each experiment. The data obtained during the measurement are exposed on a I-V graph.

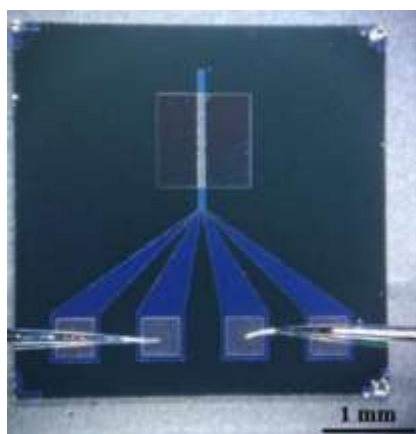


Figure 2.6. Picture of a MBE used to measure electrical properties. It shows the connection, in form of two needles, between the probe station and the sample which is located in the upper square.

With the aim of prepare coordination polymers with semiconducting properties, this technique will allow us to measure electrical properties of the material prepared.

2.1.10. Rheology

The material prepared at high concentration display interesting physical properties such as the formation of hydrogel. The study of mechanical properties of the product in hydrogel form is interesting in order to establish inherent properties of the material such as viscosity.

Rheology measurements studies the change in a non-newtonian fluid (solid or liquid material), a deformation, after applying a force on top of it. In such way it is possible to characterize the hydrogel as a supramolecular network based on polymers. Rheology will provide information about the stiffness, elasticity, viscoelasticity, viscosity and recovery properties after the pressure applied (stress) on the material. Rheology is a useful technique to determine intra- and intermolecular interactions of polymers and then outline the structure of the polymeric materials.¹⁸

The main value measured with rheology is the resistance to deformation (G^*), the result of the contribution of storage modulus (G') and loss modulus (G''). To determine if the material has a solid or liquid behavior after a shear stress applied, G' and G'' values are crucial. If there is a minimal deformation after the stress, the elastic component (G') is bigger than the plastic component (G'') and the material is considered more rigid and then a solid. On the contrary, if there is a moderate deformation after applying the stress, the viscous component predominates over the elastic component and then, the material is considered less rigid, as a liquid.³

All the rheology measurements were done in an instrument called rheometer. There are two types of rheometers, in one hand rheometers that applied extensional stress and in the other hand rheometers that applied shear stress. This last type has been used in our experiments and it consists in a plate where the sample is deposited on and connected to a temperature system. On top of it, different steel geometries (concentric cylinders, parallel plates, cone and plate) apply a rotational force on the sample, controlled by the computer connected to the instrument. The force can be an up, down and circular pressure on the sample. The result shows the shear stress 'felt' by the sample as a consequence of the force applied on it.

2.1.11. Nuclear Magnetic Resonance (NMR)

Nuclear Magnetic Resonance (NMR) is a technique widely used to determine the structure of organic molecules.

NMR is based on the absorption of electromagnetic radiation of atomic nuclei that has been oriented by a strong magnetic field, the absorption promotes the excitation and a transition between nuclear spin energy levels, normally nuclei are ^1H and ^{13}C because they have a magnetic moment not zero. Since the absorption depends on the environment of these nuclei it is easy to determine the structural properties of the molecule. As a result, the NMR spectra shows absorption lines for each kind of magnetically active nucleus in the sample.³

The preparation of a synthetic nucleoside in the experiment section used NMR as guide for the synthesis. This technique indicates if the synthesis was reliable showing the organic structure of the nucleoside prepared.

The main part of a NMR instrument consists in a stable magnet with a controller that generate an accurate magnetic field. Higher magnetic fields promote higher sensitivity and resolution of the spectra. The radio frequency coil is capable of emitting precise frequencies and it adjusts the magnetic field from the magnet. There are two coils, one transmits radio frequency pulses to the sample and the other one receives it. The sample holder has the coil that excited the nuclei and a controller of temperature of the holder. A detector will measure the radio-frequency energy absorption of the sample and finally a computer will show the spectrum after mathematical treatment.³

2.2. References

- 1- Singhal, N., Kumar, M., Kanaujia, P., Viridi, J. S., *Front Microbiol.* 2015, **6**, 791.
- 2- Hosseini, S., Martinez-Chapa, S. O., 2016, Principles and Mechanism of MALDI-ToF-MS Analysis in *Fundamentals of MALDI-ToF-MS Analysis*, 1-19, Springer, Singapore.

- 3- Rankin, D. W. H., Mitzel, N., Morrison, C., 2013, *Structural Methods in Molecular Inorg. Chem.*, Wiley.
- 4- Zhang, X., Xu, Y., *Molecules* 2011, **16**, 5655-5664.
- 5- Ashwood, B., Pollum, M., Crespo-Hernandez, C., *Photochemistry and Photobiology* 2019, **95** (1), 33-58.
- 6- Swinehart, D. F., *J. Chem. Educ.* 1962, **39**, 333-335.
- 7- Blackburn, G. M., Gait, M. J., Loakes, D., Williams, D. M., (ed.) 2006, *Nucleic Acids in Chemistry and Biology*, RCS Publishing, UK.
- 8- Khan, S., Khan, S., Khan, L., Farooq, A., Akhtar, K., Asiri, A., (ed.) 2018 Fourier Transform Infrared Spectroscopy: Fundamentals and Application in *Functional Groups and Nanomaterials Characterization in Handbook of Materials Characterization*, 317-344, Springer, Cham.
- 9- Lakowicz, J. R., 2006, *Principles of Fluorescence Spectroscopy*, Springer, Singapore.
- 10- MacKenzie, L., Palsson, L., Parker, D., Beeby, A., Pal, R., *Nat. Comm.*, 2020, **11**, 1676.
- 11- Hall, J., Renger, T., Picorel, R., Krausz, E., *Biochimica et Biophysica Acta-Bioenergetics* 2016, **1857**, 115-128.
- 12- Kumar, J., Nakashima, T., Kawai, T., *J. Phys. Chem. Lett.* 2015, **6**, 3445-3452.
- 13- Lunkley, J., Shirotani, D., Yamanari, K., Kaizaki, S., Muller, G., *J. Am. Chem. Soc.* 2008, **130**, 13814-13815.
- 14- De Greef, T., Smulders, M., Wolffs, M., Schenning, A., Sijbesma, R., Meijer, E., *Chem. Rev.* 2009, **109**, 5687-5754.
- 15- Babu, S., Kartha, K., Ajayaghosh, A., *J. Phys. Chem. Lett.* 2010, **1**, 3413-3424.
- 16- Egerton, R. F., 2016, *Physical Principles of Electron Microscopy*, Springer, Cham.
- 17- Voigtländer, B., 2019, *Atomic Force Microscopy*, Springer, Cham.
- 18- Macosko, C. W., 1994, *Rheology: Principles, Measurements, and Applications*, Wiley.

**Chapter 3. Preparation and characterization of a coordination polymer
designed from 6-thioguanosine and Ag(I)**

Table of Contents

3.1. Introduction.....	64
3.2. Materials and Methods	68
3.3. Results and Discussion	71
3.4. Conclusions.....	83
3.5. References	84

3.1. Introduction

The synthesis of nanomaterials using nucleobases derivatives from DNA and metal ions with the aim of prepare functional materials is a recent perspective.¹⁻³ With the idea of build complex nanostructures, the bottom-up preparation of these materials needs to be enhance in a more selective and efficient way in order to obtain new functionalized materials with promising applications as nanowires, logic gates or sensors (see chapter 1).

The approach follows to achieve these type of materials is the preparation of coordination polymers with coinage metals ions that can be attached through specific positions to nucleoside sulfur-derivatives, they have shown advantages in the preparation of molecular-based compounds with self-assembly properties.^{4,5} The specificity of thio-molecules to bond coinage metals ions in concrete positions often forms self-assembled one-dimensional coordination polymer structures with a sulfur-metal backbone.⁶ These thiolate-based coordination polymers can show electrical conductivity⁷ or luminescence properties,⁸ similar to semiconductors.^{9,10}

Coinage metals ions and chalcogen elements are well-known for its soft base-soft acid interaction forming metal-chalcogenolate materials.⁶ These form a variety of structures such as coordination polymers, self-assembled monolayers or clusters and they are increasing its relevance in nanotechnology because of its surface and electrical conductivity properties.^{11,12} Specifically, the use of Ag(I) and chalcogen ligands containing sulfur, lead to the formation of structurally characteristic thiolate compounds where the metal(I) is directly attached to the sulfur atom. The different bonding modes of Ag(I) when is attached to sulfur ligands or hydrogen bond interaction between ligands induce structural variations among Ag(I) thiolate compounds.⁶

There has been reported several one-dimensional crystal polymer structures for Ag(I) thiolate complexes and the linear conformation is the typical structure for these compounds when small sulfur ligands size are presents. In general, Ag(I) coordinates two ligands through sulfur atoms forming a chain and leaving the ligand substituent outside the polymer. The 3-methylpentane-3-thiolate Ag(I) shows that the main chain has two intertwining and non-connected Ag(I)-sulfur chains that interact through Ag-Ag bonds (Figure 3.1a).¹³ A similar one-dimensional Ag(I) thiolate polymer, with a bigger ligand size, 2, 4, 6-triisopropylthiophenol, shows a non-intertwine double strand with two parallel chains with argentophilic interactions between Ag(I) of each chain (Figure 3.1b).¹⁴ Another one-dimensional Ag(I) thiolate complex was reported, an Ag(I) cyclohexane thiolate exhibits small structural differences from the above compounds. In this case, the compound is arranged tubularly with Ag-Ag interactions inside the tube and Ag(I) coordinating two and three sulfur through the chain alternatively (Figure 3.1c).¹⁵

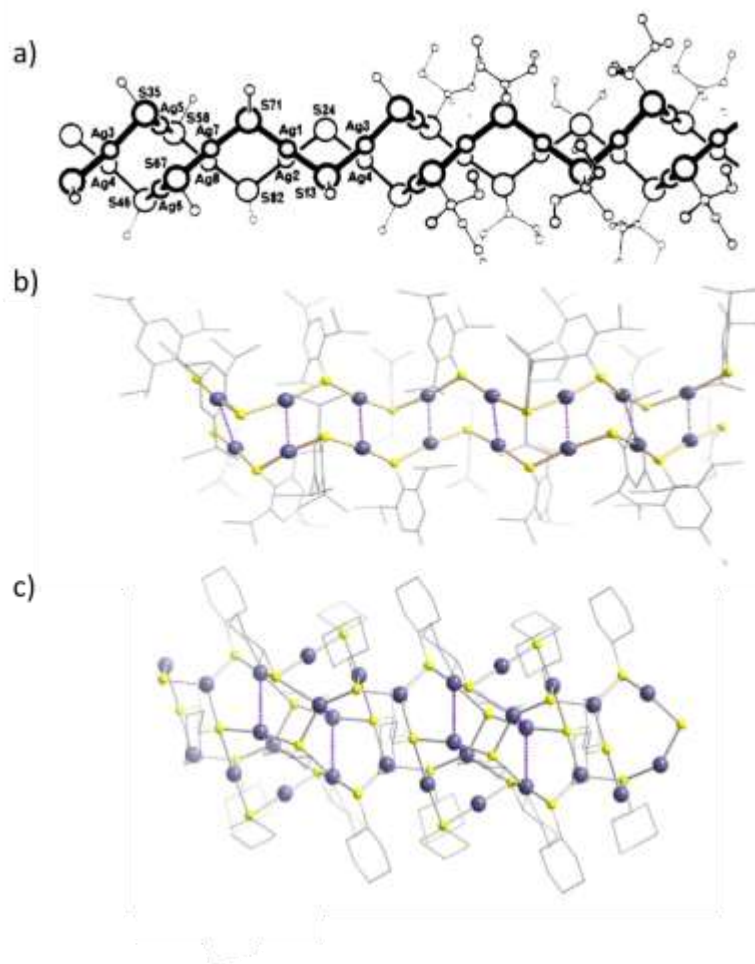


Figure 3.1. Schematic one-dimensional Ag(I) coordination polymers through the c axis of a) scheme of $[\text{AgSC}(\text{CH}_3)(\text{C}_2\text{H}_5)_2]_n$ ¹³ b) scheme of $[\text{Ag}(\text{SPh-2,4,6-}(\text{iPr})_3)]_n$ ⁶ c) scheme of $[\text{Ag}(\text{SC}_6\text{H}_{11})]_n$.⁶ In b and c sulfur atoms and Ag(I) ions are indicated as yellow and grey balls respectively. Dashed lines between Ag atoms indicate argentophilic interactions.

A non-crystal Ag(I) thiolate one-dimensional coordination polymer has been reported and it agrees with the formation of a strand made of Ag(I)-sulfur backbone.¹⁶ This self-assembly polymer is highlighting as a sensing material as chemosensors for VOCs or metal ions.¹⁷⁻¹⁹

Crystal structures for two-dimensional Ag(I) thiolate compounds has not been much explored but recently few researches shed some light in these structures. Two-dimensional Ag(I) thiolate structure was firstly suggested by Scudder *et al.* and these studies highlighted the possibility of the formation of lamellar geometries with Ag(I) bonding three sulfur alkane ligands forming a polymeric sheet seemingly to a hexagons lattice (Figure 3.2a).²⁰ The analysis of computational studies for the structure of Ag(I) benzene thiolate gives as a result the formation of layers. Ag(I) bonds three sulfur atoms from the ligand forming a polymeric layer with the benzene remaining above and below of the structure but with relatively short distances between layers.²¹ Alike, two other compounds, Ag(I) 2-pyridinethiolate and Ag(I) 2-mercaptobenzoate, forms lamellar structures with the only difference with respect to previous two-dimensional Ag(I) thiolate complexes that Ag(I) is not exclusively bound to the sulfur of the ligand. These two ligands have in their structure atoms which Ag(I) bonds, nitrogen and oxygen.^{22,23} The most recent studies about two-dimensional Ag(I) thiolates shows three lamellar structures. Ag(I) 4-mercaptobenzoate and Ag(I) 4-mercaptobezoic acid have similar conformation, they form layers of polymeric chains where Ag(I) is linked to three sulfurs and this to three other Ag(I) ions leaving the rest of the ligand outside (up and down) the main laminar structure with long distances interlayer. In addition, in this complex there are argentophilic interactions (Figure 3.2b).²⁴ The last two-dimensional Ag(I) thiolate reported to date is the complex formed by Ag(I) and 3-mercaptopropionic acid. This compound like the previous ones shows a one-dimensional coordination polymer with Ag(I)-sulfur backbone and the layer is formed when the Ag(I) coordinate three sulfur and this to three other Ag(I) atoms forming a sheet with long distance between layers.²⁵

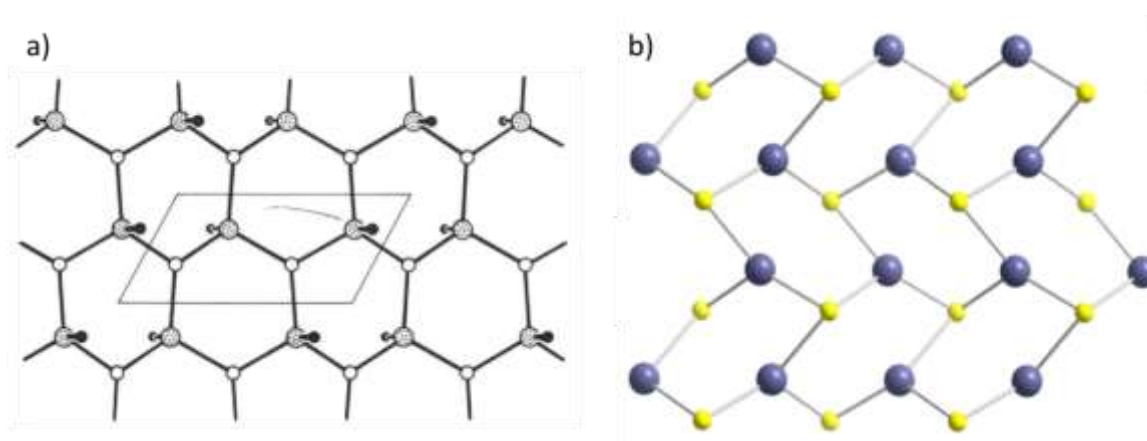


Figure 3.2. Schematic two-dimensional Ag(I) coordination polymer structures with perpendicular view of a) scheme of $[AgSR]_n$ ²⁰ b) scheme of $[Ag(p-SPhCO_2Me)]_n$.²⁴ Sulfur atoms and Ag(I) ions are indicated as white/yellow in (a) and grey/blue balls in (b).

All Ag(I) thiolate complexes structures have been described so far. In this chapter we have explored the interaction of Ag(I) as $AgNO_3$ salt with the nucleobase thio-modified, 6-thioguanosine as a ligand. Particularly, structural characterization of the complex prepared as well as chiro-optical, spectroscopic and electrical properties have been carried out in order to establish a new coordination polymer with semiconductor properties.

3.2. Materials and Methods

All chemicals used in the preparation of the complex were purchased from Sigma-Aldrich and they were used without any purification.

The preparation of 6-thioguanosine complex was carried out in water solution. A yellow aqueous suspension of 6-thioguanosine (18 mg, 0.06 mmol, 1 eq, 60 mL) was crushed and sonicated for 1 hour to achieve a fine dispersion. A molar equivalent of $AgNO_3$ (10.2 mg, 0.06 mmol, 1 eq) was added as a solid to the suspension of 6-thioguanosine.

After the addition of Ag(I) salt and a minute of strong mixing on a Vortex, a pale green solution was formed at 1 mM concentration. Higher concentrations of 6-thioguanosine Ag(I) complex were prepared and as a result, hydrogels were formed. Although its fully characterization and discussion are in chapter 5, due to instrument limitations mass spectroscopy, FTIR, SEM, AFM and conductance measures were done on dry form of hydrogels, xerogels.

Matrix-assisted laser desorption/ionization spectrometry (MALDI-ToF) was performed using a Bruker Autoflex II ToF/ToF Mass Spectrometer in Durham University by Dr. Mosely. The 6-thioguanosine Ag(I) reaction mixture (60 mM) was diluted in ultrapure water 100 times and 1 μ L of it was mixed in 9 μ L acetonitrile solution of a α -cyano-4-hydroxycinnamic acid as a matrix.

UV-Vis spectroscopy in the range of 190-850 nm was performed using a Thermo Scientific NanoDrop One Microvolume spectrometer at room temperature. Two samples were recorded, a basic solution of 6-thioguanosine (1 mM in 0.1 M of NaOH) and Ag(I) reaction mixture (1 mM) using 1.5 μ L of volume for each sample.

FTIR spectroscopy was performed using an IRAffinity-1S Fourier Transform infrared spectrophotometer (Shimadzu) with an integrated ATR accessory, in transmittance mode between 400 and 4000 cm^{-1} at 4 cm^{-1} spectral resolution, under N_2 . The sample was prepared drying the solvent on air for a day prior to analysis and then deposited on a clean p-Si (100) chip (1 cm^2). The chip was deposited on the ATR accessory sample holder and scanned 64 times, co-added and averaged. Bared ATR accessory was used as a background. Silicon chips of 1 cm^2 area were cut from 10 cm diameter wafers (dopant boron at <111> oriented p-type, resistivity 0.09-0.12 Ohm-cm) which were purchased from Pi-KEM Ltd.

Circular dichroism was performed using a Jasco J-810 spectropolarimeter, connected to a PTC-423S temperature controller at 25°C and under N₂. Two circular dichroism spectra were recorded in a demountable quartz cuvette with a path length of 0.1 mm (106-0.1-40 Hellma), a basic solution of 6-thioguanosine (10 mM in 0.1 M of NaOH) and Ag(I) reaction mixture (1 mM).

Scanning electron microscope was performed using a Tescan LMU scanning electron. Digital images of the sample were recorded for 3 µL of Ag(I) reaction mixture (60 mM) dried overnight on a clean p-Si (100) chip (1 cm²) and then mounted on an aluminium stub with double sided adhesive tape.

Atomic force microscopy was performed using a Multimode 8 atomic force microscopy with a NanoscopeV controller (Bruker) and a 'E' scanner. Nanoscope software version 9.1 was used to control the microscope. The system was operated in ScanAsyst in air mode as a peak force tapping mode at ultra-low forces to minimize damage to samples. For reducing vibrational noise, an isolation table/acoustic enclosure was used (Veeco Inc., Metrology Group). Silicon tips on silicon nitride cantilevers (ScanAsyst, Bruker) were used for imaging. The nominal tip radius was approximately 2 nm, resonant frequency 150 kHz and spring constant $k \approx 0.7 \text{ Nm}^{-1}$. The AFM data were analyzed with NanoScope Analysis 1.5 software (Bruker). The sample was prepared by adding 2 µL of Ag(I) reaction mixture (1 mM) onto a clean mica wafer and it was left for dry for two hours on air. Avogadro software version 1.2.0 was used to build the structure model of the complex prepared.

Room temperature luminescence in the range of 250-800 nm was performed using a Spex FluoroMax spectrofluorometer. Two emission spectra were recorded, a basic solution of 6-thioguanosine (1 mM in 0.1 M of NaOH) and Ag(I) reaction mixture (1 mM) using 10 µL of volume for each sample in a quartz cuvette with a path length of

1.5 mm (105-252-15-40 Hellma). Lifetime values were calculated by Dr. Horrocks following a procedure cited in the appendix.

Current-Voltage measurements were performed using a probe station (Cascade Microtech) and readings were collected using a Hewlett Packard Agilent Technologies B1500A semiconductor parameter analyzer driven by Agilent Easy EXPERT software. The applied voltage varied from +2 V to -2 V in steps of 0.05 V. All data were measured at room temperature and under N₂ atmosphere. To measure the current-voltage curves a patterned Pt microband electrode (MBE) was used. These microelectrodes were fabricated on Si/SiO₂ substrates and coated with an insulating dielectric except for an area of 2 x 2 mm² where the Pt electrodes are exposed. A drop of the sample was deposited on the exposed area and dried in air. The height of the electrodes is 200 nm and their width is 10 μm with a 10 μm between neighbouring bands (Smart Microsystems Pt MB-4000, Windsor Scientific Ltd., Slough UK). 1 μL of the reaction mixture at 1 mM was deposited onto the electrodes and it was left for dry for an hour before measurement in air.

3.3. Results and Discussion

The reaction was performed using a yellow aqueous dispersion of 6-thioguanosine and a solid Ag(I) salt, AgNO₃, in an equimolar ratio 1:1 (Figure 3.3). After a minute of mixing a pale green solution (**1**) appeared at room temperature. Attempts were made to crystallize the product, following vapour diffusion or hydrothermal methods, although they were unproductive. Then, the reaction mixture **1** was firstly analyzed in order to determine its chemical structure.

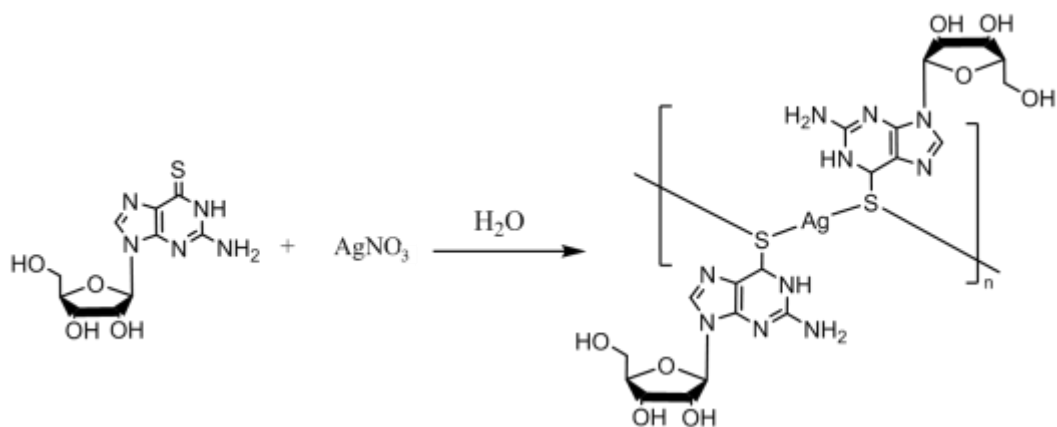


Figure 3.3. Scheme of 6-thioguanosine Ag(I) complex preparation.

Mass spectroscopy confirmed the complexation of the metal ion. MALDI-ToF mass spectroscopy show the oligomeric nature of the complex formed with peaks equivalent to oligomeric chains, 1730.9 m/z for $[Ag_5L_4]^+$, 1730.8 m/z calculated; 1326.0 m/z $[Ag_4L_3]^+$, 1325.8 m/z calculated; 921.2 m/z $[Ag_3L_2]^+$, 920.8 m/z calculated. L corresponds to a deprotonated, anionic form of 6-thioguanosine, the ion $[C_{10}H_{12}N_5O_4S]^-$ (Appendix, Figure A1). This data suggests that a coordination polymer is formed and also further analysis of **1** supports the formation of a polymeric structure as discussed below.

A comparison of UV-Vis absorbance for 1 mM of the ligand in basic solution, to help its solubility, and **1** shows changes in the spectra (Figure 3.4). The peak at 313 nm present in the ligand spectrum, corresponding to $\pi-\pi^*$ transitions in thiol form of the thio-nucleoside,^{26,27} is red shifted, to 335 nm, broadened and is less intense for the product **1**. This suggests that the sulfur is bonded to Ag(I) atom forming the expected Ag-thiolate. The peaks at 253 and 270 nm for the ligand, associated to $\pi-\pi^*$ transitions of the purine, appear to be broadened to a single broad absorbance (258 nm) in the product, again indicating the expected coordinate bond formation.²⁸

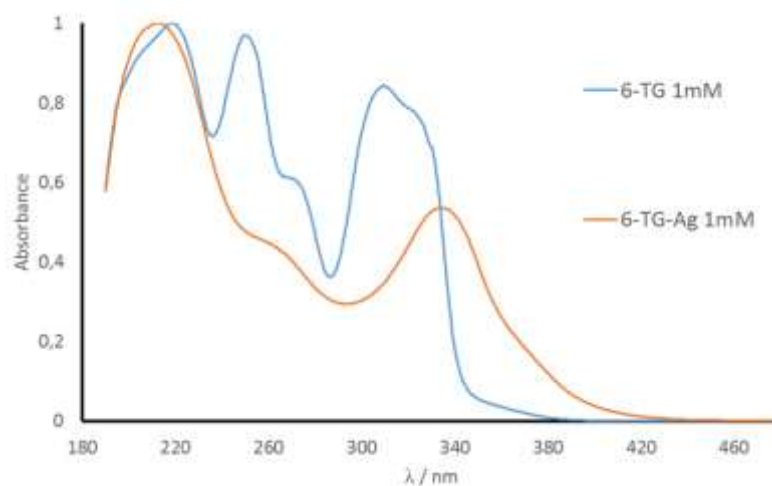


Figure 3.4. UV-Vis spectrum for a basic solution of 6-thioguanosine (blue line) and for compound **1** (orange line).

The FTIR spectrum of **1** as a dry xerogel shows fewer peaks than the ligand (Figure 3.5). The band for C=S group at around 1200 cm^{-1} is present in both spectra at 1203 cm^{-1} but the intensity of the band in **1** is reduced.²⁹ The characteristic band for the C-S group at 770 cm^{-1} is present in the ligand and in **1** but it seems to be more affected in the latter due to complexation as its intensity is much lower.³⁰ These data suggest that Ag(I) ion is bound by the sulfur atom.

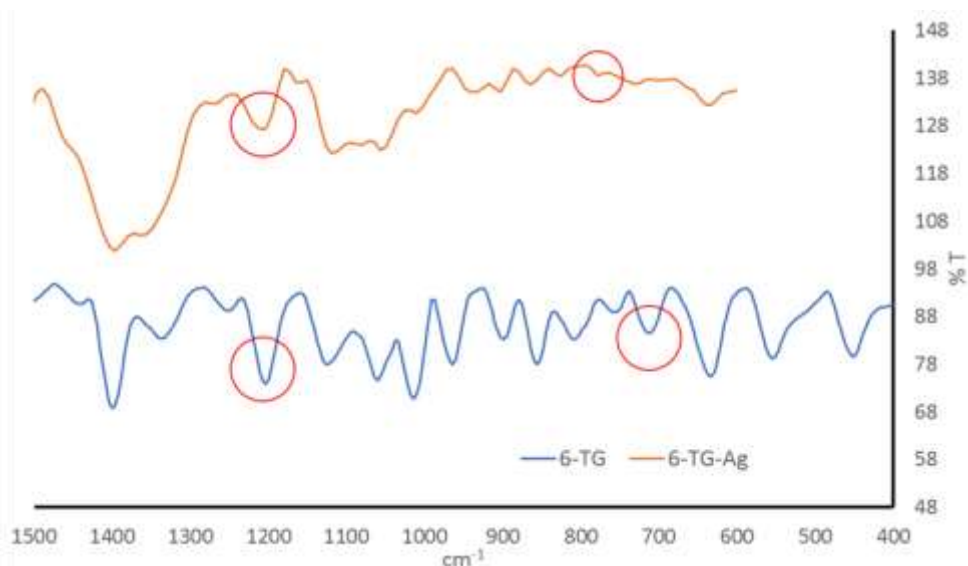


Figure 3.5. FTIR spectrum for 6-thioguanosine as a solid powder (blue line) and a dried solution of **1** (orange line). Data is showed between 400 and 1500 cm^{-1} and red circles indicates characteristic carbon-sulfur bands.

Circular dichroism (CD) spectroscopy investigates chiral properties on the product, and it is shown in Figure 3.6. The CD spectrum for a basic solution of 6-thioguanosine (10 mM) confirms the chirality of the molecule showing two positive peaks ca. 228 and 260 nm and three negatives peaks ca. 209, 246 and 322 nm. Comparing these results with the spectrum of **1** at 1 mM an increase in intensity is noted and it is associated with a rise in the molecular ordering as a consequence of a polymer formation.^{31,32} The presence of a polymer indicates the formation of a highly chiral structure which is coherent with a helical configuration,³³ the positive sign of the spectrum below 200 nm indicates the orientation of the helicity of **1**, a left-handed helix.^{32,34,35}

The association of every CD peak with a specific spectroscopic transition is difficult without computational studies but it is well known that the CD signal above 300 nm are affected by the environment of the sulfur atom of thiolates.²⁷ The change in the spectrum around 300 nm (Figure 3.6) indicates an alteration of the sulfur environment

promoted by the attachment of Ag(I) atom to 6-thioguanosine through sulfur atom forming a coordination polymer.

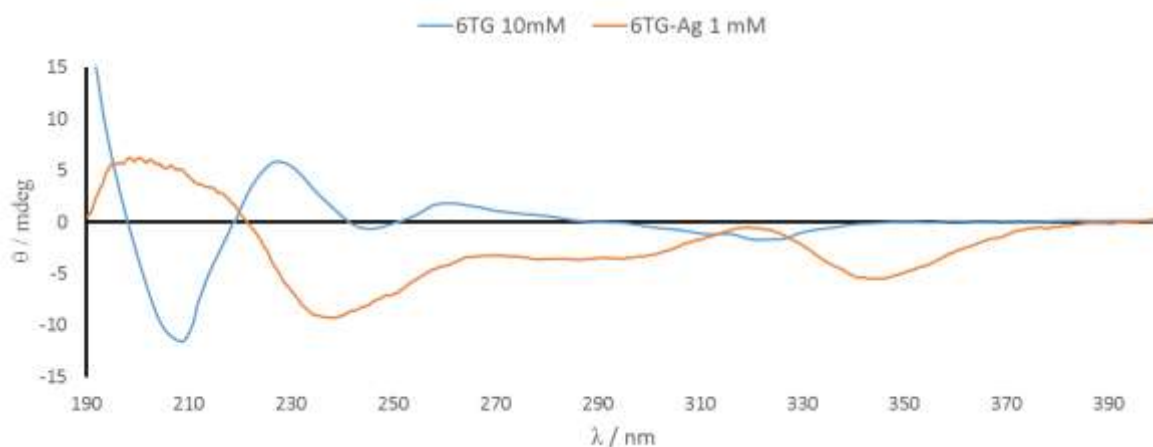


Figure 3.6. CD spectrum for a basic solution of 6-thioguanosine at 10 mM (blue line) and **1** at 1 mM (orange line).

Further analysis of **1** includes analysis of SEM microscopy on xerogel form. The sample exhibits in Figure 3.7a a supramolecular structure made of entangled fibres of microns in length covering the surface. These fibres are forming a complex net that cover all the surface of the holder (Figure 3.7a). Figure 3.7b shows a zoom in image where individual and regular fibres in shape are 10 μm of length approximately. These results are consistent with the formation of a one-dimensional coordination chain polymer, that supports as well mass spectroscopy data. To complete the structural characterization of **1**, AFM studies were tackled.

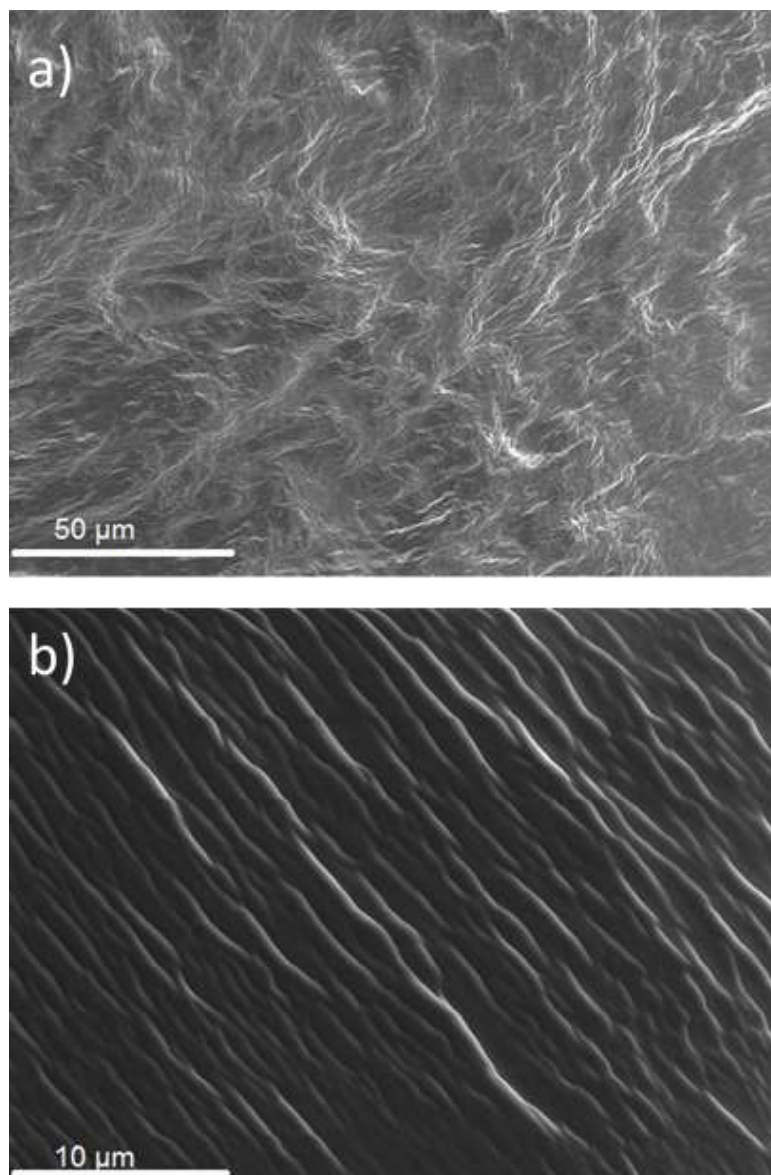


Figure 3.7. SEM image for dried sample of **1**. a) indicates a large-scale image where the polymer matrix is formed by fibres entangling. b) shows a small-scale image showing alignment of fibres on the surface of the polymer.

Compound **1** was dried, as xerogel, on mica and analyzed under AFM in order to confirm the presence of a polymeric structure. Figure 3.8 shows the structure of **1** with an extended one-dimensional structure, consistent with the formation of a coordination polymer, where strands are assembling and forming entangled networks. The length of single strands is mostly varying between 350 and 160 nm with typical average of

240 nm. The cross-sectional heights of the smallest of these fibres are around 1.8 nm (Figure 3.9a) accordingly to similar Ag(I) thiolate compounds.^{13,15} Fibres associate to form longer strands, reaching more than 400 nm in length but with similar height to shorter single fibres (Figure 3.9b). This suggests that individual fibres are interacting between them, adopting a parallel conformation on the substrate and do not necessarily lie one on top of one another. CD experiment above indicated that the molecule is chiral and it is confirmed on small range image by fibres associates revealing the formation of helical chains in a left-handed orientation (Figure 3.10), the height of helical fibres is similar to fibre associates (Appendix, Figure A2), around 2.2 nm and a regular periodicity of the helix is around 8 nm (Figure 3.10).

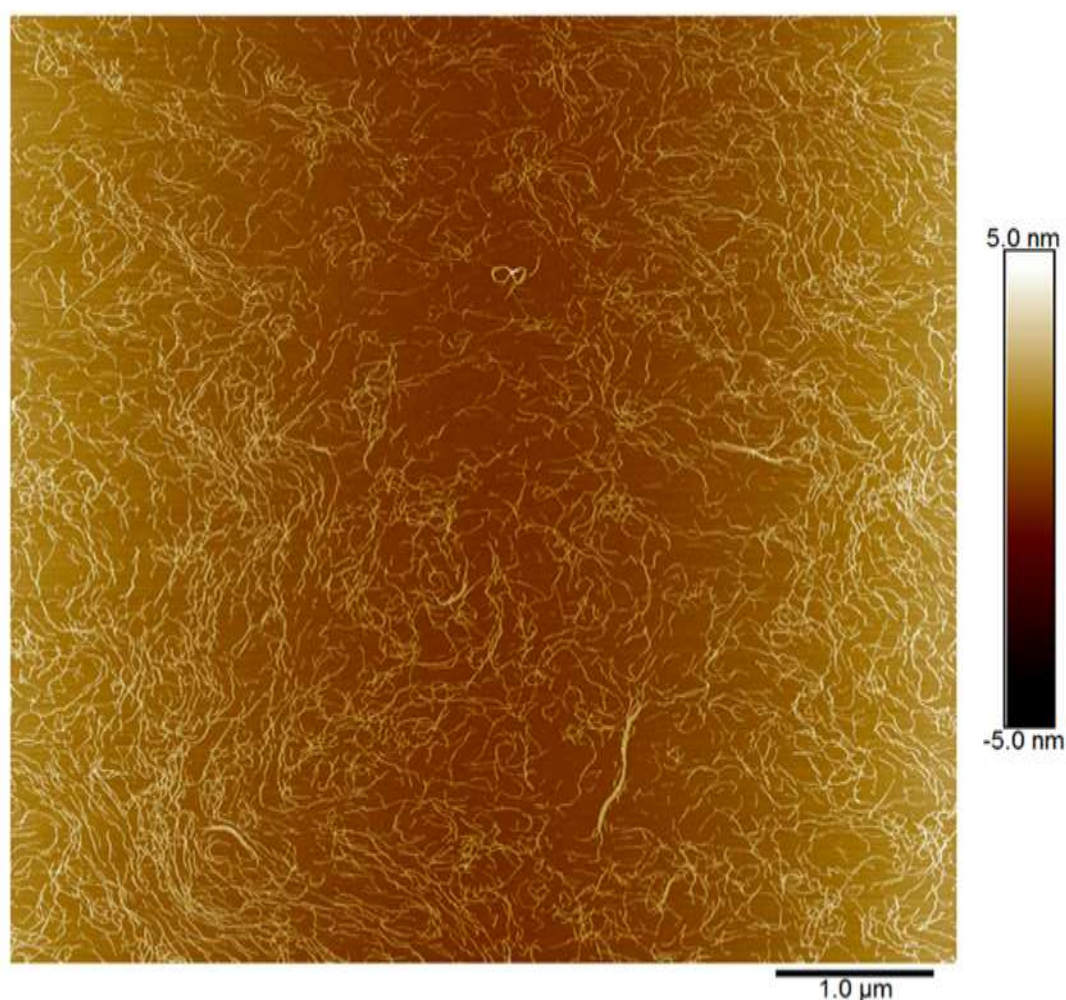


Figure 3.8. AFM image for **1** at 0.01 mM concentration in water and dried on mica.

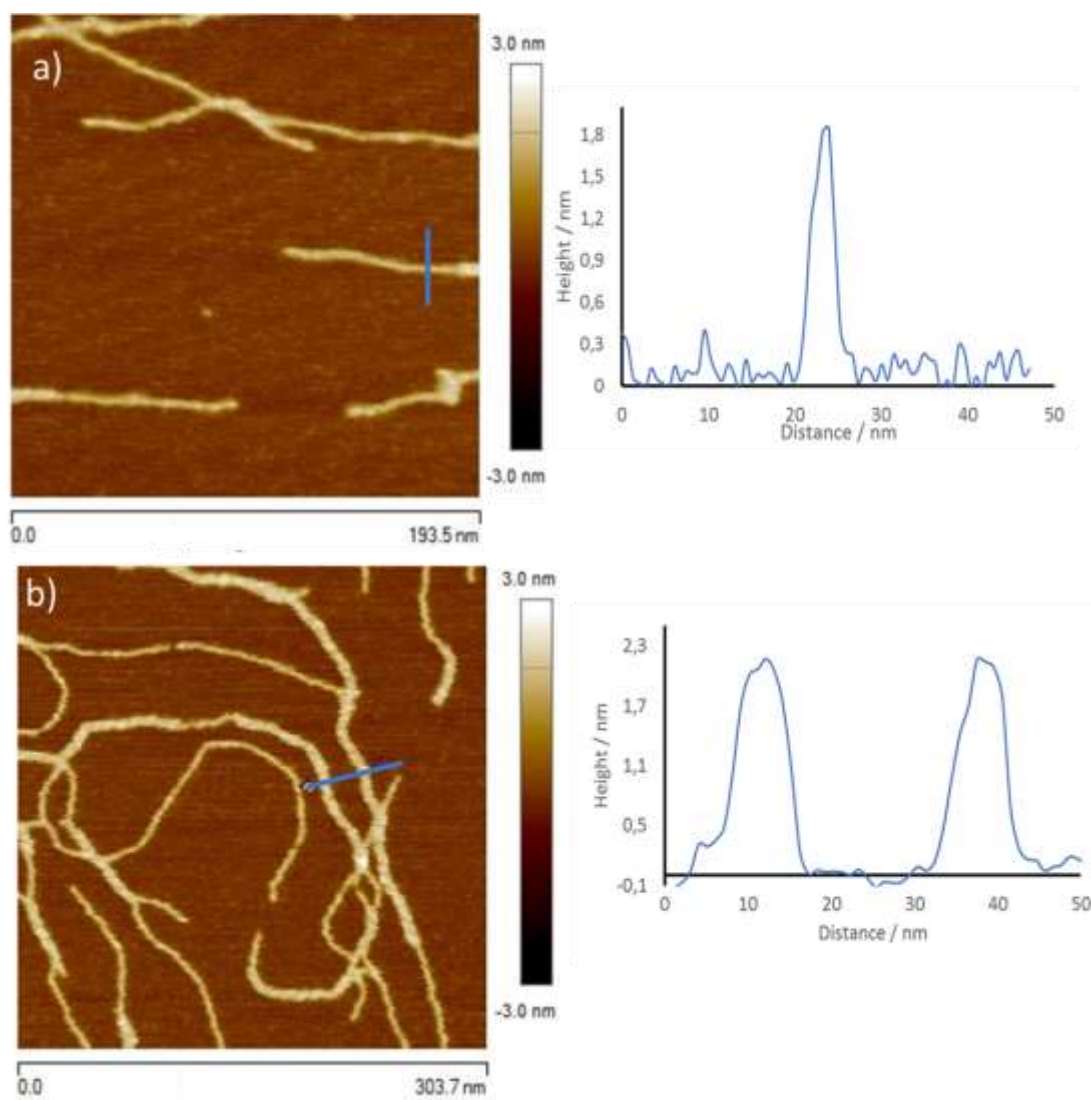


Figure 3.9. AFM images from dried solution of **1** at 0.01 mM concentration in water a) single fiber of **1** with 1.8 nm in height. b) Fibre associates of **1** with similar height as single fibres.

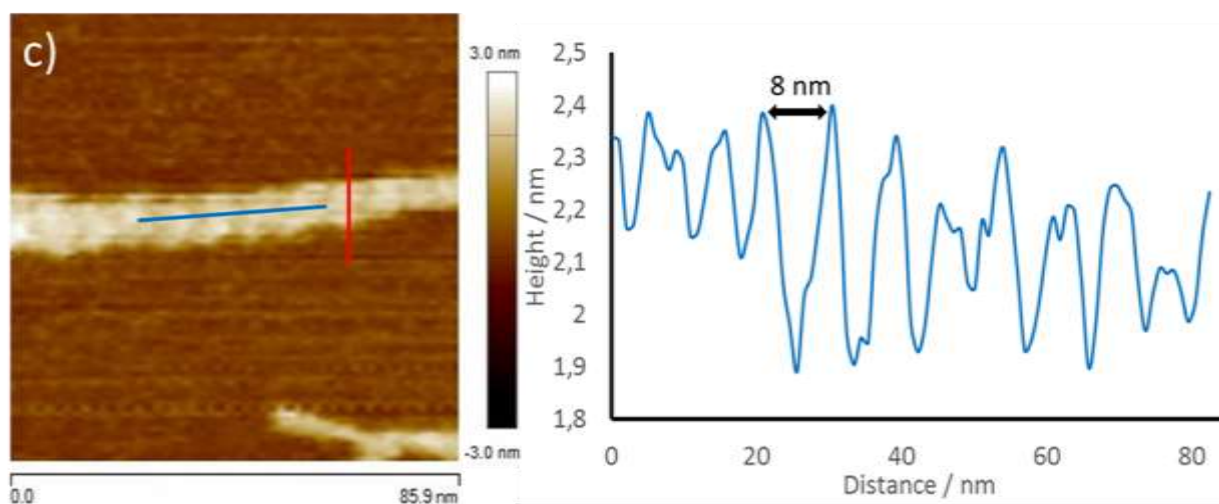


Figure 3.10. AFM image from dried solution of **1** at 0.01 mM concentration in water. Chiral fibre associates with left-handed helicity and periodicity of the helix around 8 nm (blue line). Red line indicates the height of helical fibres (Appendix, Figure A2).

After structural characterization, a structure can be proposed for compound **1**. As mass spectroscopy indicates that **1** has a oligomeric nature with the main chain of the polymer formed by Ag(I)-sulfur bonds. As it was presented in the introduction for one-dimensional crystal coordination polymer the rest of the ligand can be located above or below the chain to avoid steric impairments.¹⁴

To verify that Ag(I) is attached to the sulfur of the ligand, UV-Vis and FTIR spectroscopies were performed. They indicated that the electronic environment of sulfur was altered by the presence of Ag(I) ions and it implies that a coordinate bond is formed through Ag(I)-sulfur. The more intense CD signal of compound **1** has demonstrate the highly ordered structure with respect to the free ligand in solution and it is consistent with a polymer formation. In addition, since the polymer is chiral a helical conformation left-handed oriented is proposed.

Finally, microscopy techniques have confirmed previous assumptions. SEM images showed abundance of fibres along the sample surface and these fibres are proposed to be one-dimensional coordination polymers. This statement is corroborated with AFM that shows one-dimensional strands. These coordination polymers have comparable heights with Ag(I)-thiolate complexes, and they interact in parallel by non-covalent interactions of ligand substituent, it will be analyzed further in chapter 5.¹⁵ Also, the helicity of the polymer is confirmed. So, a coordination polymer structure is proposed for compound **1** with a Ag(I)-sulfur backbone (Figure 3.11).

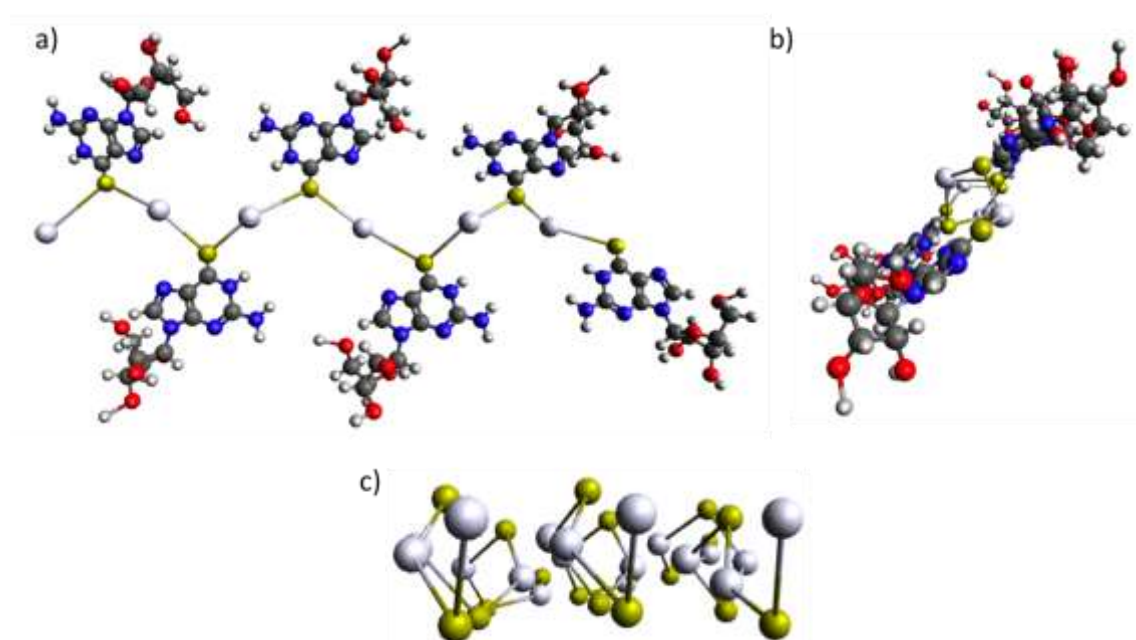


Figure 3.11. Proposed scheme models for the one-dimensional coordination polymer **1** structure, a) side view of the coordination polymer, b) viewed through the polymer axis of the one-dimensional coordination polymer and c) coordination polymers associated viewed through the polymer axis, this bundle of fibres associates turns into a left-handed orientation forming helices (grey balls represent Ag(I) ions) (ligand substituents are omitted for clarity). These models were drawn on Avogadro software 1.2.0.

In order to establish luminescence properties of compound **1**, fluorescence spectroscopy has been performed. It showed the maximum peak in the emission spectrum for **1** at 421 nm for an excitation of 350 nm, while in the ligand it is at 420 nm at the same excitation wavelength (Figure 3.12) in accordance with literature.²⁸ The spectrum shows the same wavelength for the emission peak although the intensity of the emission of the ligand is larger so, luminescence properties of **1** is mainly due to the ligand since the emission spectrum is not disturbed by the Ag(I). The emission in both compounds indicates a high energy transitions mainly due to intra ligand process,³⁶ generated by π - π^* orbitals of the ligand.³⁷ The small emission peak around 800 nm for both samples is attributed to the second order luminescence scattering.

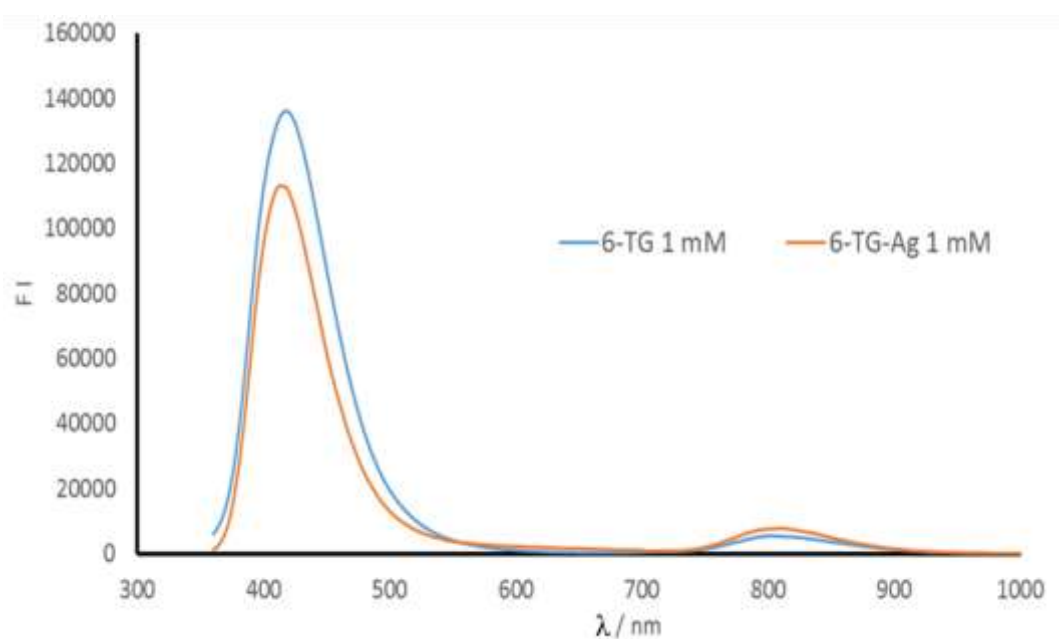


Figure 3.12. Luminescence spectrum for a basic solution of 6-thioguanosine at 1 mM (blue line) and for **1** at 1 mM (orange line) at 350 nm excitation.

It is well-known that Ag(I) complexes exhibit generally poor luminescence properties probably due to its thermal instability and light sensitivity at room temperature³⁸ but it is not the case for compound **1**. Luminescence lifetime was calculated, and it indicates

the time in which the molecule remains in an excited state before emitting a photon. Comparison of lifetime values of the ligand in solid form and compound **1** two hundred times diluted (5 μM) indicates that **1** has nearly two times longer fluorescence lifetime (0.7 ns) than the ligand (0.398 ns) (Appendix, Figure A3). This difference suggests that compound **1** has longer fluorescence properties than the ligand.

Conductance properties of the xerogel were measured on platinum microband electrodes to investigate if the fibres show nanowire behavior. It has been commented in several papers that one-dimensional arrangements of Ag(I) ions are potential nanowires.^{39,40} However, these assertions are often not backed by data on electrical conductivity.^{41,42} The current-voltage (I-V) plot in Figure 3.13 indicates the current through the fibres of the xerogel during application of a dc voltage between -2 V to +2 V. Figure 3.13 shows similar results for electrode background (blue line) and compound **1** (orange line), with maximum values of intensity of current of 0.38 pA and 0.43 pA respectively. This is a clear indication that the material is not electrically conductive since the range of values are rather similar to background levels of current. This material does not seem to be well suited as nanowires because they show the absence of electrical conductivity.^{39,40,43} The use of a doping agent was rejected for practical reasons, an oxidative doping of Ag(I) ions would require a very strong oxidant and a reductive doping will produce Ag nanoparticles.

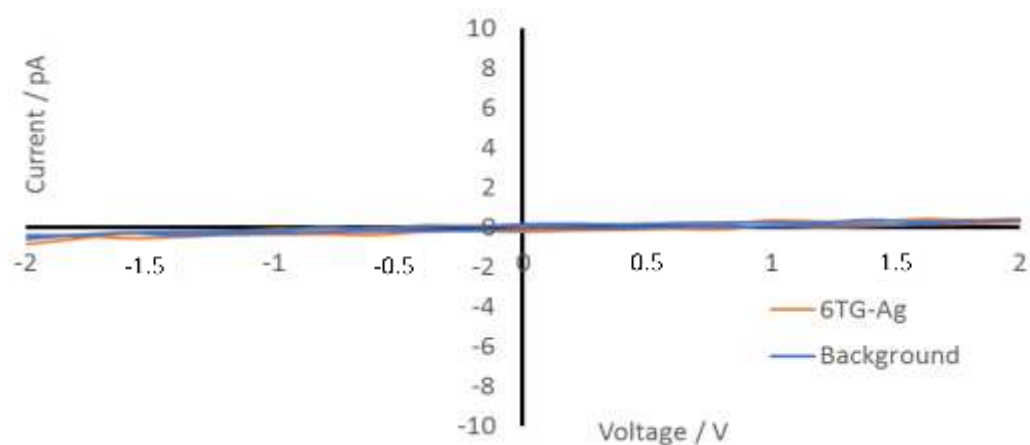


Figure 3.13. Two-terminal I-V characteristic of two samples, blue line corresponding to electrode background and orange line to **1** solution dried on the electrode.

3.4. Conclusions

We have prepared a new Ag(I) thiolate coordination polymer successfully. The reaction has demonstrated the possibility of 6-thioguanosine to attach Ag(I) ions through sulfur atoms bringing a functionalized material with luminescence properties. The product has been structurally characterized by a set of techniques and a one-dimensional coordination polymer with Ag(I)-sulfur backbone has been proposed as the structure. The polymer has also shown the formation of chiral left-handed fibres.

The interaction between the Ag(I) and sulfur in the polymer is assumed as metal sulfides compounds which exhibit semiconductor properties. One of them is optical features, which is displayed by the coordination polymer with fluorescence lifetime much bigger than the ligand. Its combination with inherent chiral properties, chiro-optics, could give a new prospective on the integration of this motif into larger oligonucleotides in order to functionalize DNA-based materials.

3.5. References

- 1- Houlton, A., Watson, S., *Annu. Rep. Prog. Chem., Sect. A: Inorg. Chem.* 2011, **107**, 21-42.
- 2- Wu, Y., Lai, R., *Biotechnology Journal* 2016, **11**, 788-796.
- 3- Carell, T., *Nature* 2011, **469**, 45-46.
- 4- Takezawa, Y., Nishiyama, K., Mashima, T., Katahira, M., Shionoya, M., *Chem. A Eur. J.* 2015, **21**, 14713-14716.
- 5- Tanaka, K., Shionoya, M., *Coord. Chem. Rev.* 2007, **251**, 2732-2742.
- 6- Veselska, O., Demessence, A., *Coord. Chem. Rev.* 2018, **355**, 240-270.
- 7- Gallego, A., Castillo, O., Gomez-Garcia, C., Zamora, F., Delgado, S., *Inorg. Chem.* 2012, **51**, 718-727.
- 8- Veselska, O., Cai, L., Podbevsek, D., Ledoux, G., Guillou, N., Pilet, G., Fateeva, A., Demessence, A., *Inorg. Chem.* 2018, **57**, 2736-2743.
- 9- Guo, Y., Wu, Q., Li, Y., Lu, N., Mao, K., Bai, Y., Zhao, J., Wang, J., Zeng, X., *Nanoscale Horiz.* 2019, **4**, 223-230.
- 10- Huang, X., Qiu, Y., Wang, Y., Liu, L., Wu, X., Liang, Y., Cui, Y., Sun, Y., Zou, Y., Zhu, J., Fang, W., Sun, J., Xu, W., Zhu, D., *Angew. Chem. Int. Ed.* 2020, **59**, 22602-22609.
- 11- Hakkinen, M., *Nat. Chem.* 2012, **4**, 443-455.
- 12- Welte, L., Calzolari, A., Felice, R., Zamora, F., Gomez-Herrero, J., *Nat. Nanotech.* 2010, **5**, 110-115.
- 13- Dance, I., Fitzpatrick, L., Rae, A., Scudder, M., *Inorg. Chem.* 1983, **22**, 3785-3788.
- 14- Tang, K., Yang, J., Yang, Q., Tang, Y., *J. Chem. Soc., Dalton Trans.* 1989, 2297-2302.
- 15- Hong, S., Olin, A., Hesse, R., *Acta Chemica Scandinavica A* 1975, **29**, 583-589.
- 16- Li, D., Shen, J., Chen, N., Ruan, Y., Jiang, Y., *Chem. Commun.* 2011, **47**, 5900-5902.
- 17- Nan, J., Yan, X., *Chem. A Eur. J.* 2010, **16**, 423-427.
- 18- Shen, J., Li, D., Cai, Q., Jiang, Y., *J. Mater. Chem.* 2009, **19**, 6219-6224.
- 19- Wang, Q., Dong, S., Tao, D., Li, Z., Jiang, Y., *Coord. Chem. Rev.* 2021, **432**, 213717.
- 20- Dance, I., Fisher, K., Banda, R. M., Scudder, M., *Inorg. Chem.* 1991, **30**, 183-187.
- 21- Massote, D., Mazzoni, M., *Appl. Phys. Lett.* 2016, **109**, 133104.
- 22- Su, W., Hong, M., Weng, J., Cao, R., Lu, S., *Angew. Chem. Int. Ed.* 2000, **39**, 2911-2914.
- 23- Sun, D., Luo, G., Zhang, N., Xu, Q., Jin, Y., Wei, Z., Yang, C., Lin, L., Huang, R., Zheng, L., *Inorg. Chem. Commun.* 2010, **13**, 306-309.

- 24- Veselska, O., Dessal, C., Melizi, S., Guillou, N., Podbevsek, D., Ledoux, G., Elkaim, E., Fateeva, A., Demessence, A., *Inorg. Chem.* 2019, **58**, 99-105.
- 25- Wang, J., Graf, R., Riedinger, A., *J. Mater. Chem. C* 2021, **9**, 11079-11084.
- 26- Zhang, Y., Zhu, X., Smith, J., Haygood, M., Gao, R., *J. Phys. Chem. B.* 2011, **115**, 1889-1894.
- 27- Repges, R., Beuck, C., Weinhold, E., Raabe, G., Fleischhauer, *Chirality* 2008, **20**, 978-984.
- 28- Rubin, Y., XVI Int. Conf. on Spectroscopy of Molecules and Crystals, Sevastopol, Ukraine, 2004.
- 29- Kamalendra, S., Yadav, R., Yadav, J., *Spectrochimica Acta* 1991, **47A**, 819-820.
- 30- Aulakh, J., Lobana, T., Sood, H., Arora, D., Kaur, R., Singh, J., Garcia-Santos, I., Kaur, M., Jasinski, *RCS Adv.* 2019, **9**, 15470-15487.
- 31- Lam, A., Guenther, R., Agris, P., *Biometals* 1995, **8**, 290-296.
- 32- Zimmer, C., Luck, G., Holy, A., *Nucleic Acids Research* 1976, **3**, 2757-2770.
- 33- Zhang, H., Zheng, X., Kwok, R., Wang, J., Leung, N., Shi, L., Sun, J., Tang, Z., Lam, J., Qin, A., Tang, B., *Nat. Commun.* 2018, **9**, 4961.
- 34- Sutherland, J., Griffin, K., Keck, P., Takacs, P., *Proc. of the Nat. Acad. of Sci. of the USA* 1981, **78**, 4801-4804.
- 35- Sprecher, C., Baase, W., Johnson, W., *Biopolymers* 1979, **18**, 1009-1019.
- 36- Chao, H., Wu, L., Li, C., Lu, W., Liu, L., Feng, X., *Z. Anorg. Allg. Chem.* 2011, **637**, 1533-1538.
- 37- Ford, P., *Chem. Sci.* 2016, **7**, 2964-2986.
- 38- Yam, V., Au, V., Leung, S., *Chem. Rev.* 2015, **115**, 7589-7728.
- 39- Mistry, L., El-Zubir, O., Dura, G., Clegg, W., Waddell, P., Pope, T., Hofer, W., Wright, N., Horrocks, B. R., Houlton, A., *Chem. Sci.* 2019, **10**, 3186-3195.
- 40- Linares, F., Garcia, E., Lopez, F., Domingo, M., Orte, A., Rodriguez, A., Galindo, M., *Chem. Sci.* 2019, **10**, 1126-1137.
- 41- Jash, B., Müller, J., *Chemistry A European Journal* 2017, **23**, 17166-17178.
- 42- Leon, J., She, Z., Kamal, A., Shamsi, M., Müller, J., Kraatz, H., *Angew. Chem. Int. Ed.* 2017, **56**, 6098-6102.
- 43- Kondo, J., Tada, Y., Dairaku, T., Hattori, Y., Saneyoshi, H., Ono, A., Tanaka, Y., *Nat. Chem.* 2017, **9**, 956-960.

**Chapter 4. Preparation and characterization of a coordination polymer
designed from 6-thioguanosine and Cu(I)**

Table of Contents

4.1. Introduction.....	88
4.2. Materials and Methods	92
4.3. Results and Discussion	93
4.4. Conclusions.....	106
4.5. References	107

4.1. Introduction

Functionalization of DNA has been increasing its interest in recent years due to its use in nanotechnology, with medical or opto-electronics applications.¹⁻³ Specifically, the bottom-up preparation of nanostructures composed by elements of DNA and other molecules such as metals ions has been increasing its importance over the years due to the particular bonding capacity and intrinsic properties of some metals to nucleosides and its derivatives.^{4,5} This highly precise combination brings potential electronic and optical properties to nano architectures prepared.⁶

The route followed in this work to obtain such molecules is the preparation of coordination polymers with coinage metals ions and nucleosides sulfur derivatives, recently demonstrated by Houlton *et al.* as the next step in the functionalization of materials.⁷ The main feature of this coordination polymer is the linkage of coinage metals ions to a specific position of the nucleoside derivative, the sulfur atom. Forcing the metal ion to bond with sulfur causes properties of metal sulfides to appear and such molecules are well-known semiconductors.^{8,9} Metal thiolates in form of coordination polymers incorporate properties of d¹⁰ metals such as conductivity and luminescence¹⁰ ensuring linear or coordination with ligands.^{11,12}

The structure of coordination polymers based on coinage metals ions and nucleosides sulfur derivatives usually forms one-dimensional chains with sulfur-metal backbone, due to specific soft base-soft acid interactions.¹³ The metal ions generally used for this type of compounds are Cu(I), Ag(I) and Au(I). In particular, the interaction between Cu(I) and sulfur ligands has led to the formation of Cu(I) thiolate compounds in form of coordination polymer with interesting semiconductor properties such as electrical conductivity¹⁴ or optical emission properties^{15,16} with singular applications,

photocatalysis, sensing, biomedical, integrated into optoelectronic devices and even getting to form nanowires.¹⁷⁻¹⁹

Various crystal structures have been studied for Cu(I) thiolates complexes, in which the main characteristic is the interaction between Cu(I) with the sulfur atom of the ligand. In general, Cu(I) tends to bond in a trigonal configuration bridging three sulfur atoms with the absence or weakness of hydrogen bonds and cuprophilic interactions within the complexes. All the ligand substituents are located outside the main chain of the polymer.¹³ This is confirmed for a one-dimensional coordination polymer crystal structure that the Cu(I) methanethiolate forms, $[\text{Cu}(\text{SMe})]_n$. This structure is a polymeric tubular chain made of a ring three Cu(I) and three sulfur atoms as repeating unit, it is a μ_3 -bridging thiolate.²⁰ An improved crystallization technique allowed to obtain a much longer chain for the above components, in this case nanowires were obtained with a significant conductivity (Figure 4.1a).²¹ Bigger ligands form as well one-dimensional coordination polymers with Cu(I), ligands like *p*-SPhH, *p*-SPhMe, *p*-SPhOMe and *p*-SPhNO₂. These compounds forms $[\text{Cu}(p\text{-SPhX})]_n$ with the same conformation as $[\text{Cu}(\text{SMe})]_n$ except $[\text{Cu}(p\text{-SPhNO}_2)]_n$ with a different bonding mode of Cu(I) when it is attached to the ligand. This last complex forms four individual chains of Cu(I)-sulfur that associated through cuprophilic interactions giving as a result a coordination polymer where Cu(I) is bridging two sulfur atoms (μ_2 -bridging thiolate). This change is due to the packaging of the *p*-substituent of the ligand in the chain because the nitro group implies hydrogen bonds throughout the polymer (Figure 4.1b).²² For bigger ligands such as diamondoids, adamantane-1-thiol and diadamantane-4-thiol, Cu(I) reacts forming two metal organic chalcogenolates (MOCs), a class of coordination polymers. The $[\text{Cu}(\text{SAdamantane})_n]$ forms a one-dimensional coordination polymer very similar to those discussed above, with Cu(I) linking three sulfur atoms and Van der Waals interactions between ligand substituent

conforming two parallel chains connected. The $[\text{Cu}(\text{SDiamantane})]_n$ presents a different conformation to the previously reported structures. In the structure of this one-dimensional coordination polymer Cu(I) bridge alternatively two and three sulfur atoms along the chain, resulting in a polymer in which the two chains are linked by alternating Cu(I) (Figure 4.1c).²³

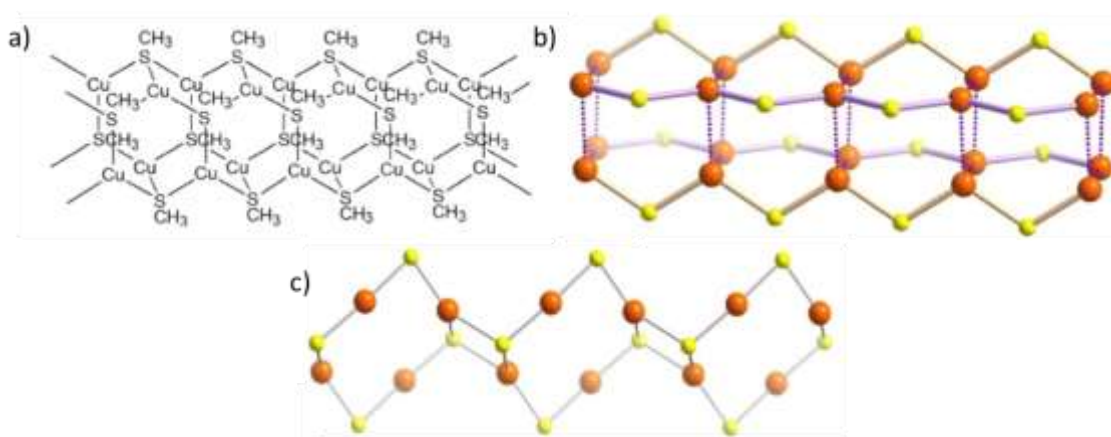


Figure 4.1. Schematic examples of one-dimensional Cu(I) thiolate coordination polymer through the *c* axis of a) $[\text{Cu}(\text{SMe})]_n$ ²¹ b) $[\text{Cu}(p\text{-SPhNO}_2)]_n$, dashed lines indicate cuprohilic interactions¹³ and c) $[\text{Cu}(\text{SDiamantane})]_n$.¹³ Yellow and orange balls are sulfur and Cu respectively. In b) and c) ligand substituent is omitted for clarity.

So far, all chain-like coordination polymer have been analyzed, the survey for crystallographic structures of two-dimensional Cu(I) thiolate compounds does not bring many examples, only several crystal structures have been analyzed in literature and all these Cu(I) coordination polymers exhibit lamellar conformations. The complex $[\text{Cu}(p\text{-SPhOH})]_n$ displays a layered structure with Cu(I) ions bonding three sulfur atoms, as a result, the complex forms hexagons of three Cu(I) and three sulfur with the ligand substituent up and down the layer, hydrogen bonds between substituents helps stabilize the two-dimensional conformation (Figure 4.2a).²⁴ Similar compounds have

been subsequently prepared as is the case of $[\text{Cu}(p\text{-SPhCO}_2\text{Me})]_n$. This compound exhibits a two-dimensional coordination polymer in form of sheets where Cu(I) adopts a trigonal geometry coordinating three sulfur atoms showing a ring of six positions, three Cu(I) and three sulfur. In such a way that ligand substituents are arranged in parallel forming an interlayer of hexagons with π stacking interactions, this complex exhibits interesting thermochromic properties (Figure 4.2b).²⁵ Another comparable structure is the $[\text{Cu}(p\text{-SPhCO}_2\text{H})]_n$ a two-dimensional Cu(I) thiolate coordination polymer that forms layers. Again, Cu(I) adopts a trigonal geometry and it is coordinated to three sulfur atoms, forming a six membered ring, three Cu(I) ions and three sulfur atoms. This complex exhibits a lamellar structure with ligand substituents located between layers, also carboxylic group of ligands cooperate in the stability of the structure establishing hydrogen bonds interactions between them (Figure 4.2c).²⁶ A last compound has been explored for two-dimensional Cu(I) thiolate coordination polymer, $[\text{Cu}(\text{ppt})]_n$ where the ligand ppt is 1-phenyl-1*H*-1,2,3,4-tetrazole-5-thiolate. This coordination polymer shows a lamellar structure with a particular bonding mode for Cu(I) ions. A molecule of ppt ligand attaches three Cu(I) ions, two by a sulfur atom and two by two different nitrogen atoms of the ligand, in such manner that Cu(I) interacts with another two ppt ligand forming sheets conformed in parallel and connected by Van der Waals interactions.²⁷

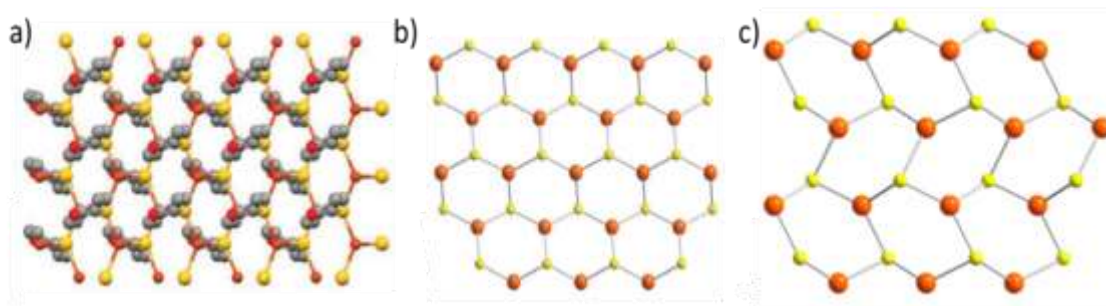


Figure 4.2. Schematic examples of two-dimensional Cu(I) thiolate coordination polymer through a perpendicular view of a) $[\text{Cu}(p\text{-SPhOH})]_n$ ²⁴ b) $[\text{Cu}(p\text{-SPhCO}_2\text{Me})]_n$ ²⁵ and c) $[\text{Cu}(p\text{-SPhCO}_2\text{H})]_n$.²⁶ Yellow and orange balls are sulfur and Cu(I) respectively. In b) and c) ligand substituent is omitted for clarity.

We have described all one and two-dimensional crystal structures known for Cu(I) thiolate coordination polymers. In this chapter we have examined the interaction of Cu(I) as $\text{Cu}(\text{MeCN})_4\text{BF}_4$ salt with the nucleobase thio-modified, 6-thioguanosine as a ligand. Mainly, we have explored the structural characterization of the complex prepared and also chiro-optical, spectroscopic and electrical properties have been studied in order to establish a new coordination polymer with semiconductor properties.

4.2. Materials and Methods

All chemicals used in the preparation of the complex were purchased from Sigma-Aldrich and they were used without any purification.

The 1:1 reaction between 6-thioguanosine and $\text{Cu}(\text{MeCN})_4\text{BF}_4$ follows a similar procedure as shown in the previous chapter. After the addition of the Cu(I) salt, five minutes of strong mixing on a Vortex were needed to form a yellow-orange solution at 1 mM.

Matrix-assisted laser desorption/ionization spectrometry (MALDI-Tof), UV-Vis spectroscopy, FTIR spectroscopy, circular dichroism spectroscopy, scanning electron microscope, atomic force microscopy and room temperature luminescence were performed in the same way as in the previous chapter, although for the latter, no calculations of lifetime values were calculated.

Also, current-voltage measurements followed the same procedure as the one shown in the previous chapter. Tris(4-bromophenyl) ammoniumyl hexachloroantimonate (Magic Blue) solution (0.1 M, 81 mg in 1 mL of anhydrous acetonitrile) was used as a p-type dopant (oxidative doping), 0.5 μL of this solution was added to the dried sample on the electrode and it was left for dry for an hour before measurement in air.

4.3. Results and Discussion

The reaction was performed using a yellow aqueous dispersion of 6-thioguanosine and a solid Cu(I) salt, $\text{Cu}(\text{MeCN})_4\text{BF}_4$, in an equimolar ratio, 1:1 (Figure 4.3). After five minutes of mixing, a yellow-orange solution (**1**) appeared at room temperature. The use of MeCN ligand was because it is a good leaving group and there is no conflict with sulfur because it binds more strongly to metal. Although attempts to crystallize were made; hydrothermal methods, solvent evaporation or solvent layering, all of them were unsuccessful. The reaction mixture **1** was first analyzed in order to determine its chemical structure.

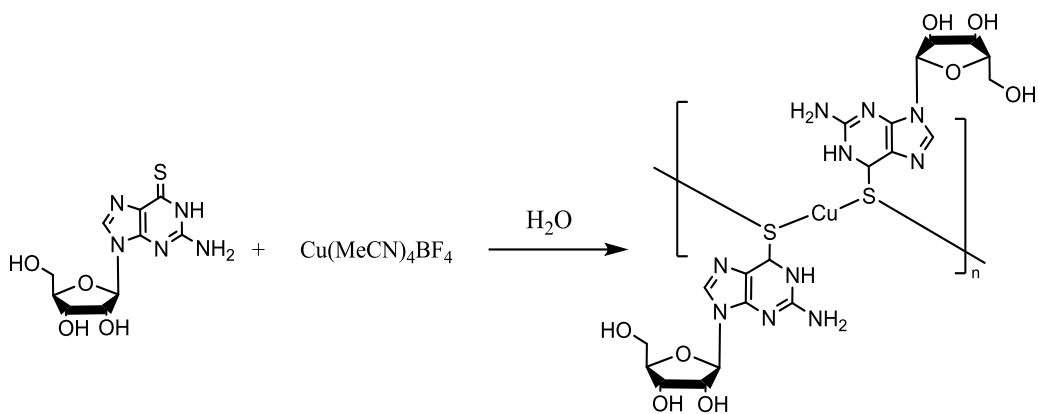


Figure 4.3. Scheme of 6-thioguanosine Cu(I) complex preparation.

Initially it was decided to determine the oxidation state of Cu ions in **1** between the two possible forms (I) and (II), for that reason a measurement of magnetic susceptibility at room temperature was carried out by Cameron Doherty. The magnetic susceptibility measured the response, attractive or repulsive, of **1** to a magnetic field induced. The reading of magnetic susceptibility in the instrument was -0.51 for a 30 mM sample of **1** meaning that it is a diamagnetic sample and then Cu(I) has an electronic configuration d^{10} , following Equation 1 (M indicates magnetic field of the sample and B magnetic field induced to the sample).²⁸

$$X = \frac{M}{B} \quad (\text{Eq. 1})$$

Mass spectroscopy confirmed the complexation of the metal ion. MALDI-Tof mass spectroscopy shows results that confirms the presence of oligomeric chains in the sample supporting the formation of a coordination polymer. The oligomeric species found correspond to, 1085.2 m/z for $[\text{Cu}_3\text{L}_3]^+$, 1084.97 m/z calculated; 1148.1 m/z for $[\text{Cu}_4\text{L}_3]^+$, 1147.9 m/z calculated; 1511.0 m/z for $[\text{Cu}_5\text{L}_4]^+$, 1510.89 m/z calculated. L corresponds to a deprotonated, anionic form of 6-thioguanosine, the ion $[\text{C}_{10}\text{H}_{12}\text{N}_5\text{O}_4\text{S}]^-$ (Appendix, Figure A4). This data suggests that a coordination polymer

is formed, further analysis of **1** it supports the formation of a polymeric structure as discussed below.

The comparison of UV-Vis absorbance for 1 mM of the ligand in basic solution, to help its solubility, and **1** display changes in the spectrum with the introduction of the metal ion as shown Figure 4.4. The main peak for the ligand, in thiol form, appears at 313 nm and it corresponds to a $\pi\text{-}\pi^*$ transitions of the thiol group.^{29,30} This peak is red shifted for **1** to 358 nm and broadened while also shows a small shoulder at around 417 nm,^{26,31} this suggests that Cu(I) ions are interacting with sulfur atoms. Also, the peaks corresponding to **1** are produced by $\pi\text{-}\pi^*$ or $n\text{-}\pi^*$ transitions, expected for Cu-thiolate compounds that confirms the presence of a coordination polymer for **1**.^{25,32} Peaks below 300 nm are due to the nucleobase,³³ associated to $\pi\text{-}\pi^*$ transitions of the purine ring,³⁴ and these are also present in **1**.

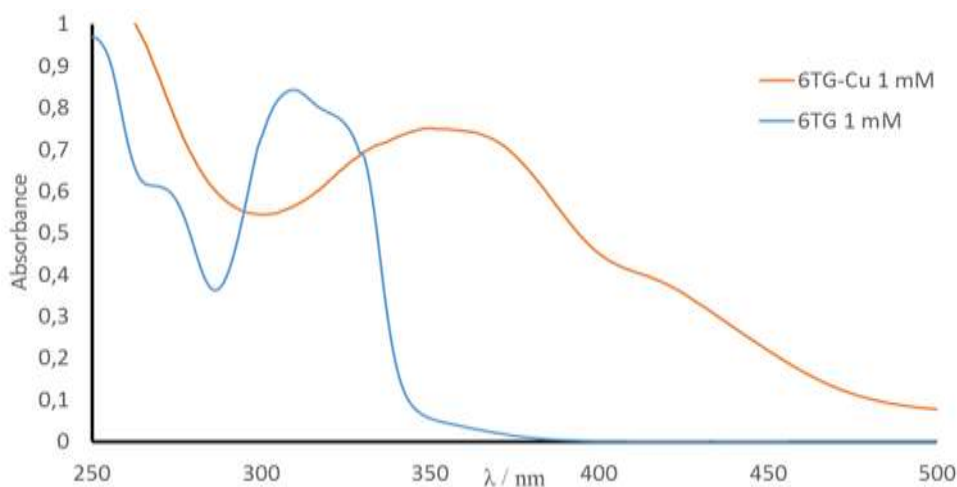


Figure 4.4. UV-Vis spectrum for a basic solution of 6-thioguanosine (blue line) and **1** (orange line).

FTIR experiment on **1** as a dry xerogel shows a different spectrum than the ligand (Figure 4.5 a,b). FTIR bands belonging to sulfur groups have been located in the ligand, they appear in the area of 1200 cm^{-1} for C=S, 770 cm^{-1} for C-S stretching

vibrations and 2525 cm^{-1} for S-H stretching band.³⁵⁻³⁷ For **1** the bands for C=S and C-S groups are less intense than in the ligand (Figure 4.5a) and the S-H disappear (Figure 4.5b). The decrease in intensity of bands related to the sulfur atoms suggests that Cu(I) is modifying the sulfur environment and it is due to the complexation of Cu(I) to sulfur atoms.

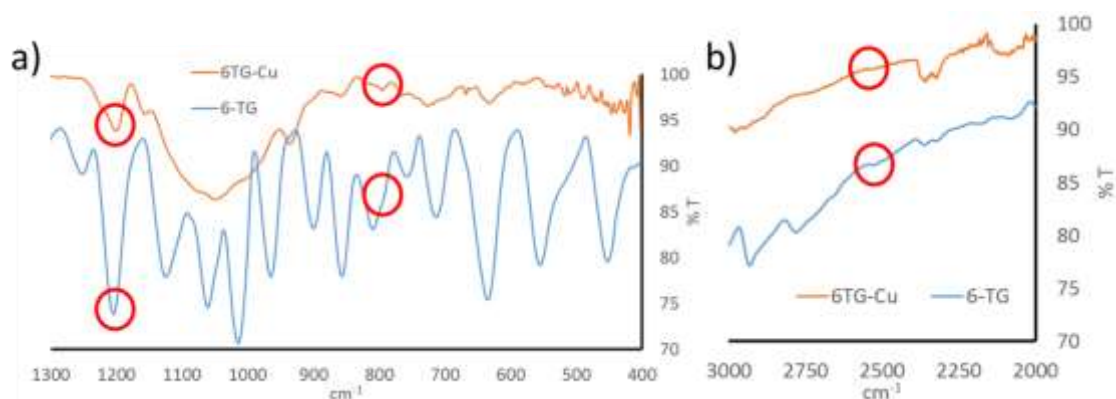


Figure 4.5. FTIR spectrum for 6-thioguanosine as a solid (blue line) and a dried solution of **1** (orange line), a) data showed between 400 and 1300 cm^{-1} and red circles indicates characteristic carbon-sulfur bands. b) data showed between 2000 and 3000 cm^{-1} and red circles indicates characteristic sulfur-hydrogen band.

Circular dichroism (CD) spectroscopy gave some insight about the structure of **1** using the chirality of the ligand as a reference. Figure 4.6 shows the CD spectrum for a basic solution of 6-thioguanosine (10 mM) with positive peaks at 228 and 260 nm and negative peaks at 209, 246 and 322 nm confirming the chirality of the molecule. Comparing these results with the spectrum of **1** at 1 mM there is a difference in the assembly process as a consequence of a coordination polymer formation and its high molecular ordered structure.^{38,39} A characteristic feature of this polymeric structure is the chirality attributed to the ribose ring but is also often ascribed to a helical configuration,⁴⁰ the negative signal in the spectrum of **1** below 200 nm is an evidence

for a right-handed orientation of the helicity, it will be discussed along with AFM data later.^{39,41,42}

Although the assignment of each band of the CD spectrum with a specific transition is difficult without the additional help of spectroscopic or computational studies, it is possible to extract further information from the CD spectrum. The signal at lower energy than 300 nm are usually affected by the sulfur environment on 6-thioguanosine³⁰ and the inversion of the signal observed for **1** around 320 nm is related to a different assembly process compared to the ligand. It suggests an interaction between Cu(I) ions and sulfur atoms of the ligand caused by the coordination polymer formation. In addition, the band due to π - π^* transitions of the purine around 260 nm is also affected in **1** so the electronic environment of the ligand has been modified by Cu(I) ions and it is reflected in a polymeric arrangement where the ligand is organized along the chain.^{43,44}

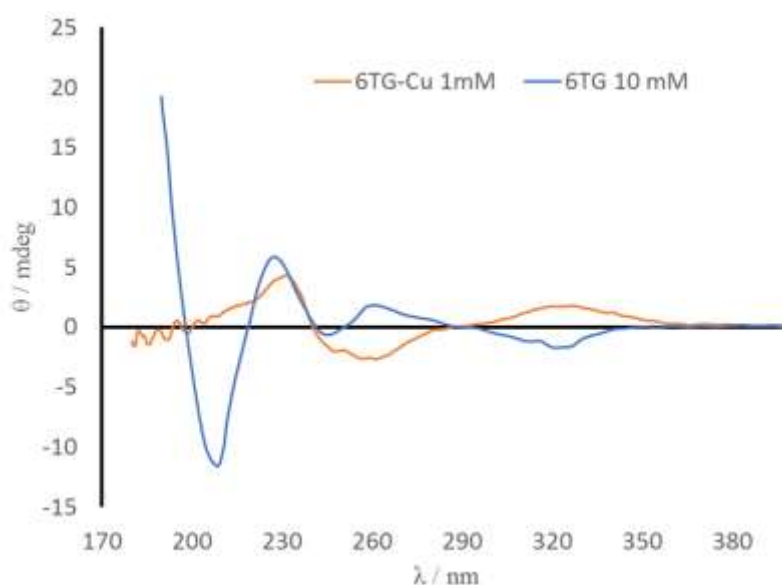


Figure 4.6. CD spectrum for a basic solution of 6-thioguanosine at 10 mM (blue line) and **1** at 1 mM (orange line).

Further structural analysis of **1** includes SEM microscopy on xerogel form. Figure 4.7 shows interesting morphological features for **1** as a material made of fibres that intertwine. In addition, such fibres of microns in length, form a layered structure that covers the surface of the dry sample. This picture clarifies the structural conformation of **1**, and they suggest the formation of a coordination polymer network in support of the MALDI-ToF mass spectroscopy and circular dichroism data. Since the resolution of SEM is not very clear, further microscopic studies with AFM were undertaken.

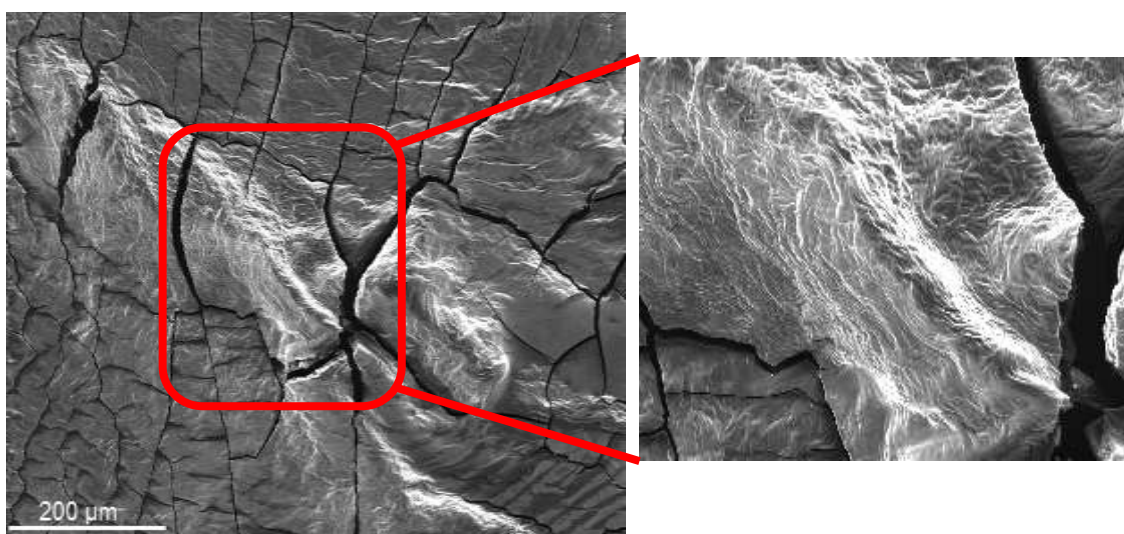


Figure 4.7. SEM image for a dried solution of **1**. Left image show the network of the polymer and right image it is possible to appreciate fibres entangling.

Atomic force microscopy analyzed **1** in xerogel form deposited on mica with the aim of confirming the presence of a polymeric structure and clarify the morphology of these strands. Figure 4.8a shows that **1** conforms layers of fibres that interact intertwining between them forming a network, it is possible to see the presence of single fibres and fibres associates. The length for single fibres varying between 130 and 550 nm with an average of 240 nm and cross-sectional heights around 2 nm (Figure 4.8b, 4.9a) in accordance to similar Cu(I) thiolate compounds where Cu(I) ions is coordinating three

thiolate ligands.²² Most of the fibres are associates, such fibres have a length varying between 800 nm and 3.5 μm with a typical average of 2.5 μm and a regular cross-sectional height around 5 nm (Figure 4.8b, 4.9a). The difference in height between single fibres and associates is coherent with an arrangement where single fibres are placed on top of each other and as a result thicker fibres are observed. Another physical difference between these two fibres arrangements is a markedly less curvature of fibres associates indicating less flexibility of the chains and it suggests strong interactions inter the fibres that constitute the fibre associate.

CD spectroscopy showed that **1** is a chiral complex and it is confirmed under AFM due to a helix formation (Figure 4.9b). The interaction of 2 individual strands lead to the formation of helical fibre associates with the height around 5 nm and a regular periodicity of the helix around 8 nm (Figure 4.9b). Features showed in Figure 4.9b by the fibre associated indicates a right-handed sense of the helix.

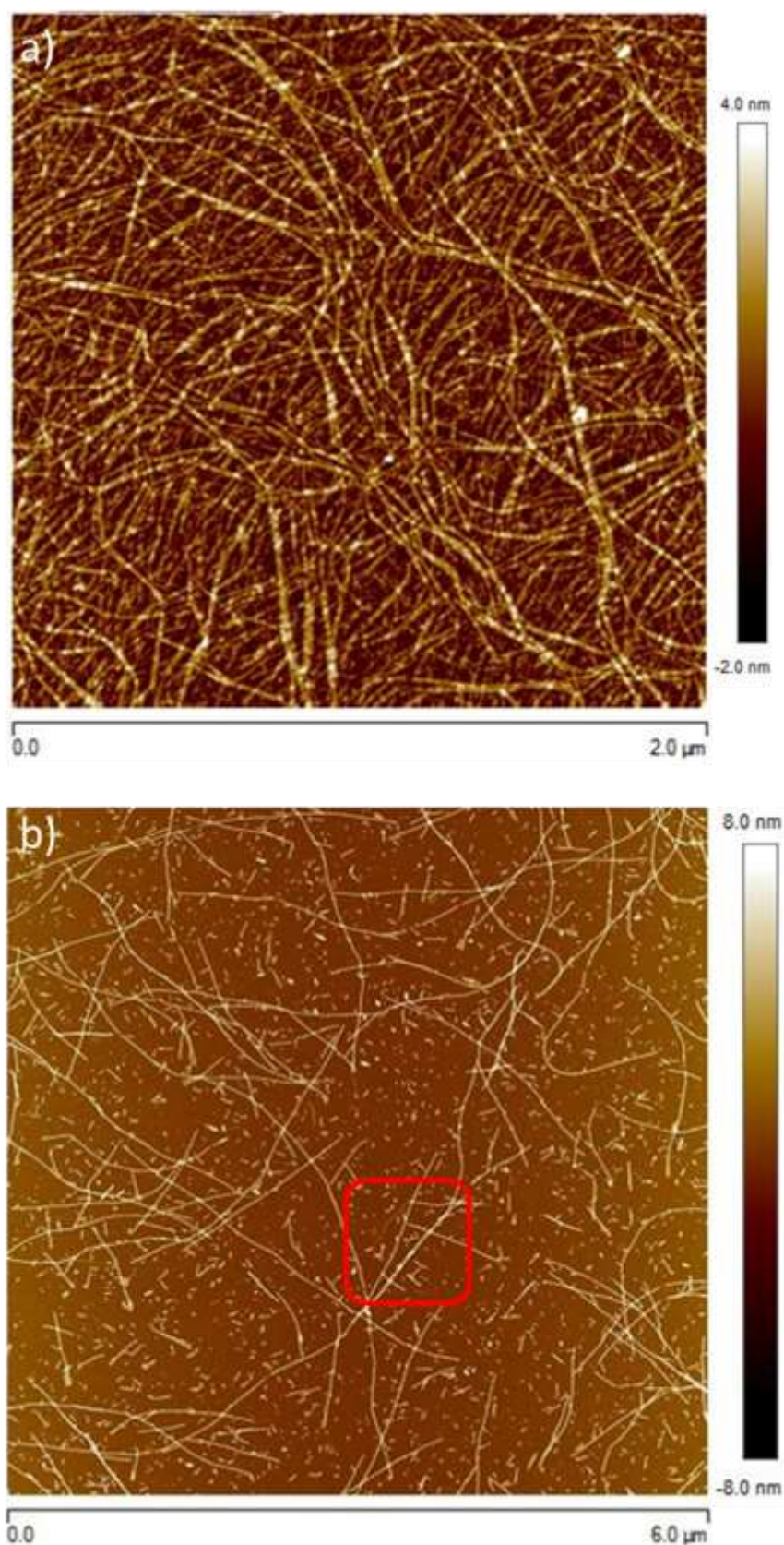


Figure 4.8. AFM image for **1** at 0.1 mM concentration in water and dried on mica (a) and **1** hundred times diluted in water and dried on mica (b). Red box indicates the difference between single fibres and associates, analyzed below.

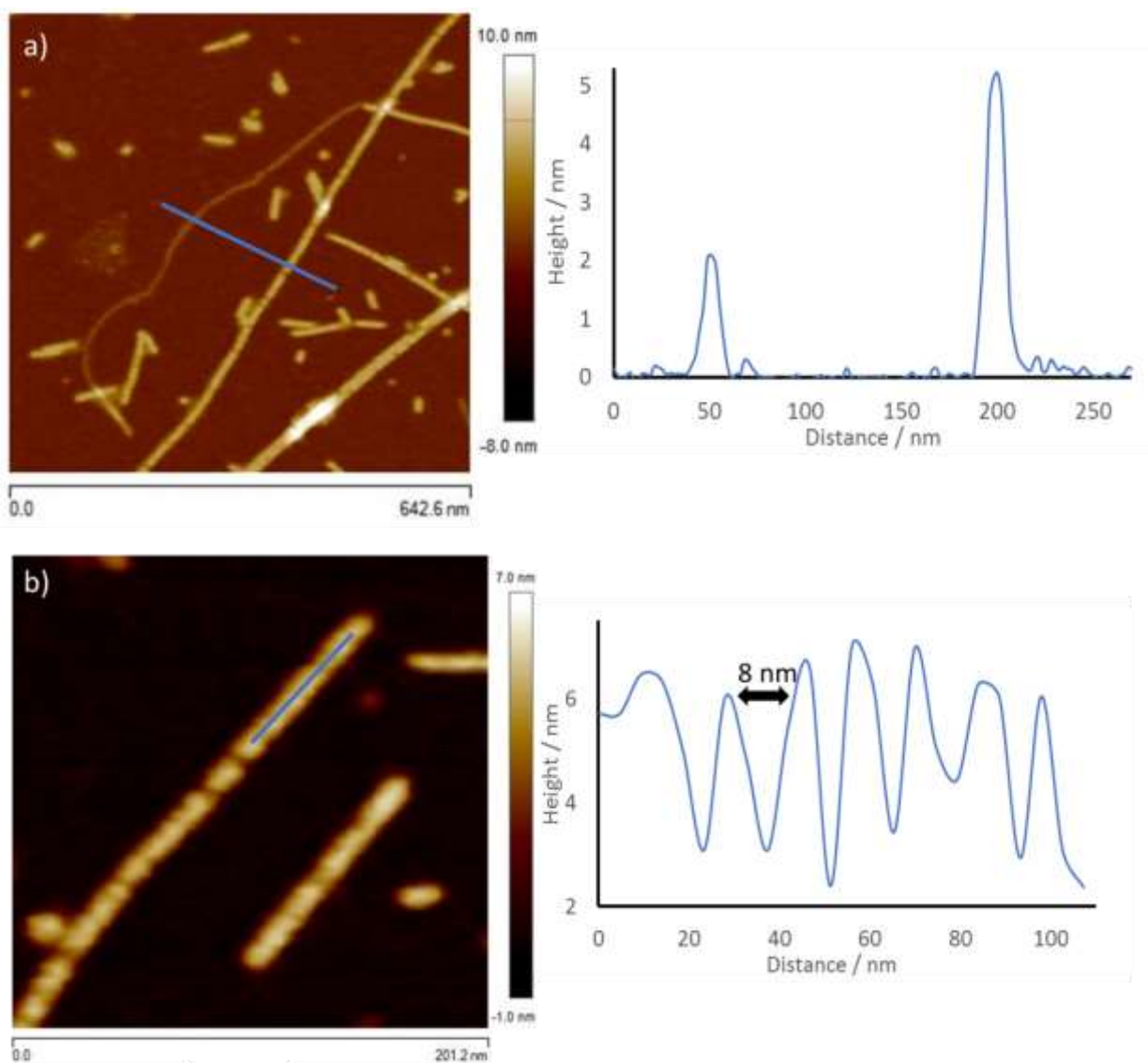


Figure 4.9. AFM image for a dried solution of **1** at 0.001 mM in water and dried on mica (a) indicating the difference in heights between single fibres and associates and (b) helical fibre associate indicating that the periodicity of the helix is 8 nm.

To finish with the structural characterization, a structure can be proposed for compound **1**. Mass spectroscopy showed the oligomeric nature of **1** confirming the interaction between Cu(I) ions and sulfur atoms forming a chain with a Cu(I)-sulfur backbone. To corroborate the Cu(I)-sulfur bond, UV-Vis and FTIR spectroscopies were performed. They showed modifications on the electronic environment of the

ligand in presence of Cu(I) ions suggesting the existence of a coordinate bond between Cu(I) ions and sulfur atoms. Besides, CD spectroscopy showed a strong signal for **1** in comparison to the free ligand in solution, coherent with an increase in the ordering of the molecules and it is due to the polymeric nature of **1**. The chiral organic part of the ligand is oriented outside the main chain of the polymer as literature showed before to avoid any steric impairments between them.²²

Microscopic techniques confirmed the formation of a one-dimensional coordination polymer with a chain like structure. SEM images showed a fibres network in all the sample surface and AFM was able to verify previous assumptions. AFM images showed one-dimensional strands equivalent in shape and heights to others Cu(I) coordination polymers,²² where Cu(I) ions are coordinating three sulfur atoms forming a tubular chain (Figure 4.10 a,b). In addition, these fibres interact one on top of each other producing helical stiff fibres associates with several microns in length. Although further calculations need to be done to find out the nature of the interaction between individual strands of Cu(I)-thiolate polymer it can be proposed that ligand substituents are interacting between them through base stacking interactions above and below the chain of the Cu(I) thiolate polymer (Figure 4.10c) similar to another Cu(I) coordination polymer.²⁵ For all the above, a one-dimensional coordination polymer is proposed as the structure of **1** with a Cu(I)-sulfur backbone (Figure 4.10).

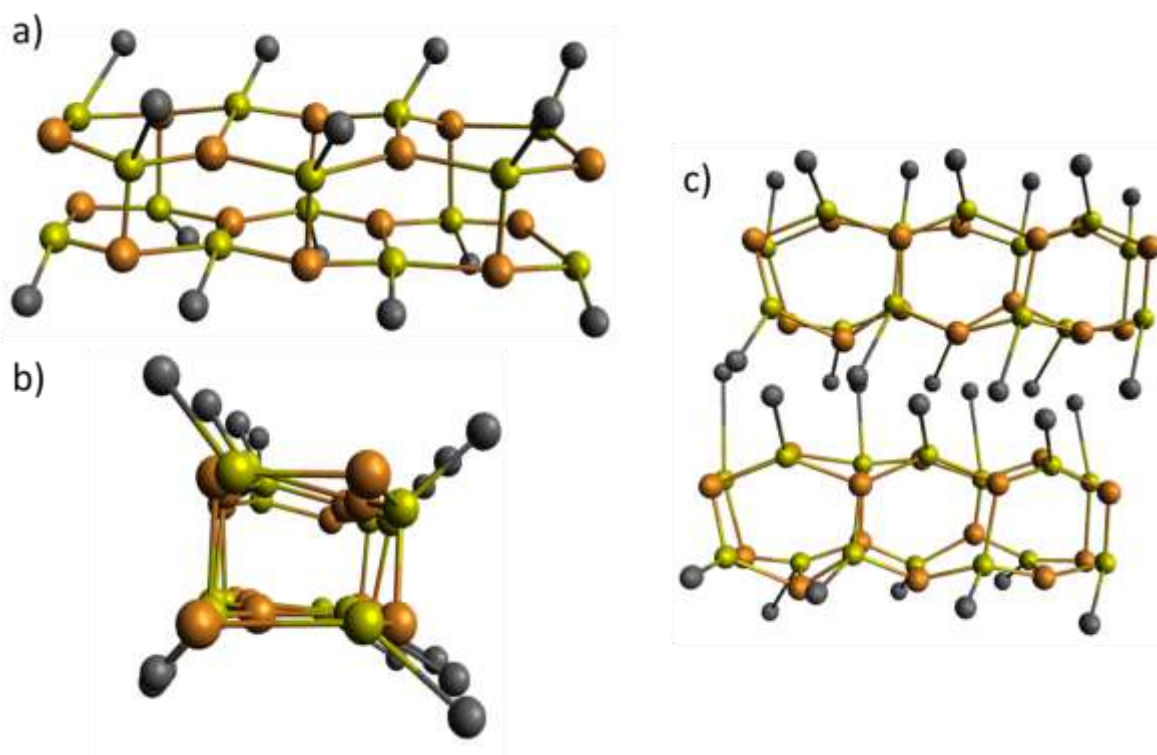


Figure 4.10. Proposed scheme models for the one-dimensional coordination polymer **1** structure. Side view (a) and central projection (b) of an individual fibre and side view of a fibre associate (c) (orange balls represent Cu(I) ions, yellow balls sulfur atoms and grey balls ligand substituent). These models were drawn on Avogadro software 1.2.0.

Opto-electronic properties of **1** were measured to establish interesting features of the Cu(I) thiolate polymer. Fluorescence spectroscopy was performed for a basic solution of 6-thioguanosine and **1**, both at 1 mM concentration. The maximum peak in the emission spectrum for the ligand is at 420 nm for excitation at 330 nm,³⁴ and for **1** appears around 580 nm and a small shoulder around 640 nm for excitation at 440 nm (Figure 4.11). Although both emission curves have a similar shape, its position is different due to the different excitation wavelength used. The main peaks are produced by the emission of the ligand, ligand-to-ligand charge transfer or intra ligand π - π^*

transitions.^{10,45} The low intensity of the shoulder at 640 nm for **1** is due to concentration effects and this peak is associated to ligand-to-metal charge transfer, metal-to-ligand charge transfer or a metal-centered transitions⁴⁶ which implies that Cu(I) is affecting luminescence properties of **1**. Similar results have been found for another Cu(I) thiolate polymer where luminescence measurements show two emission peaks that corresponds to a charge transfer between ligands and a charge transfer between the metal and the ligand.⁴⁷ The peak that appears around 800 nm for the ligand is attributed to the second order luminescence scattering.

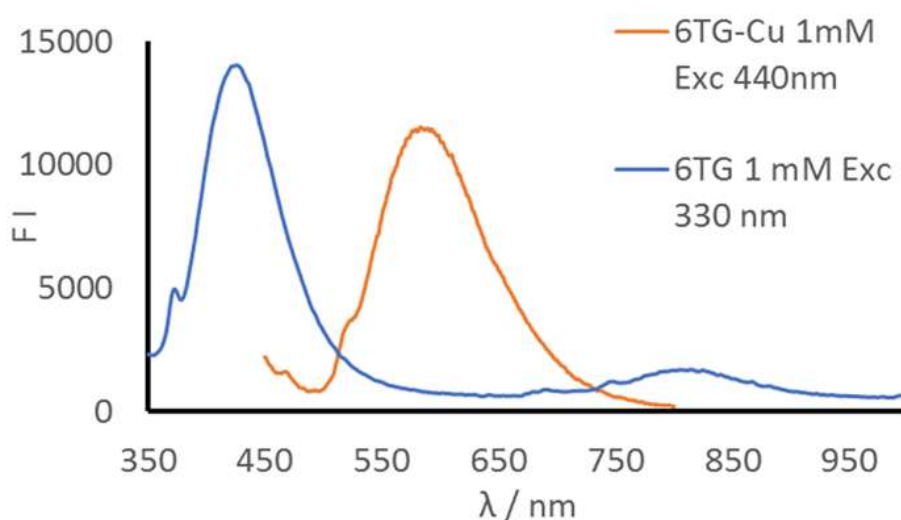


Figure 4.11. Luminescence spectra for a basic solution of 6-thioguanosine at 1 mM at 330 nm excitation (blue line) and for **1** at 1 mM at 440 nm excitation (orange line).

The electrical properties of **1** were investigated because of the possibility that the Cu(I) thiolate coordination polymer might conduct electrons in a manner analogous to those of other Cu(I) thiolate polymers.^{21,22,24} Conductance properties were measured on the xerogel form of **1** deposited on platinum microband electrodes. A dc voltage between -2 V to +2 V was applied in a series of potential steps to produce a current-voltage curve, I-V plot (Figure 4.12). Initially two measurements were performed, the bare

electrode background and **1** with maximum values of intensity of current of 320 fA and 490 fA respectively. This indicates that **1** has background levels of conductance and in this as-prepared state cannot be considered as electrically conductive. In addition, an extra measurement was performed using a redox dopant, Magic Blue, known to be a strong oxidant.⁴⁸ When the dopant was added to the sample a visible change in color was produced, from a bright orange to a darker orange. The use of the dopant improves the magnitude of the current a thousand times with respect to the background conductance (Figure 4.12) and it is a good signal in order to establish this material as an electrically conductive after doping.⁷ The same measurement was repeated three days later in order to know if the conductance remains stable. The result showed that the intensity of current decreased up to tens of picoamperes. The natural interpretation of this result is that samples in a homogeneous oxidation state are non-conductive due to the short length of polymers, but partial oxidation of the sample leads to electronic conduction by hopping of electrons from filled to empty sites. The value of conductance varied sensibly after a few days, which suggests that the polymeric chains were affected by the effect of the doping agent, perhaps breaking it.

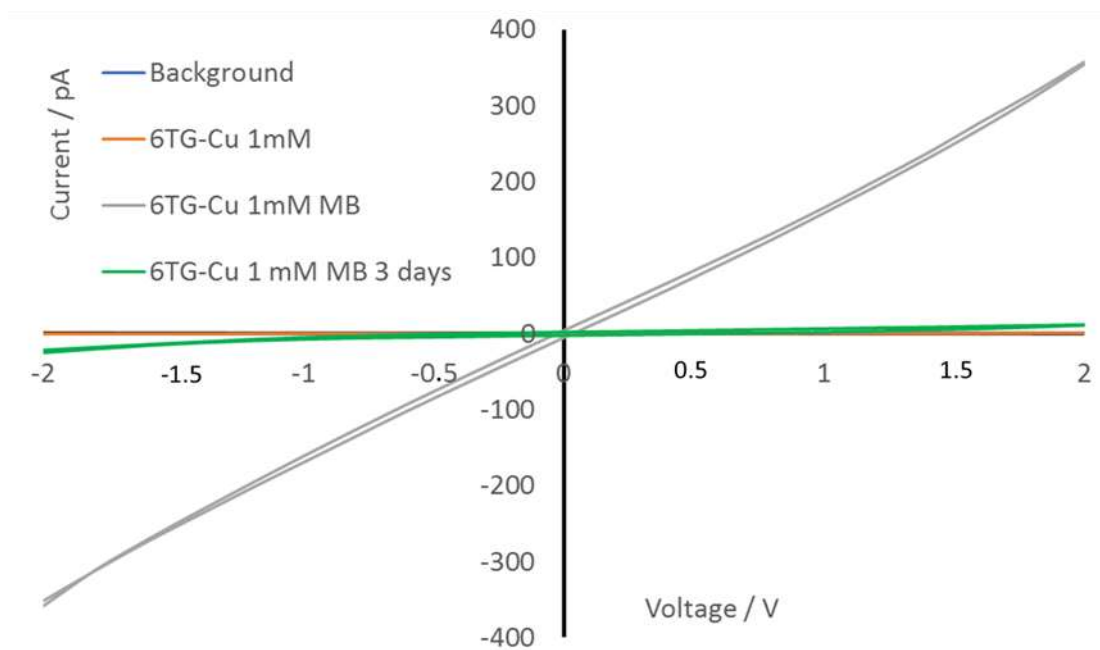


Figure 4.12. Two-terminal I-V characteristic of three samples; electrode background (blue line), 1 (orange line), 1 doped with Magic Blue (grey line) and 1 with Magic Blue measured three days later (green line).

4.4. Conclusions

We have prepared a new Cu(I) thiolate coordination polymer successfully. The reaction has been analyzed by a range of spectroscopic and microscopic techniques with the aim of proposing a structure for the reaction product. This characterization has led to propose that Cu(I) ions are attached to three sulfur atoms from the 6-thioguanosine forming a chain like structure, a one-dimensional coordination polymer with Cu(I)-sulfur backbone with interesting properties to explore.

Luminescence as well as conductance properties have been analyzed and established as the main properties of this material. Such properties, typical of semiconductors, are due to the interaction between Cu(I) ions and sulfur atoms through the polymer as metal sulfides features. The product exhibit fluorescence properties with a different

emission wavelength than the ligand and also, the product is electrically conductive after redox doping which is promising to consider that more concentrated samples will conduct electricity after doping. Therefore, the integration of this new class of material into larger DNA oligonucleotides can open a new field for the material functionalization.

4.5. References

- 1- Daniso, E., Maroh, B., Feldbacher, S., Mühlbacher, I., Schlögl, S., Melpignano, P., *Applied Surface Science* 2021, **552**, 149408.
- 2- Dong, Y., Liu, D., Yang, Z., *Methods* 2014, **67**, 116-122.
- 3- Wilner, O., Willner, I., *Chem. Rev.* 2012, **112**, 2528-2556.
- 4- Escher, D., Müller, J., *Z. Anorg. Allg. Chem.* 2021, **647**, 513-518.
- 5- Ono, A., Cao, S., Togashi, H., Tashiro, M., Fujimoto, T., Machinami, T., Oda, S., Miyake, Y., Okamoto, I., Tanaka, Y., *Chem. Commun.* 2008, 4825-4827.
- 6- Linares, F., Garcia, E., Lopez, F., Domingo, M., Orte, A., Rodriguez, A., Galindo, M., *Chem. Sci.* 2019, **10**, 1126-1137.
- 7- Al-Mahamad, El-Zubir, O., Smith, D., Horrocks, B. R., Houlton, A., *Nat. Commun.* 2017, **8**, 720.
- 8- Shinde, D., Patil, S., Cho, K., Ahn, D., Shrestha, N., Mane, R., Lee, J., Han, S., *Adv. Funct. Mat.* 2015, **25**, 5739-5747.
- 9- Guo, Y., Wu, W., Li, Y., Lu, N., Mao, K., Bai, Y., Zhao, J., Wang, J., Zeng, X., *Nanoscale Horiz.* 2019, **4**, 223-230.
- 10- Yam, V., Au, V., Leung, S., *Chem. Rev.* 2015, **115**, 7589-7728.
- 11- Carvajal, M., Novoa, J., Alvarez, S., *J. Am. Chem. Soc.* 2004, **126**, 1465-1477.
- 12- Wang, Q., Dong, S., Tao, D., Li, Z., Jiang, Y., *Coord. Chem Rev.* 2021, **432**, 213717.
- 13- Veselska, O., Demessence, A., *Coord. Chem. Rev.* 2018, **355**, 240-270.
- 14- Grozdanov, I., Najdoski, M., *J. Sol. St. Chem.* 1995, **114**, 469-475.
- 15- Achimovicova, M., Dutkova, E., Tothova, E., Bujnakova, Z., Briancin, J., Kitazono, S., *Frontiers of Chemical Science and Engineering* 2019, **13**, 164-170.
- 16- Safrani, T., Jopp, J., Golan, Y., *RSC Adv.* 2013, **3**, 23066-23074.
- 17- Roy, P., Srivastava, S., *CrystEngComm* 2015, **17**, 7801-7815.
- 18- Isac, L., Cazan, C., Enesca, A., Andronic, L., *Frontiers in Chemistry* 2019, **7**, 694.
- 19- Hsu, Y., Chen, Y., Lin, Y., *Electrochimica Acta* 2014, **139**, 401-407.
- 20- Baumgartner, M., Schmalle, H., Baerlocher, C., *J. Sol. St. Chem.* 1993, **107**, 63-75.

- 21- Zhang, Y., Xia, T., Yu, K., Zhang, F., Yang, H., Liu, B., An, Y., Yin, Y., Chen, X., *ChemPlusChem* 2014, **79**, 559-563.
- 22- Che, C., Li, C., Chui, S., Roy, V., Low, K., *Chem. A Eur. J.* 2008, **14**, 2965-2975.
- 23- Yan, H., Hohman, J., Li, F., Jia, C., Solis, D., Wu, B., Dahl, J., Carlson, R., Tkachenko, B., Fokin, A., Schreiner, P., Vailionis, A., Kim, T., Devereaux, T., Shen, Z., Melosh, N., *Nat. Mat.* 2017, **16**, 349-355.
- 24- Low, K., Roy, V., Chui, S., Chan, S., Che, C., *Chem. Commun.* 2010, **46**, 7328-7330.
- 25- Veselska, O., Podbevsek, D., Ledoux, G., Fateeva, A., Demessence, A., *Chem. Commun.* 2017, **53**, 12225-12228.
- 26- Veselska, O., Cai, L., Podbevsek, D., Ledoux, G., Guillou, N., Pilet, G., Fateeva, A., Demessence, A., *Inorg. Chem.* 2018, **57**, 2736-2743.
- 27- Zhou, F., Yue, C., Zhang, H., Lei, X., *Acta Crystallographica Section C* 2013, **69**, 1478-1481.
- 28- Nguyen, P., Do, T., Nguyen, T., (ed.) 2020, *Smart Nanocontainers*, Elsevier, ch. 14, 229-250.
- 29- Zhang, Y., Zhu, X., Smith, J., Haygood, M., Gao, R., *J. Phys. Chem. B* 2011, **115**, 1889-1894.
- 30- Repges, R., Beuck, C., Weinhold, E., Raabe, G., Fleischhauer, J., *Chirality* 2008, **20**, 978-984.
- 31- Yam, V., Lo, K., Wang, C., Cheung, K., *J. Phys. Chem. A* 1997, **101**, 4666-4672.
- 32- Zhang, M., Li, H., Li, H., Lang, J., *Dalton Trans.* 2016, **45**, 17759-17769.
- 33- Sapunar, M., Domcke, W., Doslic, N., *Phys. Chem. Chem. Phys.* 2019, **21**, 22782-22793.
- 34- Rubin, Y., XVI Int. Conf. on Spectroscopy of Molecules and Crystals, Sevastopol, Ukraine, 2004.
- 35- Kamalendra, S., Yadav, R., Yadav, J., *Spectrochimica Acta* 1991, **47A**, 819-820.
- 36- Aulakh, J., Lobana, T., Sood, H., Arora, D., Kaur, R., Singh, J., Garcia, I., Kaur, M., Jasinski, J., *RSC Adv.* 2019, **9**, 15470-15487.
- 37- Odriozola, I., Ormategui, N., Loinaz, I., Pomposo, J., Grande, H., *Macromolecular Symposia* 2008, **266**, 96-100.
- 38- Lam, A., Guenther, R., Agris, P., *Biometals* 1995, **8**, 290-296.
- 39- Zimmer, C., Luck, G., Holy, A., *Nucleic Acids Research* 1976, **3**, 2757-2770.
- 40- Zhang, H., Zheng, X., Kowk, R., Wang, J., Leung, N., Shi, L., Sun, J., Tang, Z., Lam, J., Qin, A., Tang, B., *Nat. Commun.* 2018, **9**, 4961.
- 41- Sutherland, J., Griffin, K., Takacs, P., *Proc. Natl. Acad. Sci. USA* 1981, **78**, 4801-4804.
- 42- Sprecher, C., Baase, W., Johnson, C., *Biopolymers* 1979, **18**, 1009-1019.

- 43- Khani, S., Faber, R., Santoro, F., Hättig, C., Coriani, S., *J. Chem. Theory Comput.* 2019, **15**, 1242-1254.
- 44- Gladysz, M., Andralojc, W., Czapik, T., Gdaniec, Z., Kierzek, R., *Scientific Reports* 2019, **9**, 4385.
- 45- Xie, H., Kinoshita, I., Karasawa, T., Kimura, K., Nishioka, T., Akai, I., Kanemoto, K., *J. Phys. Chem. B* 2005, **109**, 9339-9345.
- 46- Song, J., Li, S., Zhou, R., Shao, J., Qiu, X., Jia, Y., Wang, J., Zhang, X., *Dalton Trans.* 2016, **45**, 11883-11891.
- 47- Delgado, S., Sanz, P., Priego, J., Jimenez, R., Gomez, C., Zamora, F., *Inorg. Chem.* 2008, **47**, 9128-9130.
- 48- Hofmann, A., Kroon, R., Zokaei, S., Järsvall, E., Malacrida, C., Ludwigs, S., Biskup, T., Müller, C., *Adv. Elec. Mat.* 2020, **6**, 2000249.

**Chapter 5. Preparation and characterization of coordination polymers
hydrogels designed from 6-thioguanosine with Ag(I) and Cu(I) coinage metal
ions**

This chapter is partially based upon the following publication:

Osama El-Zubir, Pablo Rojas Martinez, Gema Dura, Lamia L. G. Al-Mahamad,
Thomas Pope, Thomas J. Penfold, Lewis E. Mackenzie, Robert Pal, Jackie Mosely,
Fabio Cucinotta, Liam F. McGarry, Benjamin R. Horrocks, Andrew Houlton, *J. Mater
Chem C* 2022, **10**, 7329-7335

Table of Contents

5.1. Introduction.....	112
5.2. Materials and Methods	119
5.3. Results and Discussion	121
5.3.1. 6-Thioguanosine and Ag(I)	121
5.3.2. 6-Thioguanosine and Cu(I).....	131
5.4. Conclusions.....	144
5.5. References	145

5.1. Introduction

In chapter 1 it has been defined what is a hydrogel and its classification between chemical and physical gels. Specifically, supramolecular gels are referred to physical gels where fibres, of low molecular weight gelators (LMWGs), self-assemble and crosslink non-covalently to form a gel network with water molecules trapped inside.^{1,2} The route of formation of such three-dimensional gels start with microscopic entities that assemble into large one-dimensional fibres and ends by the fibres forming bundles that interact between them to form self-assembled fibrillar network.¹

These supramolecular gels and in particular, low-molecular weight gelators, are of a great interest due to their versatile structural and functional capabilities. They can be built from a variety of gelators such as amides,³ *n*-alkanes⁴ or dendrimers⁵ by combination of different low-molecular weight gelators.⁶⁻⁸ It is important to report that supramolecular gels can be also prepared by metal coordination complexes and they are called metallogels (Figure 5.1).⁹ Metallogels are compounds where metals can participate in different ways inside the gel network. These metals can be part of coordination complexes or coordination polymers, usually linking organic ligands and as nanoparticles attached to the gel.⁹ Mainly, the formation of coordination polymers that self-intertwine are responsible of the formation of a three-dimensional network with water molecules caught inside the net.¹⁰

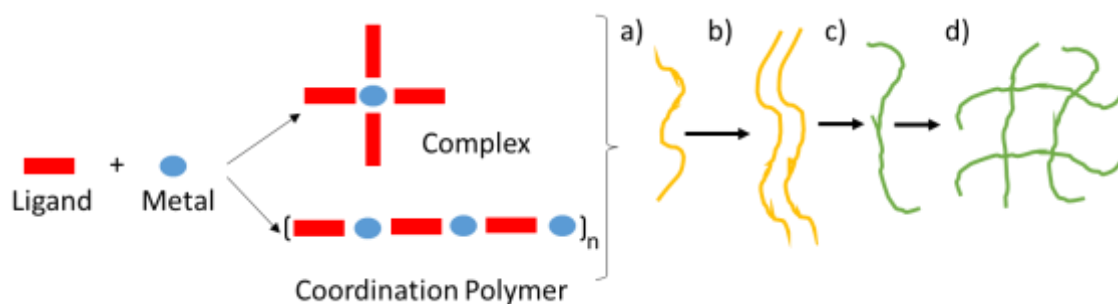


Figure 5.1. Scheme of the preparation of metallogels. These supramolecular hydrogels can be prepared from complexes or coordination polymers and ligands act as a gelator. The complexes or coordination polymers can form fibres (a) that self-assemble (b) forming larger nanofibers (c) that entangled forming a supramolecular network where water molecules get trapped (d).

Metallogels formed from metal ions like Ag(I) or Cu(II) with pyridyl ligands have showed interesting luminescence features.^{11,12} Besides, other metallogels coordination polymers have found interest in sensing,¹³ catalysis¹⁴ or magnetism¹⁵ and other applications due to the physical properties of gel networks.¹⁶ In addition, it has been reported studies related to the design of gelators with specific bonding sites to metal ions that potentially bring a supramolecular gel with tunable properties.¹⁷ These gelators are based on different parts with a specific function for each one, e.g. a cholesteryl moiety provides hydrophobic interactions and a pyridine derivative contributes with metal interactions. Different metal ions have been used in this regard such as Ag(I), Zn(II) and Pd(II).¹⁷

The fact that supramolecular gels are based on self-assemble interactions makes the use of molecules derivatives from DNA or RNA with specific non-covalent interactions a very interesting approach to prepare gels. So, the capacity of nucleosides, nucleotides or nucleic acids to self-interact specifically by hydrogen bonds following

the Watson-Crick model, bring the possibility to design supramolecular assemblies.^{18,19} Generally, in a nucleoside it is possible to distinguish specific non-covalent locations where hydrogen bond occurs as well as metal coordination interaction (Figure 5.2).¹⁹ The self-assembly properties of nucleobases are not equivalent to affirm that they form hydrogels, only guanine forms it without modification on its molecule.¹ Also, guanosine monophosphate hydrogel has been explored since early twentieth century^{20,21} and it was established that its structure is based on the formation of helical arrangements settle by the stacking of the nucleobases that forms G4-quarters with the aid of metal ions (Figure 5.3).^{1,22} It has also presented different structures of guanosine such as linear tapes²³ or macrocycles²⁴ and recently it has been discovered interesting biological applications for those complexes, such as aptamers for therapeutical treatment.²⁵

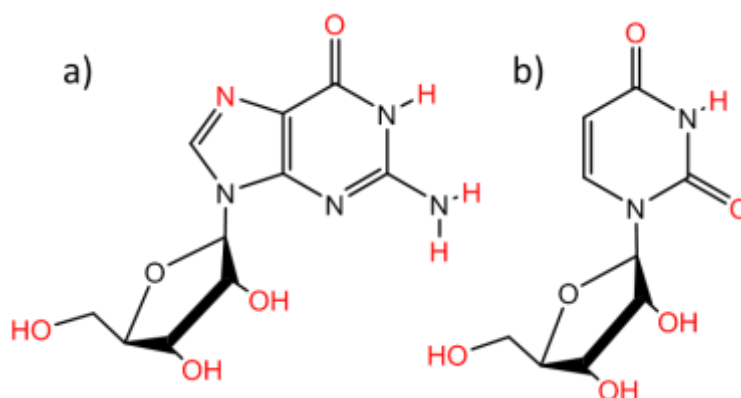


Figure 5.2. Nucleoside representation of a) guanosine and b) uridine. In red positions are highlighted chemical groups where non-covalent interactions may occur. In addition, metal interactions can be located in position N3 and O4.

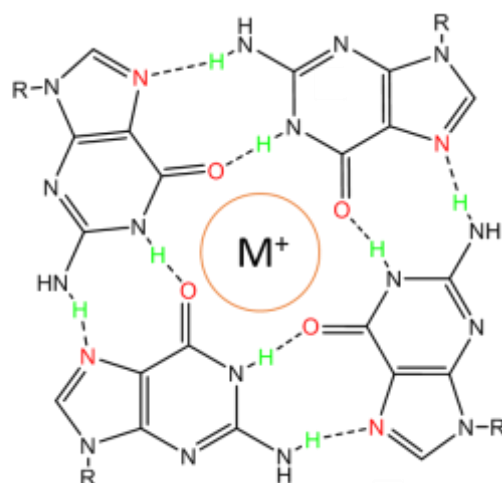


Figure 5.3. Hydrogen bonds interactions between guanine molecules to form G-quartets formed in presence of metal ions, e.g. K^+ . R= ribose ring.

Although other studies have focused in the combination of natural nucleosides by hydrogen bond with different molecules to prepare hydrogel systems,^{26,27} most of the approaches have used derivatized nucleoside and nucleotide as low molecular weight gelators.¹ The general method follows to modified nucleosides and nucleotides is to attach lipophilic groups to them in order to increase hydrophobicity on the system without loss of hydrophilicity in order to produce hydrogelation.¹ This, in combination with inherent hydrogen bonds and π stacking capabilities of nucleobases, causes stable gel networks.¹⁸ Some of the examples that illustrate this approach is the modification of cytidine with acyl chains (Figure 5.4a),²⁸ 2'-deoxyadenosine (Figure 5.4b)²⁹ or more complexes structures built on the combination of nucleobases with other biomolecules like peptides³⁰ or sugars (Figure 5.4c).³¹

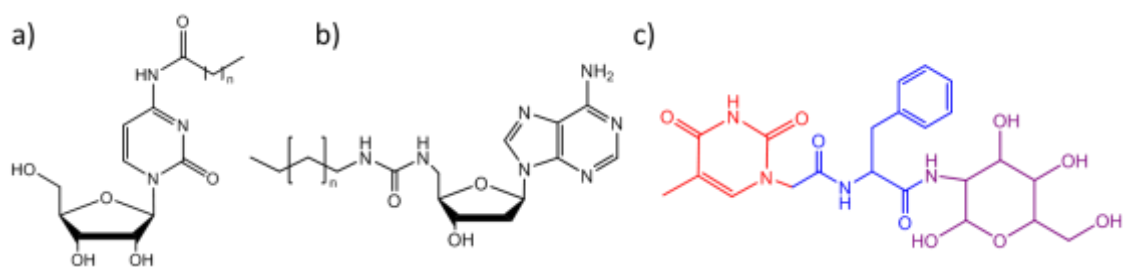


Figure 5.4. Examples of LMWG derived from nucleosides; a) cytidine functionalized with fatty acid ($n=10, 12, 14, 16$), b) 2'-deoxyadenosine modified with alkyl chain ($n=3, 5, 9$) and c) combination of a nucleoside (thymine in red), an amino acid (phenylalanine in blue) and a glycoside (glucosamine in purple).

The interaction of nucleobases with metal ions has been analyzed in chapter 1 but here we will delve into the hydrogel formation process. The presence of metal ions can modify the supramolecular properties of nucleobases, the effect on guanosine to form G-quartets was cited above but also the fact that the coordination bond substitutes hydrogen bond could affect the stability of the gel. Besides, inherent metal properties, such as electrical or magnetic, can be introduced in the supramolecular network.¹⁹ Here are highlighted some of metal ions used in metal-nucleobase interaction that form supramolecular networks like Zn(II)³² or Pt(II).³³ In addition, all of these supramolecular structures based on low molecular weight gelators are highlighting in potential applications.⁶ There is a current interest in the use of these compounds in sensing,³⁴ optoelectronics,³⁵ or drug delivery.³⁶

The focus of our investigation is the use of thio-modified nucleobases with the capacity to attach metal ions forming coordination polymers. So, specifically, there are few examples where thiolate coordination polymers are forming hydrogels. The first one reported consists in a self-assembly of Au(I) glutathione polymers with biomedical applications, such as drug delivery.³⁷ The two-dimensional thiolate coordination

polymer that forms the hydrogel is composed by a Au(I)-glutathione one-dimensional polymeric structure that self-assemble into a lamellar structure where Au(I) atoms are coordinating three sulfur atoms through the plane and glutathione hydrophilic substituents are in top or above the plane.³⁸ This polymer is stabilized by Au(I)-Au(I) interactions, metallophilic interactions.³⁹ To form the three-dimensional structure characteristic of a hydrogel, these layers are self-interacting with water molecules inter-layered allowing non-covalent connection between layers.³⁷ Later, the same research group extended the study to the rest of coinage metal ions, Ag(I) and Cu(I) and their interaction with glutathione (Figure 5.5a). These studies stated the importance of metallophilic interactions to adhere coordination polymers and then form hydrogels with biomedical applications, such as in tissue engineering and in controlled drug release.⁴⁰ These metallophilic hydrogels⁴¹ are also formed with a small thiol, *N,N*-dimehtyl-3-mercaptopropanamide and Ag(I) ions. The hydrophilic properties of the ligand substituents make possible self-assembly interactions between two-dimensional coordination polymers to form a supramolecular hydrogel with thermo-reversible properties (Figure 5.5b).⁴² The same group has also investigated the interaction of coinage metals with a drug, *N*-acetyl-L-cysteine, to form a hydrogel with drug-delivery properties.⁴¹ The hydrogels were formed by the self-assemble of thiolate coordination polymers and they exhibit different thermal stabilities possibly due to the different degree of metallophilic interactions within them.⁴¹ The last study directly related to the above, is the preparation of argentophilic hydrogels.⁴³ The formation of supramolecular hydrogels composed by coordination polymers stabilized by metallophilic interactions, that self-assemble through non-covalent interactions, can be modified by changing the nature of thiols.⁴³ In such a way that the interaction between Ag(I) with neutral thiols like 1-thioglycerol or *N*-acetyl-L-cysteine methyl ester results in a tetrameric fibrillar structure; or with acidic thiols like *N*-acetyl-L-cysteine or

glutathione lead to the formation of long polymers with a layered structure (Figure 5.5c).⁴³

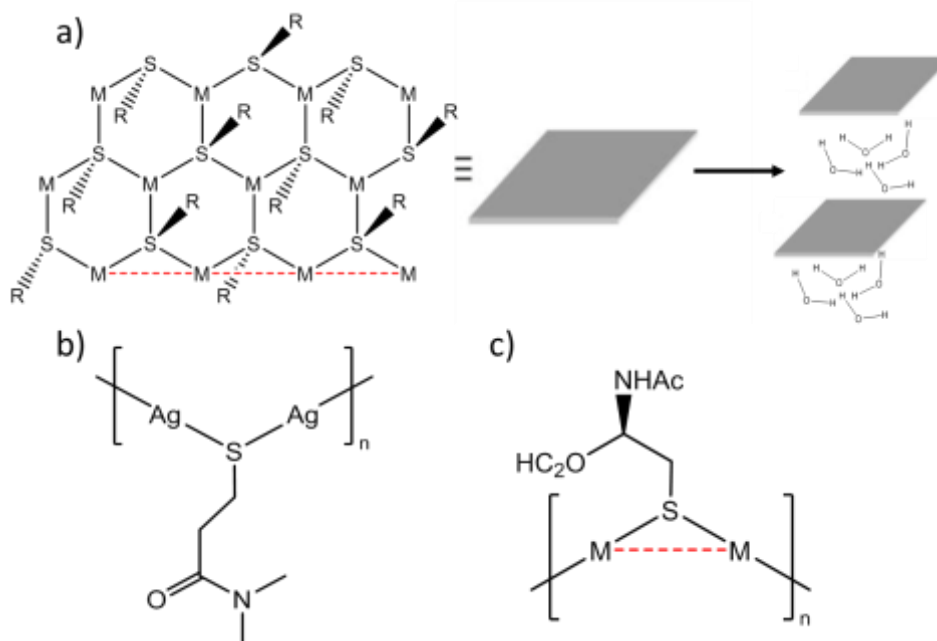


Figure 5.5. Structural schemes of metallogels based on coinage metals thiolate coordination polymer. A polymeric two-dimensional structure in lamellar form that trap water molecules inside the network forming a supramolecular hydrogel (a), a one-dimensional scheme of a metallo-supramolecular gel prepared from Ag(I) ions and *N,N*-dimethyl-3-mercaptopropanamide (b) and one-dimensional scheme of a metallogel based on coinage metal ions and *N*-acetyl-L-cysteine (c). Red dashes lines correspond to metallophilic interactions. M indicates Cu(II), Ag(I) and Au(III) ions. Ligand substituents (R= glutathione) have been removed for clarity.

At this point of this introduction, all hydrogels reported based on coordination polymer with coinage metals and thiolate ligands have been presented. In this chapter we have explored the formation of two hydrogels as a product of the reaction between Ag(I) and Cu(I) salts with the thio-modified nucleoside, 6-thioguanosine as a ligand. Characterization of these compounds include descriptions of the structure,

measurement of their luminescence and electrical properties as well as the study of chiro-optics properties in order to establish hydrogels with semiconductor behavior.

5.2. Materials and Methods

All chemicals used in the preparation of the complex were purchased from Sigma-Aldrich and they were used without any purification.

The synthesis of 6-thioguanosine complexes was carried out similar to the previous two chapters although at different concentrations. Aqueous yellow suspensions of 6-thioguanosine (18 mg, 0.06 mmol, 1 eq, 6 mL for 10 mM; 4 mL for 15 mM; 3 mL for 20 mM, 2 mL for 30 mM and 1 mL for 60 mM) were crushed and sonicated for 1 hour to achieve a fine dispersion. A molar equivalent of AgNO_3 (10.2 mg, 0.06 mmol, 1 eq) and $\text{Cu}(\text{MeCN})_4\text{BF}_4$ (18.9 mg, 0.06 mmol, 1 eq) were added as solids to each of the five suspensions of 6-thioguanosine. After the addition of metal(I) salts and 1 hour of strong mixing on a magnetic stirrer, a pale green and an orange viscous liquid were formed for Ag(I) and Cu(I) samples, respectively. The viscosity varied for each of the ten samples depending on concentration and metal ion added. The reaction instantly formed hydrogels for Ag(I) samples, 60, 30, 20, 15 mM and it took minimum a week for the high concentrated sample of Cu(I), 60 mM, and more than nine days for 30, 20 and 15 mM. Samples at 10 mM remain as viscous liquids in both cases regardless of time. Also, the color of all samples turned darker with time.

Rheology was performed using a HR-2 Discovery Hybrid Rheometer from TA Instrument, with a standard steel parallel-plate geometry of 20 mm diameter with a 1 mm gap, the volume of sample used was 1 ml. The strain and the frequency were set to 1 % and 1 Hz, respectively. All measurements were performed at room temperature by Dr. Dura. Rheological measurements were recorded for two Ag(I) complexes at 15 and 30 mM and two Cu(I) complexes at 30 and 60 mM.

UV-Vis spectroscopy in the range of 190-800 nm was performed using a Varian Cary 100 Bio UV-Vis spectrophotometer with all data collected at room temperature. Cary WinUV software was used to control the spectrophotometer. Three samples were recorded, a basic solution of 6-thioguanosine (30 mM in 0.1 M of NaOH) and Ag(I) and Cu(I) complexes (30 mM) using a demountable quartz cuvette with a path length of 0.1 mm (106-0.1-40 Hellma), the sample was trapped between the layers of the cuvette. The blank used for the measurements was nanopure water produced in Direct-Q® 3 UV Water purification system from Merck at 18 MΩcm resistivity. Melting temperature experiments were performed in the same instrument at 260 nm for Cu(I)-6-thioguanosine complex at 30 mM and the range of temperatures used were 35 °C to 75 °C with 0.5°C per minute of increment for each measurement.

Circular dichroism was performed following the procedure showed in the two previous chapters although at different complex concentrations, Ag(I) complexes at 10, 15, 20 and 30 mM and Cu(I) complexes at 10, 15, 20, 30 and 60 mM.

For the atomic force microscopy imaging two samples were prepared by adding 2 µL of Ag(I) and Cu(I) reaction mixtures (20 mM) onto a clean mica wafer and it was left for dry for two hours on air. The measure procedure followed the same structure as the two previous chapters.

Room temperature luminescence was measured for Ag(I) complexes at 10 mM and 30 mM and Cu(I) complexes at 10 mM and 30 mM, using a demountable quartz cuvette with a path length of 0.1 mm (106-0.1-40 Hellma) and following the same procedure as two previous chapters. Lifetime values were calculated by Dr. Horrocks following a procedure cited in the appendix.

Circular polarized luminescence was performed using a custom-build CPL spectrometer in the range of 400-800 nm with a 410 nm excitation source in Durham

University by Dr MacKenzie.⁴⁴ The data was analyzed using a custom-written Matlab scripts (Matlab 2019b, Mathwork) and smoothed using an intensity-preserving Savitzky-Golay filter. Seven samples had CPL measured, six times, for a basic solution of 6-thioguanosine at 10, 30 and 60 mM, for Ag(I) complex at 10 and 30 mM and for Cu(I) complex at 20 and 60 mM using an open-topped quartz cuvette (101-10-40 Hellma).

Current-Voltage measurements followed the same structure as it was showed in the two previous chapter, although here the sample consisted of 1 μL of the Cu(I) complex at 60 mM.

5.3. Results and Discussion

5.3.1. Ag(I)-6-thioguanosine complexes

Samples of $[\text{Ag(I)-6-thioguanosine}]_n$ (**1**) were prepared at different concentrations (10 mM, 15 mM, 20 mM, 30 mM and 60 mM) by reaction of an aqueous suspension of 6-thioguanosine and solid Ag(I) salt, AgNO_3 , in an equimolar ratio 1:1. After an hour of strong mixing a pale green product appeared and the viscosity of the sample increased with increased concentration. For higher concentration samples, 60, 30, 20, 15 mM, a hydrogel is formed immediately after mixing, inferred by the vial inversion test (Figure 5.6), and for 10 mM sample a viscous liquid is formed. As crystallization proved unproductive for these samples, chapter 3 reports the detailed analysis of the lowest concentration of **1** (1 mM). The section here reports characterization of the hydrogels formed and how particular morphology affects its properties.

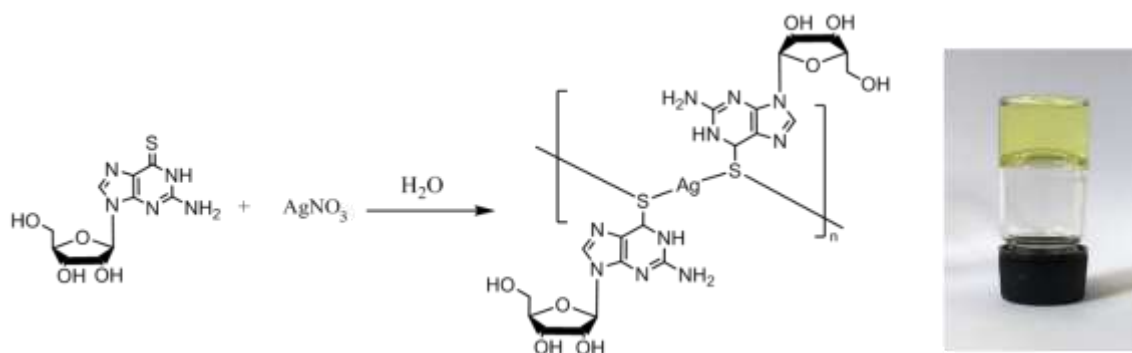


Figure 5.6. Scheme for the reaction between Ag(I) salt and 6-thioguanosine. An image for a 60 mM concentration sample confirming the formation of a hydrogel by the vial inversion test.

Two samples at 15 mM and 30 mM concentration, were first analyzed by rheology with the aim of establishing their gel-like nature in addition to structural and mechanical properties of these compounds. Oscillatory sweep tests were performed to confirm the gel behavior of these two samples exhibiting G' values bigger than G'' values (Figure 5.7 a,b).⁴⁵ The stiffness of 15 mM and 30 mM samples were 22 Pa and 58 Pa, respectively, suggesting an increase of rigidity with increased concentration. (Figure 5.7 a,b) Also, frequency sweep experiments supported the elastic nature of gels with a larger storage modulus than loss modulus (Figure 5.7 c,d) in the range of frequencies between 0.1 to 100 rad/s.

Oscillatory sweep tests assessed the viscoelastic property of gels. The linear region, where G' is independent of the strain applied (10% and 6% for 15 and 30 mM respectively), confirmed the stability of the gel structure upon deformation. At larger values of strain, bigger than 125% and 100% for 15 and 30 mM respectively, the storage and loss modulus are equivalent suggesting the deformation of gels and their transition to liquid phase (Figure 5.7 e,f).^{46,47} Further rheological measurements includes a shear rate experiment to explore the viscosity of gels (Figure 5.7 g,h) and

they confirmed that these hydrogels showed a shear-thinning behavior, reducing the viscosity by two orders of magnitude as the shear rate increased, typical of a non-Newtonian fluid.⁴⁸ Additionally, backward experiments showed the capacity of hydrogels to self-repair after inducing a deformation on its structure. This suggest the presence of non-covalent interactions inside hydrogels, which confirms supramolecular hydrogel characteristics. In chapter 3, AFM showed fibres or fibres aggregates for the coordination polymer **1** at 1 mM which, together with rheological results, make it possible to state the non-covalent interaction between these fibres to form a hydrogel network. Also, the differences in length showed for such fibres in chapter 3, can be ascribed to the reversibility of the metal(I)-sulfur bond and it confirms self-healing properties inherent to the nature of hydrogels.

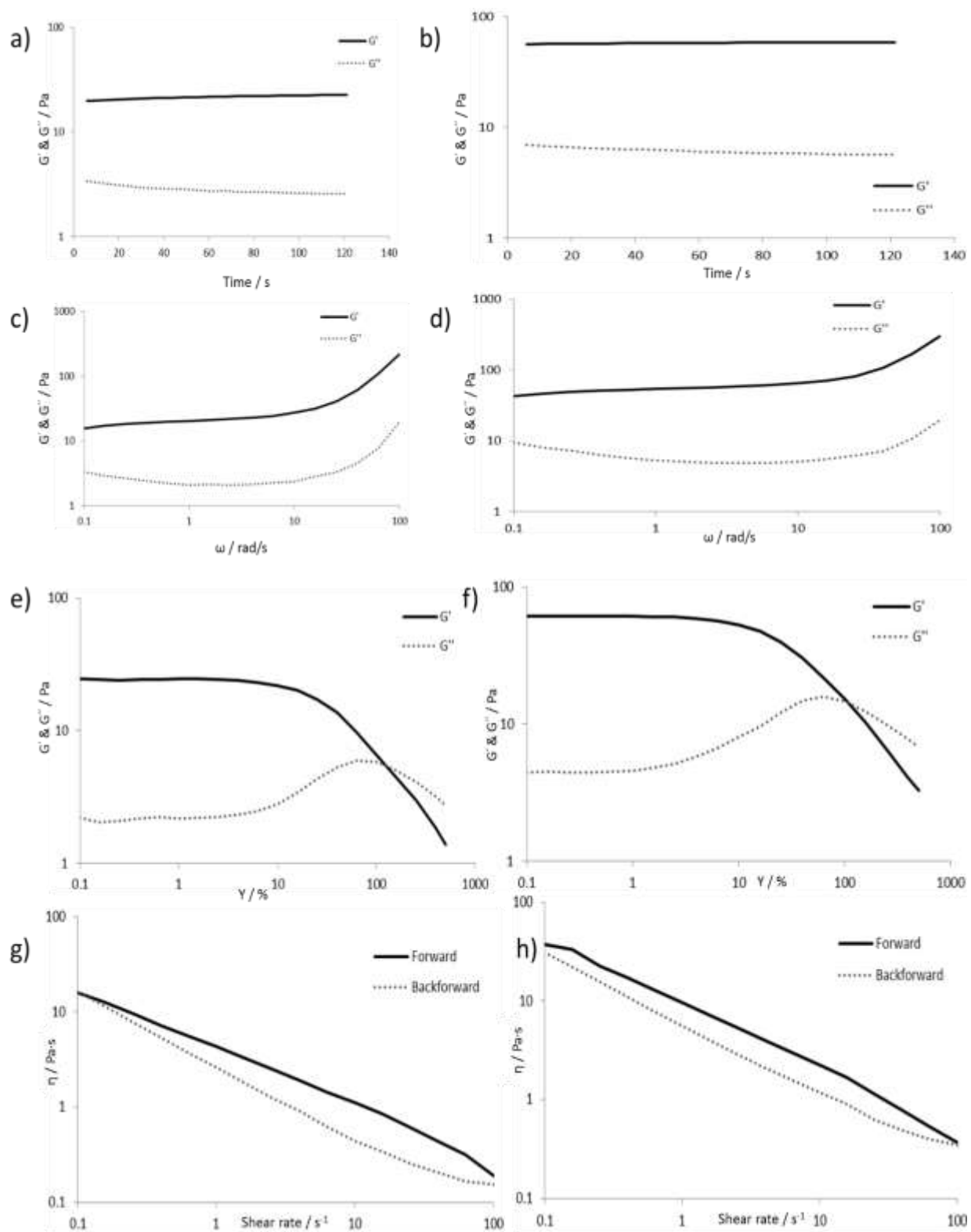


Figure 5.7. Rheological results for Ag(I) complex at 15 mM (a, c, e, g) and 30 mM (b, d, f, h). a) and b) are time sweep experiments; c) and d) frequency sweep experiments; e) and f) amplitude sweep experiments; g) and h) shear rate experiments.

The change from colourless solution of 6-thioguanosine to a pale-yellow hydrogel for **1** indicated that there must be a modification of the UV-Vis spectrum. Then, both samples were analyzed by UV-Vis spectroscopy at 30 mM. The comparison of UV-Vis absorbance for 30 mM of 6-thioguanosine in basic solution, to help its solubility, and hydrogel **1** at 30 mM exhibit a change in the spectra shown in Figure 5.8. It is observed by a red shift of the signal of the hydrogel, from the maximum of absorption at 357 nm of 6-thioguanosine to 401 nm of the hydrogel. Such variation is due to the change of electronic transitions from π - π^* of the thiol in 6-thioguanosine to π - π^* or n - π^* in hydrogel **1**.⁴⁹ It confirms the interaction between Ag(I) ions and sulfur atoms from 6-thioguanosine as mass spectrum in chapter 3 also supported.

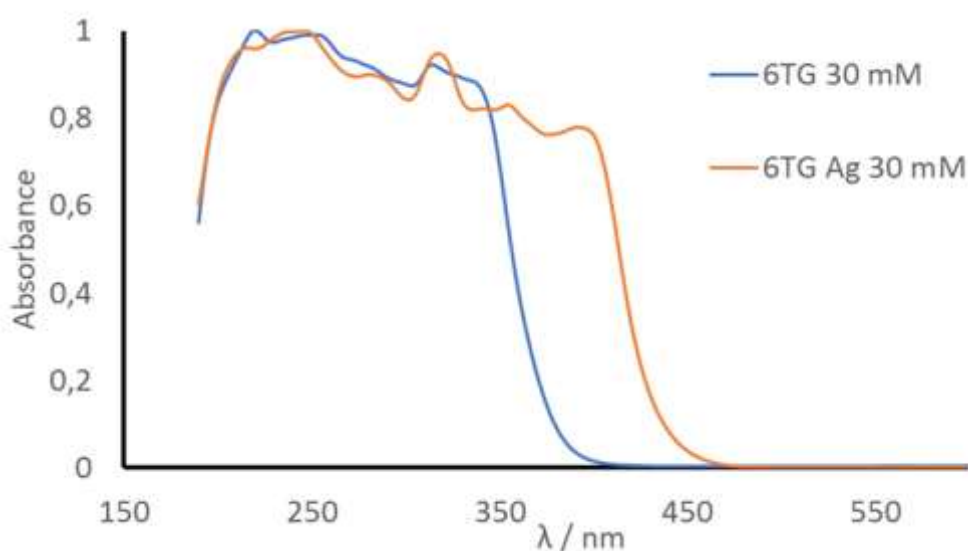


Figure 5.8. UV-Vis spectra for a basic solution of 6-thioguanosine (blue line) and **1** at 30 mM (orange line).

In chapter 3, **1** at 1 mM concentration showed circular dichroism (CD) signal due to chiral properties of 6-thioguanosine. This is expanded to the CD study of **1** to more concentrated samples, 30 mM, 20 mM, 15 mM and 10 mM as well as 6-thioguanosine at 10 mM. The CD signal for all of those complexes confirms their chirality (Figure 5.9).

Comparing the spectrum for the ligand and the four samples of **1** at different concentrations, a big increase in intensity is noted as concentration increases. It is proposed that this is connected with a hierarchical molecular ordering of the polymeric structures.^{50,51} Then, it confirms that the polymers of **1** self-interact to form hydrogels depending on concentration. Besides, the large increase of CD signal is associated with a large chiro-optic property of the compound,^{52,53} and it is confirmed with the presence of left-handed helical fibres associates as it was showed in chapter 3.^{51,54,55} For higher concentrations of hydrogels such as 30, 20 and 15 mM, there is a reversed dichroism signal with an opposing sign above 300 nm, that is known to be affected by the environment of sulfur atoms of metal-thiolate chains.⁵⁶ This change in CD signal indicates that the higher assembly produces changes to the chirality of the initial individual chains only on the metal-thiolate region, indicating a different assembly process between the ligand and **1**.

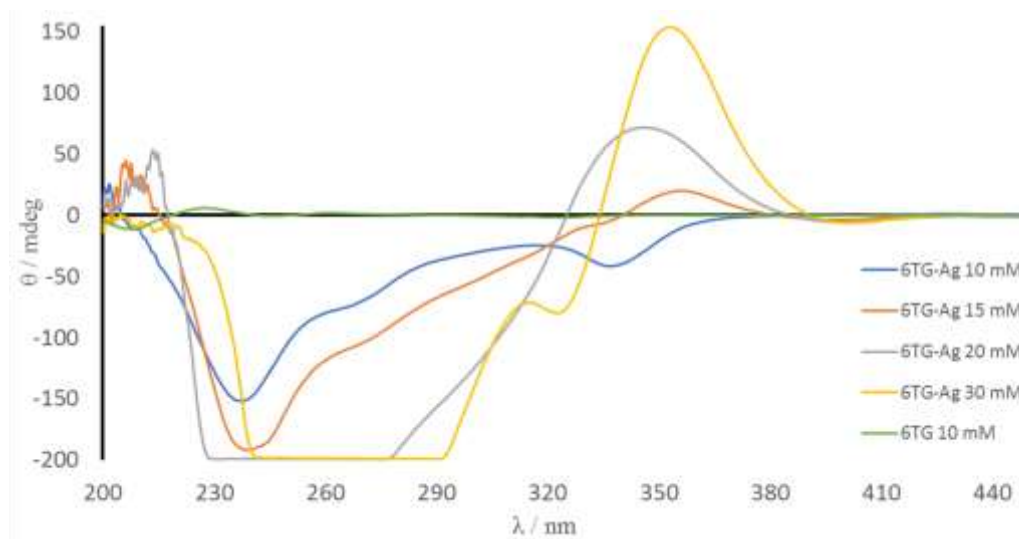


Figure 5.9. CD spectra for a basic solution of 6-thioguanosine at 10 mM (green line) and **1** at four different concentrations.

This characterization on the hydrogels leads to propose a structure for **1** at different concentration. Former structural characterization shown in chapter 3 for a less concentrated **1**, 1 mM, indicates the polymeric nature of the complex in the form of a one-dimensional coordination polymer with a Ag(I)-sulfur backbone. Recall, AFM clearly showed helical fibres for this compound (chapter 3). Starting from these proposals, the hydrogels are based on one-dimensional Ag(I) thiolate coordination polymer (μ_2) that are assembled to form supramolecular networks. Non-covalent interactions between fibres of **1** coordination polymers were confirmed by rheology and they are due metallophilic interactions, base stacking interactions or hydrogen bonding (Figure 5.10a).⁵⁷⁻⁶⁰ So, these self-assembly interactions between the strands of the polymer form bundles of nanofibers that intertwining to set up a three-dimensional fibrillar network in form of supramolecular hydrogel (Figure 5.10b)^{61,62} due to water molecules trapped within the network and their hydrogen bonds interactions with nanofibres.^{45, 63,64} This structure is confirmed by AFM for a concentrated sample of **1** at 20 mM. In Figure 5.10c it is possible to see fibres associates of the thiolate coordination polymer that are inter-crossing and although the picture is in two-dimensions, it suggests the formation of a three-dimensional network where water molecules are trapped as a main characteristic of a hydrogel formation.⁶⁵

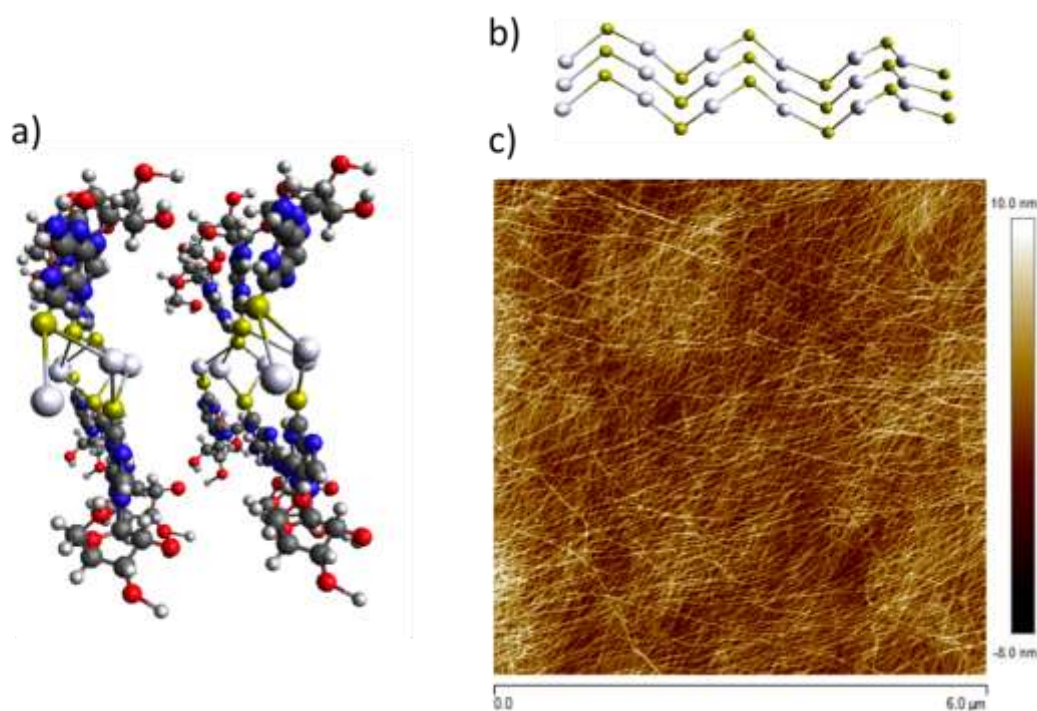


Figure 5.10. Proposed scheme models for the coordination polymer hydrogels **1** structure; a) front view of the self-assembly of two coordination polymers by base stacking, b) side view of coordination polymers that self-assemble forming fibres aggregates, ligand substituents were removed for clarity (white and yellow balls represent Ag(I) ions and sulfur atoms, respectively). These models were drawn on Avogadro software 1.2.0. C) AFM image of hydrogel of **1** at 20 mM demonstrating the intercrossing between fibres aggregates forming the supramolecular network of a hydrogel.

Fluorescence spectroscopy was performed to explore the luminescence properties of hydrogels of **1**. Figure 5.11 shows the maximum peaks in the emission for the ligand at 420 nm for an excitation of 350 nm and for the hydrogel **1** at 30 mM at 550 nm for an excitation of 430 nm.⁶⁶ They both have a comparable fluorescence emission intensity but there is a red shift in the signal after complexation of approximately 120 nm and it indicates that Ag(I) ions are affecting luminescence properties of the

compound. While the emission of the ligand is a well-defined sharp peak arising from the transitions between π - π^* orbitals, high energy transitions characteristic of intra-ligand emission processes,^{67,68} the emission principles for the Ag(I) product is more complex. The broad emission band of Ag(I) compound and its low energy can be ascribed to metal-ligand charge transfer, metal-metal charge transfer or metal centered transitions,^{69,70} also, the Stokes shift not bigger than 200 nm confirms that the hydrogel **1** at 30 mM is fluorescent.⁷¹ The effect of the concentration has been analyzed and a large difference in fluorescence intensity is observed between 30 mM and 10 mM samples indicating, possibly, an aggregation induced emission effect (Figure 5.11).⁷² The formation of a self-assembled complex network in the hydrogel form promotes a stiff entity with non-covalent interactions that enhances luminescence properties.^{73,74} Lifetime values of luminescence were calculated of the 6-thioguanosine as a solid and for **1** at 30 mM. Comparison of lifetime values indicates that **1** has nearly twenty times longer fluorescence lifetime (7 ns) than the ligand (0.398 ns) (Appendix, Figure A5). In addition, an increase of ten times in lifetime value was calculated between **1** at 30 mM and **1** at 5 μ M. These values indicate a long fluorescence process of **1** when concentration increases.

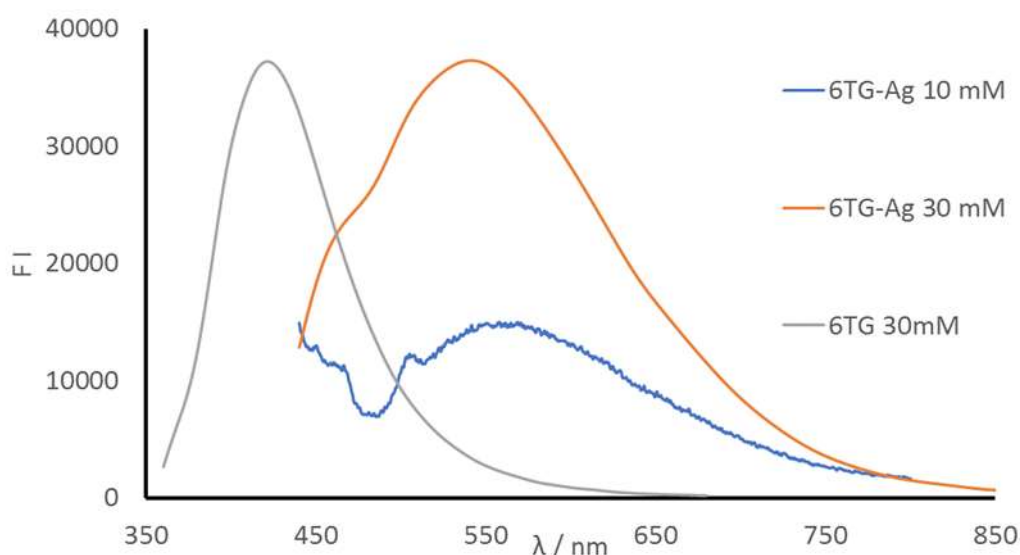


Figure 5.11. Luminescence spectra for a basic solution of 6-thioguanosine at 30 mM (grey line) at 350 nm excitation and for **1** at 10 mM (blue line) and 30 mM (orange line) at 430 nm excitation.

As it has been shown, **1** are fluorescent chiral molecules that increase its optical properties due to a supramolecular organization in form of hydrogel. To deepen the study of luminescent properties of these compounds and taking advantage of the fact that they are chiral, circular polarized luminescence measurements were performed. This measures the difference in intensity between left and right circularly polarized emission giving the luminescence dissymmetry factor (g_{lum}), **1** at 30 mM shows a maximum of g_{lum} of -0.05 at 610 nm (Figure 5.12). By comparison, 6-thioguanosine at 10 mM showed no measurable CPL (Figure 5.12). Additionally, it was shown that **1** at 10 mM did not show circular polarization of the luminescence either (Appendix, Figure A6). The value of g_{lum} for Ag(I) complex at 30 mM is the strongest found for supramolecular hydrogels so far.⁷⁵⁻⁷⁷ The difference of g_{lum} values confirms the effect of the self-assembly to enhance luminescence properties of Ag(I) complex at 30 mM,⁷⁸

and also, the formation of helical fibres for **1**, seen in chapter 3, with left-handed orientation are mainly responsible for this high value of CPL.⁷⁹

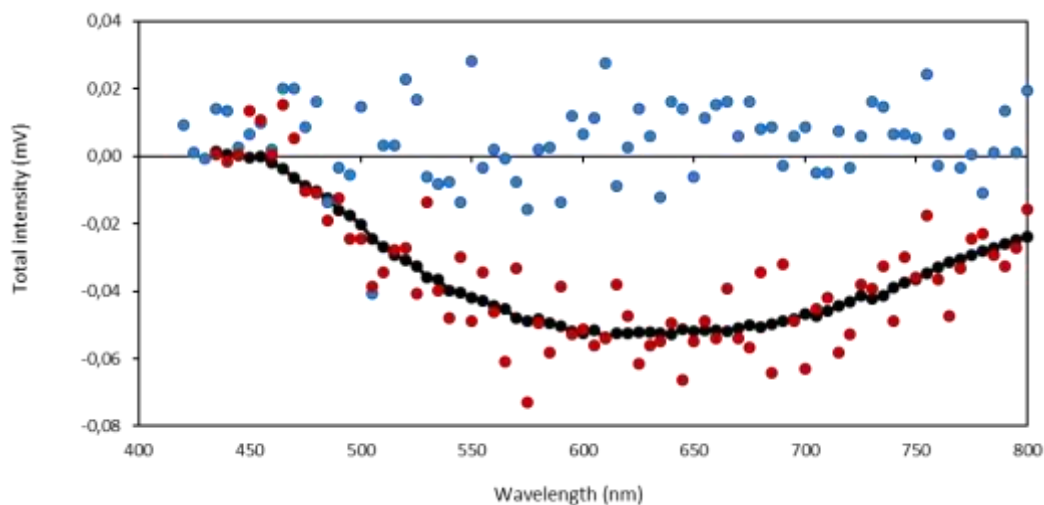


Figure 5.12. CPL raw spectra showing g_{lum} values between 400 and 800 nm for **1** at 30 mM (red dots and their smoothing into a black line) and 6-thioguanosine at 10 mM (blue dots).

5.3.2. Cu(I)-6-thioguanosine complexes

Samples of [Cu(I)-6-thioguanosine]_n (**2**) were prepared at different concentrations (10 mM, 15 mM, 20 mM, 30 mM, 60 mM) by reaction of an aqueous suspension of 6-thioguanosine and solid Cu(I) salt, Cu(MeCN)₄BF₄, in an equimolar ratio 1:1. After an hour of strong mixing an orange product appeared and the viscosity of the sample increased with concentration. For the highest concentration sample, 60 mM, a hydrogel is formed after a week, inferred by the vial inversion test (Figure 5.13), and for the rest of samples, 30, 20, 15 mM more than nine days are needed to form hydrogels; 10 mM sample remains as a viscous liquid over time. The difference in time for the hydrogel formation compared to [Ag(I)-6-thioguanosine]_n could be due to the slow kinetics that rule the reaction between the ligand and Cu(I) or due to different interactions between

coordination polymers inside the network. As crystallization proved unproductive for these samples, chapter 4 reports the detailed analysis of the lowest concentration of **2** (1 mM). The section here describes characterization of the hydrogels formed, its particular morphology and chiro-optics properties.

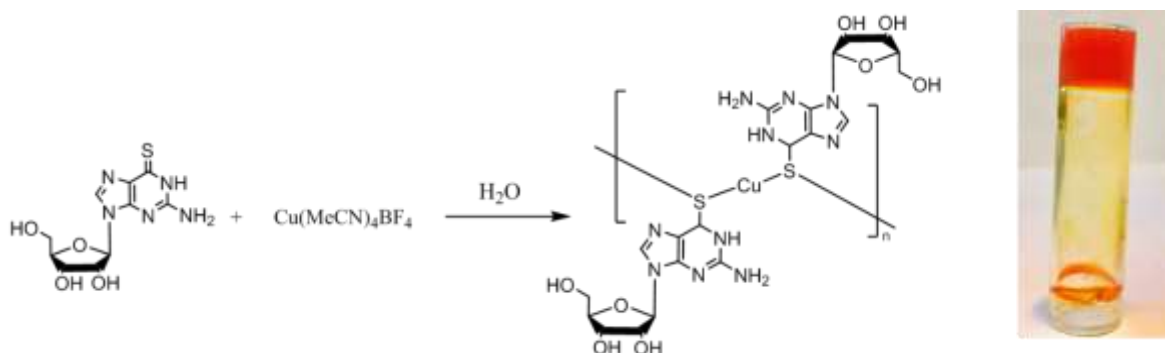


Figure 5.13. Scheme for the reaction between Cu(I) salt and 6-thioguanosine. An image for a 60 mM concentration sample confirming the formation of a hydrogel by the vial inversion test.

Two samples at 30 mM and 60 mM concentration, were first analyzed by rheology with the aim of determine their gel-like structure and structural and mechanical properties. Rheological analysis using oscillatory sweep test confirmed the gel-like nature of these two compounds due to larger values of storage modulus than loss modulus (Figure 5.14 a,b).⁴⁵ The stiffness of 30 mM and 60 mM samples were 10.6 Pa and 29 Pa, respectively, suggesting an increase of rigidity with increased concentration (Figure 5.14 a,b). In addition, frequency sweep experiments displayed elastic behavior of these compounds with larger storage modulus than loss modulus (Figure 5.14 c,d) in the range of frequencies between 0.1 to 100 rad/s. However, higher frequencies reversed the relation between storage modulus and loss modulus in the complex at 60 mM, indicating that the gel network broke. It suggests a weak gel nature.

Oscillatory studies assessed the viscoelastic property of Cu(I) complexes. The linear region, where storage modulus is independent of the strain applied (40%) in both complexes, supported the stability of the gel network upon deformation. At values of strain larger than 364% and 234% for 30 and 60 mM respectively, storage modulus and loss modulus are identical and it suggests a deformation of gels and their transition to liquid phase (Figure 5.14 e,f).^{46,47} In addition, the viscosity of Cu(I) complexes was studied under shear rate experiments (Figure 5.14 g,h). These results showed a shear-thinning behavior, reducing the viscosity by three orders of magnitude as the shear rate increased, typical of a non-Newtonian fluid.⁴⁸ In addition, backward experiments showed self-healing properties of Cu(I) complexes after an induced deformation of its structure. This suggests the presence of non-covalent interactions inside the gel, which confirms supramolecular hydrogel characteristics.

In chapter 4, AFM showed fibres or fibres associates for the coordination polymer **2** at 1 mM. These results are in accordance with rheological studies displayed here, where these fibres are interacting through non-covalent interactions to form hydrogel network. Likewise, the differences in length for such fibres, showed in chapter 4, can be related to the reversibility of such interactions and self-healing properties of hydrogels.

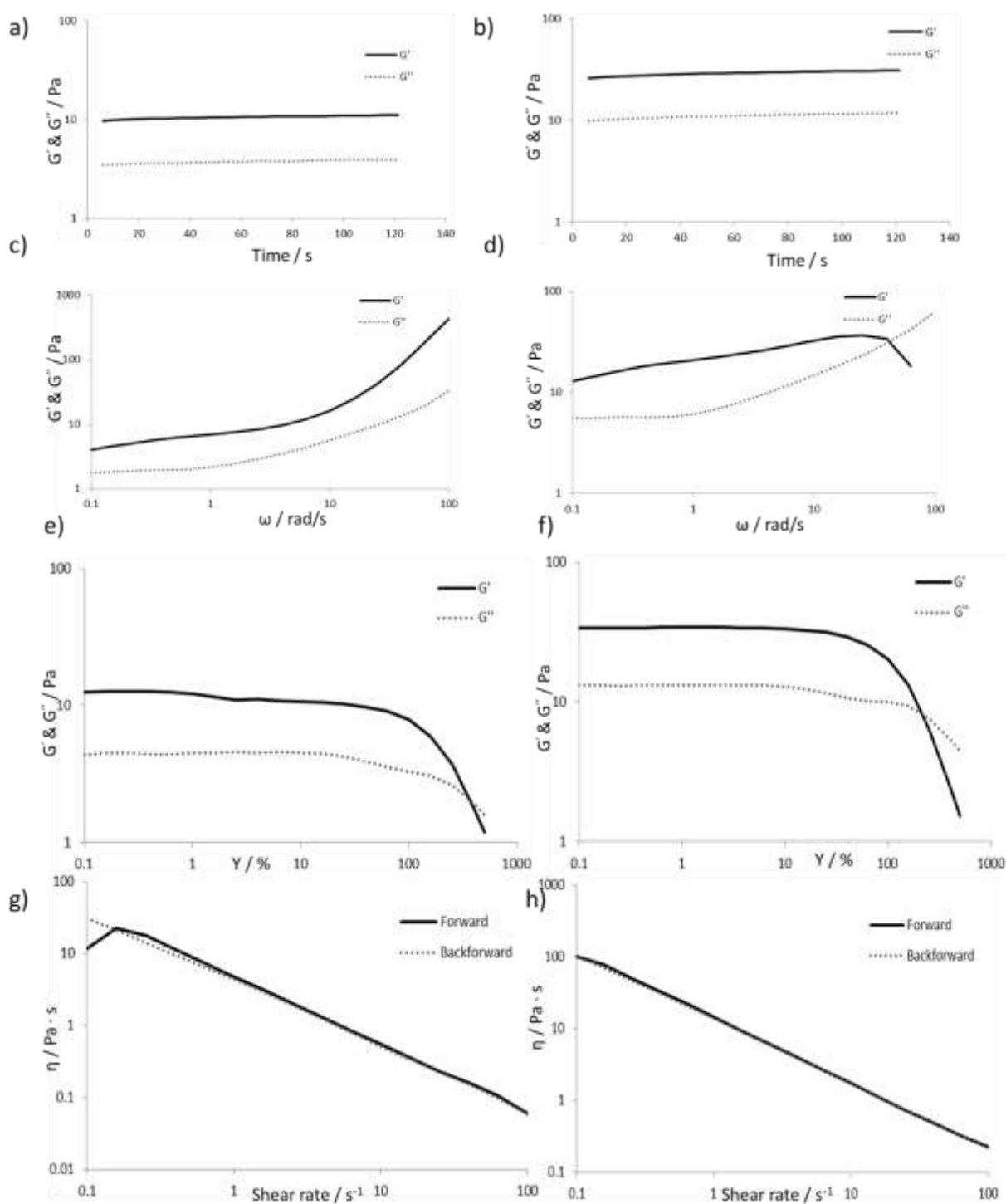


Figure 5.14. Rheological results for Cu(I) complex at 30 mM (a, c, e, g) and 60 mM (b, d, f, h). a) and b) are time sweep experiments; c) and d) frequency sweep experiments; e) and f) amplitude sweep experiments; g) and h) shear rate experiments.

These hydrogels were analyzed by UV-Vis spectroscopy. The transition from colorless solution of 6-thioguanosine to an orange hydrogel for **2** indicates that UV-Vis should change after complexation. The comparison of absorbance for 30 mM of 6-thioguanosine in basic solution, to help its solubility, and **2** in hydrogel form at 30 mM exhibit some changes in the spectra shown in Figure 5.15. The main band for the ligand, in thiol form,⁴⁹ is at 328 nm and it corresponds to a $\pi\text{-}\pi^*$ transition of the thiol group.^{49,56} This peak is red shifted and more intense for the hydrogel **2** at 355 nm, showing a shoulder at 413 nm.^{80,81} The peaks for the **2** as hydrogel correspond to $\pi\text{-}\pi^*$ or $n\text{-}\pi^*$ transitions, expected for Cu-thiolate compounds confirming that Cu(I) is interacting with sulfur atoms forming a polymeric structure as mass spectrum results also suggest in chapter 4.⁸²⁻⁸⁴

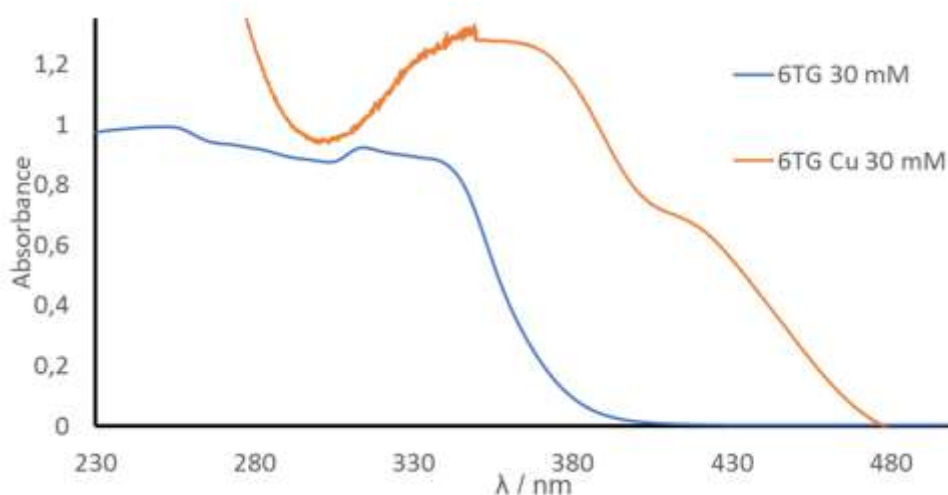


Figure 5.15. UV-Vis spectra for a basic solution of 6-thioguanosine (blue line) and **2** at 30 mM (orange line).

To analyze interactions within the hydrogel, melting temperature experiment was performed. Base stacking non-covalent interactions in Cu(I) hydrogels are due to the nucleobases of the ligand and it is well-known that the peaks below 300 nm in absorbance spectrum are due to nucleobase $\pi\text{-}\pi^*$ transitions.^{66,85} Figure 5.16a shows

the change of intensity of absorbance for hydrogel **2** at 30 mM at constant wavelength, 260 nm, when the temperature increases. From 40°C to 63°C there is an increase in absorption intensity and suggests the presence of base stacking interactions within the hydrogel. This is similar to the melting behavior of duplex DNA where there is a hyperchromic shift as the individual aromatic nucleobase groups are no longer stacked.⁸⁶ After the cooling process hydrogel **2** showed a higher value of absorption than the initial value. To confirm recovery properties of hydrogel **2**, a UV-Vis spectrum was run a day before in order to see if the initial absorbance value was reached, but the results were inconclusive. This maybe occurs due to the viscous medium where **2** is so, it is not possible to confirm self-repair properties after being exposed to changes in temperature.

When the **2** was heated above 63°C a decrease in absorbance intensity was observed, expected for a xerogel, where there are no base stacking interactions (Figure 5.16b). These results indicate that **2** is a self-assembled supramolecular hydrogel, built from non-covalent interactions between **2** coordination polymers based on base stacking interactions of 6-thioguanosine.

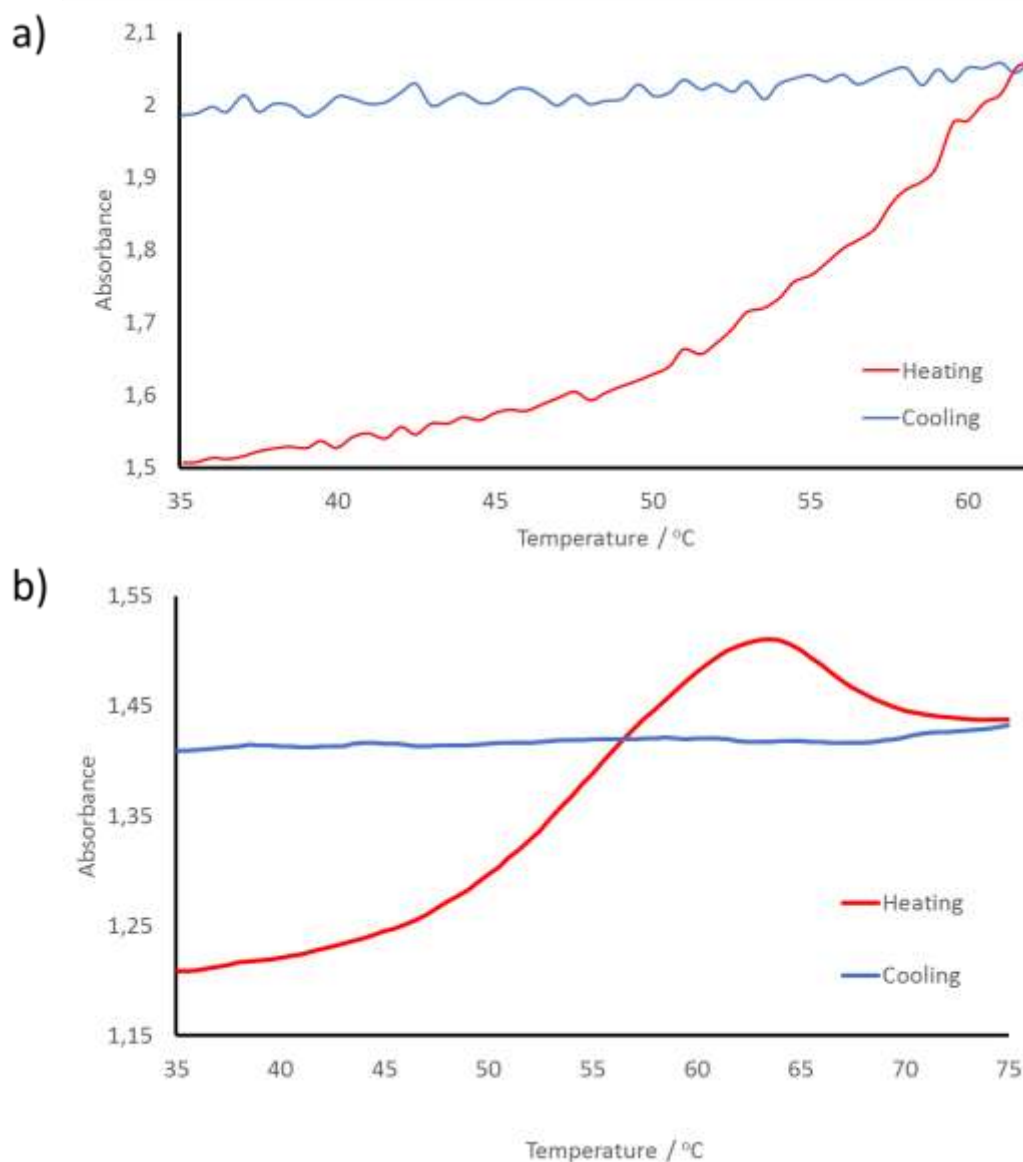


Figure 5.16. Melting temperature experiments for a 30 mM **2** at 250 nm; a) indicates the change in absorbance of **2** when the temperature increases up to 63°C (red line) and when it decreases to 35°C (blue line); b) indicates the change in absorbance of the complex when temperature reaches 75 °C (red line) and decreases up to 35°C (blue line).

Experiments of circular dichroism (CD) performed in chapter 4 confirms the chirality of **2** at 1 mM. Figure 5.17 shows CD spectra for complexes of **2** at 60, 30, 20, 15 and 10 mM and 6-thioguanosine at 10 mM. Comparing these spectra, the main change is the

large difference in intensities between complexes of **2** and the ligand and it suggests that the complex is adopting a high ordered polymeric structure.^{50,51} Figure 5.17 clearly shows that the CD signal depends on the concentration and this effect can be observed in the band that starts at 420 nm which depends on metal-to-ligand charge transfer.^{82,83} For 10, 15 and 20 mM this band remain negative but for 30 mM and 60 mM it is positive. This reversed circular dichroism signal may be due to higher concentrations of metal thiolate polymers that produce higher assemblies than low concentration samples, a different assembly process.

Although it is expected that the intensity of the CD signal is greater for the highest concentrations, it was not so experimentally since the viscosity of such samples prevents a homogeneous distribution in the cuvette. So CD confirms the chirality of all the Cu(I) hydrogels and also their self-assembly properties, a structural feature of these compounds that form supramolecular networks made of polymeric chains.⁵⁶

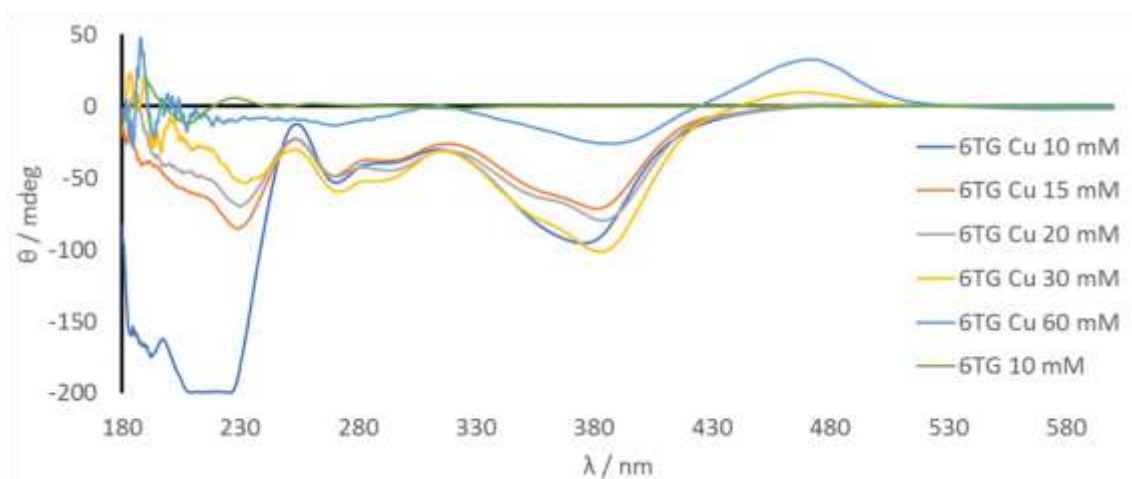


Figure 5.17. CD spectra for a basic solution of 6-thioguanosine at 10 mM (green line) and hydrogels of complexes at five different concentrations.

This characterization of hydrogels of **2** lead to suggests a molecular structure them. Chapter 4 cover all characterization for a low concentrated **2** complex (1 mM) and it

shows that it is made of Cu(I)-sulfur backbone in a polymeric chain forming a one-dimensional coordination polymer (μ_3) (Figure 5.18a). Also, AFM showed strands for **2** at 1 mM concentration (chapter 4). The characterization of hydrogels of **2** by UV-Vis confirmed the presence of a polymeric structure as mass spectroscopy reported in chapter 4 suggested. Besides, rheology and melting temperature experiment verified that to form a supramolecular network in form of hydrogels, these polymers interact between them through non-covalent interactions, in particular, base stacking interactions (Figure 5.18b).⁸⁷⁻⁸⁹ The chirality of hydrogels of **2** was validated with circular dichroism spectroscopy indicating a reverse in the signal, it was ascribed to the formation of aggregated bundles of the polymer for high concentrated samples. Therefore, the structure of hydrogel **2** is formed by the self-entangling of individual coordination polymer fibres that interacts through π - π stacking to form nanofibres that associate to form a three-dimensional network where water molecules are trapped (Figure 5.18b).⁹⁰⁻⁹² AFM images for a high concentrated sample of Cu(I) hydrogel (Figure 5.18c), 60 mM, confirms the presence of nanofibres associates entangled that forms the characteristic fibrillar network of a hydrogel.⁶⁵

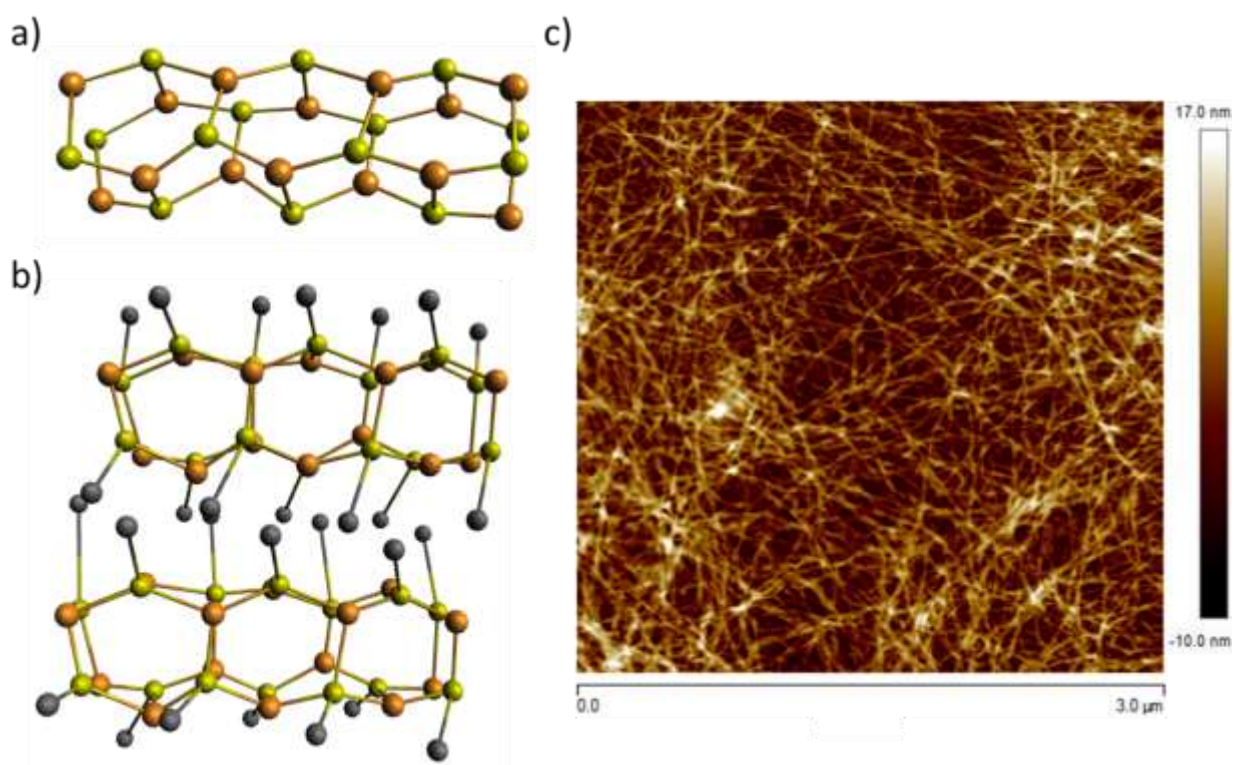


Figure 5.18. Proposed scheme models for the coordination polymer hydrogels **2** structure; a) side view of the assembly of the Cu(I) thiolate coordination polymer with a tubular chain, b) side view of two coordination polymers that self-assemble forming fibres aggregates by base stacking, ligand substituents were removed for clarity (orange, yellow and grey balls represent Cu(I) ions, sulfur atoms and ligand substituent respectively). These models were drawn on Avogadro software 1.2.0. C) AFM image of a hydrogel **2** at 20 mM that demonstrate the intercrossing between fibres aggregates forming the supramolecular network of a hydrogel.

Fluorescence spectroscopy was performed for a basic solution of 6-thioguanosine and complexes of **2**. For the ligand, the maximum peak in emission is at 420 nm for an excitation of 350 nm,⁶⁶ and for complexes of **2** at 10 mM and 30 mM, two emission peaks appeared, ca. 560 nm and 670 nm, for an excitation of 470 nm (Figure 5.19). The sharp emission peak of the ligand and the most intense for the complex have been

assigned to ligand-to-ligand charge transfer or intra ligand π - π^* transitions.^{93,94} The broad band in complexes of **2** around 670 nm is related to ligand-to-metal charge transfer, metal-to-ligand charge transfer or a metal-centered transitions^{95,96} confirming that Cu(I) ions are affecting luminescence properties of the ligand. Comparing the intensity of the emission, the difference between complexes of **2** at 30, 10 and 1 mM and 6-thioguanosine at 1 mM, is not large, only the band at 670 nm is more pronounced for Cu(I) complex at 10 mM. It suggests that the emission of complexes of **2** is not highly affected by concentration effects. Also, self-quenching effects are affecting the emission of **2** at 30 mM concentration hydrogel compared to 10 mM Cu(I)-6-thioguanosine viscous liquid.⁹⁷ Other Cu(I) thiolates have exhibit similar photophysical properties with two emission peaks corresponding to ligand-ligand for the high energy transition and metal-ligand charge transfer for a low energy transition.^{80,98} The peak that appears around 800 nm for the ligand is attributed to the second order luminescence scattering.

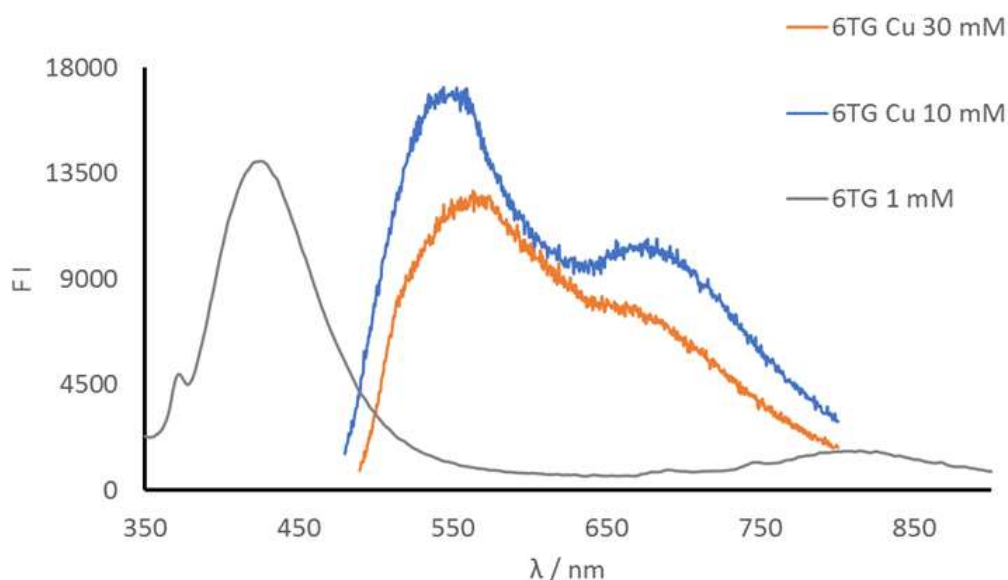


Figure 5.19. Luminescence spectra for a basic solution of 6-thioguanosine at 1 mM (grey line) at 350 nm excitation and for complexes of **2** at 10 mM (blue line) and 30 mM (orange line) at 470 nm excitation.

CD has confirmed that hydrogels of **2** at different concentrations are chiral and also, they have exhibited luminescence properties. Then, circular polarized luminescence was performed in order to study if self-assembly properties make these complexes suitable for CPL.⁹⁹ Two hydrogels of **2** samples were measured at 60 mM and 20 mM concentration respectively. Both of these exhibited CPL signals; the maximum of g_{lum} for 60 mM was +0.01 at 700 nm and for 20 mM was -0.015 at 735 nm (Figure 5.20). The measure of CPL for the ligand at 30 mM was zero so there is no interference of the ligand in the circular polarized emission of complexes of **2**, confirming the self-assembly chiral arrangement of luminophores and, therefore, the chiral nature of the luminescence emission for these supramolecular networks.^{76,78}¹⁰⁰ The values of g_{lum} obtained for these complexes of **2** are rather high compared to other Cu(I) complexes previously reported.¹⁰¹

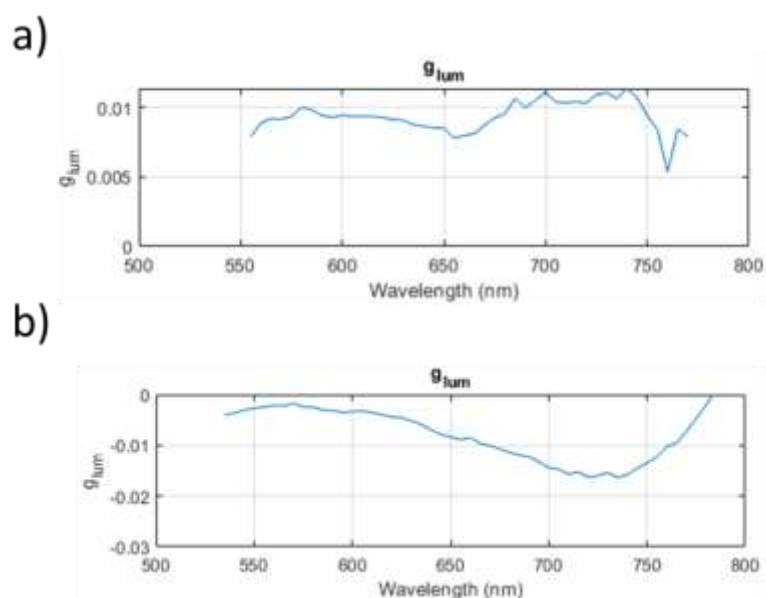


Figure 5.20. CPL experiment showing g_{lum} values for hydrogels of **2** at a) 60 mM and at b) 20 mM.

Electrical properties of **2** at 60 mM concentration in xerogel form were examined to establish if this polymer can conduct electrons as is known for other similar Cu(I) thiolate polymers.¹⁰²⁻¹⁰⁴ To obtain **2** in xerogel form it was prepared as a hydrogel, deposited on the platinum microband electrodes and dried in air for an hour before measurement. Then a direct current voltage between -2 V to +2 V was applied giving as a result a current-voltage, I-V plot, (Figure 5.21). First, the maximum current measured, 10 fA, for the bare electrode background indicates that there is no interference of the microband electrode. The maximum current measured for the **2** xerogel prepared at 60 mM was 0.497 nA. This indicates that the as-prepared compound is electrically conductive.¹⁰⁵ Further, redox doping with Magic Blue turned dark the color of the xerogel and significantly improves the electrical conductance of the complex. The maximum current reaches 2 nA and the conductivity is 4 times greater than the original complex. These results indicate that increasing the concentration of **2** complex up to 60 times it is possible to obtain a large amount on conductivity compared to that demonstrated in chapter 4, owing to the formation of long polymers that interact forming a supramolecular network in form of a xerogel. As in chapter 4, oxidative doping is established as a useful strategy to introduce charge carriers in inorganic complexes.¹⁰⁶ The increase in electrical conductivity of **2** at 60 mM could be explained by the injection of positive charges through the oxidation of Cu(I) ions to Cu(II) ions as has been shown in previous studies.¹⁰⁵ Partial oxidation of the Cu centers is expected to increase conductivity because the hopping rate will depend on the product of the local concentrations of Cu(I) and Cu(II) sites. To determine if the conductance is stable with time the same measurement was repeated five days later. The results showed that the intensity of current decreases up to 33 pA, suggesting that the polymer structure of Cu-thiolate is not stable due to the effect of the doping agent.

Time did not allow to characterize chemical or structurally **2** 60 mM xerogel. However, it has been demonstrated that a highly concentrated (60 mM) xerogel of **2** shows higher values of electrical conductivity than low concentrated (1 mM) xerogel for the same compound as chapter 4 proved with background levels of conductivity and it is due to the formation of a supramolecular network consistent on fibre-like bundles of **2** that improve the current-carrying properties of the material.

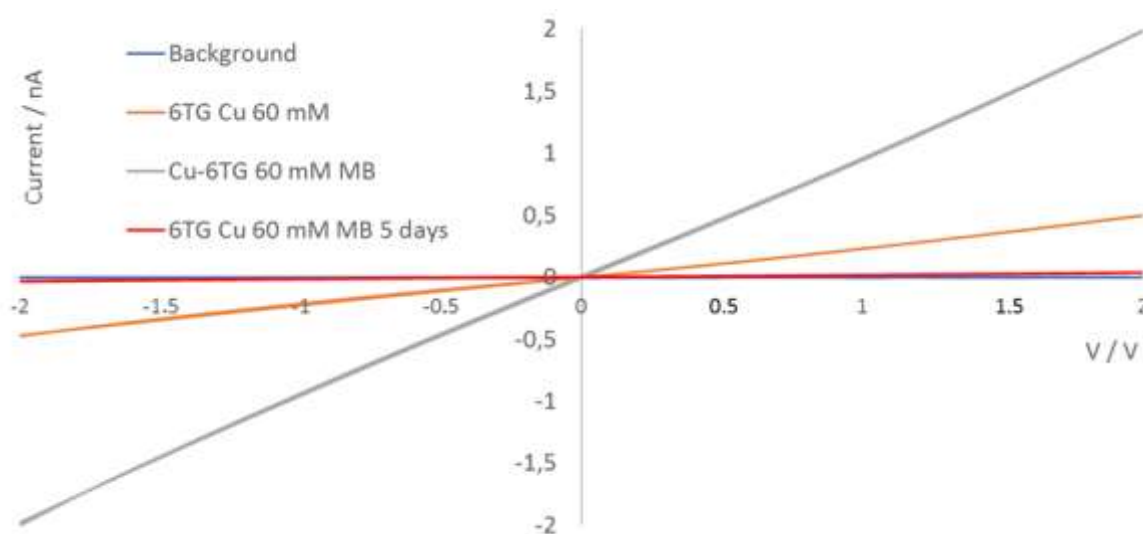


Figure 5.21. Two-terminal I-V characteristic of three samples; electrode background (blue line), **2** xerogel at 60 mM (orange line), **2** xerogel at 60 mM doped with Magic Blue (grey line) and **2** xerogel at 60 mM doped with Magic Blue measured 5 days later (red line).

5.4. Conclusion

We have prepared Ag(I) and Cu(I) thiolate coordination polymers at different concentrations and they form hydrogels. The reaction has probed the interactions between one-dimensional coordination polymers to form a three-dimensional network with chiro-optics properties. The hydrogels have been structurally analyzed proving the formation of a supramolecular network made of fibers associates of Ag(I) and Cu(I)

thiolate polymers. Besides, the chirality of the components of the hydrogel has been confirmed and it increases by forming such structures.

Rheological results for Cu(I) hydrogels and Ag(I) hydrogels show, in both cases, a similar gel behavior but there are some distinctions. The difference in stiffness values indicates that Ag(I) hydrogels are fairly more rigid even at lower concentrations but also more fragile when a deformation is induced as lower values of critical strain indicates when it is compared with Cu(I) complexes.

Luminescence properties have been investigated for the hydrogels evidencing its high fluorescence due to the organization into a supramolecular system. In addition, the high concentrated hydrogel exhibits a strong circular polarized luminescence what encourages to think that the chiro-optics properties of these compounds are enhanced when supramolecular networks are formed. Besides, high concentrated Cu(I) thiolate xerogel showed a very promising conductivity properties which confirms semiconductor behavior of this compound. All these properties are promoted by the formation of supramolecular networks and they are potential applications on DNA functionalization.

5.5. References

- 1- Peters, G., Davis, J., *Chem. Soc. Rev.* 2016, **45**, 3188-3206.
- 2- Liu, X., 2005, Gelation with small molecules: from formation mechanism to nanostructurearchitecture in *Low Molecular Mass Gelator*, **256**, 1-37, Springer, Berlin.
- 3- Fages, F., Vögtle, F., Zinic, M., 2005, Systematic design of amide- and urea-type gelators with tailored properties in *Low Molecular Mass Gelators*, **256**, 77-131, Springer, Berlin.
- 4- Abdallah, D., Weiss, R., *Langmuir* 2000, **16**, 352-355.
- 5- He, H., Chen, S., Tong, X., An, Z., Ma, M., Wang, X., Wang, X., *Langmuir* 2017, **33**, 13332-13342.
- 6- Raeburn, J., Adams, D., *Chem. Commun.* 2015, **51**, 5170-5180.
- 7- Jayawarna, V., Ali, M., Jowitt, T., Miller, A., Saiani, A., Gough, J., Ulijn, R., *Adv. Mat.* 2006, **18**, 611-614.

- 8- Abul, Y., Roy, S., Frederix, P., Javid, N., Jayawarna, V., Ulijn, R., *Small* 2014, **10**, 973-979.
- 9- Dastidad, P., Ganguly, S., Sarkar, K., *Chem. An Asian J.* 2016, **11**, 2484-2498.
- 10- Ganta, S., Chand, D., *Chem. An Asian J.* 2018, **13**, 3777-3789.
- 11- Kim, H., Lee, J., Lee, M., *Angew. Chem.* 2005, **117**, 5960-5964.
- 12- Gee, W., Batten, S., *Chem. Commun.* 2012, **48**, 4830-4832.
- 13- Sarkar, S., Dutta, S., Chakrabarti, S., Bairi, P., Pal, T., *ACS Applied Materials & Interfaces* 2014, **6**, 6308-6316.
- 14- Huang, J., He, L., Zhang, J., Chen, L., Su, C., *J. of molecular catalysis A: Chemical* 2010, **317**, 97-103.
- 15- Grondin, P., Roubeau, O., Castro, M., Saadaoui, H., Colin, A., Clerac, R., *Langmuir* 2010, **26**, 5184-5195.
- 16- Adarsh, N., Sahoo, P., Dastidar, P., *Crystal Growth & Design* 2010, **10**, 4976-4986.
- 17- Svodoba, H., Nonappa, Lahtinen, M., Wimmer, Z., Kolehmainen, E., *Soft Matter* 2012, **8**, 7840-7847.
- 18- Araki, K., Yoshikawa, I., 2005, Nucleobase-Containing Gelators in *Low Molecular Mass Gelator*, **256**, 133-165, Springer, Berlin.
- 19- Sivakova, S., Rowan, S., *Chem. Soc. Rev.* 2005, **34**, 9-21.
- 20- Bang, I., *Biochem. Z.* 1910, **26**, 293-311.
- 21- Gellert, M., Lipsett, M., Davies, D., *Proc. Natl. Acad. Sci. USA* 1962, **48**, 2013-2018.
- 22- Fresco, J., Massoulié, J., *J. Am. Chem. Soc.* 1963, **85**, 1352-1353.
- 23- Giorgi, T., Grepioni, F., Manet, I., Mariani, P., Masiero, S., Mezzina, E., Pieraccini, S., Saturni, L., Spada, G., Gottarelli, G., *Chem. A Eur. J.* 2002, **8**, 2143-2152.
- 24- Davis, J., *Angew. Chem. Int. Ed.* 2004, **43**, 668-698.
- 25- Spindler, L., Fritzsche, W., (ed.), 2012, *Guanine Quartets: Structure and Applications*, RSC Publishing.
- 26- Bairi, P., Chakraborty, P., Mondal, S., Roy, B., Nandi, A., *Soft Matter* 2014, **10**, 5114-5120.
- 27- Kumar, A., Gupta, S., *Green Chem.* 2015, **17**, 2524-2437.
- 28- Skilling, K., Ndungu, A., Kellam, B., Ashford, M., Bradshaw, T., Marlow, M., *J. Mater. Chem. B* 2014, **2**, 8412-8417.
- 29- Park, S., Kim, B., *Soft Matter* 2008, **4**, 1995-1997.
- 30- Li, X., Kuang, Y., Lin, H., Gao, Y., Shi, J., Xu, B., *Angew. Chem. Int. Chem.* 2011, **50**, 9365-9369.
- 31- Li, X., Yi, K., Shi, J., Gao, Y., Lin, H., Xu, B., *J. Am. Chem. Soc.* 2011, **133**, 17513-17518.

- 32- Bazzicalupi, C., Bencini, A., Berni, E., Bianchi, A., Ciattini, S., Giorgi, C., Paoletti, P., Valtancoli, B., *EurJIC* 2001, **2001**, 629-632.
- 33- Lippert, B., *Coord. Chem. Rev.* 2000, **200-202**, 487-516.
- 34- Berdugo, C., Escuder, B., Miravet, J., *Org. Biomol. Chem.* 2015, **13**, 592-600.
- 35- Babu, S., Praveen, V., Ajayaghosh, A., *Chem. Rev.* 2014, **114**, 1973-2129.
- 36- Skilling, K., Citossi, F., Bradshaw, T., Ashford, M., Kellam, B., Marlow, M., *Soft Matter* 2014, **10**, 237-256.
- 37- Odriozola, I., Loinaz, I., Pomposo, J., Grande, H., *J. Mater. Chem.* 2007, **17**, 4843-4845.
- 38- Parikh, A., Gillmor, S., Beers, J., Beardmore, K., Cutts, R., Swanson, B., *J. Phys. Chem. B* 1999, **103**, 2850-2861.
- 39- Pyykkö, P., *Angew. Chem. Int. Ed.* 2004, **43** (34), 4412-4456.
- 40- Odriozola, I., Ormategui, N., Loinaz, I., Pomposo, J., Grande, H., *Macromolecular Symposia* 2008, **266**, 96-100.
- 41- Casuso, P., Carrasco, P., Loinaz, I., Grande, H., Odriozola, I., *Org. Biomol. Chem.* 2010, **8**, 5455-5458.
- 42- Casuso, P., Loinaz, I., Möller, M., Carrasco, P., Pomposo, J., Grande, H., Odriozola, I., *Supramolecular Chemistry* 2009, **21**, 581-884.
- 43- Casuso, P., Carrasco, P., Loinaz, I., Cabañero, G., Grande, H., Odriozola, I., *Soft Matter* 2011, **7**, 3627-3633.
- 44- Carr, R., Puckrin, R., McMahon, B., Pal, R., Parker, D., Palsson, L., *Meth. And Appl. In Fluorescence* 2014, **2**, 024007.
- 45- Piepenbrock, M., Lloyd, G., Clarke, N., Steed, J., *Chem. Rev.* 2010, **110**, 1960-2004.
- 46- Mistry, L., El-Zubir, O., Dura, G., Clegg, W., Waddell, P., Pope, T., Hofer, W., Wright, N., Horrocks, B. R., Houlton, A., *Chem. Sci.* 2019, **10**, 3186-3195.
- 47- Dash, J., Patil, A., Das, R., Dowdall, F., Mann, S., *Soft Matter* 2011, **7**, 8120-8126.
- 48- Gabelle, J., Morchain, J., Archard, D., Augier, F., Line, A., *AIChE J.* 2013, **59**, 2251-2266.
- 49- Zhang, Y., Zhu, X., Smith, J., Haygood, M., Gao, R., *J. Phys. Chem. B* 2011, **115**, 1889-1894.
- 50- Lam, A., Guenther, R., Agris, P., *Biometals* 1995, **8**, 290-296.
- 51- Zimmer, C., Holy, L., *Nucleic Acids Research* 1976, **3**, 2757-2770.
- 52- Greenfield, J., Evans, E., Nuzzo, D., Antonio, M., Friend, R., Nitschke, J., *J. Am. Chem. Soc.* 2018, **140**, 10344-10353.
- 53- Zhang, H., Zheng, X., Kwok, R., Wang, J., Leung, N., Shi, L., Sun, J., Tang, Z., Lam, J., Qin, A., Tang, B., *Nat. Commun.* 2018, **9**, 4961.
- 54- Sutherland, J., Griffin, K., Keck, P., Tacaks, P., *Proc. Natl. Acad. Sci. USA* 1981, **78**, 4801-4804.

- 55- Sprecher, C., Baase, W., Johnson, C., *Biopolymers* 1979, **18**, 1009-1019.
- 56- Repges, R., Beuck, C., Weinhold, E., Raabe, G., Fleischhauer, J., *Chirality* 2008, **20**, 978-984.
- 57- Panja, S., Seddon, A., Adams, D., *Chem. Sci.* 2021, **12**, 11197-11203.
- 58- Koskinen, L., Jääskeläinen, S., Hirva, P., Haukka, M., *Solid State Sciences* 2014, **35**, 81-87.
- 59- Wang, W., Zhang, Y., Liu, W., *Progress in Polymer Science* 2017, **71**, 1-25.
- 60- Toupanloo, H., Rahmani, Z., *Applied Biological Chemistry* 2018, **61**, 209-226.
- 61- Kim, H., Zin, W., Lee, M., *J. Am. Chem. Soc.* 2004, **126**, 7009-7014.
- 62- Wu, Z., Du, Y., Liu, J., Yao, Q., Chen, T., Cao, Y., Zhang, H., Xie, J., *Angew. Chem. Int. Ed.* 2019, **58**, 8139-8144.
- 63- Pradas, M., Ribelles, J., Aroca, A., Ferrer, G., Anton, J., Pissis, P., *Colloid and Polymer Science* 2001, **279**, 323-330.
- 64- Popa, V., Volf, I., (ed.), 2018, *Biomass and Renewable raw material to obtain bioproducts of high-tech value*, ch. 11, 401-439, Elsevier.
- 65- Feng, H., Du, Y., Tang, F., Ji, N., Zhao, X., Zhao, H., Chen, Q., *RSC Adv.* 2018, **8**, 15842-15852.
- 66- Rubin, Y., XVI Int. Conf. on Spectroscopy of Molecules and Crystals, Sevastopol, Ukraine, 2004.
- 67- Chao, H., Wu, L., Li, C., Lu, W., Liu, L., Feng, X., *Z. Anor. Allg. Chem.* 2011, **637**, 1533-1538.
- 68- Ford, P., *Chem. Sci.* 2016, **7**, 2964-2986.
- 69- Forward, J., Bohmann, D., Fackler, J., Staples, R., *Inorg. Chem.* 1995, **34**, 6330-6336.
- 70- Wang, X., Guerzo, A., Schmehl, R., *J. of Photoc. And Photob. C: Photoc. Reviews*, 2004, **5**, 55-77.
- 71- Luo, Z., Yuan, X., Yu, Y., Zhang, Q., Leong, D., Lee, J., Xie, J., *J. Am. Chem. Soc.* 2012, **134**, 16662-16670.
- 72- Veselska, O., Dessal, C., Melizi, S., Guillou, N., Podbevsek, D., Ledoux, G., Elkaim, E., Fateeva, A., Demessence, A., *Inorg. Chem.* 2019, **58**, 99-105.
- 73- Fermi, A., Bergamini, G., Roy, M., Gingras, M., Ceroni, P., *J. Am. Chem. Soc.* 2014, **136**, 6395-6400.
- 74- He, Z., Ke, C., Tang, Z., *ACS Omega* 2018, **3** (3), 3267-3277.
- 75- Li, C., Jin, X., Zhao, T., Zhou, J., Duan, P., *Nanoscale Adv.* 2019, **1**, 508-512.
- 76- Wang, F., Ji, W., Yang, P., Feng, C., *ACS Nano* 2019, **16**, 7281-7290.
- 77- Shen, Z., Wang, T., Shi, L., Tang, Z., Liu, M., *Chem. Sci.* 2015, **6**, 4267-4272.
- 78- MacKenzie, L., Pal, R., *Nat. Rev. Chem.* 2021, **5**, 109-124.
- 79- Kameta, S., Shimizu, T., *Nanoscale* 2020, **12**, 2999-3006.

- 80- Veselska, O., Cai, L., Podbevsek, D., Ledoux, G., Guillou, N., Pilet, G., Fateeva, A., Demessence, A., *Inorg. Chem.* 2018, **57**, 2736-2743.
- 81- Yam, W., Lo, K., Wang, C., Cheung, K., *J. Phys. Chem. A* 1997, **101**, 4666-4672.
- 82- Zhang, M., Li, H., Li, H., Lang, J., *Dalton Trans.* 2016, **45**, 17759-17769.
- 83- Veselska, O., Podbevsek, D., Ledoux, G., Fateeva, A., Demessence, A., *Chem. Commun.* 2017, **53**, 12225-12228.
- 84- Rosas, R., Reyes, Y., Morales, J., Gomez, V., Garcia, I., *Journal of Chem.* 2017, **2017**, 7623210.
- 85- Sapunar, M., Domcke, W., Doslic, N., *Phys. Chem. Chem. Phys.* 2019, **21**, 22782-22793.
- 86- Ackerman, M., Ricciardi, C., Weiss, D., Chant, A., Kraemer, M., *J. Chem. Educ.* 2016, **93**, 2089-2095.
- 87- Lyu, Y., Azevedo, H., *Molecules* 2021, **26**, 873.
- 88- Li, F., Zhu, Y., You, B., Zhao, D., Ruan, Q., Zeng, Y., Ding, C., *Adv. Funct. Mat.* 2010, **20**, 669-676.
- 89- Zhang, Y., Zhu, L., Tian, J., Zhu, L., Ma, X., He, X., Huang, K., Ren, F., Xu, W., *Adv. Sci.* 2021, **8**, 2100216.
- 90- Fichman, G., Gazit, E., *Acta Biomaterialia* 2014, **10**, 1671-1682.
- 91- Braun, G., Ary, B., Dear, A., Rohn, M., Payson, A., Lee, D., Parry, R., Friedman, C., Knowles, T., Linse, S., Akerfeldt, K., *Biomacromolecules* 2020, **21**, 4781-4794.
- 92- Zheng, J., Fan, R., Wu, H., Yao, H., Yan, Y., Liu, J., Ran, L., Sun, Z., Yi, L., Dang, L., Gan, P., Zheng, P., Yang, T., Zhang, Y., Tang, T., Wang, Y., *Nat. Commun.* 2019, **10**, 1604.
- 93- Xie, H., Kinoshita, I., Karasawa, T., Kimura, K., Nishioka, T., Akai, I., Kanemoto, K., *J. Phys. Chem. B* 2005, **109**, 9339-9345.
- 94- Yam, V., Au, V., Leung, S., *Chem. Rev.* 2015, **115**, 7589-7728.
- 95- Song, J., Li, S., Zhou, R., Shao, J., Qiu, X., Jia, Y., Wang, J., Zhang, X., *Dalton Trans.* 2016, **45**, 11883-11891.
- 96- Ford, P., Cariati, E., Bourassa, J., *Chem. Rev.* 1999, **99**, 3625-3648.
- 97- Bae, W., Yoon, T., Jeong, C., *PLoS ONE* 2021, **16**, e0247326.
- 98- Delgado, S., Sanz, P., Priego, J., Jimenez, R., Gomez, C., Zamora, F., *Inorg. Chem.* 2008, **47**, 9128-9130.
- 99- Deng, Y., Wang, M., Zhuang, Y., Liu, S., Huang, W., Zhao, Q., *Light: Science & Applications* 2021, **10**, 76.
- 100- Liu, M., Zhang, L., Wang, T., *Chem. Rev.* 2015, **115**, 7304-7397.
- 101- Zhang, M., Li, K., Zang, S., *Adv. Opt. Mat.* 2020, **8**, 1902152.
- 102- Hassanein, K., Cappuccino, C., Amo, P., Lopez, J., Maini, L., Bandini, E., Ventura, B., *Dalton Trans.* 2020, **49**, 10545-10553.

- 103- Low, K., Roy, V., Chui, S., Chan, S., Che, C., *Chem. Commun.* 2010, **46**, 7328-7330.
- 104- Zhan, Y., Xia, T., Yu, K., Zhang, F., Yang, H., Liu, B., An, Y., Yin, Y., Chen, X., *ChemPlusChem* 2014, **79**, 559-563.
- 105- Al-Mahamad, L., El-Zubir, O., Smith, D., Horrocks, B. R., Houlton, A., *Nat. Commun.* 2017, **8**, 720.
- 106- Hofmann, A., Kroon, R., Zokaei, S., Järsvall, E., Malacrida, C., Ludwigs, S., Biskup, T., Müller, C., *Adv. Elect. Mat.* 2020, **6**, 2000249.

Chapter 6. A nanowire-based gas sensor

Table of Contents

6.1. Introduction.....	153
6.2. Materials and Methods	155
6.2.1. Sensing System	159
6.2.2. Sensing properties studies	161
6.3. Results and Discussion	162
6.3.1. Spectroscopic, microscopic and electrical characterization	162
6.3.2. Sensing by Cu(I)-6-thioguanosine films.....	169
6.3.3. T90 reaction times in Cu(I)-6-thioguanosine films	173
6.3.4. VOCs sensing in Au(I)-6-thioguanosine/MWCNTs composites.....	175
6.3.5. T90 reaction times in Au(I)-6-thioguanosine/MWCNTs composites ..	181
6.4. Conclusions.....	182
6.5. References	183

6.1. Introduction

Researchers and commercial institutions have faced a challenge by chemical sensors to the classic model of analytical measurement with instrumentation.¹ The differences between instrumentation and sensors have become increasingly more important and the optimum choice of technique for a given application often depends on these factors in addition to analytical performance.² In general, analytical instrumentation has higher sensitivity and selectivity than chemical sensors. Examples include mass spectrometry, chromatography and various types of spectroscopy. Such instruments, however, suffer from disadvantages: they may not be portable, they require trained operators and sample preparation techniques and they are often confined to centralized laboratories.³ In contrast, chemical sensors are, by design, small, portable and cheap devices.⁴ They typically do not require a trained operator to carry out the measurement. Chemical sensors are therefore most useful in situations where great precision is not required, but the cost of the analysis or the ability to perform the measurement in the field or distributed over many sites is crucial.⁵ This is often the case for the measurement of gases in industrial safety or environmental contexts.^{6,7} Gas sensors are based on the change of one or more of physical properties when in contact with gases and calibration of this property against the gaseous analyte allows determination of various gases.^{8,9}

Some applications of gas sensors are of increasing interest owing to current environmental concerns and how they affect the health of people. Mainly, those sensors are committed to study harmful analytes present in the air that we breathe. Common, hazardous analytes present in the air are ozone, carbon monoxide, nitrogen dioxide or sulfur dioxide.¹⁰ To analyze the air quality there are different methods of sensing. These include electrochemical reactions (amperometric sensors), solid state semiconductors devices based on the conductivity response of metal oxides,

photoionization or optical methods such as light scattering.¹¹ Using these techniques, the response of the sensor, which governs the time taken for the analysis, is typically between 10 s and 60 s and the limit of detection lies in the ppm range.^{12,13} Whilst these figures are typical, it is also possible for gas sensors to reach ppb detection limits and the upper limit of their dynamic range may be as high as 1000 ppm.¹⁴

Analysis of the composition of breath has relevance in healthcare. In breath there are many relevant analytes including carbon dioxide, nitrogen oxides, ammonia or VOCs (hydrocarbons, alcohols, terpenes or aldehydes). To measure them there are different sensing methods that stand out for their greater reliability and sensitivity for the analytes quoted.^{15,16} The chemiluminescence sensors and chemiresistors (similar to metal oxide semiconductor devices) have a limit of detection around 2 ppb for nitrogen oxide. Amperometric electrochemical sensors and the use of spectroscopy as a detection technique are well known. The use of metal oxide semiconductors and optical sensors are also useful for acetone and ammonia.¹⁷⁻¹⁹

Specifically, the utility of electronic sensors arises from their low cost, reliability, low power consumption and long operational lifespan; in these respects, they often have advantages over optical/spectroscopic methods because no light source or optical components are required.²⁰ Electronic devices rely on changes in conduction upon interaction with the analyte.²¹ Such effects may be small for bulk materials but increase as the surface to volume ratio increases when the material reaches nanoscale dimensions.²² That guides us to choose self-assembled nanowires as a system for electronic gas sensors. The semi-conductive materials investigated in this thesis are of particular interest because of their known sensitivity to oxidation.²³ The combination of the semiconducting coordination polymers with CNTs materials allow us to merge the high conductance and surface area of the CNTs²⁴⁻²⁵ with the possibility of alteration

of conductance from the coordination polymer when its surface is exposed to different vapours.²⁶

In this chapter we have analyzed the behavior of a coordination polymer based on Cu(I) as a sensor for ozone and VOCs and we have measured the effect of coating CNTs, specifically of type MWCNTs, with the metal(I)-thionucleobase coordination polymers to enhance the sensitivity of the sensors.

6.2. Materials and Methods

Most of chemicals used in the preparation of the complex were purchased from Sigma-Aldrich and they were used without any purification.

The coordination polymer was prepared by metal/nucleoside complexation in aqueous media. The first coordination polymer proposed for sensing used, as a metal-containing reagent, tetrakis (acetonitrile) Cu(I) tetrafluoroborate. The second polymer was based on chloroauric acid. (-)-2-amino-6-mercaptapurine riboside hydrate was the nucleoside used. The chloroauric acid is Au(III) and prior to complexation must be reduced to Au(I). The reducing agent used was 2,2'-thiodiethanol. The solvent to prepare the coordination polymer was highly purified nanopure deionized water (with nominal resistivity of 18.2 MΩ·cm) from a Barnstead NANOpure® Diamond™ Life Science ultra-pure water system attached to a Diamond™ reverse osmosis system. Absolute ethanol for HPLC, acetone for HPLC and chloroform for 99.8% were purchased from Fisher Scientific Ltd., UK. The multi-wall carbon nanotubes (MWCNTs Elicarb™) were purchased from Thomas Swan, UK with diameter 2-10 nm and dispersed in methanol (obtained from Fisher Scientific Ltd., UK). Interdigitated Pt on glass microelectrodes (DRP-G-IDEPT10) with an electrode width of 10 microns and an inter-electrode gap also of 10 microns (DropSens) were purchased from Metrohm

Ltd., UK. The number of digits was 125x2, and the nominal cell constant of the device is 0.0118 cm^{-1} (Figure 6.1).



Figure 6.1. Interdigitated Pt on glass microelectrodes (DRP-G-IDEPT10). The sample is deposited on the right grey part of the electrode.

The preparation of the Cu(I)-6-thioguanosine coordination polymer was performed in aqueous solution. (-)-2-amino-6-mercaptapurine riboside hydrate (18 mg) was crushed and added to water (1 mL) and sonicated for one hour. Tetrakis (acetonitrile) Cu(I) tetrafluoroborate (18.9 mg) was then added to the 6-thioguanosine suspension and strongly mixed with stirring for one hour on a magnetic stirrer. The resulting orange mixture was left for 7 days to form a gel.

The preparation of the Au(I)-6-thioguanosine coordination polymer was performed in aqueous solution. (-)-2-amino-6-mercaptapurine riboside hydrate (0.5 mg) was crushed and added to water (1 mL). Chloroauric acid (0.5 mg) was dissolved in deionized water (1 mL) and then the Au(III) was reduced to Au(I) using the reducing agent 2,2'-thiodiethanol (0.35 mg) before mixing with the 6-thioguanosine suspension and carbon nanotube dispersion in various ratios given below. A dispersion of multi-wall carbon nanotubes was prepared after sonicating 0.1 mg MWCNTs in methanol (10 mL) for 3 h using a micro tip (750 W, 20 kHz, amplitude 20%, 230 Volt, ultrasonic processor) to avoid aggregation of MWCNTs at the bottom of the vial.

Three samples were prepared with three different ratios of Au(I)-6-thioguanosine:MWCNTs by adding $1\mu\text{L}:1\mu\text{L}$, $2.5\mu\text{L}:2.84\mu\text{L}$ and $5\mu\text{L}:5.68\mu\text{L}$ of the 6-

thioguanosine and Au(I) solutions respectively to 50 μL of the MWCNT dispersion. An additional sample prepared from 50 μL of MWCNTs alone was explored as a control for the effect of the polymer on the sensing response. The mole ratio of Au:C in the composites on a percentage basis was 3.5%, 10% and 20% respectively plus the control sample (0%). One sample of Cu composite was prepared, Cu(I)-6-thioguanosine:MWCNTs, 1 μL :1 μL of the 6-thioguanosine and Cu(I) solutions were added to 50 μL of the MWCNT dispersion.

Multiple techniques were used to investigate the formation of the composites Cu(I)-6-thioguanosine/MWCNTs and Au(I)-6-thioguanosine/MWCNTs. The interaction of the coordination polymer and MWCNTs, essential for sensing application, were characterized by atomic force microscopy (AFM), Raman spectroscopy (only Au(I)-6-thioguanosine/MWCNTs), scanning electron microscopy (SEM) and electrical measurements (Au(I)-6-thioguanosine/MWCNTs and Cu(I)-6-thioguanosine).

Atomic force microscopy data were obtained using a Multimode 8 atomic force microscope with a NanoscopeV controller (Bruker) and a 'E' scanner. Nanoscope software version 9.1 was used to control the microscope. The system was operated in ScanAsyst in Air mode as a peak force tapping mode at ultra-low forces to minimize damage to the samples. A silicon tip on silicon nitride cantilevers (ScanAsyst, Bruker) was used as the tips for imaging. The nominal tip radius was approximately 2 nm, resonant frequency 150 kHz, and spring constant $k \approx 0.7 \text{ nm}^{-1}$. The AFM data were analyzed with NanoScope Analysis 1.5 software (Bruker). Cu(I)-6-thioguanosine/MWCNTs and Au(I)-6-thioguanosine/MWCNTs samples were drop cast from solution (3 μL) onto interdigitated electrodes and were dried at room temperature for 15 min. All measurements were performed at room temperature in air.

For Raman spectra a Confocal Raman Imaging microscope (alpha CRM200, Witec GmbH) was used. The back scattered light was collected by a multimode fiber, which served as the confocal pinhole, dispersed on a grating and detected by a Peltier-cooled CCD. The laser excitation wavelength was 488 nm using a diode laser of 60 mW output power. The measured light intensity at the sample was 12 mW. MWCNTs and Au(I)-6-thioguanosine/MWCNTs sample was drop cast from solution (3 μ L) onto interdigitated electrodes and were dried at room temperature for 15 min.

A TESCAN VEGA LMU Scanning Electron Microscope, housed within EM Research Services, Newcastle University was used. Digital Images were collected with TESCAN supplied software. CNTs, Cu(I)-6-thioguanosine/MWCNTs and Au(I)-6-thioguanosine/MWCNTs samples were prepared by drop-casting 3 μ L of solution into Si chips and drying at room temperature overnight. The samples were then mounted on an aluminum stub with double sided adhesive tape. Silicon chips of 1 cm² area were cut from 10 cm diameter wafers (dopant boron and <111> oriented p-type, resistivity 0.09-0.12 Ohm-cm) which were purchased from Pi-KEM Ltd.

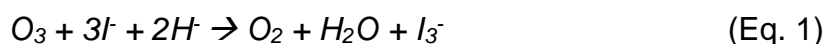
Current-voltage measurements were performed on a probe station (Cascade Microtech) and readings were collected using a Hewlett Packard Agilent Technologies B1500A semiconductor parameter analyzer driven by Agilent Easy EXPERT software. The applied voltage was varied from +2 V to -2 V in steps of 0.05 V. Nitrogen was flowed through the probe station sample chamber to keep the measurement area dry. All data were measured at room temperature after 30 min of nitrogen flow. Cu(I)-6-thioguanosine sample was drop cast on the electrode (~100 μ L) and spread as a thin film. It was then allowed to dry in vacuo to form the xerogel which comprises an orange-brown film in which networks of Cu(I)-6-thioguanosine nanowires span the inter-electrode gaps. Au(I)-6-thioguanosine/MWCNTs sample (3 μ L) was dried on inter digitated electrode and it was dried for 15 min before any measurement. Prior to use,

the interdigitated electrodes were cleaned by sonication for 15 minutes in acetone before being washed with acetone and dried under a stream of nitrogen gas.

6.2.1. Sensing system

The performance of the devices was evaluated using a test rig to provide flows of controlled gas composition over the sensors. Two configurations were employed: one for ozone testing and one for volatile organic compounds (VOCs).

Ozone was generated in a flow of synthetic air (aka zero air, 4:1 dry N₂ : dry O₂) by irradiation with a shortwave UV tube lamp ($\lambda = 185$ nm). The tube lamp runs parallel to the gas flow line and is covered by a ruled aluminum shield (Figure 6.2, part A). The relative concentration of ozone is controlled by removing the shield to reveal a known fraction of the tube lamp. The absolute concentration of ozone was determined by calibration using the reaction of ozone with iodide (equation 1) in a Dreschel bottle in place of the sensor compartment:



Triiodide (I₃⁻) has a characteristic band at $\lambda = 350$ nm and was determined by UV spectrophotometry of the solution after passage of the gas stream for 10, 20, 30, 40, 50 and 60 min. At a volume flow rate of 100 mL min⁻¹ the ozone concentration could be controlled in the range between 5 and 25 ppm.

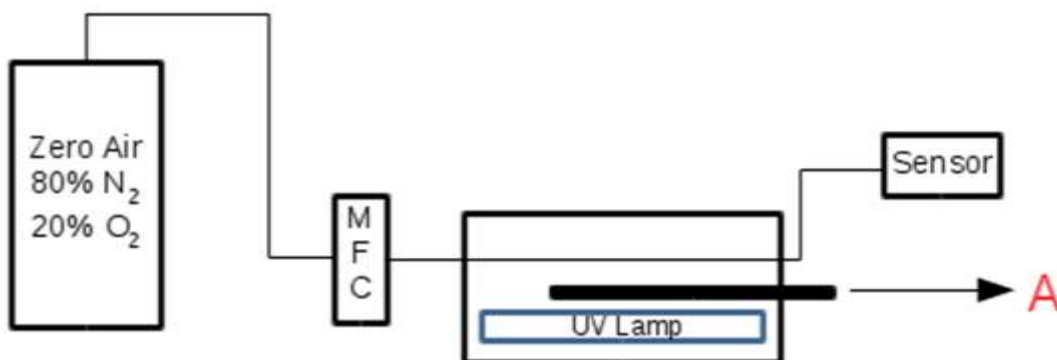


Figure 6.2. Schematic of the ozone rig. Synthetic (zero) air flows from a gas bottle through a mass flow controller (MFC) and past a shortwave (185 nm) UV lamp. The partial pressure of ozone flowing to the sensor is determined by the volume flow rate and the extent to which the aluminium shield A is retracted from the UV lamp. The solid lines indicate 6 mm i.d. PVC tubing.

The configuration employed for VOCs is shown in Figure 6.3. Two MFCs (mass flow controllers, Figure 6.3 a,b) were used to control the volume flow rate of VOC-saturated air and zero air. Pure synthetic air (zero air; 80% N₂, 20% O₂, BOC Ltd) was passed through a Dreschel bottle (Figure 6.3c) to saturate it with the chosen VOC and then mixed with zero air before passing to the gas cell/sensor as shown in Figure 6.3. The volume flow rate of zero air and VOC-saturated air varied from 400;100, 300;200, 200;300, 100;400 and 0;500 mL min⁻¹ respectively throughout the experiment. For the control measurement (zero air) the volume flow rate was fixed at 400 mL min⁻¹. A thermocouple connected to the sensor and the Dreschel bottle was used to monitoring the temperature of each separately.

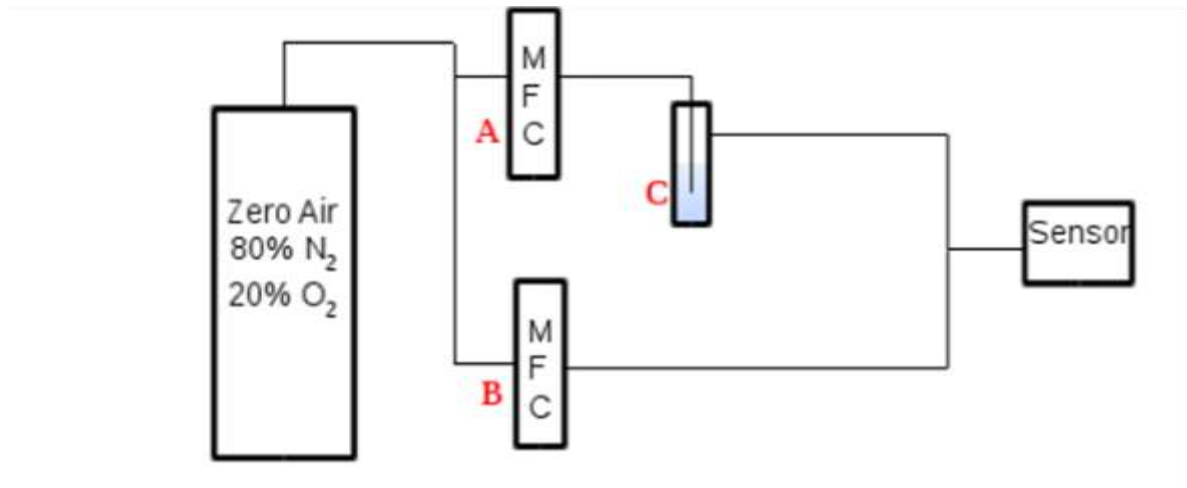


Figure 6.3. Schematic of the VOC sensing test rig. Synthetic (zero) air flows from a Gas bottle via two independent mass flow controllers (MFC A and MFC B). The air streams A passes through a Dreschel bottle where it is saturated with the vapor of an organic liquid (C). The two flows are combined before passing to the sensor. The solid lines indicate 6 mm i.d. PVC tubing.

6.2.2. Sensing properties studies

A stream of VOC at controlled partial pressures in synthetic air was generated by adjusting the volume flow rates in the two lines of Figure 6.3. The partial pressure of the analyte at the sensor is then determined by the mixing ratio and the saturated vapor pressure at the temperature of the Dreschel bottle, p^* , via equation 2.

$$p = p^* \cdot \frac{V_{air}}{V_{voc} + V_{air}} \quad (\text{Eq. 2})$$

Where V_{voc} and V_{air} are the volume flow rates of the VOC-saturated air and of the pure synthetic air. The saturated vapor pressure p^* was obtained from the Antoine equation, equation 3.

$$\log_{10} p^* = A - \frac{B}{T + C} \quad (\text{Eq. 3})$$

The parameters A, B and C for particular VOCs were obtained from the National Institute of Standards and Technology (NIST) database (<http://webbook.nist.gov/>).

In both the ozone or the VOC experiments, the response of the sensor was monitored either using a digital multimeter (Agilent 34401A, controlled with LabView) to record directly the device resistance or using a potentiostat to apply a fixed bias voltage and to record the direct current flowing across the device.

To quantify the sensor performance, the film sensitivity was calculated by observing the fractional change in film resistance, equation 4.

$$S = \frac{R - R_0}{R_0} \quad (\text{Eq. 4})$$

Where R_0 is the film resistance on the zero air (background) and R is the film resistance during exposure to the analyte (VOCs:dry air).

6.3. Results and Discussion

6.3.1. Spectroscopic, microscopic and electrical characterization

The coordination polymer, Cu(I)-6-thioguanosine, Au(I)-6-thioguanosine, and composites Cu(I)-6-thioguanosine/MWCNTs and Au(I)-6-thioguanosine/MWCNTs were characterized using different techniques. Mainly the nanocomposites were characterized using AFM to determine the effect of mixing the coordination polymer with carbon nanotube as well as mixing volume. Figure 6.4a and b shows a Au(I)-6-thioguanosine and Cu(I)-6-thioguanosine AFM image of individual strands respectively. Two distinct heights (nanowire diameters) are discernible in the image. We interpret these as the formation of double-strands by the intertwining of individual strands – the helical nature of this self-assembly is evident in the apparent corrugation along the double-stranded regions.

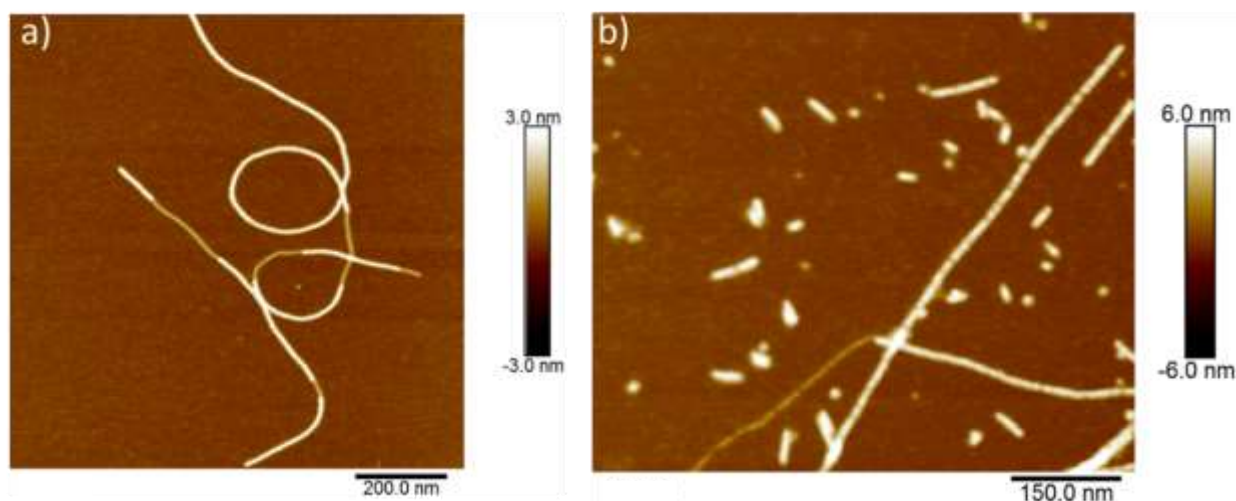


Figure 6.4. AFM image on air of polymer strands of drop-cast a) Au(I)-6-thioguanosine and b) Cu(I)-6-thioguanosine after drying.

Atomic force microscopy was also used to image the topography of composites. The samples were drop cast from a small volume of solution (3 μL) onto mica wafer, dried for 15 min and finally imaged in air. The scan over the sample surface is produced by the tip marking intermittent contact with the sample. The control MWCNT sample (Figure 6.5a) and the Cu(I)-6-thioguanosine/MWCNTs sample show the presence of individual nanotubes (Figure 6.5c), however the composite Au(I)-6-thioguanosine/MWCNTs (Figure 6.5b), which tends to readily absorb moisture from the atmosphere, has the appearance of a film and individual nanotubes are not easy to discern.

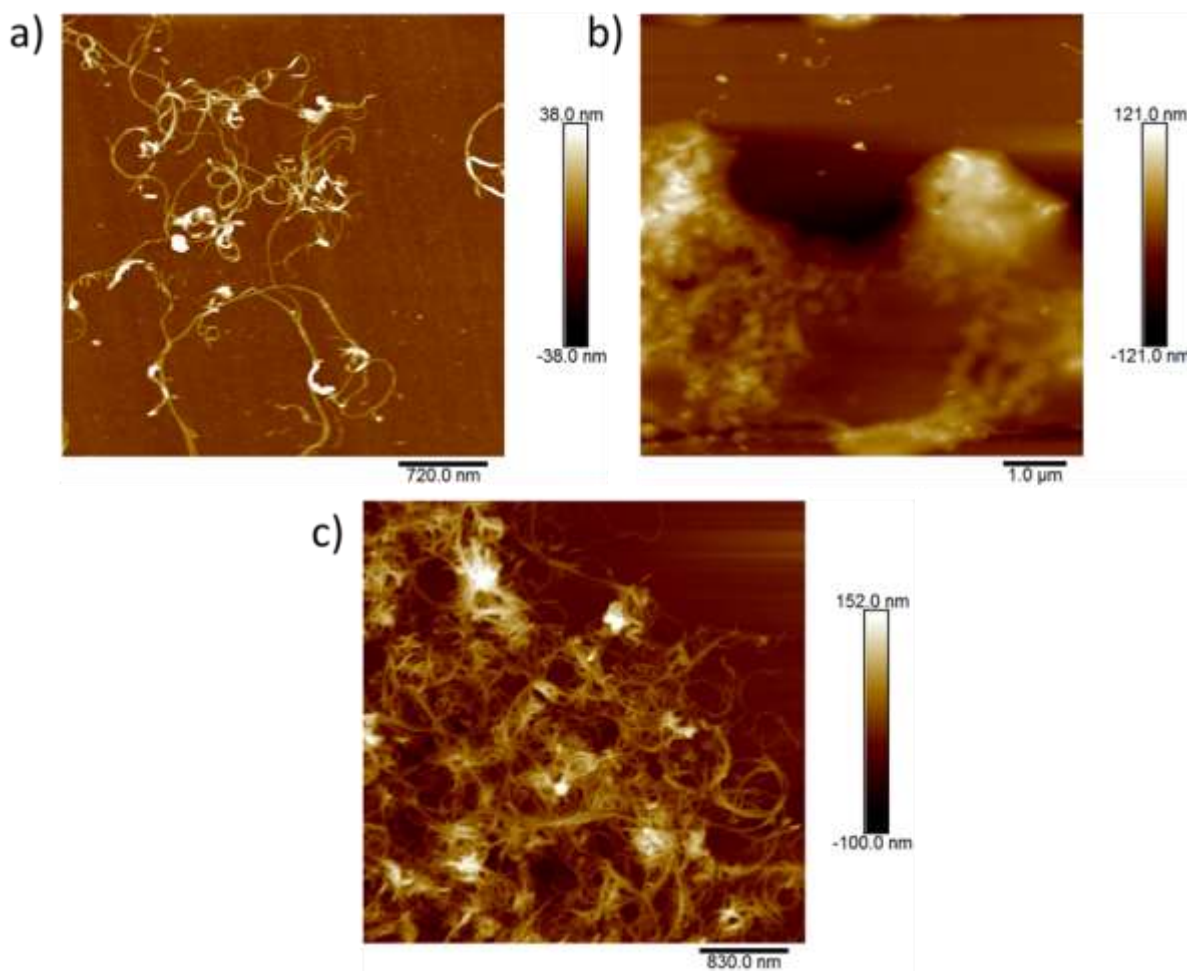


Figure 6.5. AFM images a) bare MWCNTs, b) Au(I)-6-thioguanosine/MWCNTs composite and c) Cu(I)-6-thioguanosine/MWCNTs composite.

It is clearly difficult to confirm the presence of CNTs in the composites only with AFM images, so we have analyzed the same samples using SEM. These two types of microscopy exhibit differences, especially in the imaging mechanism. AFM tip is very sensitive to the organic material because it depends on tip/sample forces, but SEM is less sensitive to the organic material and the electrons scatter more strongly from the CNTs.

SEM was used to image the MWCNTs, Cu(I)-6-thioguanosine/MWCNTs and Au(I)-6-thioguanosine/MWCNTs nanocomposites in order to determine the effect of adding the

coordination polymer to the carbon nanotubes. Characterization by SEM reveals differences between these systems. Figure 6.6a and 6.6b reveal one dimensional fibres of MWCNTs, Figure 6.6c shows the Cu(I)-6-thioguanosine/MWCNTs nanocomposite film. Those are difficult to see but it clearly shows that the Cu(I) coordination polymer, forming spherical aggregates and MWCNTs are interacting with each other.

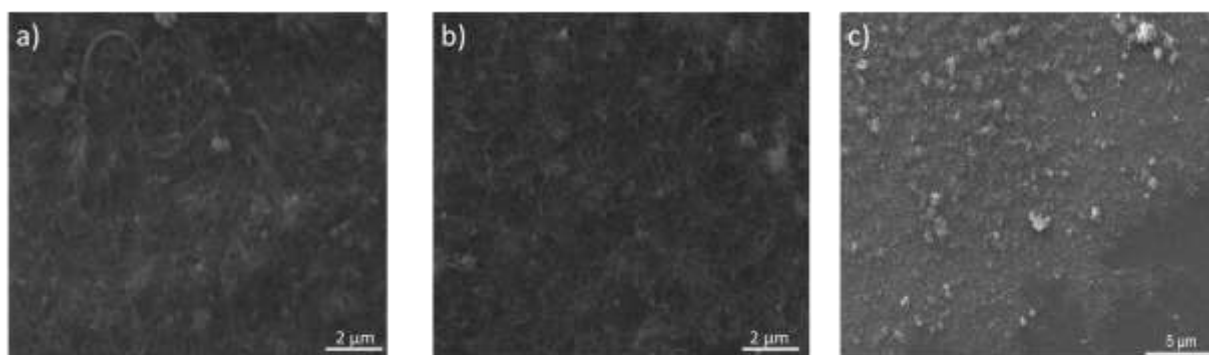


Figure 6.6. SEM images a) bare MWCNTs b) Au(I)-6-thioguanosine/MWCNTs composite and c) Cu(I)-6-thioguanosine/MWCNTs composite.

Examining images from AFM and SEM together, there is a clear evidence of the presence of MWCNTs in the composites. MWCNTs have a similar morphology in the composites as they do in pure MWCNTs sample, under SEM they look almost the same for the composite as for the control, but there is evidence they are coated with the coordination polymer (Cu-6-thioguanosine or Au(I)-6-thioguanosine) because of the difference between AFM images of composite and the bare CNTs control.

Raman spectroscopy can be used to monitor the change in composition and structure of MWCNTs and Au(I)-6-thioguanosine/MWCNTs nanocomposites.²⁷ Figure 6.7 did confirm the presence of MWCNTs in the composite by the expected bands at Raman shifts of 1365 cm^{-1} (D-band), 1588 cm^{-1} (G-band) and 2706 cm^{-1} (2D).²⁸

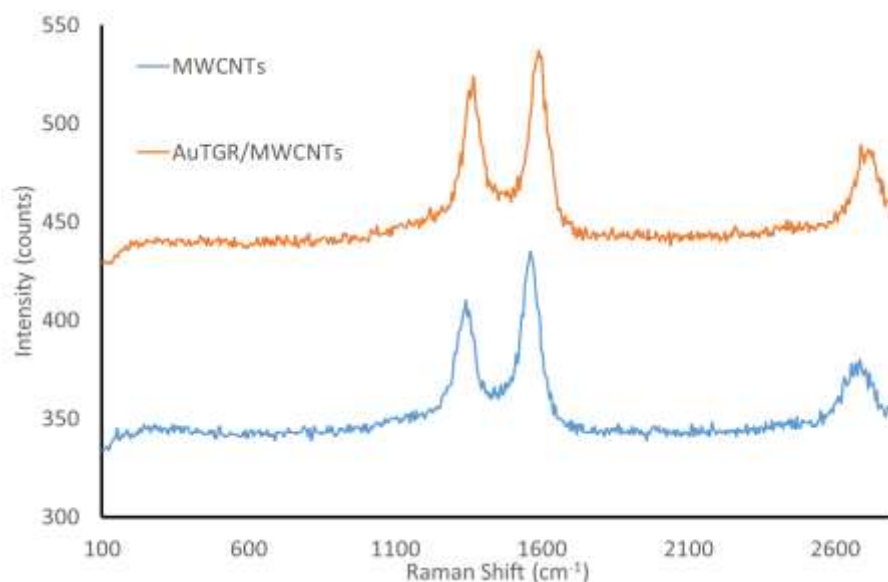


Figure 6.7. Raman spectra of bare MWCNTs (blue line) and Au(I)-6-thioguanosine/MWCNTs (orange line). (Note: the dark count of the CCD is about 325 and the spectrum for the composite has been offset on the y-axis for clarity).

Since D band is due to sp^3 carbons and G band to sp^2 carbon hybridization²⁹ we can assume that the slightly greater ratio D/G in the composite compared to the MWCNTs control is the only indication of sp^3 carbons of the composite in the spectrum.

For electrical characterization, bare MWCNTs and Au(I)-6-thioguanosine/MWCNTs composites at different ratios were investigated using a two-point current-voltage (I-V) measurement on a probe station. Figure 6.8 shows the I-V plots of bare MWCNTs and nanotube-polymer composites at different ratios: all show an ohmic behavior. The four samples plotted indicate the change in the current during application of a direct current voltage between -2 V and +2 V. The horizontal portion of the data merely indicates the maximum current that can be passed by the instrument of about 5 mA. The data shows that the current decreases after Au(I)-6-thioguanosine is added to the MWCNTs and as the ratio Au:C increases, the conductance decreases from 5.0 mS for a control

sample of MWCNTs to 0.43 mS for the 20% sample, which has the largest amount of Au(I)-6-thioguanosine polymer (Figure 6.8).

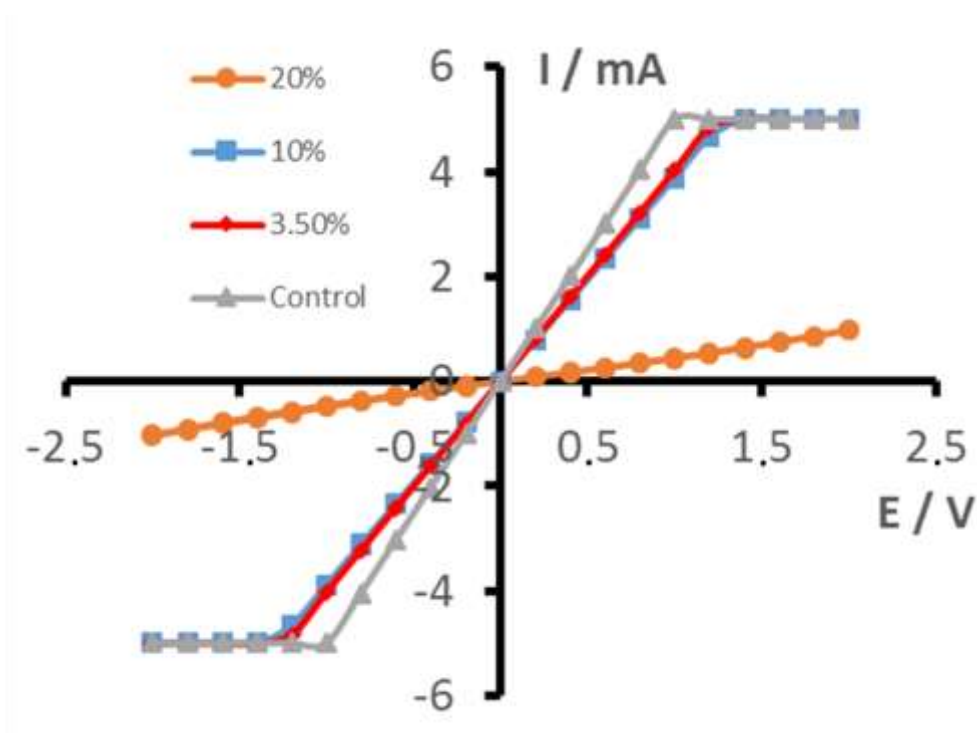


Figure 6.8. Two-terminal I-V characteristics of three samples with different ratios Au(I)-6-thioguanosine/MWCNTs and bare MWCNTs control. The ratios are reported as percentages calculated on the basis of the molar ratio of Au:C in the composite.

The monotonic decrease in conductance with the mole ratio of polymer is interpreted as the effect of the semiconducting polymer coating the metal-like MWCNTs and introducing additional inter-tube tunneling barriers for charges to pass through the composite (Figure 6.9). The reason for the sharp decrease in conductance between the 10% (3.89 mS) and 20% sample (0.43 mS) is unclear, but percolation effects are well-known in metal/insulator composites.³⁰

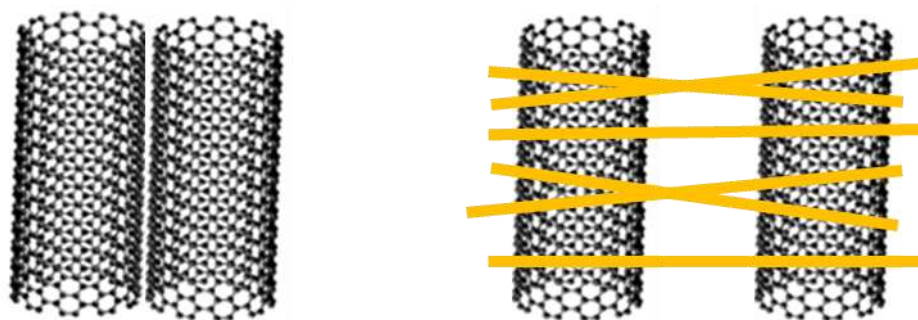


Figure 6.9. Schematic diagram showing two MCNTs in solution before (left) and after (right) be coated and dispersed with coordination polymer (yellow lines).

Electrical characterization of pure Cu(I)-6-thioguanosine was also performed in a two-point measurement on the probe station. Cu(I)-6-thioguanosine devices showed non-linear I-V characteristics, which are typical for hopping conductors. Here, the carriers are localized and make tunneling transitions between sites following a simple nearest-neighbour hopping model in which a given charge has only one possible hop.³¹ In our polymer system, there is also the possibility to have a significant contribution to the overall resistance from the interfacial charge transfer at the contacts because one of them would always be reverse-biased resulting a sigmoidal I-V curve (Figure 6.10). Nevertheless, the devices have an easily measurable differential conductance at zero bias suitable for using in sensing. Figure 6.10 shows the I-V characteristic curve for the pure polymer Cu(I)-6-thioguanosine and following other related experiments in our group, it shows differences in conductance in relation to Au(I)-6-thioguanosine since Cu(I)-6-thioguanosine conducts a little bit when is chemically undoped whereas Au(I)-6-thioguanosine need to be doped to conduct.²³ We suggest that the reason for this is the accessibility of the Cu(II) oxidation state.

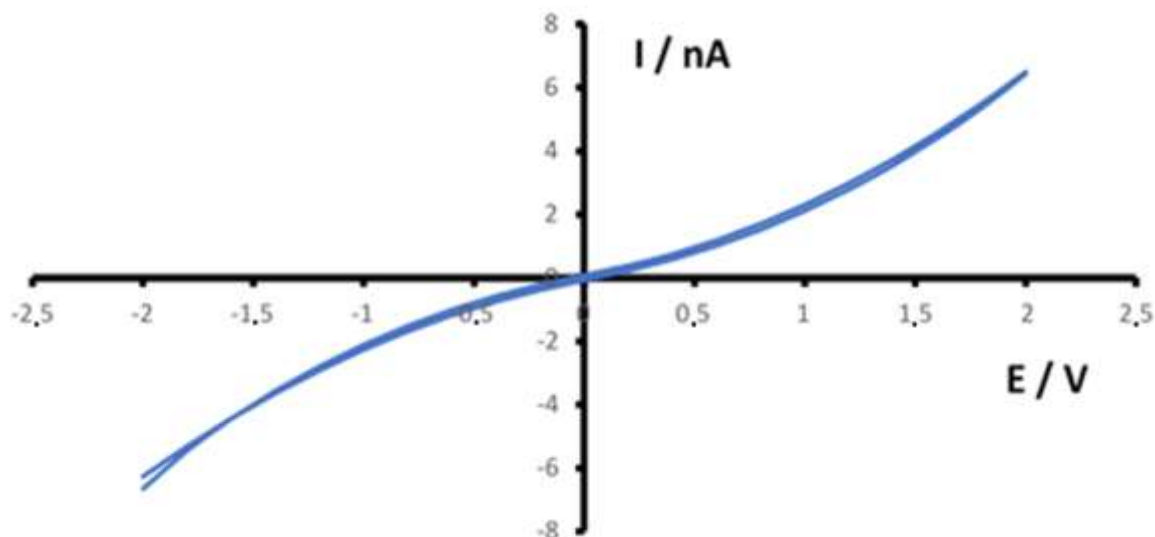


Figure 6.10. Two-terminal I-V characteristic for a typical pure Cu(I)-6-thioguanosine device.

6.3.2. Sensing by Cu(I)-6-thioguanosine films

The detection of ozone in Cu(I)-6-thioguanosine is shown in Figure 6.11. It shows typical data for the response of a Cu(I)-6-thioguanosine device to 23.5 ppm ozone. As expected, there is a drop-in resistance upon exposure to ozone – similar polymers have been successfully oxidatively doped.²³ However, the response time of >5 min is rather long and the resistance does not recover upon shielding the UV lamp to return the sensor to pure air. In fact, repeated exposure of the device to ozone resulted in degradation of the film. This is considered to most likely be a result of the extreme oxidizing power of ozone and we were unable to produce re-usable sensing devices. We therefore switched to a study of the response to VOCs.

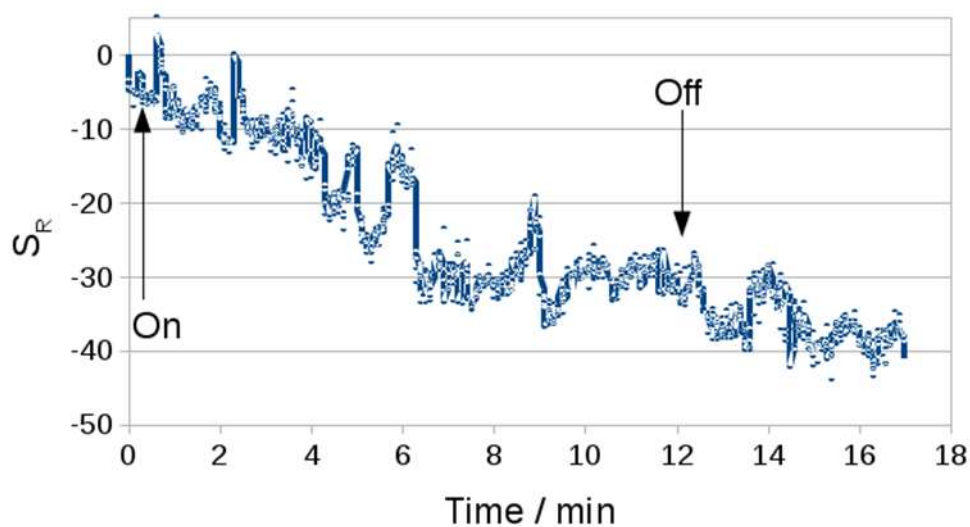


Figure 6.11. Data for the response of the resistance of a Cu(I)-6-thioguanosine to 23.5 ppm ozone at a volume flow rate of 100 mL/min. The arrows indicate the times at which the device was exposed to ozone and at which the ozone was removed.

In the detection of volatile organic compounds, a reversible response of the Cu(I)-6-thioguanosine device to all three vapours (acetone, chloroform and ethanol) was observed. Example data for chloroform is given in Figure 6.12.

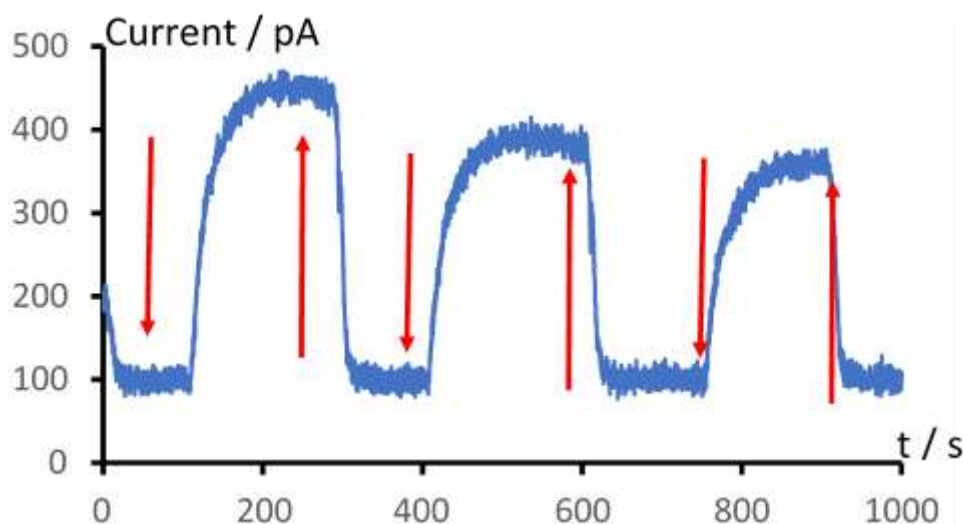


Figure 6.12. Typical raw data showing the reversibility of the current response of Cu(I)-6-thioguanosine to chloroform vapour. Down arrows indicate exposure of the sensor to 300 ppm chloroform and up arrows indicate return to pure synthetic air. The flow rate was constant at 100 mL min^{-1} throughout and steady applied voltage of 0.5 V .

Response times to achieve 90% of the steady value of S_i , reported as a percentage change in current following equation 5, were of the order of $t_{90}=40 \text{ s}$ or less. Figure 6.10 is an indication that this material is not highly conductive, so the multimeter is not capable of making reliable resistance measurements. In these cases, a direct measurement of current by the potentiostat is better (in Figure 6.13 pA currents correspond to TOhm resistance and the multimeter can only measure GOhm resistances at maximum).

The presence of the VOCs on the surface of the electrode makes the current decrease since the resistance is increasing.

$$S = \frac{(I-I_0)}{I_0} \quad (\text{Eq. 5})$$

The sensitivity of the device was lowest for chloroform and larger for the polar molecules, acetone and ethanol (Figure 6.13). The shape of the $\ln S_i$ vs p curve (Figure 6.13) suggest an adsorption process is responsible for the analytical response. BET theory can be applied to systems of multilayer adsorption and it aims to explain the adsorption of gas molecules on solid surfaces (microporous solids) without any chemical reaction between them; once the micropores are filled by the gas molecules there are not free surface for further sorption. Specifically, Figure 6.13 gives rise to a similar shape as that of a type I isotherm if the analytical signal is assumed to be proportional to the volume of gas absorbed onto the surface of the sample as pressure increases.³² At high pressure the pores start to fill and therefore the additional response to the VOCs decreases at high pressure – the curve is sublinear.

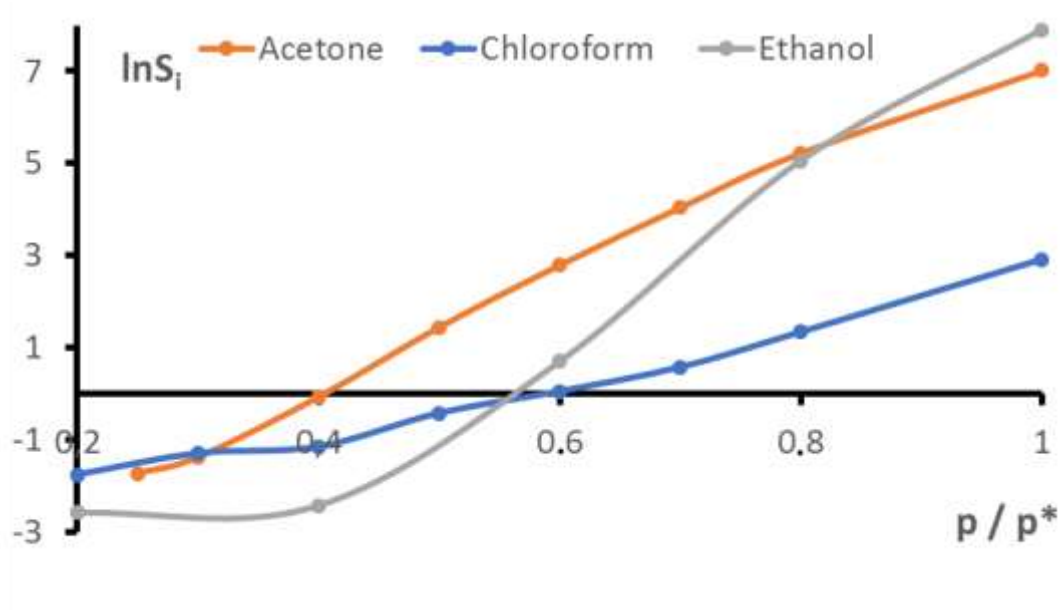


Figure 6.13. Data for the response of the dc current at fixed bias of 1V for a Cu(I)-6-thioguanosine to three VOCs. p/p^* is the fraction of the saturated vapour pressure of the VOC.

6.3.3. t_{90} reaction times in Cu(I)-6-thioguanosine films

The standard measure of device response time is the t_{90} parameter.³³ This is defined as the time taken for the response to attain 90% of the steady-state response in the presence of the analyte. It can be simply obtained from Figure 6.12 by measuring the time required for S to achieve 90% of the steady-state value after switching the gas flow from air to analyte. This measurement includes a small overestimate equal to the dead volume of the system (length of tubing x cross-section area) divided by the absolute volume flow rate. Also, the response time is dependent on the size of the gas sensing chamber or the working temperature inside it.³⁴⁻³⁵ In our apparatus, the dead-time is less than 2 s and is therefore insignificant in most of the reported measurements. Typical value of t_{90} for commercial amperometric gas sensing systems (e.g. O₂, CO, Cl₂) are around 50 s³³ and the difference between these values and our shorter times is mainly because the sensors studied here rely simply on adsorption on the surface of the material. Thickness or porosity play an important role in the diffusion of the VOC through the material. Figure 6.14 shows the 90% response time for Cu(I)-6-thioguanosine to ethanol; t_{90} increases with partial pressure, reaching a value of 40 s near the saturated vapour pressure. These values are comparable to commercial amperometric sensor t_{90} s for gases, such as carbon monoxide used in safety applications.³³

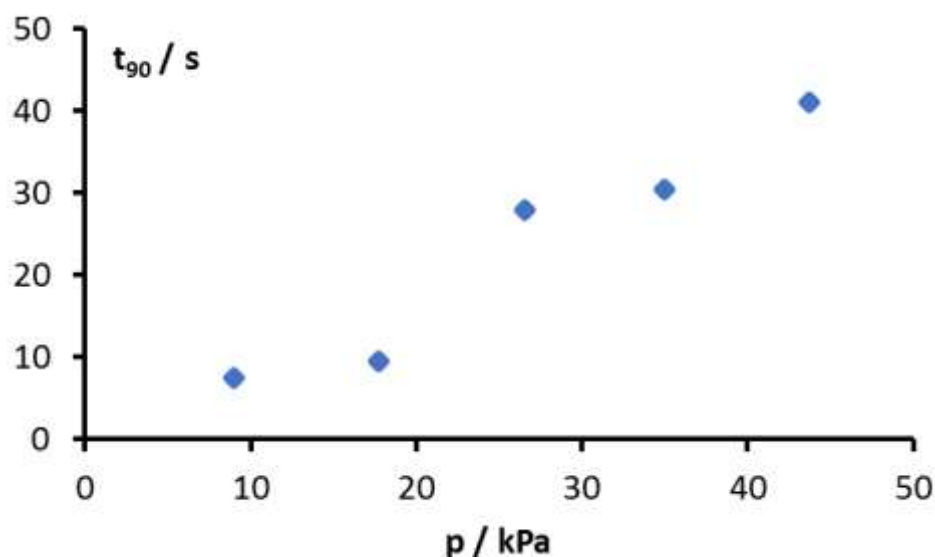


Figure 6.14. 90% response time for Cu(I)-6-thioguanosine to ethanol vapour as a function of the partial pressure of ethanol at the sensor.

Changes in current observed in Figure 6.13 and the t_{90} reaction time, Figure 6.14, are promising. However, it is necessary to make a study of the continual exposure of Cu(I)-6-thioguanosine to VOCs, chloroform and ethanol, required in order to understand if the current response is maintained over a long duration of exposure.

Figure 6.15 shows the effect of continual exposure of Cu(I)-6-thioguanosine to (a) chloroform and (b) ethanol with time. The signal reaches a maximum after which the current decreases strongly, although it does not return all the way to the baseline. The analytical response S_i , based on current following equation 5, was followed over about 15 min. Although the initial response is very large, it decays with continuous exposure until an approximate plateau is observed at about 4000 s in the case of chloroform (Figure 6.15a) and 2000 s in the case of ethanol (Figure 6.15b). The value of current remains larger than the pre-exposure baseline, however the fact that the current decreases very slowly when the partial pressure of the VOCs is constant would make distinguishing slow changes in analyte concentration from purely time-dependent

effects of the sensor difficult. Further, in Figure 6.15, ethanol shows a larger normalized signal at long times than chloroform, but chloroform shows a large response at short times; this would make any attempt to distinguish different analytes difficult.

These long exposure test also show that the response to chloroform is reversible in the sense that the current returns to the baseline value before exposure when the analyte flow is switched to zero air again ($t = 4500$ s, Figure 6.15a). A reasonable interpretation of the data is that adsorption of the VOC creates a swelling effect that varies slowly with time and is reversed upon evaporation of the analyte. Confirmation of this would require further investigation using AFM to explore the influence of the VOC on the morphology of the coordination polymer. However, it is clear that the coordination polymer alone is not suitable as a sensing material.

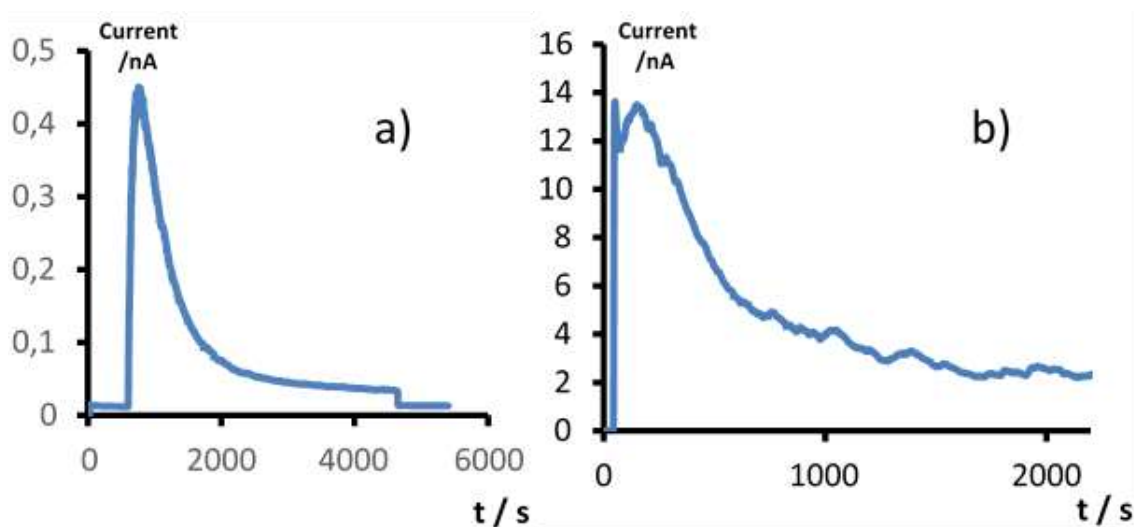


Figure 6.15. Long term exposure raw current data for Cu(I)-6-thioguanosine for (a) chloroform at 16.6 kPa and (b) ethanol at 43.8 kPa.

6.3.4. VOCs sensing in Au(I)-6-thioguanosine/MWCNTs composites

Gas sensing properties of Au(I)-6-thioguanosine/MWCNTs composites to different volatile organic compounds in gas phase were investigated motivated as an attempt

to improve on the known issues with bare MWCNTs and the observations above regarding the coordination polymer. Bare MWCNTs respond weakly to VOCs, and the coordination polymer Cu(I)-6-thioguanosine responded strongly, but in a complex manner. In this section sensors prepared by coating MWCNTs with an insulating coordination polymer, Au(I)-6-thioguanosine, were analyzed.³⁶⁻³⁸ Inclusion of MWCNTs in the polymer film increases the overall conductivity and it was hoped would also stabilize the response.

Before any detection measurement we studied the resistance against time for a MWCNTs device in the absence of coordination polymer as a control (Figure 6.16). The device was exposed to pulses of each of the VOCs of increasing concentration and the response is notably stable and reaches a steady-state within a few minutes of exposure that does not substantially decay. The response is also reversible and returns to the baseline after the gas stream is switched to zero air. Increasing partial pressures of the VOC also produce signals of increasing magnitude. The sensitivity, S , was calculated following equation 4 and it varied between VOCs, it is of the order of 0.1 for ethanol, 0.04 for chloroform and 0.0005 for acetone.

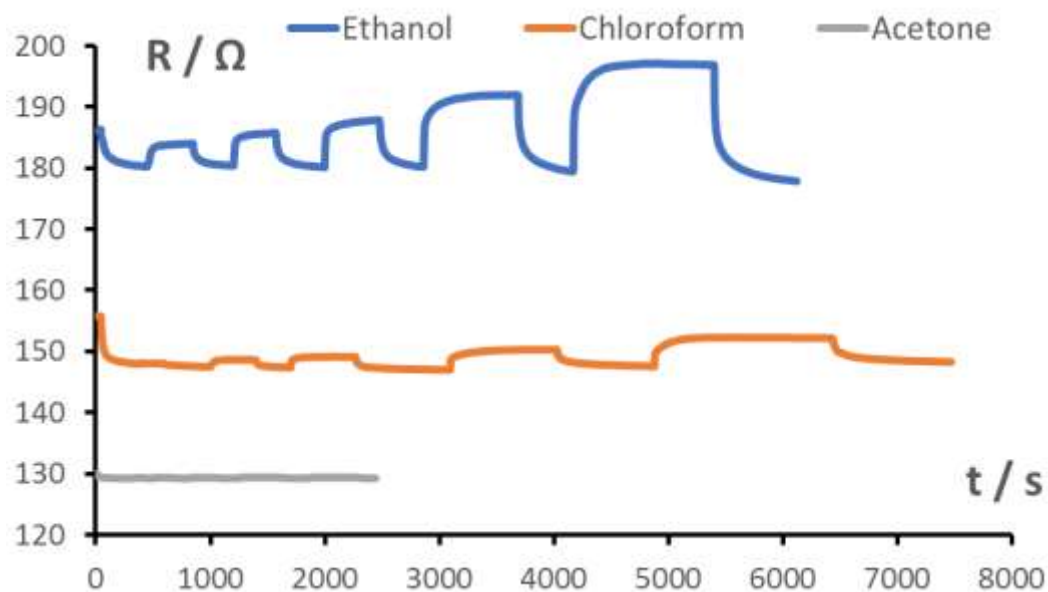


Figure 6.16. Typical raw data showing the reversibility of the current response of a control device based on MWCNTs alone to ethanol, chloroform and acetone.

The MWCNTs control device shows a similar level of response to both ethanol and chloroform (Figure 6.16). However, when the Au(I)-6-thioguanosine/MWCNTs composite is employed, the pattern of selectivity changes with a much larger response to ethanol observed (Figure 6.17). Importantly, the response to ethanol does not show the steep decline observed in Figure 6.15b.

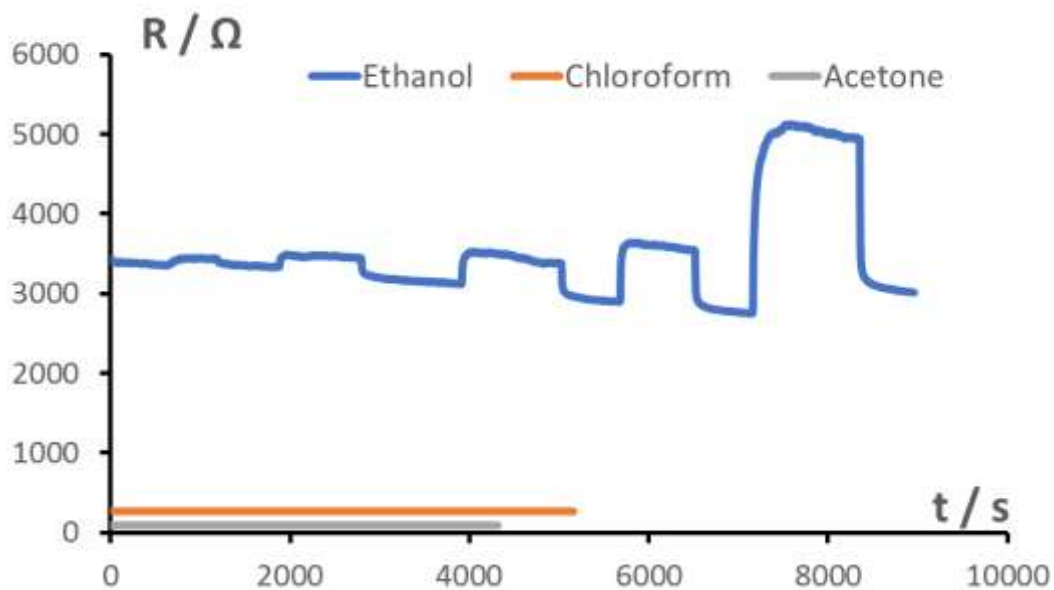


Figure 6.17. Raw data showing response of Au(I)-6-thioguanosine/MWCNTs (20%) to ethanol, chloroform and acetone. It is clear that there is much larger change in the film resistance during ethanol exposure.

We have analyzed the impact of varying partial pressures of the three VOCs and different polymer-MWCNTs compositions. As shown in Figure 6.18, as the ratio Au:C increased in the composite, a larger response to ethanol was observed. However, the linearity of the calibration curves is degraded for the 10% and 20% composites (Figure 6.18). The 3.5% composite shows a good linear response up to the saturated vapour pressure ($r^2 = 0.9996$), however the 20% composite shows evidence of an effect of condensation of ethanol near the saturated vapour pressure as a rapid increase in the value of S near $p/p^* = 1$ (Figure 6.18).

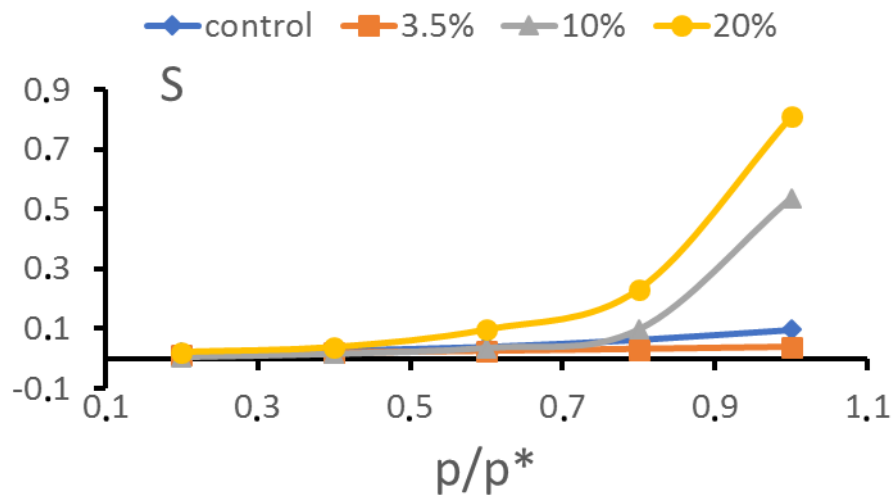


Figure 6.18. Fractional change in resistance, S , upon exposure to ethanol at various partial pressure and for difference compositions of the sensing material. The ethanol partial pressure is expressed as a ratio to the saturated vapour pressure at the temperature of the experiment (17.1 °C).

Although the device responses to chloroform an acetone are much weaker, similar data can be obtained. Although with an increase of partial pressure the sensitivity to the gases increase, linearity is lost due to similar condensation effects as in ethanol.

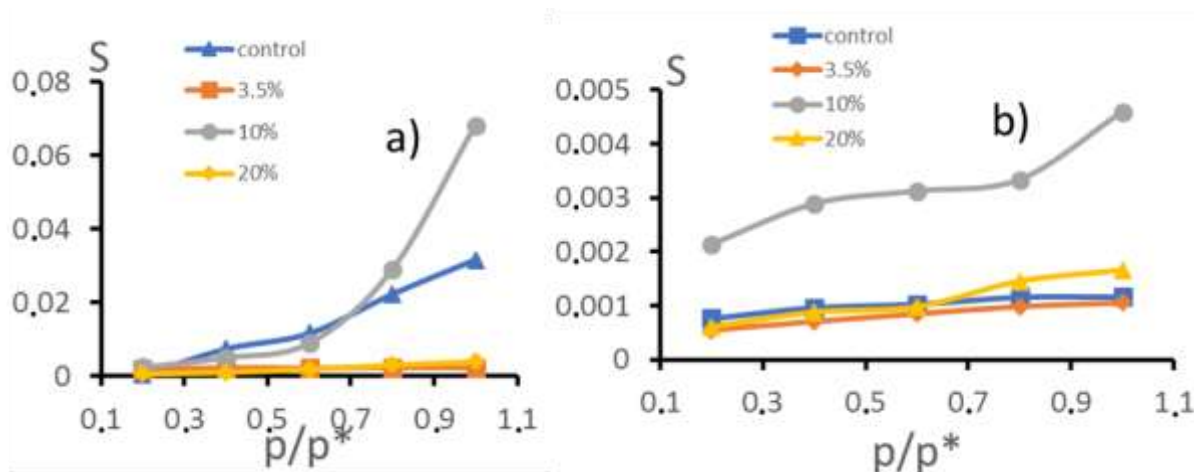


Figure 6.19. Fractional change in resistance, S , in response to VOCs at various fractions of their saturated vapour pressure and different compositions of the sensing material. a) chloroform, b) acetone. The temperature was 15-16 °C.

Figure 6.19 shows that the response to chloroform and acetone is at least an order of magnitude lower than to ethanol. Interestingly, an increase in the mole ratio of Au(I)-6-thioguanosine eventually leads to a suppression of the response to either of these compounds- the values of S are of order 10^{-3} for the 20% Au(I)-6-thioguanosine/MWCNTs composites.

The comparison of the values of sensitivity between MWCNTs control sample and Au(I)-6-thioguanosine/MWCNTs also shed light on some aspects. First, whereas the size of sensitivity to ethanol and chloroform are very similar between control and composite in the linear region, acetone showed a difference with a higher size of sensitivity in the composite sample (10%) than the control sample. This is an indication that the sensitivity using a coordination polymer coating the MWCNTs is enhancing the sensitivity for the sensing of acetone. On the other hand, the values of sensitivity for acetone are rather smaller than the other two VOCs. Overall, the size of the values of sensitivity also indicate that the composite Au(I)-6-thioguanosine/MWCNTs becomes

more sensitive for ethanol than the other VOCs. We attribute this to the low polarity of MWCNTs compared to the metal ion-containing polymer.

In addition to device sensitivity and linearity, the response time of the sensor is important. Slow device response times (minutes) may be acceptable in urban air quality monitoring where the typical variations occur throughout the day over timescales of hours.¹⁴ However, industrial safety applications and breath analytics in a clinical setting may require more rapid response to observe VOCs breath-by-breath.

6.3.5. t_{90} reaction times in Au(I)-6-thioguanosine/MWCNTs

The t_{90} values for the response to ethanol are about 3 minutes and actually decline slightly with increasing polymer mole fraction (Figure 6.20). The magnitude of these values is consistent with rate limiting diffusion of the analyte in a thin composite polymer/MWCNTs film. The response to acetone is much faster (<1 minute), but also much weaker (Figure 6.19b). The behavior of chloroform is intermediate: at low polymer mole fractions, the response times are similar to those for ethanol, but they decline at higher mole fractions. We interpret this in terms of the rejection of chloroform from the relatively hydrophilic environment of the polymer. The response times are slower than commercial amperometric gas sensors ($t_{90} \approx 30$ s)³³ but are nevertheless sufficient for long-term monitoring applications.

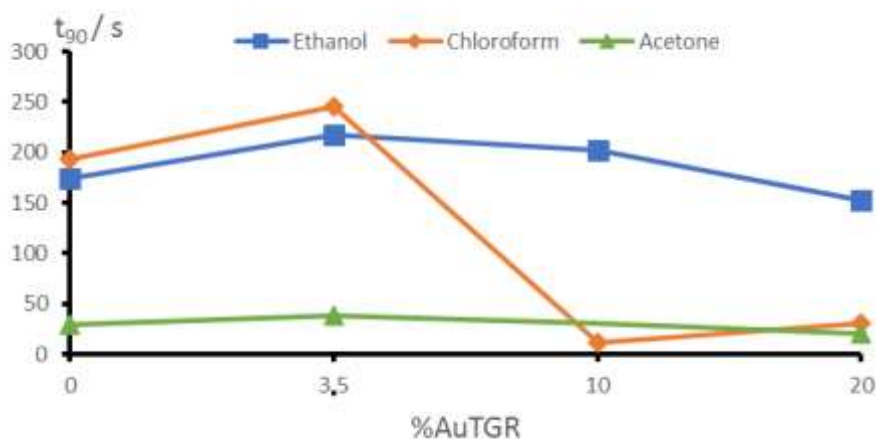


Figure 6.20. t_{90} values for various compositions Au(I)-6-thioguanosine/MWCNTs for each analyte studied. This data shows the response to switching from air to analyte.

6.4. Conclusions

The synthesis of the nanocomposites Au(I)-6-thioguanosine/MWCNTs has helped to overcome the limitation in terms of sensing of the pure coordination polymer systems. As we saw, Cu(I)-6-thioguanosine suffer the oxidizing effect from ozone and the material was unable to recover after exposure, also the humidity of the system causes the material to degrade and then the electrode become unusable. Apart from that, Cu(I)-6-thioguanosine sensor system showed a large response upon exposure to three VOCs (acetone, chloroform, ethanol), however the response was complex and time-dependent. However, this simple polymer system motivated a move towards polymer/CNT nanocomposites and the study of their performance as VOC sensing materials.

After synthesis, the nanocomposites were characterized by a range of techniques, AFM, Raman spectroscopy or scanning electron microscopy. Electrical characterization of those materials shows the decrease in current with increase of the ratio of Au(I)-6-thioguanosine to MWCNTs but the sensitivity to VOCs improved and a

stable response was observed. Au(I)-6-thioguanosine/MWCNTs become more sensitive for ethanol than other VOCs in the gas phase. Also, a faster response of the sensor to ethanol was observed.

6.5. References

- 1- Meng, Z., Stolz, R. M., Mendecki, L., Mirica, K. A. *Chem. Rev.* 2019, **119**, 478-598.
- 2- Cammann, K. *Phys. Chem. Chem. Phys.* 2003, **5**, 5159-5168.
- 3- Wolfbeis, O., S. *Fresenius' J. of Anal. Chem.* 1990, **337**, 522-527.
- 4- Janata, J., Josowicz, M., Vanýsek, P., DeVaney, D. M. *Anal. Chem.* 1998, **70**, 179-208.
- 5- Janata, J., Josowicz, M., DeVaney, D. M. *Anal. Chem.* 1994, **66**, 207-228.
- 6- Wang, P., Chen, W., Wang, J., Zhou, F., Hu, J., Zhang, Z., Wan, F. *Anal. Chem.* 2021, **93**, 15474-15481.
- 7- Hanf, S., Keiner, R., Yan, D., Popp, J., Frosch, T. *Anal. Chem.* 2014, **86**, 5278-5285.
- 8- McGrath, M. J., Scanail, C. N., 2013, *Sensing and Sensor Fundamentals in Sensor Technologies*, Ch. 2, 15-50, Apress, Berkeley, CA.
- 9- *Sensors in Analytical Chemistry in Techniques and Instrumentation in Anal. Chem.* 1994, **16**, 13-47.
- 10- Zhang, H., Srinivasan, R., *Sustainability* 2020, **12**, 9045.
- 11- Stetter, J. R., Li, J., *Chem. Rev.* 2008, **108**, 352-366.
- 12- Yi, W., Lo, K., Mak, T., Leung, K., Leung, Y., Meng, M., *Sensors* 2015, **15**, 31392-31427.
- 13- Thompson, J. E., *Trends in Environm. Anal. Chem.* 2016, **11**, 23-34.
- 14- Baron, R., Saffell, J., *ACS Sens.* 2017, **2**, 1553-1566.
- 15- Righettoni, M., Amann, A., Pratsinis, S. E., *Materials Today* 2015, **18**, 163-171.
- 16- Di Natale, C., Paolesse, R., Martinelly, E., Capuanu, R., *Anal. Chim. Acta* 2014, **824**, 1-17.
- 17- Mogera, U., Sagade, A. A., George, S. J., Kulkarni, G. U., *Scientific Reports* 2014, **4**, 4103.
- 18- Ellis, J. E., Star, A., *ChemPlusChem* 2016, **81**, 1248-1265.
- 19- Tai, H., Wang, S., Duan, Z., Jiang, Y., *Sensors and Actuators B: Chemical* 2020, **318**, 128104.
- 20- Chen, X., Zhou, G., Mao, S., Chen, J., *Environ. Sci.: Nano* 2018, **5**, 837-862.
- 21- Javid, M., Haleem, A., Rab, S., Singh, R. P., Suman, R., *Sensors International* 2021, **2**, 100121.

- 22- Moldovan, O., Iñiguez, B., Deen, M. J., Marsal, L. F., *IET Circuits, Devices & Systems* 2015, **9**, 446-453.
- 23- Al-Mahamad, L., El-Zubir, O., Smith, D. G., Horrocks, B. R., Houlton, A., *Nat. Commun.* 2017, **8**, 720.
- 24- Zhang, Q. D., Piro, B., Noel, V., Reisberg, S., Pham, M., *Adv. in Nat. Sci.: Nanoscience and Nanotechnology* 2010, **1**, 045011.
- 25- Zuniga, C., Rinaldi, M., Khamis, S. M., Jones, T. S., Johnson, A. T., Piazza, G., IEEE 22nd Int. Conf. on Micro Electromechanical System, Sorrento, Italy, 2009.
- 26- Qi, P., Vermesh, O., Grecu, M., Javey, A., Wang, Q., Dai, H., Peng, S., Cho, K. J., *Nano Letters* 2003, **3**, 347-351.
- 27- Osswald, S., Flahaut, E., Ye, H., Gogotsi, Y., *Chem. Phys. Letters* 2005, **402** (4-6), 422-427.
- 28- Gogotsi, Y., Presser, V., (ed.) 2006, *Carbon Nanomaterial*, 1st Ed., Taylor and Francis, Boca Raton.
- 29- Jawari, T., Roid, A., Casado, J., *Carbon* 1995, **33** (11), 1561-1565.
- 30- Toker, D., Azulay, D., Shimoni, N., Balberg, I., Millo, O., *Physical Review B* 2003, **68**, 041403.
- 31- Watson, S., Hedley J., Galindo, M., Horrocks, B., Houlton, A., *Chem. A Eur. J.* 2012, **18**, 12008-12019.
- 32- Brunauer, S., Deming, L. S., Deming, W. E., Teller, E., *J. Am. Chem. Soc.* 1940, **62**, 1723-1732.
- 33- Alphasense Ltd technical notes on amperometric gas sensors. Available at: www.alphasense.com (Accessed: 25 May 2020).
- 34- Wilson, D. M., DeWeerth, S. P., *Sensors and Actuators B: Chemical* 1997, **41**, 63-70.
- 35- Xiao, S., Nie, J., Tan, R., Duan, X., Ma, J., Li, Q., Wang, T., *J. of Mat. Chem. C* 2019, **3**, 11397-11405.
- 36- Salavagione, H. J., Diez-Pascual, A., Lazaro, E., Vera, S., Gomez-Fatou, M., *J. of Mat. Chem. A* 2014, **2**, 14289-14328.
- 37- Kanoun, O., Lazarevic-Pasti, T., Pasti, I., Nasraoui, S., Talbi, M., Brahem, A., Adiraju, A., Sheremet, E., Rodriguez, R., Ali, M., Al-Hamry, A., *Sensors* 2021, **21**, 4131.
- 38- Lee, C., Bhandari, S., Tiwari, B., Yapici, N., Zhang, D., Yap, Y., *Molecules* 2016, **21**, 922.

Chapter 7. Synthesis of 4-thiouridine. Preparation and characterization of coordination polymers designed from 4-thiouridine with Ag(I), Au(I) and Cu(I) coinage metal ions

Table of Contents

7.1. Introduction.....	187
7.2. Material and Methods.....	194
7.2.1. Reagents and techniques.....	194
7.2.2. 4-Thiouridine synthesis.....	196
7.2.2.1. Protection	196
7.2.2.2. Thiolation.....	197
7.2.2.3. Deprotection	198
7.2.3. Ag(I)-4-thiouridine complex preparation	199
7.2.4. Au(I)-4-thiouridine complex preparation	199
7.2.5. Cu(I)-4-thiouridine complex preparation	200
7.3. Results and Discussion	200
7.3.1. Synthesis of 4-Thiouridine	200
7.3.2. Reaction between 4-thiouridine and coinage metal(I) ions	203
7.3.2.1. Ag(I) and 4-thiouridine	203
7.3.2.2. Au(I) and 4-thiouridine	213
7.4. Conclusions.....	220
7.5. References	221

7.1. Introduction

The interaction of modified nucleic acids and metal ions is a promising route to design functionalized materials with properties on demand.^{1,2} In particular, the idea is to attach metal ions to modified nucleosides through specific interactions to build materials with opto-electronic³ or semiconductor properties⁴ for its use in technological applications.

An approach to design these materials consists in the bottom-up preparation of coordination polymers from specific interaction between coinage metal ions and nucleosides derivatives⁵ since, as has been successfully demonstrated,³ such route of preparation lead to the formation of functionalized materials.

Modified nucleosides are usually prepared to extend features of oligonucleotides, e. g. altering their original formula to attach specific molecules or chemical groups to them.^{3, 6-8} The modification explored here consists in the use of a thio-modified nucleoside derived from RNA to force specific interactions with coinage metal ions and then form a coordination polymer with a sulfur-metal ion backbone. The sulfur-metal ion pairing is based on the hard and soft acids and bases Lewis theory, HSAB theory, that established that there is an affinity between a soft base, sulfur, and a soft acid, coinage metal ions.^{9,10}

The formation of metal-chalcogenolate materials⁵ lead to show interesting properties for technological application, such as luminescence¹¹ or electrical conductivity,¹² derived from the interaction between sulfur atoms and metal ions similar to metal sulfides, well-known semiconductors.^{13,14}

The coinage metal ions usually used are, Ag(I), Au(I) and Cu(I). These metal ions are able to attach sulfur groups from ligands forming metal(I) thiolate compounds in form of coordination polymer that display equivalent properties as semiconductors, optical

emission¹⁵ or electrical conductivity.¹⁶ Because of that, these coordination polymers found use as a sensors or nanowires.^{17,18}

In addition to coinage metal ions, 4-thiouridine has been used as the sulfur contain ligand. It is a thio-modification from the original nucleoside uridine present on tRNA (Figure 7.1) that has the aim of protecting the cells from near-UV exposure. It is produced in bacteria cells (*E. coli*), where uridine suffers a usual mutation in the fourth position by two enzymes, cysteine desulfurase and tRNA sulfurtransferase,¹⁹ and as a result, this thiol derivative can be found at position eight of tRNAs.^{20,21} Also, it is possible to prepare 4-thiouridine synthetically²² and it can be exportable to short oligonucleotides.²³ So, the sulfur atom of 4-thiouridine will provide a specific bonding site to coinage metal ions.²⁴

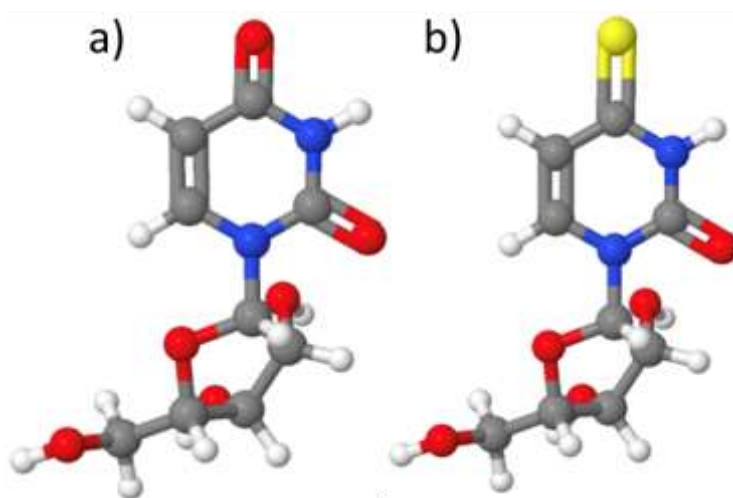


Figure 7.1. Three-dimensional model structure for a) uridine and b) 4-thiouridine.

There are not many examples of crystal structures of complexes based on 4-thiouridine and metal ions, only three have been analyzed in order to determine their structure and properties. The simplest reported crystal structure consists in a complex based on 1-methyl-4-thiouracil that coordinate linearly a *p*-mercuribenzoic acid through the

sulfur atom.²⁵ Another study focusses on the interaction and stability of complexes based on Mo metal ions with different thiouracil ligands.²⁶ Crystal structures based on these systems are described as 4-thiouracil attaching Mo(IV) through N3 and S(C4) (Figure 7.2a). The study also compare this system with a complex based on a 4-methylthiouracil that link Mo(IV) through N3 and O(C2) indicating that this compound is less stable than the complex formed with 4-thiouracil which suggests a high affinity of Mo(IV) to sulfur atoms than to oxygen.²⁶ In addition, there is another study that explores the interaction of 4-thiouracil with Pt(II).²⁷ The attachment of Pt(II) to the ligand 4-thiouracil occurs exclusively through the sulfur atom and it is justified by the intense donor properties of sulfur atom (Figure 7.2b).²⁷ Moreover, they explored the interaction between Pt(II) ions and a deprotonated molecule of 4-thiouracil, resulting in the formation of a complex where 4-thiouracil attach Pt(II) ions through S(C4) and N3 (Figure 7.2c).²⁷ These examples illustrated that only particular metal ions have affinity for sulfur atom of 4-thiouracil ligands to form mono- and di-nuclear complexes.

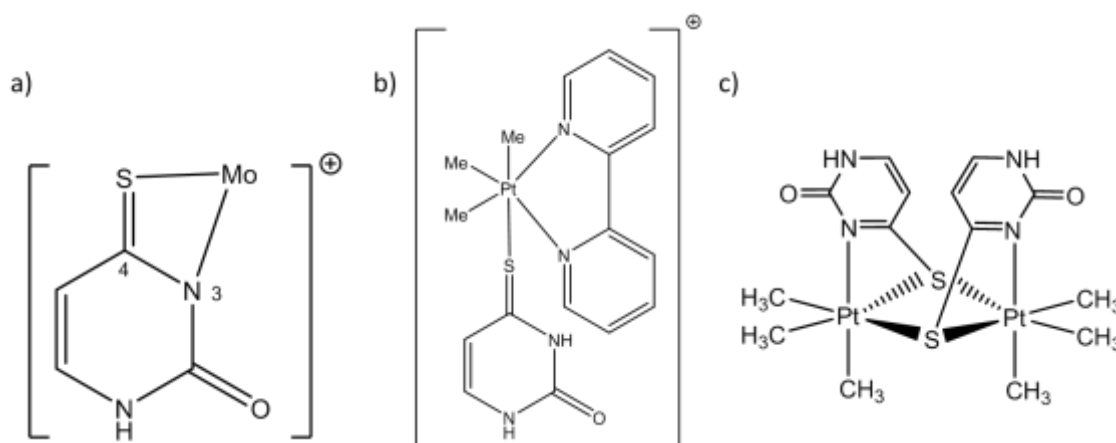


Figure 7.2. Scheme of crystal structures based on 4-thiouracil and metal ions, a) $[\text{Mo}(4\text{-SN}_2\text{OC}_4\text{H}_3)]^+$, b) $[\text{PtMe}_3(\text{bpy})(\text{s}^4\text{Ura-kS})]^+$ and c) $[(\text{PtMe}_3)_2(\text{u-s}^4\text{Ura-H})_2]$.

Because there is a lack of crystal structures based on 4-thiouridine and coinage metals, crystal structures based on 2-thiouridine and coinage metal ions have been explored since a similar reactivity has been assumed for both ligands.

A crystal structure for Ag(I) ions and 2-thiouracil, confirms the interaction through the S(C2) forming a mononuclear complex with trigonal planar geometry around the Ag(I) and it owns antimicrobial bioactivity (Figure 7.3).²⁸ Another complex formed with a derivative of 2-thiouridine, 2-mercapto-4-(3H)-quinazolinone, and Ag(I) verify that the preferred coordination site for Ag(I) is S(C2) atom. The tetrahedral complex formed around the metal ion possess antibacterial activity.²⁹

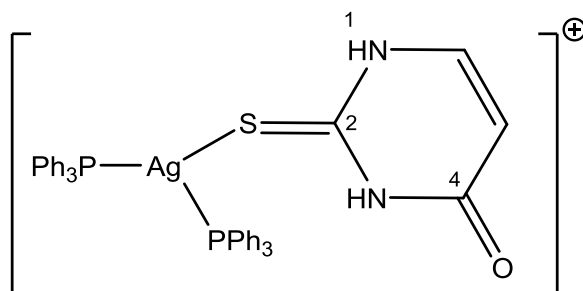


Figure 7.3. Scheme of a crystal structure based on 2-thiouracil and Ag(I) ions, $[Ag(S-tucH_2)(PPh_3)_2]^+$.

Studies of crystal structures based on Au(I) and thiouridine derivatives showed interesting results. The coordination of two Au(I) ions with S(C2) and N3 of 2-thiouridine produced a short distance between them and as a result, aurophilic interactions appeared. This complex can extend its configuration to form a helical polymer with Au(I)-Au(I) motif joined by aurophilic interactions (Figure 7.4) with photoluminescence properties.³⁰ Another crystal structure based on Au(I) and 2-thiouridine has been reported and it confirmed the affinity of Au(I) to S(C2) of 2-thiouridine forming a linear mononuclear complex with metal ion substituent.³¹ Further crystal structures includes

a complex based on Au(I) and pteridine based ligands. The linear coordination between a Au(I) ion and a sulfur atom from the ligand included aurophilic interactions with another Au(I) ion (Figure 7.5a), this complex exhibit optical properties with luminescence emission.³² A long luminescence polymer chain has been explored in the interaction of Au(I) ions and a ligand derived from the deprotonated thiobarbituric acid. Crystal structures have showed a complex based on Au(I) ions that coordinate linearly a sulfur ligand that can interact with another ligand, attached to another Au(I), through hydrogen bonding (Figure 7.5b). In addition, this complex can incorporate other Au(I) ions by aurophilic interactions.³³

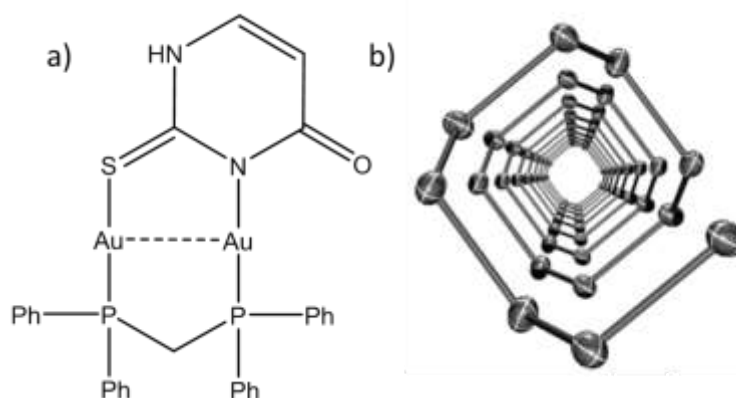


Figure 7.4. Scheme of a) the crystal structure based on 2-thiouracil and Au(I) ions, $[Au_2(\mu-TU)(\mu-dppm)]$ and b) a model of the helical arrangement of Au(I) ions (grey balls) (ligands are omitted for clarity).³⁰

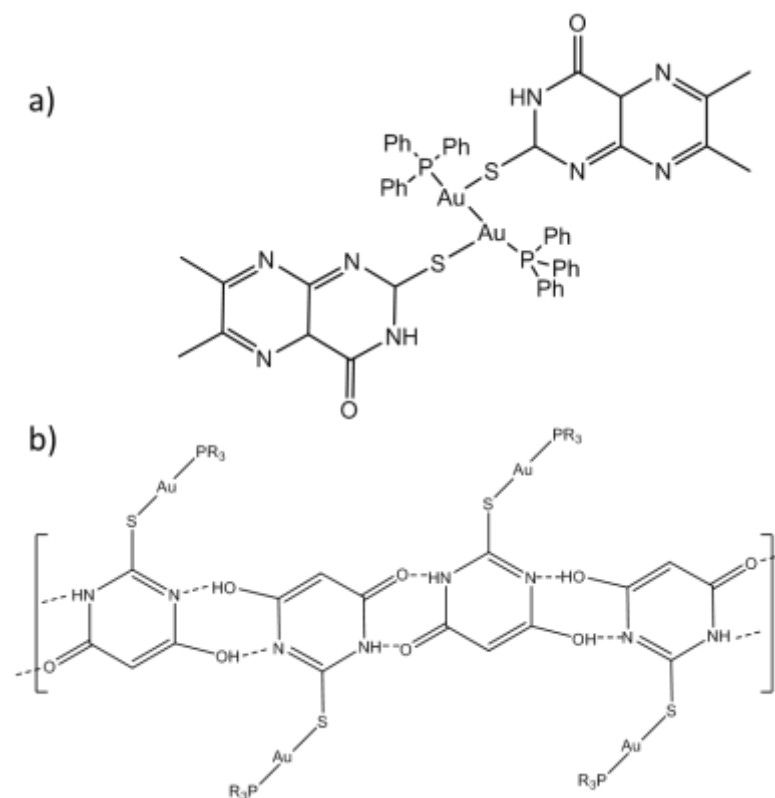


Figure 7.5. Scheme of some of crystal structures based on Au(I) ions and thiouracil derivatives, a) $[\text{Au}(\text{2SpteridinylMe}_2)(\text{PPh}_3)]_2$ and b) $[\text{Ph}_3\text{PAuSC}_4\text{H}_3\text{N}_2\text{O}_2]_n$, dashed lines correspond to hydrogen bonds ($\text{R}=\text{Ph}$).

Also, Cu(I) ions and thiouracil derivatives complexes have been studied. A crystal structure based on a Cu(I) ion bridging two sulfur atoms from 2-thiouracil has been reported.³⁴ In addition, this complex is the unit of a long polymeric chain where derivatives of 2-thiouracil interact through hydrogen bond, N1-O(C6) and O(C6)-N1, forming a one-dimensional coordination polymer (Figure 7.6a).³⁵ Another complex reported for Cu(I) ion is the formation of a di-nuclear complex based on 2,4-thiouridine that bridge two Cu(I) ions, each one attached to a 2,4-thiouridine. This complex can be modified introducing a Br substituent of Cu(I) ion and it induce the formation of a one-dimensional coordination polymer with a Cu(I)-sulfur backbone (Figure 7.6b).³⁶

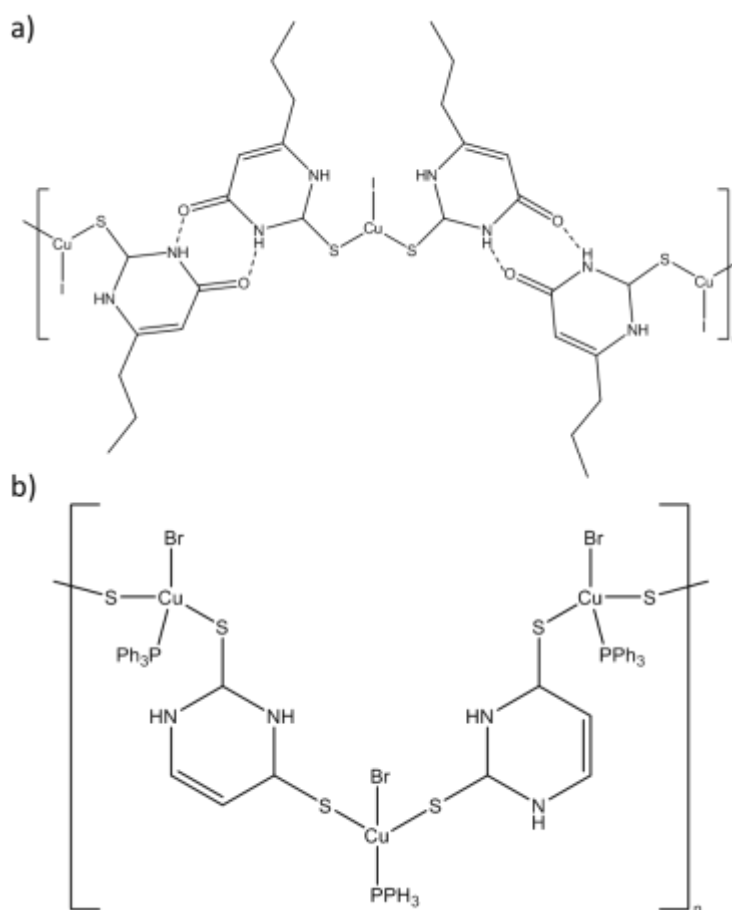


Figure 7.6. Scheme of crystal structures based on Cu(I) ions and thiouracil derivatives, a) $[CuI(ptu)_2]_n$ and b) $[CuBr(\mu\text{-}S,S\text{-}dtucH_2)(PPh_3)]_n$.

Also, thiouridines has been studied for their interactions with Cd(II),³⁷ and Tl(III).³⁸ All of these studies have highlighted the large affinity for sulfur in C2 and C4 of metal ions than for oxygen. Although N3 could be involved in the complexation, the complex formation is not thermodynamically favorable.³⁷

As a new perspective using thiouridine derivatives, our work focusses on the coordination of monovalent coinage metal ions with 4-thiouridine in an effort to prepare coordination polymers analogous to those formed with 6-thioguanosine.³ The fact that we designed a coordination polymer using 6-thioguanosine and coinage metal ions in previous chapters encouraged us to consider that analogous compounds based on a

pyrimidine nucleobase derivative from nucleic acid will be formed. Therefore, in this chapter we have investigated the interaction of a fully synthesized 4-thiouridine with different monovalent coinage metal ions. Structural and spectroscopic studies have been carried out in order to characterize the products of these reactions.

7.2. Materials and Methods

7.2.1. Reagents and Techniques

All chemicals used on the synthesis were purchased from Sigma-Aldrich and Fisher Scientific and they were used without any purification.

NMR, ^1H and ^{13}C experiments, were carried out in a Bruker Avance III at 300 MHz and 75 MHz, respectively, with $\text{DMSO-}d_6$ as a solvent. The data was analyzed using MestReNova software.

Mass spectrometry analysis was done using a Waters Xevo G2-XS Quadrupole Time of Flight Mass Spectrometer, with Electrospray Ionisation source in Positive Ion mode. Three samples were analyzed, 4-thiouridine, Ag(I) reaction mixture (10 mM) and Au(I) reaction mixture (10 mM). For each sample 2 μL was injected into the mass spectrometer in MeOH:H₂O (9:1), the flow rate into the instrument was 0.2 mL/min and the collision energy was 5 eV.

FTIR spectroscopy was performed using an IRAffinity-1S Fourier Transform infrared spectrophotometer (Shimadzu) with an integrated ATR accessory, in transmittance mode between 400 and 4000 cm^{-1} at 4 cm^{-1} spectral resolution, under N_2 . Samples were prepared drying the solvent on a vacuum oven during 30 min and then deposited on a clean p-Si (100) chip (1 cm^2). The chip was deposited on the ATR accessory sample holder and scanned 50 times, co-added and averaged. Bared ATR accessory was used as a background. Silicon chips, purchased from Pi-KEM Ltd, of 1 cm^2 area

were cut from 10 cm diameter wafers (dopant boron at <111> oriented p-type, resistivity 0.09-0.12 Ohm·cm).

The pH was measured on a Hanna HI 90103 instrument and previously calibrated using commercial buffer solutions from Sigma-Aldrich. Aliquots NaOH 0.1 M were used to increase the pH value.

UV-Vis spectroscopy in the range of 190-800 nm was performed using a Thermo Scientific NanoDrop One Microvolume spectrometer with all data collected at room temperature. Three samples were recorded, a water solution of 4-thiouridine (0.1 mM) and Ag(I) and Au(I) reaction mixtures (0.1 mM) using a quartz cuvette with a path length of 10 mm (108-000-10-40 Hellma). The blank used for the measurements was nanopure water produced in Direct-Q[®] 3 UV Water purification system from Merck at 18 MΩ·cm resistivity, this water was used for all the solutions made in the experiments.

Circular dichroism was performed using a Jasco J-810 spectropolarimeter, connected to a PTC-423S temperature controller at 25°C and under N₂. Three circular dichroism spectra were recorded in a demountable quartz cuvette with a path length of 0.1 mm (106-0.1-40 Hellma), 4-thiouridine solution at 10 mM, Ag(I) (10 mM) and Au(I) (10 mM) reaction mixtures.

Scanning electron microscope was performed using a Tescan Vega LMU scanning electron. Digital images of the sample were recorded for 20 µL of Ag(I) reaction mixture (100 mM) dried on a vacuum oven for 30 min on a clean p-Si (100) chip (1 cm²) and then mounted on an aluminium stub with double sided adhesive tape.

Atomic force microscopy was performed using a Multimode 8 atomic force microscopy with a NanoscopeV controller (Bruker) and a 'E' scanner. Nanoscope software version 9.1 was used to control the microscope. The system was operated in ScanAsyst in air mode as a peak force tapping mode at ultra-low forces to minimize damage to the

samples. For reducing vibrational noise, an isolation table/acoustic enclosure was used (Veeco Inc., Metrology Group). Silicon tips on silicon nitride cantilevers (ScanAsyst, Bruker) were used for imaging. The nominal tip radius was approximately 2 nm, resonant frequency 150 kHz, and spring constant $k \approx 0.7 \text{ nm}^{-1}$. The AFM data were analyzed with NanoScope Analysis 1.5 software (Bruker). Samples were prepared by adding 3 μL of Ag(I) reaction mixture (0.01 mM) and Au(I) reaction mixture (0.1 mM) onto a clean 1 cm^2 mica wafer and it was left for dry for 15 min at room temperature on air. Different diluted solutions of such samples were used to image. All measurements were done at room temperature on air. Avogadro software version 1.2.0 was used to build the structure model of complexes prepared.

Room temperature luminescence in the range of 300-900 nm was performed using a Spex FluoroMax spectrofluorometer. Four emission spectra were recorded, a water solution of 4-thiouridine (60 mM), Ag(I) reaction mixture at 100 mM and two for Au(I) reaction mixture at 100 mM, using a quartz cuvette with a path length of 1.5 mm (105-252-15-40 Hellma).

7.2.2. 4-Thiouridine synthesis

7.2.2.1. Protection

Uridine (5 g, 20.47 mmol, 1 eq) was dissolved in dry pyridine (30 ml) and acetic anhydride (6.44 ml, 68.18 mmol, 3.33 eq) was added dropwise under an inert atmosphere at 60°C. The reaction was stirred for 7 hours, with TLC monitoring (ethyl acetate:petrol; 9:1), and then quenched with the addition of ice. The product was isolated by rotary evaporation producing a colourless oil, and it was partitioned between 100 ml of chloroform and 100 ml of water. The organic layer was washed with 100 ml of HCl 1N, 100 ml of H₂O and 100 ml of brine. The liquid was dried with Na₂SO₄ overnight and the solvent was rotary evaporated until an oil appears. The addition of

40 ml of ethanol yielded a white powder, isolated by air vacuum and dry inside a vacuum oven at 40 °C (Figure 7.7).^{22,39} ¹H-NMR (300 MHz, DMSO- δ 6) δ 2.02 (s, 3H), 2.04 (s, 3H), 2.06 (s, 3H), 4.27-4.40 (m, 2H), 4.41-4.6 (m, 1H), 5.39 (t, 1H), 5.48 (t, 1H), 5.7 (d, 1H), 5.9 (d, 1H), 7.6 (d, 1H), 11.5 (s, 1H). ¹³C-NMR (75 MHz, DMSO- δ 6) δ 20.2, 20.21, 20.22, 62.8, 69.91, 71.8, 79.4, 88.8, 102.6, 142.4, 150.1, 164.1, 171.2 ppm. FT-IR (wavenumber, cm^{-1}): 3050 (N-H), 1750 (C=O, ester), 1680 (C=O, amide), 1380 (C-H, alkyl), 1250 (C-N, aromatic amine), 1000 (C=C, alkene), 850 (C-H). ESI/MS ($\text{C}_{15}\text{H}_{19}\text{N}_2\text{O}_9$)⁺: Theoretical: 371.11 m/z. Actual: 371.11 m/z. Yield: 87%

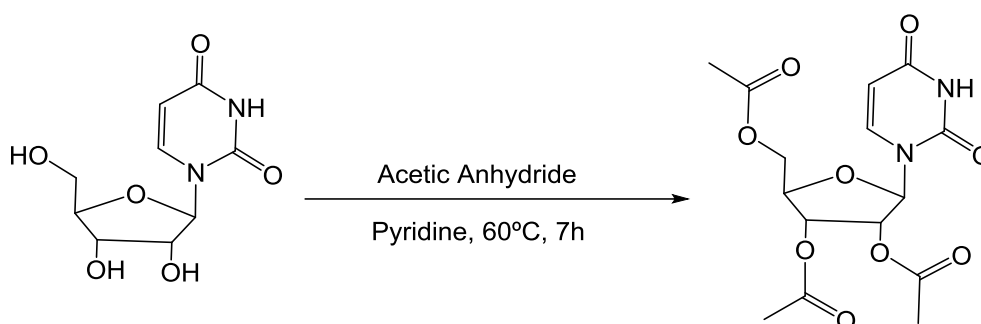


Figure 7.7. Reaction scheme of uridine protection.

7.2.2.2. Thiolation

Uridine protected (3 g, 8 mmol, 1 equiv) and Lawesson's reagent (6.55 g, 16.21 mmol, 2 eq) were dissolved in anhydrous toluene (30 ml) and stirred for 24 hours under an inert atmosphere at 110°C. A yellow solution with a precipitate was formed. The solid was removed under vacuum filtration and the liquid was isolated by rotary evaporation, producing a yellow gummy solid. It was purified by a column of silica gel (ethyl acetate:hexane; 16:33) and isolated by rotary evaporation which gave a yellow caramel (Figure 7.8).^{22,40,41} ¹H-NMR (300 MHz, DMSO- δ 6) δ 2.02 (s, 3H), 2.04 (s, 3H), 2.06 (s, 3H), 4.37-4.44 (m, 3H), 5.4 (t, 1H), 5.49 (t, 1H), 5.8 (d, 1H), 6.4 (dd, 1H), 7.53 (d, 1H), 12.8 (s, 1H). ¹³C-NMR (75 MHz, DMSO- δ 6) δ 21.1, 20.14, 20.18, 64, 69.9,

72.3, 79.69, 89.4, 103.82, 137.7, 147.5, 169.4, 191.1 ppm. ESI/MS

$[(C_{15}H_{18}N_2O_8S)Na]^+$: Theoretical: 409.07 m/z. Actual: 408.87 m/z. Yield: 19%

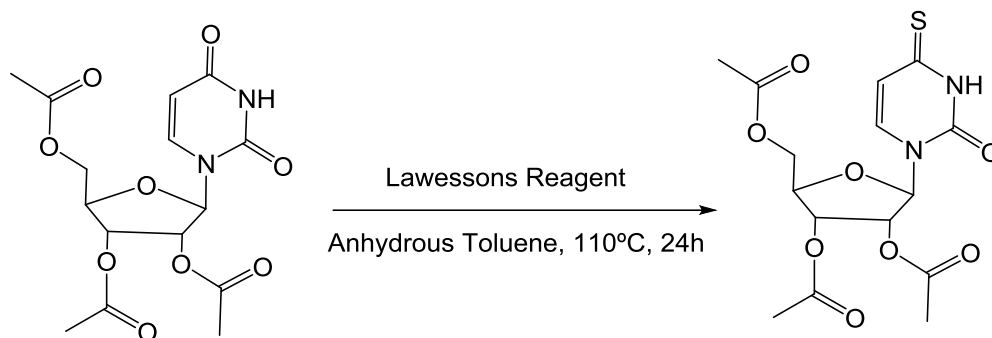


Figure 7.8. Reaction scheme for the thiolation in carbon 4 (C4).

7.2.2.3. Deprotection

4-Thiouridine protected (0.589 g, 1.52 mmol) was dissolved in 10 ml of ammonia in methanol (7 N) under inert atmosphere, stirred overnight and monitored by TLC (DCM:Methanol; 3:1). The solution was neutralized (from pH 3 to 7) using a DOWEX-50 WX-8 ion exchange resin in proton form (2 g) previously washed with methanol. The product was isolated by rotary evaporation and 20 ml of water were added. After two washes of 30 ml of diethyl ether the sample was lyophilized for two days and a yellow solid was obtained (Figure 7.9).²² 1H -NMR (300 MHz, DMSO- d_6) δ 3.5-3.68 (m, 2H), 3.8-4.2 (m, 3H), 5.2 (m, 2H), 5.49 (d, 1H), 5.7 (d, 1H), 6.38 (dd, 1H), 7.7 (d, 1H), 12.69 (s, 1H). ^{13}C -NMR (75 MHz, DMSO- d_6) δ 60.02, 69.85, 73.68, 85.1, 89.06, 111.2, 135.4, 149.2, 190.01 ppm. FT-IR (wavenumber, cm^{-1}): 3300 (O-H, alcohol), 3000 (N-H), 1693 (C=O, amide), 1608 (C=C, alkene), 1458 (C-H, alkyl), 1269 (C-N, aromatic amine), 1100 (C=S), 850 (C-H). ESI/MS $[(C_9H_{12}N_2O_5S)Na]^+$: Theoretical: 283.04 m/z. Actual: 283.03 m/z. Yield: 79%

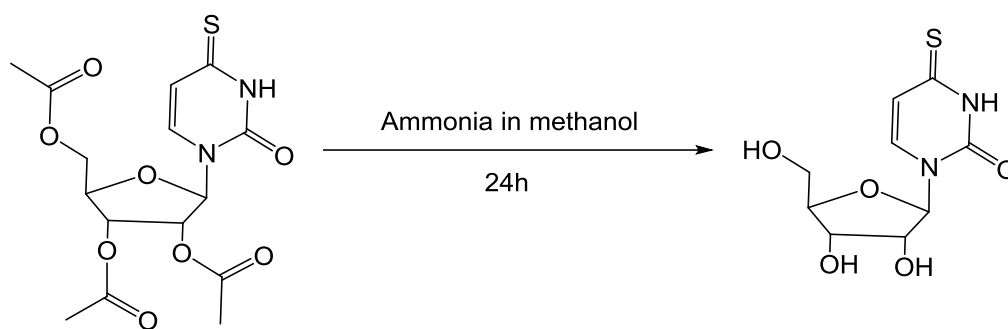


Figure 7.9. Reaction scheme for the deprotection of 4-thiouridine.

7.2.3. Ag(I)-4-thiouridine complex preparation

The preparation of 4-thiouridine complex was carried out in water solution. A yellow aqueous solution of 4-thiouridine (26 mg, 0.1 mmol, 1 eq, 1 mL) was added to AgNO₃ in powder form (17 mg, 0.1 mmol, 1 eq) at room temperature. After 10 min of strong mixing on a Vortex, a yellow hydrogel was formed at 100 mM and over 24 hours is confirmed by the vial inversion test. Due to instrument limitations measurements of mass spectroscopy, FTIR, SEM and AFM were performed on dry form of the hydrogel, xerogel, to make them possible.

7.2.4. Au(I)-4-thiouridine complex preparation

The preparation of 4-thiouridine complex was carried out in water solution. A colourless aqueous solution of Au(I) (34 mg, 0.1 mmol, 1 eq, 100 μ L) prepared by reduction of HAuCl₄ with 2 equivalents of thiodiglycol was added to a yellow aqueous solution of 4-thiouridine (26 mg, 0.1 mmol, 1 eq, 900 μ L) at room temperature. After 10 min of strong mixing on a Vortex, an orange liquid was formed at 100 mM. Due to instrument limitations measurements of FTIR, SEM and AFM were performed on dry form of the orange liquid to make them possible.

7.2.5 Cu(I)-4-thiouridine complex preparation

The preparation of 4-thiouridine complex was carried out in water solution. A yellow aqueous solution of 4-thiouridine (26 mg, 0.1 mmol, 1 eq, 1 mL) was added to $\text{Cu}(\text{MeCN})_4\text{BF}_4$ in powder form (31.5 mg, 0.1 mmol, 1 equiv) at room temperature. After 10 min of strong mixing on a Vortex, a black solution with a black precipitate was formed. No characterization was made on this material.

7.3. Results and Discussion

7.3.1. Synthesis of 4-thiouridine

The synthesis of 4-thiouridine was successfully achieved in three steps. The first step consisted on the protection of alcohol groups of uridine with hydroxyl groups through an esterification (Figure 7.10). ESI mass spectroscopy confirmed the protection of uridine showing a peak equivalent to a cationic single molecule of protected uridine, 371.1106 m/z for $(\text{C}_{15}\text{H}_{19}\text{N}_2\text{O}_9)^+$, 371.11 m/z calculated (Appendix, Figure A7). In addition, ^1H and ^{13}C NMR confirmed the protection with triplets at 2 ppm and 20 ppm, respectively, corresponding to the hydroxyl groups (Appendix, Figure A8). Also FTIR confirmed the protection of uridine (Appendix, Figure A9)

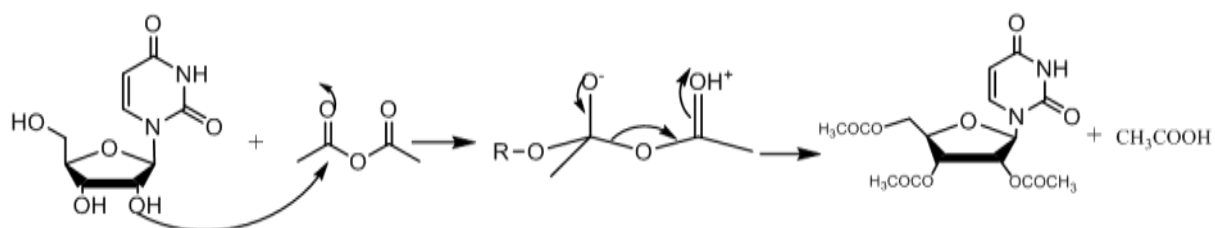


Figure 7.10. Scheme of the mechanism for the protection of alcohol groups in uridine, R=uridine.

The second step consisted in the thiolation of the fourth position of uridine by the Lawesson's reagent (Figure 7.11). ESI mass spectroscopy indicates the formation of a sodium adduct molecule equivalent to the acetyl-protected 4-thiouridine, 408.8760 m/z for $[(C_{15}H_{18}N_2O_8S)Na]^+$, 409.07 m/z calculated (Appendix, Figure A10). NMR also suggested the thiolation of protected uridine with singlets for 1H at 13 ppm and for ^{13}C at 190 ppm, corresponding to the proton of the thiol group and the carbon linked to the sulfur group, respectively, in agreement with literature values (Appendix, Figure A11).²² In addition, due to steric hindrance Lawesson's reagent will only sulfurize the position 4 of uridine protected.²²

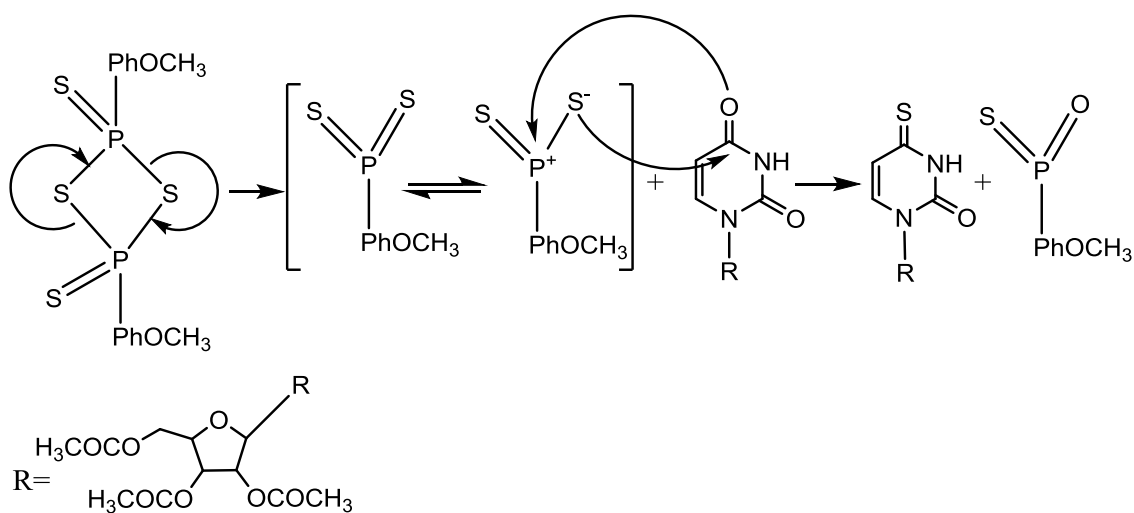


Figure 7.11. Scheme of the mechanism for the thiolation in position 4 of acetyl-protected uridine by Lawesson's reagent. R indicates the acetyl-protected ribose group of uridine.

The final step consists in a deprotection via ester alcoholysis (Figure 7.12).²² ESI mass spectrum on the synthesis product indicates the formation of a 4-thiouridine sodium adduct, 283.0362 m/z for $[(C_9H_{12}N_2O_5S)Na]^+$, 283.04 m/z calculated (Appendix, Figure A12). 1H and ^{13}C NMR also indicates a successful deprotection with the disappearance of peaks related to protected groups (Appendix, Figure A13). This data suggests that

deprotection was successful and further analysis of 4-thiouridine will support its formation.

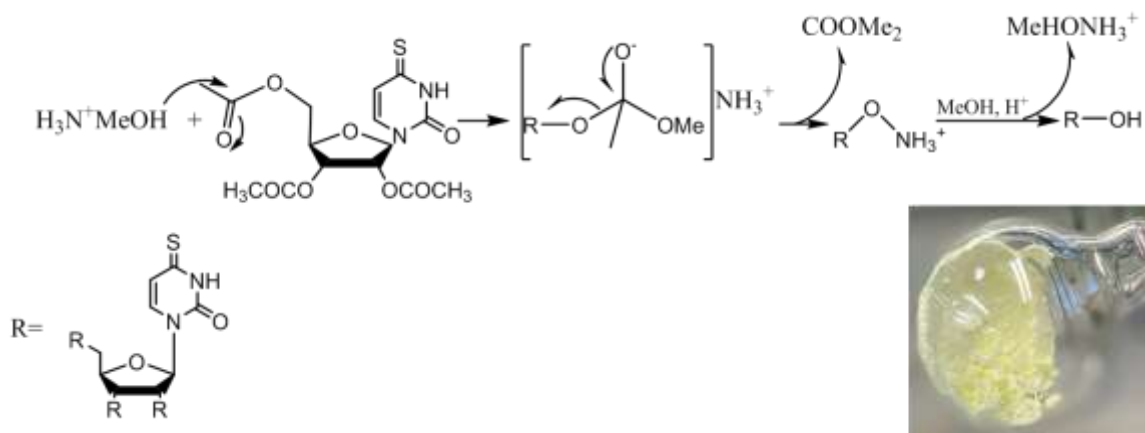


Figure 7.12. Scheme of the mechanism for the deprotection of acetyl-protected 4-thiouridine to obtain a yellow solid, 4-thiouridine. R indicates the 4-thiouridine group.

Additional characterization of 4-thiouridine included UV-Vis absorption, FTIR, CD and fluorescence spectroscopies. The UV-Vis spectrum showed two maximum peaks at 333 nm and 248 nm and these are assigned to π - π^* transitions of the thione group⁴² and π - π^* transitions of the pyrimidine ring, respectively (Appendix, Figure A14).⁴³⁻⁴⁶ FTIR spectroscopy showed a characteristic C=S stretch mode band at 1112 cm⁻¹ confirming the formation of 4-thiouridine (Appendix, Figure A15).⁴⁷ CD spectrum confirms the chirality of 4-thiouridine with two positive peaks at around 335 nm and 267 nm and one negative at around 231 nm, that correspond to π - π^* transitions (Appendix, Figure A16).^{43,48,49} Finally, fluorescence spectroscopy of an aqueous solution of 4-thiouridine showed a maximum emission at 470 nm for an excitation of 380 nm confirming luminescence properties of 4-thiouridine. In accordance with literature, this emission is produced by transitions between π - π^* orbitals of 4-thiouridine (Appendix, Figure A17).^{50,51} These results confirmed that 4-thiouridine was

successfully prepared and therefore, it was possible to analyze its interaction with coinage metal ions.

7.3.2 Reaction between 4-thiouridine and coinage metal(I) ions

In an effort to prepare coordination polymer analogues of the 6-thioguanosine derivatives reported in chapters 3 and 4, reactions with univalent coinage metal ions were performed. The following sections show the results obtained for each of the reactions between 4-thiouridine and metal(I) salts used in previous chapter, i.e. AgNO_3 and Au(I) derived from reduction of HAuCl_4 .

7.3.2.1. 4-Thiouridine and Ag (I)

The reaction was performed using a yellow aqueous solution of 4-thiouridine and a solid Ag(I) salt, AgNO_3 , in an equimolar ratio 1:1 (Figure 7.13). After a minute of strong mixing a yellow-green hydrogel (**1**) appeared immediately at room temperature, inferred by the vial inversion test. The reaction mixture **1** was firstly analyzed in order to determine its chemical structure.

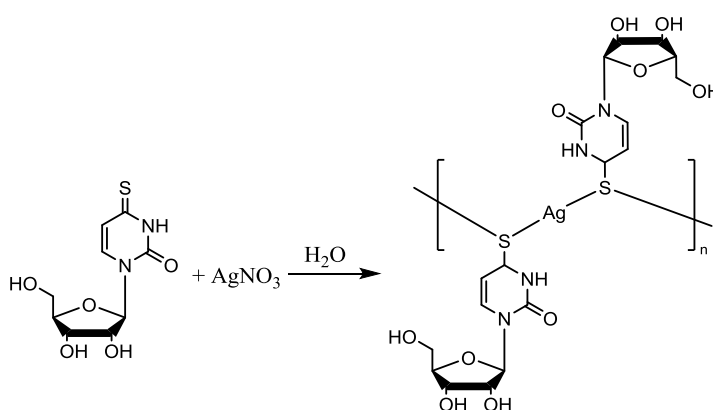


Figure 7.13. Scheme of Ag(I)-4-thiouridine complex preparation.

Mass spectroscopy confirmed the complexation of the metal ion. ESI mass spectroscopy showed a peak equivalent to an oligomeric chain, 628.9990 m/z for $[\text{AgL}_2]^+$, 629.000 m/z calculated (Appendix, Figure A18). L corresponds to a neutral charge molecule of 4-thiouridine, $[\text{C}_9\text{H}_{12}\text{N}_2\text{O}_5\text{S}]$. This data suggests that a coordination polymer is formed through a Ag(I)-sulfur bond, further analysis of **1** supports the formation of a polymeric structure as discussed below.

The comparison of UV-Vis absorbance for an aqueous solution of 4-thiouridine (0.1 mM) and **1** (0.1 mM), shows changes in the spectra (Figure 7.14). The main peak for the ligand, in thione form, appears at 333 nm and it corresponds to a $\pi\text{-}\pi^*$ transitions of the thione group.⁴² This peak is red shifted to 338 nm, broadened and less intense for **1**. This suggests that the sulfur atoms are affected by Ag(I) ions forming the expected Ag(I)-thiolate. Peaks below 300 nm are due to $\pi\text{-}\pi^*$ transitions of the pyrimidine ring,⁴³ and they appear at 248 nm for the ligand and 245 nm for **1**.

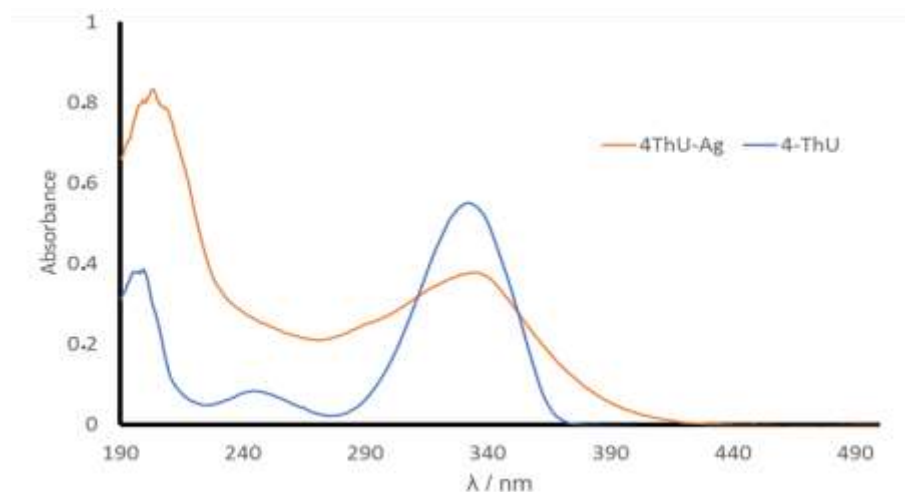


Figure 7.14. UV-Vis spectrum for 4-thiouridine (blue line) and **1** (orange line).

The FTIR spectra of **1** as a dry xerogel shows a similar spectrum than the ligand (Figure 7.15). The characteristic band for the C=S group at 1112 cm^{-1} and for C-S group at

770 cm^{-1} are present in 4-thiouridine.^{28,52} For **1** the band for C=S is less intense while for C-S more intense (Figure 7.15). It suggests that there is a modification in the sulfur environment due to the interaction between Ag(I) ions and sulfur atoms.

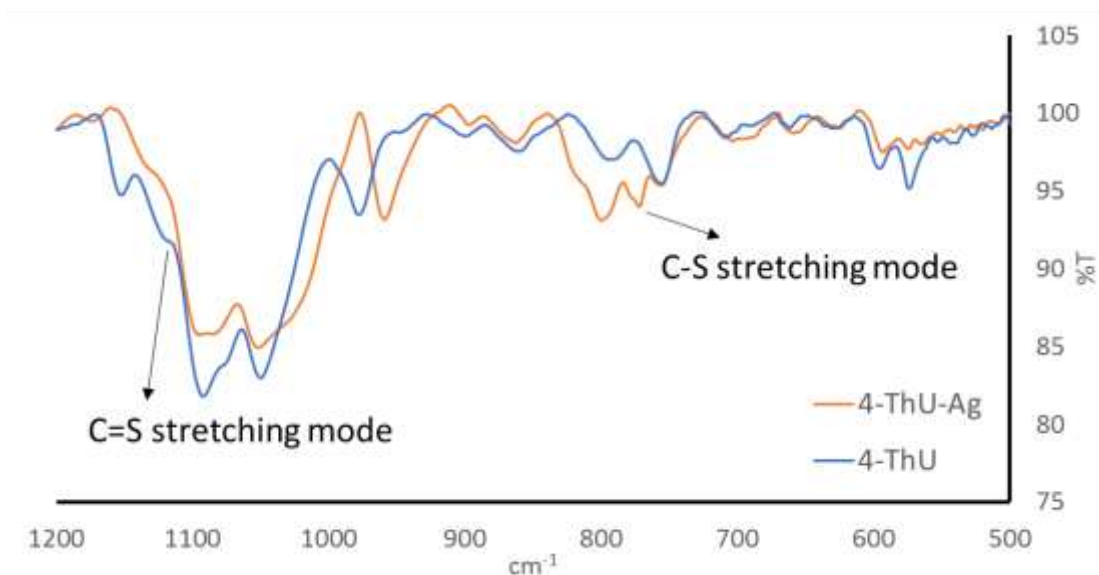


Figure 7.15. FTIR spectra for 4-thiouridine (blue line) and **1** (orange line). Data showed between 500 and 1200 cm^{-1} .

Circular dichroism (CD) spectroscopy helped to determine the structure of **1** based on the chirality of 4-thiouridine. The CD spectrum of an aqueous solution of 4-thiouridine (10 mM) shows two positive peaks at 268 and 315 nm and one negative at 231 nm confirming the chirality of the molecule (Figure 7.16). Comparing these peaks with the spectrum of **1** at 10 mM there is a red shift to 300 and 360 nm and also these peaks are broadened and more intense than in 4-thiouridine (Figure 7.16). Although it is difficult to assign each peak with a spectroscopic transition without computational calculations, peaks above 300 nm are usually assigned to $\pi\text{-}\pi^*$ transitions of C=S group in 4-thiouridine⁵³ and it indicates that the change in the spectra observed is due to a modification of the sulfur environment. This change can be explained by the Ag(I) ions coordinating sulfur atoms of 4-thiouridine. In addition, the increase of intensity

suggests a rise in the molecular ordering as a consequence of a polymer formation.^{54,55} The confirmed chirality of **1** is often ascribed to a helical configuration⁵⁶ and the negative CD signal below 200 nm is an indication for a right-handed orientation of the helicity, it will be discussed along with AFM data later.^{55,57,58}

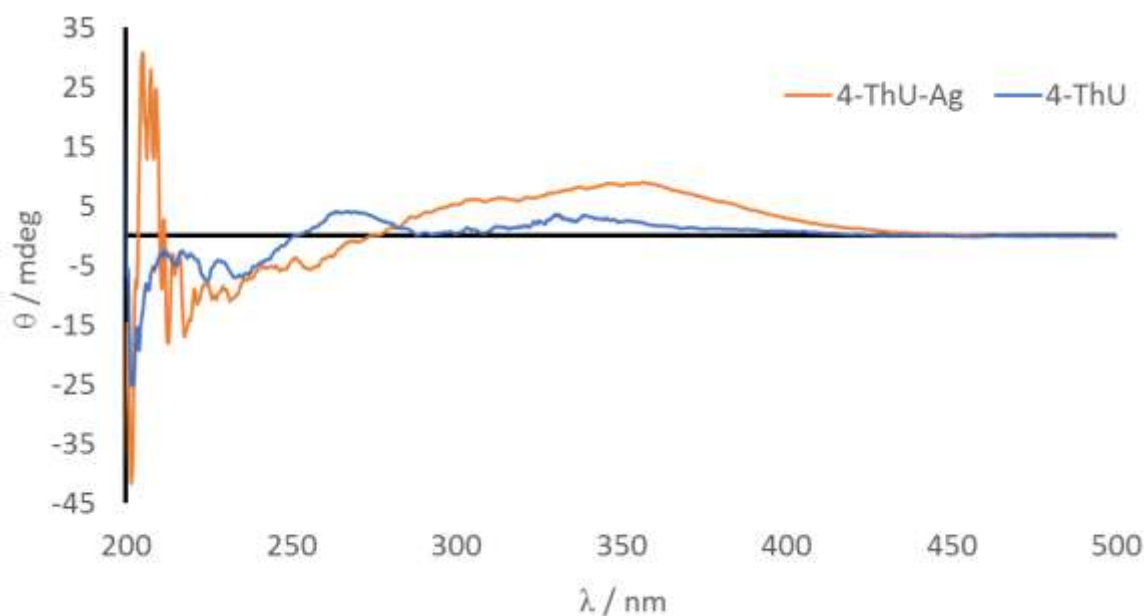


Figure 7.16. CD spectra for 4-thiouridine (blue line) and **1** (orange line).

Further analysis of **1** includes analysis of SEM microscopy on xerogel form. Figure 7.17a reveals the formation of a supramolecular network made of one-dimensional polymers with microns in length, that entangle forming layers of polymers. These polymers, in form of fibres, are consistent with the formation of coordination polymers that cover all the surface of the holder. Figure 7.17b shows a zoom in image where the formation of such strands is discernible. These results suggest the formation of a one-dimensional coordination polymer made with Ag(I)-sulfur backbone, that support as well mass spectroscopy data. Since the resolution for the size of the fibers under SEM is not very clear, further studies with AFM may show better details.

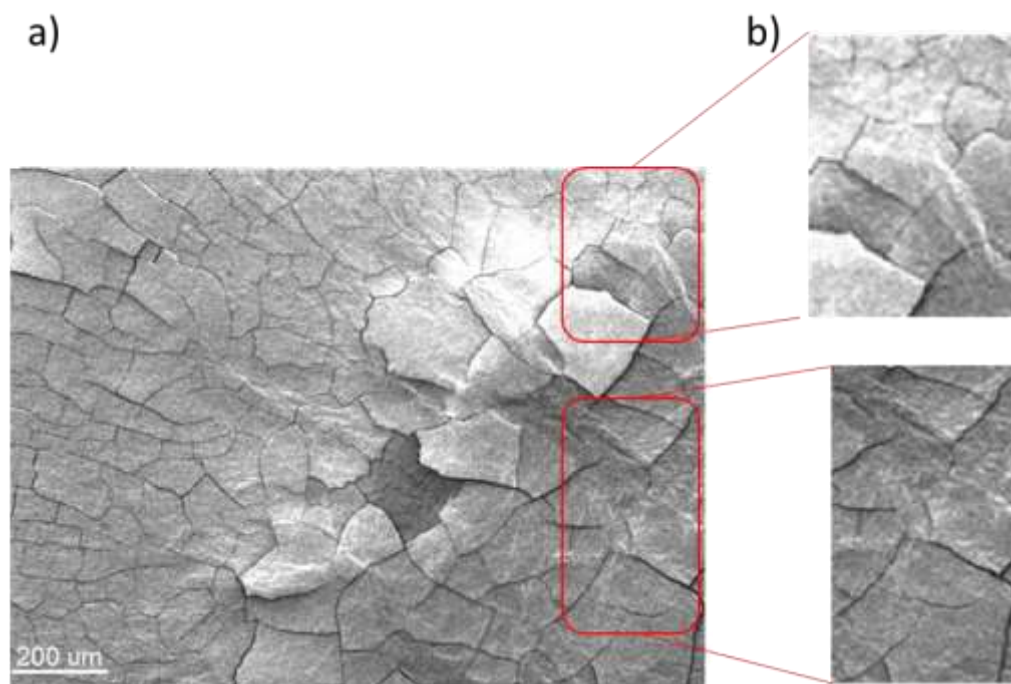


Figure 7.17. SEM image for Ag(I) product at 200 μm (a). Two zoom images show the conformation of the material in layers (b).

Atomic force microscopy analyzed **1** in xerogel form deposited on mica to gain better insight into its structure. Figure 7.18 shows that **1** formed a layer of fibres associates that assemble forming an entangled supramolecular network, characteristic of a hydrogel. Also, it is possible to observe fibres thicker than others. The length of single fibres varying between 100 to 200 nm with an average of 140 nm (Figure 7.19a) and cross-sectional heights around 2 nm (Figure 7.19b) similar to other Ag(I) thiolate compounds.^{59,60} Individual fibres associate to form much longer strands, ca. 2 μm , forming extended bundles (Figure 7.20a) with equivalent height to shorter individual fibres (Figure 7.20b). This is an indication that individual fibres self-interact in parallel to associate. In addition, as CD experiment suggested, **1** is chiral and it is confirmed in Figure 7.20c were a fibre associate reveals the formation of an individual helical

chain with a regular periodicity of the helix around 9 nm and cross-sectional height around 2 nm.

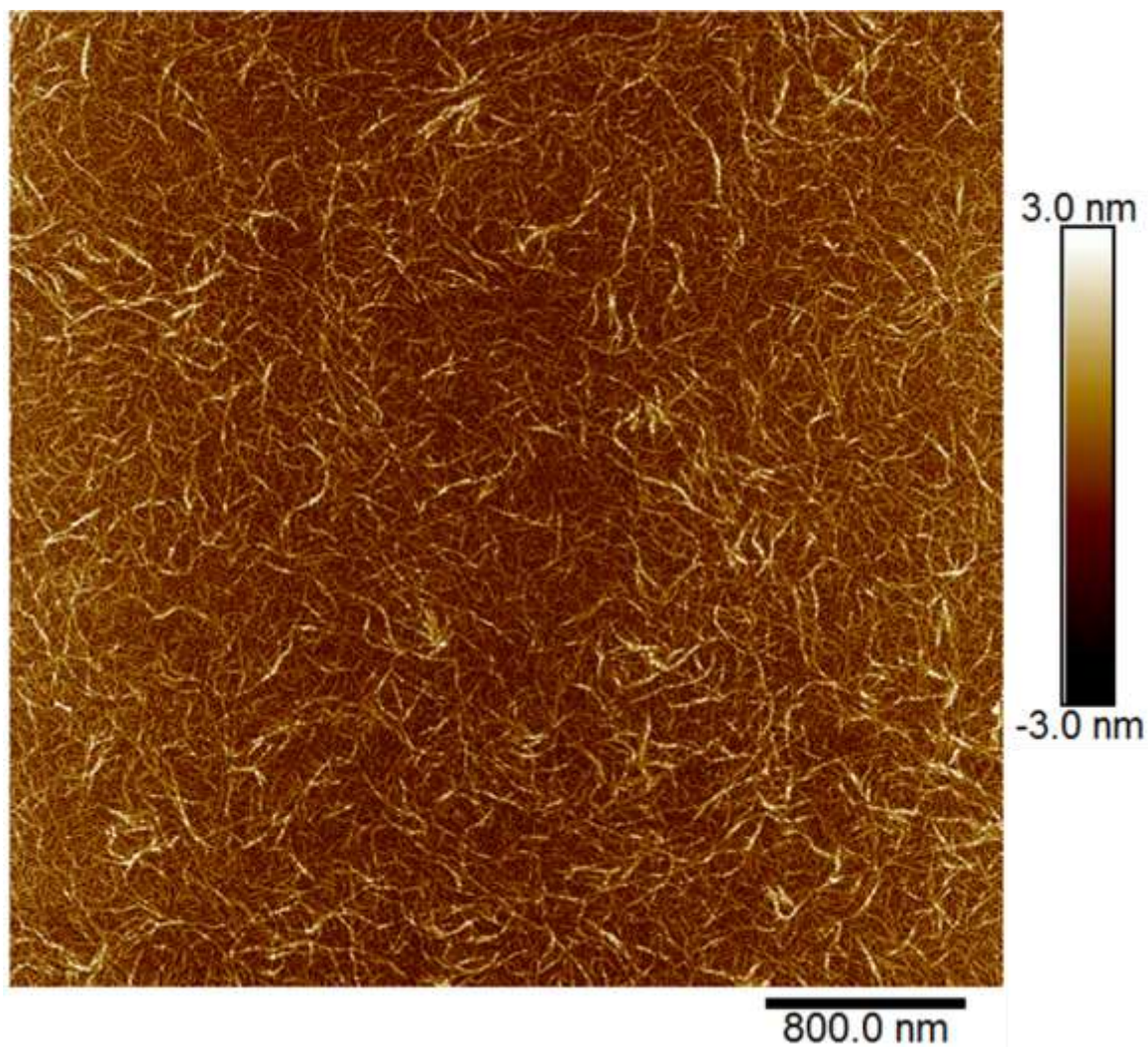


Figure 7.18. AFM image for **1** at 0.1 mM concentration in water and dried on mica, showing fibres associates that entangle, forming a characteristic network of a hydrogel.

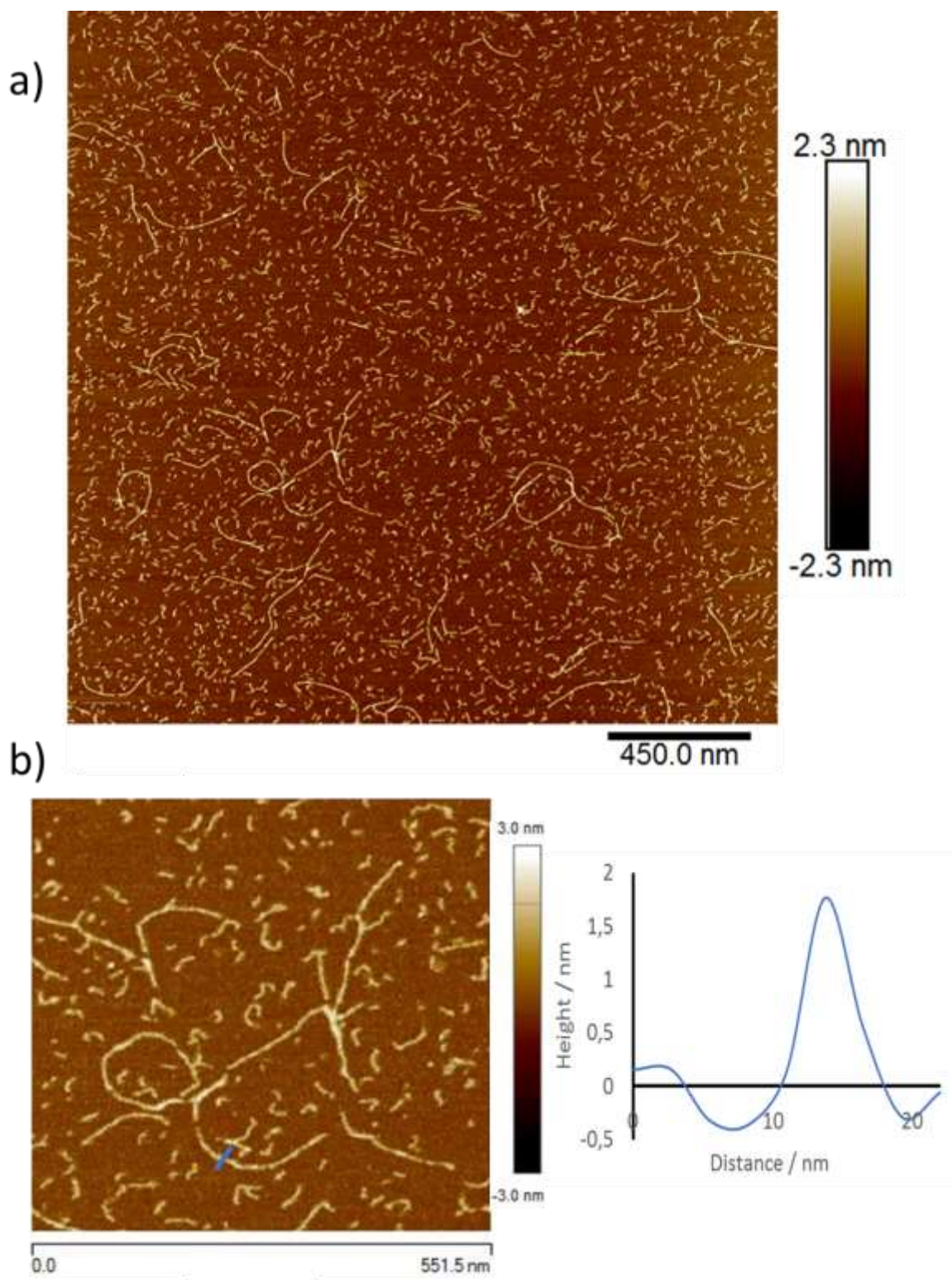


Figure 7.19. AFM images for **1** at 0.01 mM concentration in water and dried on mica, showing single fibres, a) shows large individual fibres and b) shows that the height of an individual fibre is around 2 nm.

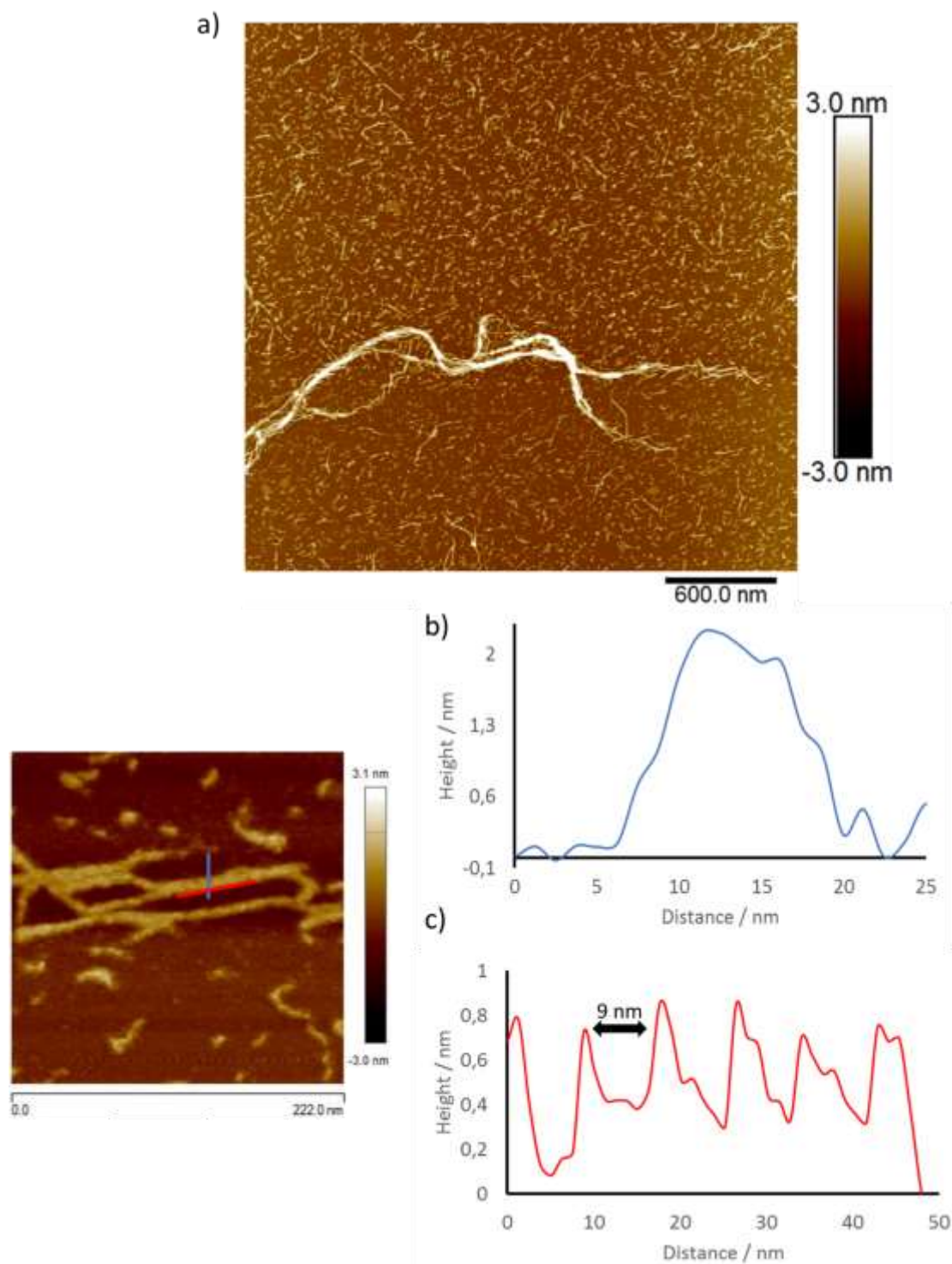


Figure 7.20. AFM images for **1** at 0.01 mM concentration in water and dried on mica, showing fibres associates, a) shows an extended bundle of individual fibres, b) shows that the height of these associates is around 2 nm and c) shows a helical feature of these fibres associates, the periodicity of a helix, which is around 9 nm.

At this point it is possible to propose a structure for **1**. Mass spectroscopy indicated the oligomeric nature of **1** with Ag(I)-sulfur motif and it is in agreement with the formation of a coordination polymer. Spectroscopic techniques, UV-Vis, FTIR and CD, confirmed the interaction of sulfur atoms with Ag(I) ions due to the modifications on the electronic environment of sulfur atoms. It implies the coordination of 4-thiouridine by Ag(I) ions. In addition, CD spectroscopy showed an increase in the intensity of the chiral signal for **1** suggesting that molecular ordering is larger than in 4-thiouridine ligand and it is consequence of a polymer formation. Microscopic techniques showed the formation of a one-dimensional coordination polymer in form of fibres that could associate into helical bundles for **1** (Figure 7.21a). The formation of associates is based on the non-covalent self-interaction between individual fibres by base stacking or hydrogen bonding (Figure 7.21b).^{61,62} As a result, these fibre associates entangled to form the three-dimensional network of a supramolecular hydrogel where water molecules are trapped.⁶³⁻⁶⁵ In addition, these chiral fibre associates have a right-handed helical orientation.

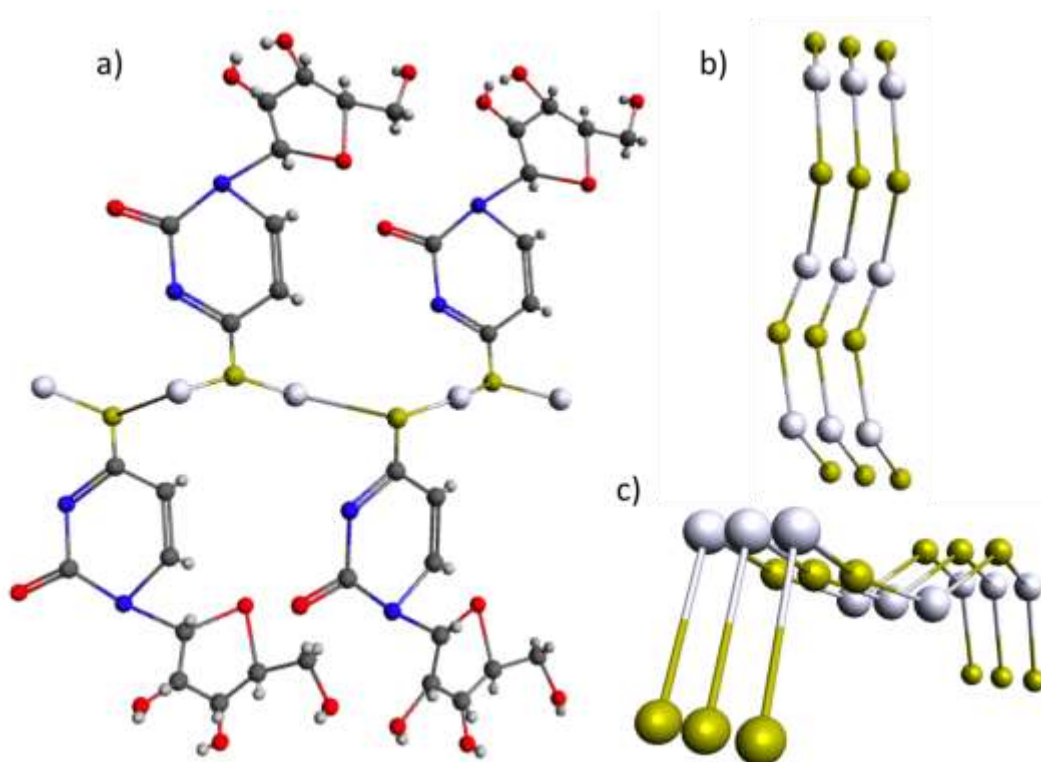


Figure 7.21. Proposed scheme models for the one-dimensional coordination polymer **1** structure, a) indicates a perpendicular view of the coordination polymer, b) and c) shows the association of coordination polymers in parallel viewed from the top (b) and onto the polymer axis (c). These bundles of fibres associates turn into a helix with a right-handed orientation (grey balls represent Ag(I) ions) (in b and c ligand substituents are omitted for clarity). These models were drawn on Avogadro software 1.2.0.

Luminescence emission was measured to determine optical features on the coordination polymer **1**. The maximum peak in the emission spectrum of **1** appears around 522.5 nm for an excitation of 380 nm while in 4-thiouridine it is at 470 nm for the same excitation wavelength (Figure 7.22). The red shift and the large increase in emission intensity after complexation suggests a ligand to metal charge transfer process.⁶⁶⁻⁶⁸ Also the broad emission band of **1** can be associates with a metal-ligand

charge transfer, metal-metal charge transfer or metal centered transitions.^{69,70} In addition, the Stokes shift near 200 nm along with a broad emission peak, are often indicatives of a phosphorescence emission process.⁷¹⁻⁷³

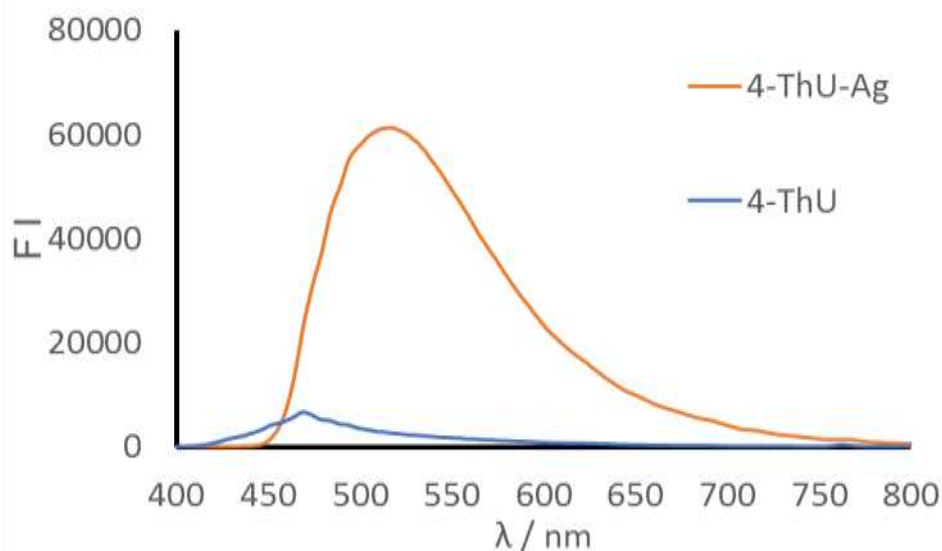


Figure 7.22. Luminescence spectra for an aqueous solution of 4-thiouridine at 60 mM (blue line) and **1** at 100 mM (orange line) at 380 nm excitation.

7.3.2.2. 4-Thiouridine and Au (I)

The reaction was performed using a yellow aqueous solution of 4-thiouridine and an aqueous solution of Au(I), prepared by the reduction of HAuCl_4 with thiodiglycol, in an equimolar ratio 1:1 (Figure 7.23). After 10 min of strong mixing an orange liquid (**2**) is formed at room temperature. The reaction mixture **2** was firstly examined to determine its chemical structure.

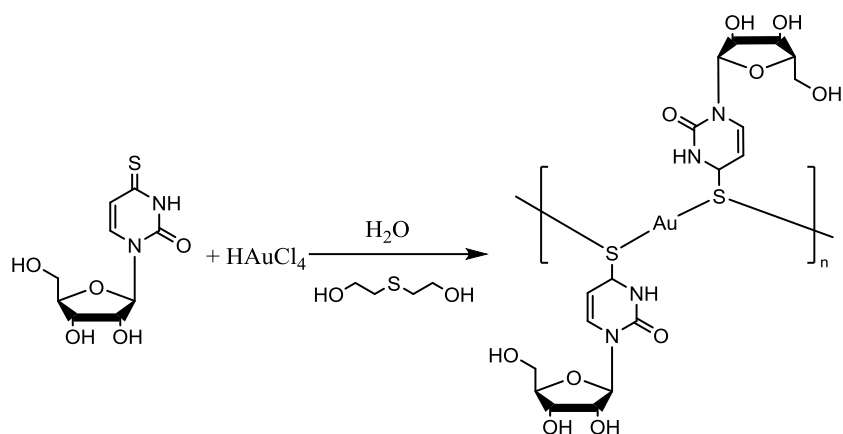


Figure 7.23. Scheme of Au(I)-4-thiouridine complex preparation.

Mass spectroscopy proved the complexation of Au(I) and the oligomeric nature of **2**. ESI mass spectroscopy showed a peak equivalent to an oligomeric chain, 717.0573 m/z for $[\text{AuL}_2]^+$, 717.06 m/z calculated (Appendix, Figure A19). L corresponds to a neutral charge molecule of 4-thiouridine, $[\text{C}_9\text{H}_{12}\text{N}_2\text{O}_5\text{S}]$. This data suggests the formation of a coordination polymer where Au(I) is attached to sulfur of 4-thiouridine as a thione in accordance with literature.²⁴ Further examinations of **2** supports its polymeric structure as discussed below.

A comparison of UV-Vis absorbance for an aqueous solution of 4-thiouridine (0.1 mM) and **2** (0.1 mM) shows differences in the spectra (Figure 7.24). The main peak of 4-thiouridine at 333 nm, due to $\pi\text{-}\pi^*$ transitions of the thione group,⁴² is red shifted to 350 nm, broadened and more intense for **2**. This suggest that sulfur atoms are interacting with Au(I) ions forming the expected Au(I)-sulfur thiolate.²⁴ Peaks below 300 nm are related to $\pi\text{-}\pi^*$ transitions of the pyrimidine ring,⁴³ and they appear at 248 nm for the ligand and 260 nm for **2**.

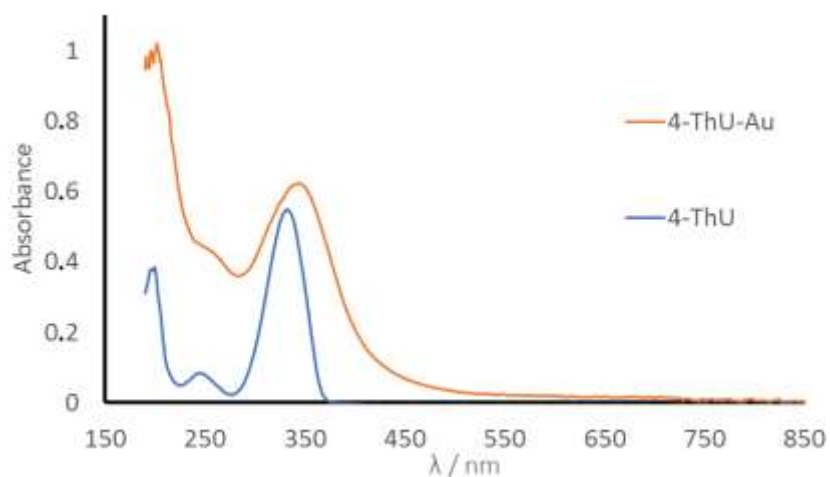


Figure 7.24. UV-Vis spectra for 4-thiouridine (blue line) and **2** (orange line).

Circular dichroism (CD) spectroscopy contributed with important features to determine the structure of **2**. The CD spectrum of an aqueous solution of 4-thiouridine (10 mM) showed a signal with positive and negative peaks, confirming its chiral properties (Figure 7.25). Comparing this with the spectrum of **2** at 10 mM there is an increase in intensity of the CD signal related to a polymer formation, where molecules adopt an ordered structure.^{55,56} In addition, the number of peaks increased after complexation. Positive peak of 4-thiouridine at 268 nm is red shifted to 297 nm for **2**; 315 nm is red shifted and unfolded to 330 and 371 nm for **2** that also showed a new peak at 440 nm. The peaks above 300 nm are related to the electronic environment of the sulfur atoms⁷⁴ so the change in the spectra above 300 nm is associated to the coordination of Au(I) ions with sulfur atoms. For long wavelength, peaks are usually assigned to metal to ligand charge transfer³ so the new peak at 440 nm also supports the complexation. Both the chiral properties and the formation of a polymer with a Au(I)-sulfur motif were therefore confirmed for **2**.

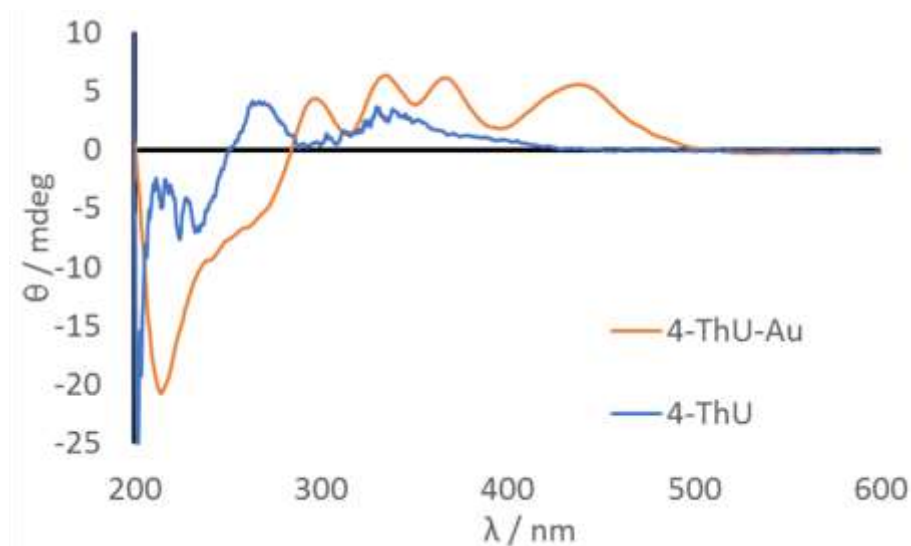


Figure 7.25. CD spectra for 4-thiouridine (blue line) and **2** (orange line).

Structural characterization eventually included AFM microscopy for **2**, after being dried on mica. The examination of **2** dried reveals the formation of aggregates, with cross-sectional heights varying between 1.4 and 2.7 nm with an average of 2.5 nm (Figure 7.26). The size distribution of these aggregates varies between 5 and 40 nm with an average of 20 nm, this wide range of size distribution is associated with the poor uniformity of the aggregates (Figure 7.27). The fact that **2** is a liquid suggest that there is not a supramolecular network supported by fibres entangling. Instead, AFM suggests the formation of aggregates with undefined shapes. These have some thick parts where the material seems to gather together strongly (Figure 7.27).

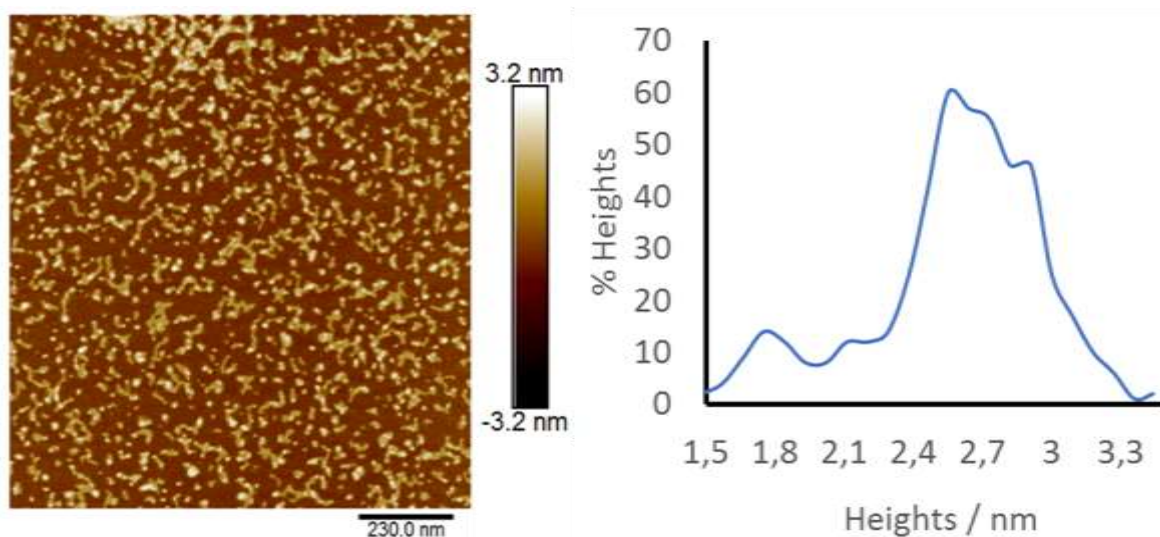


Figure 7.26. AFM image for **2** at 0.1 mM concentration in water and dried on mica and its cross-sectional heights distribution (right).

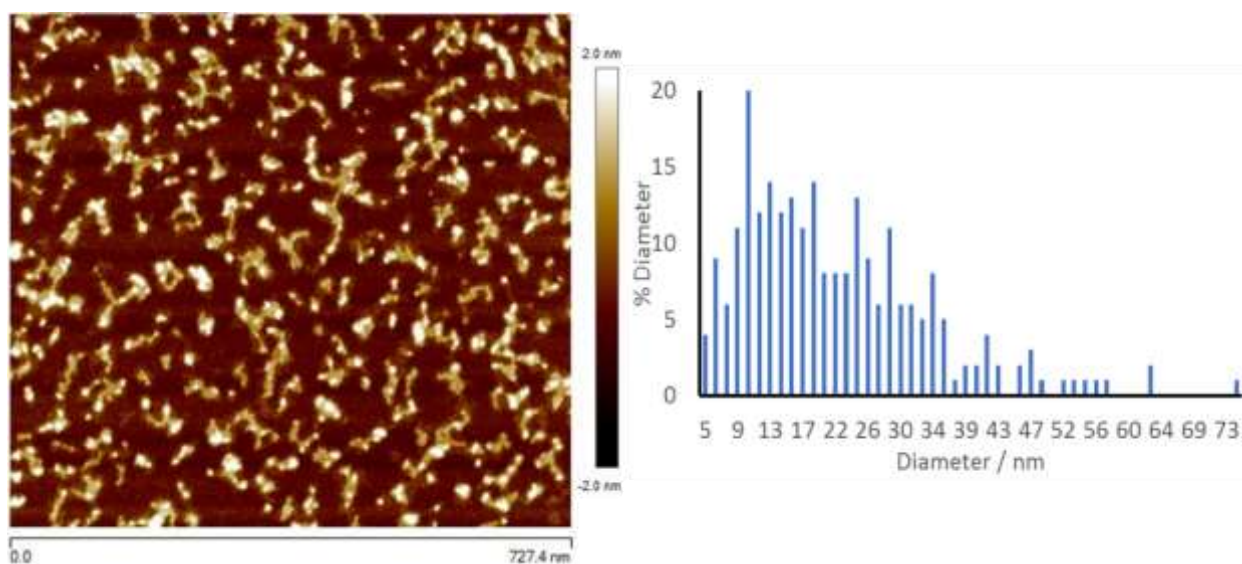


Figure 7.27. AFM image for **2** at 0.1 mM concentration in water and dried on mica (left) and its size distribution diameter (right).

The structural characterization of **2** started with mass spectroscopy, which indicated the formation of a polymer with a Au(I)-sulfur backbone. To confirm that the polymeric nature of **2** is based on a Au(I) thiolate chain, UV-Vis and CD spectroscopies were performed. They showed a change in the electronic environment of sulfur atoms after

reaction with Au(I) ions, which indicates formation of a coordination polymer based of Au(I)-sulfur chains. In addition, CD spectroscopy indicated that **2** possess chiral properties. AFM indicated that **2** forms non-uniform aggregates. To propose a structure for **2**, aurophilic interactions should be considered as a possible interaction between Au(I) ions as some of crystal structures reported showed. Also, the fact that the aggregation of **2** can be related with aurophilic interactions,⁷⁵⁻⁷⁷ leads to the conclusion that the structure of **2** is based on shorts Au(I) thiolate coordination polymer that aggregate due to aurophilic interactions (Figure 7.28). The presence of aurophilic interactions will be further investigated with the study of luminescence properties of **2**.

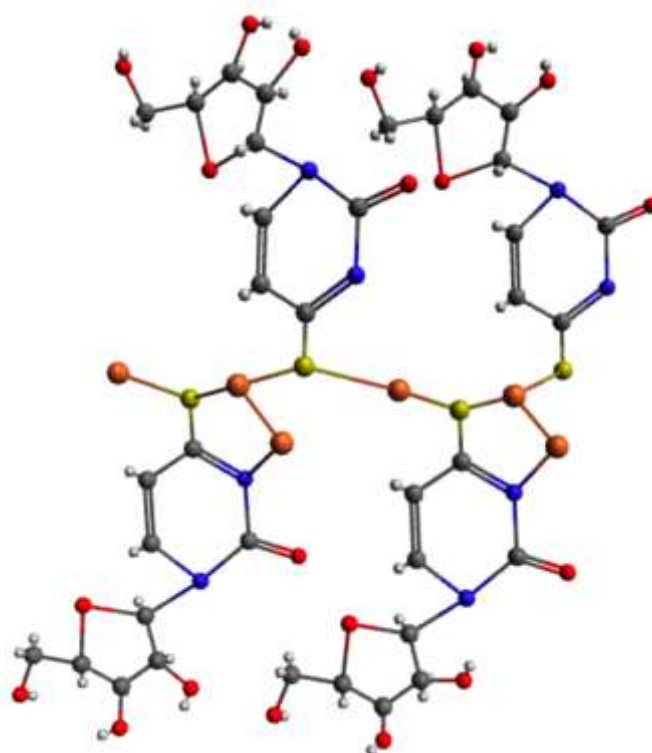


Figure 7.28. Proposed scheme model for the one-dimensional coordination polymer **2** structure. It shows a perpendicular view of the coordination polymer where Au(I) ions are bridging 4-thiouridine ligands and another Au(I) ion by aurophilic interactions, this Au(I) is interacting with N3 of 4-thiouridine (orange balls represent Au(I) ions) (ligand substituents are omitted for clarity). This model was drawn on Avogadro software 1.2.0.

Luminescence emission was measured to determine optical properties on the coordination polymer **2**. The maximum peak of the emission for **2** appears at 623 nm for an excitation of 450 nm while in 4-thiouridine it appears at 470 nm for an excitation of 380 nm (Figure 7.29). The emission peak for **2** is red shifted and is broader than that of the ligand and it suggest a ligand to metal, metal to ligand or metal centered transition processes.^{67,69,70} Another emission peak appears at 832 nm when **2** is excited at 550 nm (Figure 7.29). This peak displays a much larger increase in emission intensity as well as a large Stokes shift, which suggests a phosphorescence emission process attributed to a Au(I) centered transition due to aurophilic interactions and a ligand to metal charge transfer.^{30,69,78-82} The high intensity of this emission is related to the formation of aggregates of the Au(I) thiolate coordination polymer and it is due to the large amount of aurophilic interactions between Au(I) ions within the aggregate.^{80,}

83-85

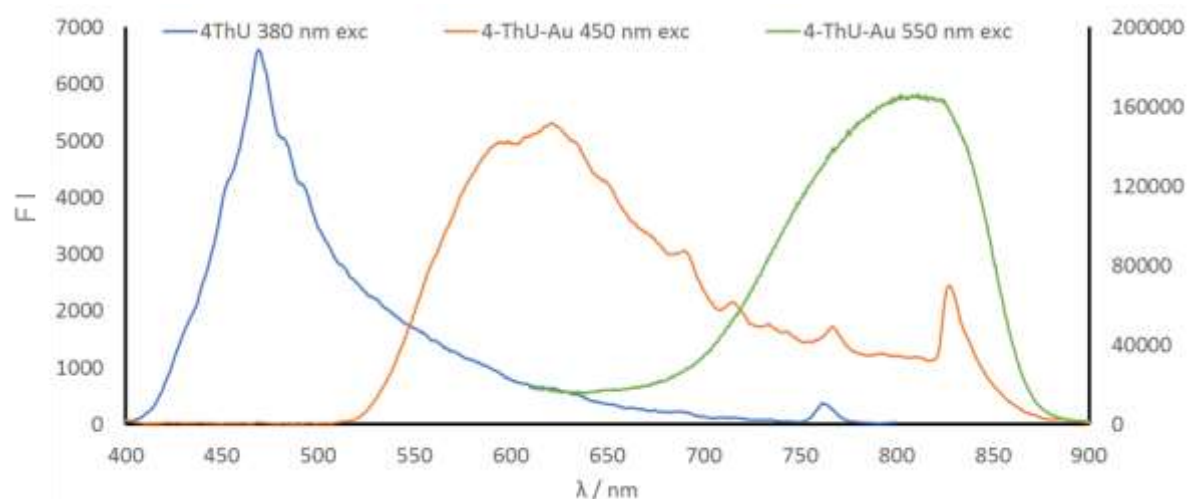


Figure 7.29. Emission spectra of 4-thiouridine with excitation at 380 nm (blue line) and **2** with excitation at 450 nm (orange line) and 550 nm (green line).

7.4. Conclusion

A thio-modified nucleoside, 4-thiouridine, has been successfully prepared following an organic synthesis method. Once the completion of the synthesis was successful, 4-thiouridine has been spectroscopically and structurally characterized to confirm its morphology.

The preparation of coordination polymers with pyrimidine thio-nucleoside and coinage metal ions was explored. First, the interaction between Ag(I) ions and 4-thiouridine was examined using ESI mass spectroscopy, UV-Vis, FTIR, CD, SEM and AFM. The structural analysis on [Ag(I)-4-thiouridine]_n hydrogel proved the formation of a chiral one-dimensional coordination polymer based on Ag(I)-sulfur motif as building-block of a supramolecular network. Also, optical properties of [Ag(I)-4-thiouridine]_n indicates that luminescence emission intensity increased compared to the ligand and thus confirming the chiro-optical properties of [Ag(I)-4-thiouridine]_n.

In addition, the preparation of [Au(I)-4-thiouridine]_n was achieved. Its structural characterization included ESI mass spectroscopy, UV-Vis, CD and AFM. They showed the formation of a chiral coordination polymer based on Au(I)-sulfur interactions that aggregate due to aurophilic interactions. Optical properties of [Au(I)-4-thiouridine]_n were explored and the formation of aggregates led to a large increase of luminescence emission compared to the ligand.

To conclude, it has been shown that it is possible to prepare coordination polymers based on coinage metal ions and thio-modified pyrimidine nucleosides. Although [Ag(I)-4-thiouridine]_n and [Au(I)-4-thiouridine]_n possess promising characteristics, such as chiro-optical properties, similar to semiconductor compounds, further experiments need to be done in order to prove these materials as appropriate candidates for electrical conductivity or magnetic properties.

7.5. References

- 1- Carell, T., *Nature* 2011, **469**, 45-46.
- 2- Naskar, S., Guha, R., Müller, J., *Angew. Chem. Int. Ed.* 2020, **59**, 1397-1406.
- 3- Al-Mahamad, L., El-Zubir, O., Smith, D., Horrocks, B. R., Houlton, A., *Nat. Comm.* 2017, **8**, 720.
- 4- Al-Tai, H., Periasamy, V., Amon, Y., *PLoS ONE* 2016, **11**, e0145423.
- 5- Veselska, O., Demessence, A., *Coord. Chem. Rev.* 2018, **355**, 240-270.
- 6- Mistry, L., El-Zubir, O., Dura, G., Clegg, W., Waddell, P., Pope, T., Hofer, W., Wright, N., Horrocks, B. R., Houlton, A., *Chem. Sci.* 2019, **10**, 3186-3195.
- 7- Chai, Y., Guo, X., Leonard, P., Seela, F., *Chem. A Eur. J.* 2020, **26**, 13973-13989.
- 8- Pant, P., Fisher, M., *Biophysical Chemistry* 2021, **269**, 106525.
- 9- Heitner, H., Lippard, S., Sunshine, H., *J. Am. Chem. Soc.* 1972, **94**, 8936-8937.
- 10- Sigel, A., Operschall, B., Matera, A., Swiatek, J., Sigel, H., *Coord. Chem. Rev.* 2016, **327-328**, 200-220.
- 11- Veselska, O., Cai, L., Podbevsek, D., Ledoux, G., Guillou, N., Pilet, G., Fateeva, A., Demessence, A., *Inorg. Chem.* 2018, **57**, 2736-2743.
- 12- Gallego, A., Castillo, O., Gomez, C., Zamora, F., Delgado, S., *Inorg. Chem.* 2012, **51**, 718-727.
- 13- Zhang, K, Guo, L., *Catal. Sci. Technol.* 2013, **3**, 1672-1690.
- 14- Tributsch, H., Rojas, A., *Electrochimica Acta* 2000, **45**, 4705-4716.
- 15- Safrani, T., Jopp, J., Golan, Y., *RSC Adv.* 2013, **3**, 23066-23074.
- 16- Grozdanov, I., Najdoski, M., *J. Sol. St. Chem.* 1995, **114**, 469-475.
- 17- Isac, L., Cazan, C., Enesca, A., Andronic, L., *Front. Chem.* 2019, **7**, 694.
- 18- Hsu, Y., Chen, Y., Lin, Y, *Electrochimica Acta* 2014, **139**, 401-407.
- 19- Liu, Y., Zhu, Z., Nakamura, A., Orlando, R., Söll, D., Whitman, W., *J. of Biological Chem.* 2012, **287**, 36683-36692.
- 20- Borek, C., Reichle, V., Kellner, S., *ChemBioChem* 2020, **21**, 2768-2771.
- 21- Pal, B., Uziel, M., Doherty, D., Cohn, W., *J. Am. Chem. Soc.* 1969, **91**, 3634-3638.
- 22- El-Tayeb, A., Qi, A., Nicholas, R., Müller, C., *J. Med. Chem.* 2011, **54**, 2878-2890.
- 23- Palafox, M., Rastogi, V., Singh, S., *J. of Biom. Structure and Dynamics* 2017, **36**, 1225-1254.
- 24- Ericson, A., Arthur, J., Coleman, R., Elding, L., Elmroth, S., *J. Chem. Soc., Dalton Trans.* 1998, 1687-1692.
- 25- Hawkinson, S., Pal. B., Einstein, J., *Cryst. Struct. Comm.* 1975, **4**, 557.
- 26- Dias, A., Duarte, M., Galvao, A., Garcia, M., Marques, M., Salema, M., Masi, D., Mealli, C., *Polyhedron* 1995, **14**, 675-685.

- 27- Vetter, C., Kaluderovic, G., Paschke, R., Kluge, R., Schmidt, J., Steinborn, D., *Inorganica Chimica Acta* 2010, **363**, 2452-2460.
- 28- Aulakh, J., Lobana, T., Sood, H., Arora, D., Kaur, R., Singh, J., Garcia, I., Kaur, M., Jasinski, J., *RSC Adv* 2019, **9**, 15470-15487.
- 29- Varna, D., Kapetanaki, E., Koutsari, A., Hatzidimitrou, A., Psomas, G., Angaridis, P., Papi, R., Pantazaki, A., Aslanidis, P., *Polyhedron* 2018, **151**, 131-140.
- 30- Lee, Y., Eisenberg, R., *J. Am. Chem. Soc.* 2003, **125**, 7778-7779.
- 31- Harker, C., Tielink, E., Whitehouse, M., *Inorg. Chim. Acta* 1991, **181**, 23-30.
- 32- Mullice, L., Mottram, H., Hallet, A., Pope, S., *EurJIC* 2012, **2012**, 3054-3060.
- 33- Hunks, W., Jennings, M., Puddephatt, R., *Inorg. Chem.* 2002, **41**, 4590-4598.
- 34- Hunt, G., Griffith, E., Amma, E., *Inorg. Chem.* 1976, **15**, 2993-2997.
- 35- Paizanos, K., Charalampou, D., Kourkoumelis, N., Kalpogiannaki, D., Hadjiarapoglou, L., Spanopoulou, A., Lazarou, K., Manos, M., Tasiapoulos, A., Kubicki, M., Hadjikakou, S., *Inorg. Chem.* 2012, **51**, 12248-12259.
- 36- Lobana, T., Kaur, A., Sharma, R., Bala, M., Jassal, A., Duff, C., Jasinski, J., *J. of Chem. Sci.* 2015, **127**, 1859-1869.
- 37- Kowalik, T., Varnagy, K., Swiatek, J., Jon, A., Sovago, I., Sochacka, E., Malkiewicz, A., Sychata, J., Koztowski, H., *J. of Inorg. Biochem.* 1997, **65**, 257-262.
- 38- Baindur, S., Douglas, K., *Biochimica et Biophysica Acta – General Subjects* 1987, **923**, 66-73.
- 39- Laduree, D., Fossey, C., Delbederi, Z., Sugeac, E., Schmidt, S., Laumond, G., Aubertin, A., *J. of Enzyme Inhibition and Medical Chem.* 2005, **20**, 533-549.
- 40- Griffon, J., Mathe, C., Faraj, A., Aubertin, A., De Clercq, E., Balzarini, J., Sommadossi, J., Gosselin, G., *Eur. J. of Medicinal Chem.* 2001, **36**, 447-460.
- 41- Kaleta, Z., Makowski, B., Soos, T., Dembinski, R., *Org. Lett.* 2006, **8**, 1625-1628.
- 42- Komatsu, Y., Ohtsuka, E., 1999, Chemical RNA Synthesis in *Comprehensive Natural Products Chemistry*, **6**, 81-96.
- 43- Igarashi, N., Tajiri, A., Hatano, M., Shibuya, S., Ueda, T., *Biochim. et Bioph. Acta – Nucleic Acids and Protein Synthesis* 1981, **656**, 1-15.
- 44- Zou, X., Dai, X., Liu, K., Zhao, H., Song, D., Su, H., *J. Phys. Chem. B* 2014, **118**, 5864-5872.
- 45- Sapunar, M., Domcke, W., Doslic, N., *Phys. Chem. Chem. Phys.* 2019, **21**, 22782-22793.
- 46- Arslanacan, S., Martinez, L., Corral, I., *Molecules* 2017, **22**, 998.
- 47- Cao, P., Yao, J., Ren, B., Gu, R., Tian, Z., *J. Phys. Chem. B* 2002, **106**, 10150-10156.
- 48- Samejima, T., Kita, M., Saneyoshi, M., Sawada, F., *Bioch. Et Bioph. Acta – Nucleic Acids and Protein Synthesis* 1969, **179**, 1-9.

- 49- Palyi, G., Zucchi, C., Caglioti, L., 2004 (ed), *Progress in Biological Chirality*, ch. 32, 397-404.
- 50- Favre, A., *Photochemistry and Photobiology* 1974, **1**, 15-19.
- 51- Feitelson, J., Shalitin, N., *Biochemistry* 1976, **15**, 2092-2097.
- 52- Shanker, R., Yadav, R., Singh, I., *Spectrochimica Acta Part A: Molecular Spectroscopy* 1994, **50**, 1251-1258.
- 53- Watanabe, K., *Biochemistry* 1980, **19**, 5542-5549.
- 54- Lam, A., Guenther, R., Agris, P., *Biometals* 1995, **8**, 290-296.
- 55- Zimmer, C., Luck, G., Holy, A., *Nucleic Acids Research* 1976, **3**, 2757-2770.
- 56- Zhang, H., Zheng, X., Kwok, R., Wang, J., Leung, N., Shi, L., Sun, J., Tang, Z., Lam, J., Qin, A., Tang, B., *Nat. Comm.* 2018, **9**, 4961.
- 57- Sutherland, J., Griffin, K., Keck, P., Takacs, P., *Proc. Natl. Acad. Sci. USA* 1981, **78**, 4801-4804.
- 58- Sprecher, C., Baase, W., Johnson, C., *Biopolymers* 1979, **18**, 1009-1019.
- 59- Hong, S., Olin, A., Hesse, R., *Acta Chemica Scandinavica A* 1975, **29**, 583-589.
- 60- Dance, I., Fitzpatrick, L., Rae, A., Scudder, M., *Inorg. Chem.* 1983, **22**, 3785-3788.
- 61- Panja, S., Seddon, A., Adams, D., *Chem. Sci.* 2021, **12**, 11197-11203.
- 62- Koskinen, L., Jääskeläinen, S., Hirva, P., Haukka, M., *Solid State Sciences* 2014, **35**, 81-87.
- 63- Kim, H., Zin, W., Lee, M., *J. Am. Chem. Soc.* 2004, **126**, 7009-7014.
- 64- Wu, Z., Du, Y., Liu, J., Yao, Q., Chen, T., Cao, Y., Zhang, H., Xie, J., *Angew. Chem. Int. Ed.* 2019, **58**, 8139-8144.
- 65- Popa, V., Volf, I., (ed.), 2018, *Biomass as renewable raw material to obtain bioproducts of high-tech value*, ch. 11, 401-439.
- 66- Zhou, Y., Chen, W., Wang, D., *Dalton Trans.* 2008, 1444-1453.
- 67- Jin, S., Wang, S., Song, Y., Zhou, M., Zhong, J., Zhang, J., Xia, A., Pei, Y., Chen, M., Li, P., Zhou, M., *J. Am. Chem. Soc.* 2014, **136**, 1555-15565.
- 68- Li, G., Lei, Z., Wang, Q., *J. Am. Chem. Soc.* 2010, **132**, 17679-17679.
- 69- Forward, J., Bohmann, D., Fackler, J., Staples, R., *Inorg. Chem.* 1995, **34**, 6330-6336.
- 70- Wang, X., Guerzo, A., Schmehl, R., *J. of Photoc. and Photob. C: Photochemistry Rev.* 2004, **5**, 55-77.
- 71- Yang, T., Peng, B., Shan, B., Zong, Y., Jiang, J., Wu, P., Zhang, K., *Nanomaterials* 2020, **10**, 261.
- 72- Ji, S., Guo, H., Yuan, X., Li, X., Ding, H., Gao, P., Zhao, C., Wu, W., Wu, W., Zhao, J., *Org. Lett.* 2010, **12**, 2876-2879.
- 73- Veselska, O., Dessal, C., Melizi, S., Guillou, N., Podbevsek, D., Ledoux, G., Elkaim, E., Fateeva, A., Demessence, A., *Inorg. Chem.* 2019, **58**, 99-105.

- 74- Reppes, R., Beuck, C., Weinhold, E., Raabe, G., Fleischhauer, J., *Chirality* 2008, **20**, 978-984.
- 75- Romo, G., Gavara, R., *Inorganics* 2021, **9**, 32.
- 76- White, R., Olmstead, M., Balch, A., *J. Am. Chem. Soc.* 2003, **125**, 1033-1040.
- 77- Fujisawa, K., Yamada, S., Yanagi, Y., Yoshioka, Y., Kiyohara, A., Tsutsumi, O., *Scientific Reports* 2015, **5**, 7934.
- 78- Li, Q., So, W., Huang, J., Li, M., Kauffman, D., Cotlet, M., Higaki, T., Peteanu, L., Shao, Z., Jin, R., *J. Am. Chem. Soc.* 2019, **141**, 5314-5325.
- 79- Goswami, N., Yao, Q., Luo, Z., Li, J., Chen, T., Xie, J., *J. Phys. Chem. Lett.* 2016, **7**, 962-975.
- 80- Cantelli, A., Guidetti, G., Manzi, J., Caponetti, V., Montalti, M., *EurJIC* 2017, **2017**, 5068-5084.
- 81- Barbieri, A., Accorsi, G., Armaroli, N., *Chem. Commun.* 2008, 2185-2193.
- 82- Veselska, O., Guillou, N., Ledoux, G., Huang, C., Newell, K., Elkaïm, E., Fateeva, A., Demessence, A., *Nanomaterials* 2019, **9**, 1408.
- 83- Fernandez, E., Laguna, A., Lopez, J., Monge, M., Sanchez, E., *Dalton Trans.* 2011, **40**, 3287-3294.
- 84- Lavenn, C., Okhrimenko, L., Guillou, N., Monge, M., Ledoux, G., Dujardin, C., Chiriac, R., Fateeva, A., Demessence, A., *J. Mater. Chem. C* 2015, **3**, 4115-4125.
- 85- Yam, V., Cheng, W., *Chem. Soc. Rev.* 2008, **37**, 1806-1813.

Chapter 8. Conclusions & Outlook

8.1. Conclusions and Outlook

The work in this thesis has developed a series of new coordination polymers based on thio-nucleosides and coinage metal ions that display a range of technologically useful properties.

Previous studies on DNA-based nanomaterials have showed an absence of valuable properties for their use in nanotechnology such as electrical conduction or magnetism.¹ To overcome these limitations, our group has worked on the preparation of a one-dimensional coordination polymer based on Au(I) and 6-thioguanosine and it has showed luminescence and electrical conductivity after being oxidative doped. In addition, it was integrated on DNA sequence.²

Continuing with this proposal, the main body of this thesis has been focused on the synthesis of $[\text{Ag(I)-6-thioguanosine}]_n$ and $[\text{Cu(I)-6-thioguanosine}]_n$ coordination polymers, determining their molecular structures. The interaction between monovalent coinage metal ions and 6-thioguanosine has been examined and established as the union through the metal-sulfur bond (Figure 8.1 a,b). Thus, the formation of one-dimensional coordination polymers is based on this interaction, similar to semiconductors, and it provides chiro-optical and conductivity features not observed so far for similar thiolate coordination polymers. A future prospective is the idea of using these polymers as building blocks to design a specific route of functionalization of molecules derivatives from DNA and RNA.

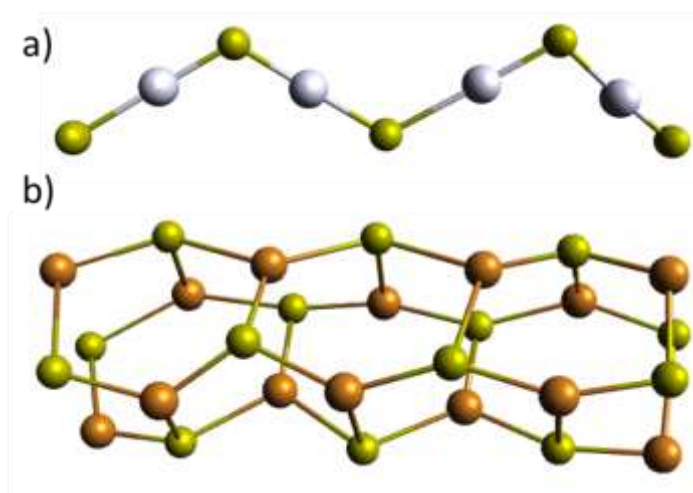


Figure 8.1. Side view of a proposed scheme models of a one-dimensional coordination polymer for Ag(I)-thiolate (a), and for Cu(I)-thiolate (b). They show the metal ions (white balls for Ag(I) and orange balls for Cu(I)) coordinating sulfur atoms (μ_2 and μ_3 respectively) (yellow balls) to form the metal-sulfur backbone of a coordination polymer. These models were drawn on Avogadro software 1.2.0.

The preparation of the $[\text{Ag(I)-6-thioguanosine}]_n$ was characterized structurally and it confirmed the formation of a chiral one-dimensional coordination polymer with a Ag(I)-sulfur backbone. Some details on the structure indicated that individual polymer chains associate to form left-handed helical strands. In addition, optical properties of $[\text{Ag(I)-6-thioguanosine}]_n$ showed an increase in luminescence emission after coordination polymer formation.

The synthesis of the $[\text{Cu(I)-6-thioguanosine}]_n$ was characterized similarly to $[\text{Ag-6-thioguanosine}]_n$ and it results as the formation of a chiral one-dimensional coordination polymer with a Cu(I) coordinating three sulfur atoms. These individual chains, in form of fibres, were associated to produce long helical polymeric chains. Additionally, optical and electrical properties of $[\text{Cu(I)-6-thioguanosine}]_n$ were analyzed, obtaining luminescence emission and conductivity behavior after redox doping.

When prepared at high concentrations, both complexes, $[\text{Ag(I)-6-thioguanosine}]_n$ and $[\text{Cu(I)-6-thioguanosine}]_n$, formed hydrogels. These three-dimensional supramolecular networks with self-healing properties, showed enhanced chiro-optical properties compared to themselves at low concentrations due to larger self-assembly processes and the homochirality of their chains. The combination between homochirality and luminescence emission originated that these coordination polymers showed CPL emission. Specifically, $[\text{Ag(I)-6-thioguanosine}]_n$ displayed the largest value of CPL reported for thiolate coordination polymers so far. In addition, $[\text{Cu(I)-6-thioguanosine}]_n$ exhibited electrical conductivity and this confirmed its behavior as a nanowire.

The idea of developing a practical route of nucleic acid functionalization using the coordination polymer approach has been successfully achieved. The new materials prepared in form of thiolate coordination polymers have displayed useful optical and conductivity properties that could be integrated into DNA as previous studies in our group have demonstrated, as is the case with $[\text{Au(I)-6-thioguanosine}]_n$. In addition, inherent structural properties of such self-assembled hydrogels in combination with opto-electronics properties possess features appreciated in technological fields.³

High concentration $[\text{Cu(I)-6-thioguanosine}]_n$ and $[\text{Au(I)-6-thioguanosine}]_n$ coordination polymers in form of hydrogels were successfully designed and tested for their use as nanowire-based gas sensors. The sensing properties shown by $[\text{Cu(I)-6-thioguanosine}]_n$ indicated that suffered the oxidizing effect from ozone and it was incapable to recover after degradation. However, $[\text{Cu(I)-6-thioguanosine}]_n$ exhibited larger response to three VOCs although it was time-dependent. To overcome these limitations, the use of a nanocomposite of $[\text{Au(I)-6-thioguanosine}]_n$ and Multi-Walled Carbon Nanotubes (MWCNTs) showed an enhancement in sensing capabilities exhibiting a stable response for VOCs. In addition, $[\text{Au(I)-6-thioguanosine}]_n/\text{MWCNTs}$ showed a sensitive and faster response for ethanol. Excellent results showed on gas

sensing for these hydrogels confirm a useful application of thiolate coordination polymers. This will encourage further studies on soft-materials based on thio-derivatives nucleosides and coinage metal ions for their use in the versatile design of materials with potential applications in recognition processes or catalysis.

The preparation of analogous coordination polymers was expanded to another thio-modified nucleoside, 4-thiouridine, in order to explore the coordination of coinage metal ions to pyrimidine bases. The synthesis of 4-thiouridine and its interaction with Ag(I) and Au(I) ions, successfully formed two coordination polymers, [Ag(I)-4-thiouridine]_n and [Au(I)-4-thiouridine]_n. [Ag(I)-4-thiouridine]_n formed a supramolecular network in form of hydrogel composed by chiral one-dimensional coordination polymers based on Ag(I)-sulfur interactions while in the case of [Au(I)-4-thiouridine]_n aggregates were formed by the interaction between chiral Au(I) thiolate coordination polymers, suggesting the presence of aurophilic interactions between them. For both systems, optical properties showed an improve in luminescence emission compared to 4-thiouridine. Therefore, it confirmed that the preparation of coordination polymers with a pyrimidine thio-nucleoside derived from nucleic acids lead to the formation of similar complexes as thiopurine did and consequently the study of coordination polymer can be expanded to other soft-mutated nucleobases.

The work shown in this thesis allows to affirm that coordination polymer approach is a potential route of functionalization of larger biomolecules through soft modification of nucleobases. The interaction between sulfur atoms and monovalent coinage metal ions provide an interesting starting point in order to provide specific functions that metal ions entail. Also, the design of larger biomolecules with specific places to link these metal ions also provide an advantage to other nanomaterial designs since it is possible to build complexes architectures with particular capacities for opto-electronics in nanotechnology.

The future prospects of such studies will need to establish the molecular ordering of these coordination polymer. As a first step, a NMR titration experiment could be established in order to determine the effect of the metal(I) after complexation and follow the change in NMR signal of the complex according to the hydrogel concentration. With this technique it would be possible to determine structural changes produced by the metal(I) in the system and therefore, have a better insight of the chemical structure of the coordination polymer. Subsequently, perform a TEM-EDX experiment will bring information about which atoms form the fibres showed in AFM. Also, one should proceed in the design of specific experiments with the aim of obtaining crystals suitable for X-ray diffraction and determine the coordination mode of metal(I) ions. These experiments should include the modification of the thio-nucleoside, replacing the ribose ring by alkyl groups, and its reaction with metal(I) ions. This perspective will focus on avoiding a high number of hydrogen bonds interactions and then the formation of hydrogels. Thus, it will be possible to understand and clarify potential structural properties of these coordination polymers. As has been done in this thesis, the coordination polymer studies should be expanded to other nucleobases, modified or not, and metal ions. Probably they will show properties unexpected that can accommodate the development of previously unknown nanomaterials.

In addition, the integration of such motifs into DNA or RNA should be the next step for this field of knowledge. The possibility to extent the properties of coordination polymers, as shown in this thesis, to larger nucleic acids with their structure-building capabilities provides a new approach to integrate technologically useful properties into nucleic acid-based molecular architectures in a simple and controllable manner.

8.2. References

- 1- Sönmezoglu, S., Sönmezoglu, O., Çankaya G., Yildirim, A., Serin, N., *J. of Applied Physics* 2010, **107**, 124518.
- 2- Al-Mahamad, L., El-Zubir, O., Smith, D., Horrocks, B. R., Houlton, A., *Nat. Commun.* 2017, **8**, 720.
- 3- Yuan, Y., Hu, M., Zhang, K., Zhou, T., Wang, S., Liu, M., Zheng, Y., *Mater. Horiz.* 2020, **7**, 3209-3216.

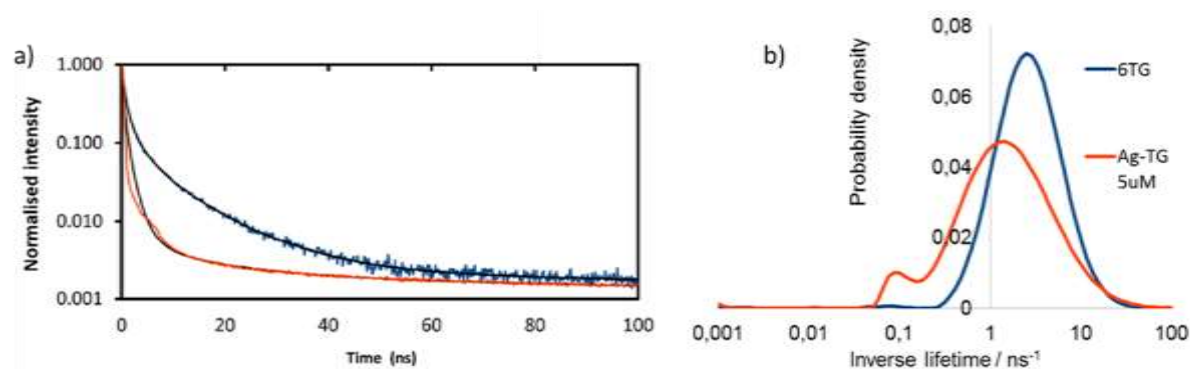


Figure A3. (a) Normalised intensity against time for the luminescence decay of ligand (6-thioguanosine, red line) and [Ag(I)-6-thioguanosine]_n (blue line) at 5 μM concentration and fits. The excitation wavelength was 371 nm and the emission at 430 nm was recorded against delay time in a TCSPC experiment with 10^6 counts. (b) Distribution of inverse lifetimes extracted from the fitting of the PL decays. Blue curve ligand, red line [Ag(I)-6-thioguanosine]_n at 5 μM .¹

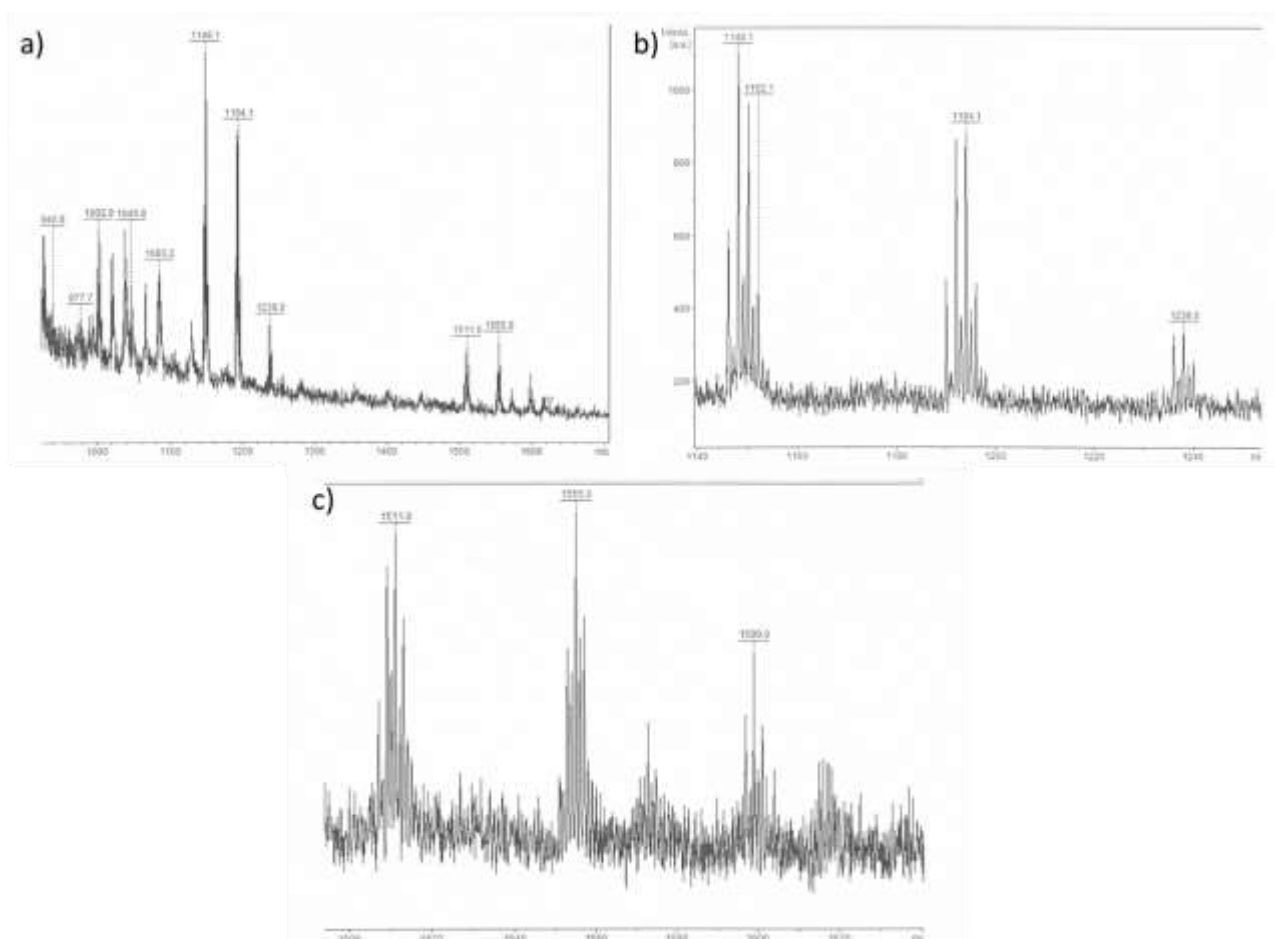


Figure A4. MALDI-ToF data measured for [Cu(I)-6-thioguanosine]_n.

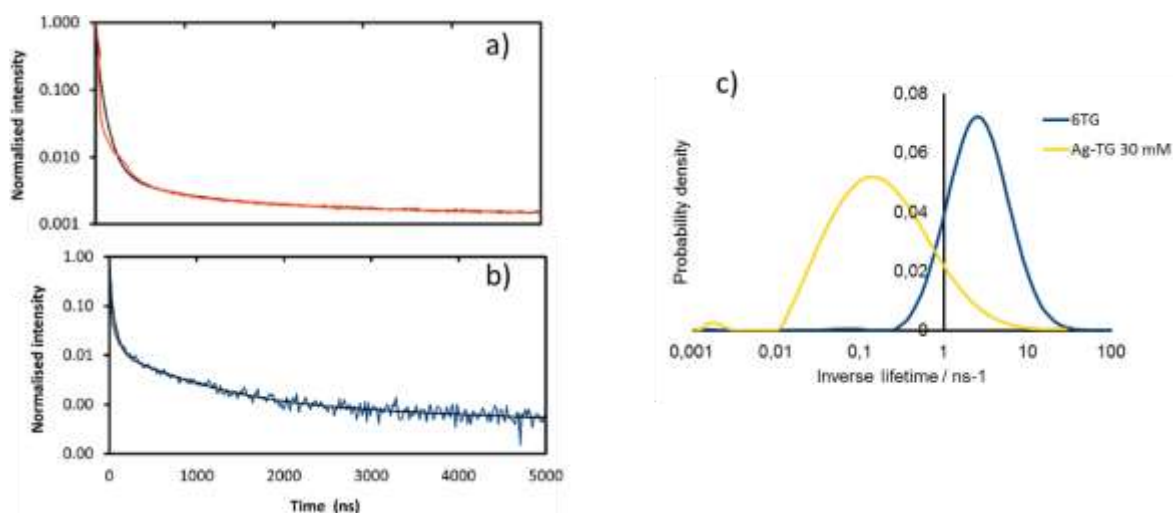


Figure A5. (a) Normalised intensity against time for the luminescence decay of ligand (6-thioguanosine) and (b) [Ag(I)-6-thioguanosine]_n (blue line) at 30 mM concentration and fits. The excitation wavelength was 371 nm and the emission at 430 nm was recorded against delay time in a TCSPC experiment with 10⁶ counts. (c) Distribution of inverse lifetimes extracted from the fitting of the PL decays. Blue curve ligand, red line [Ag(I)-6-thioguanosine]_n at 30 mM.¹

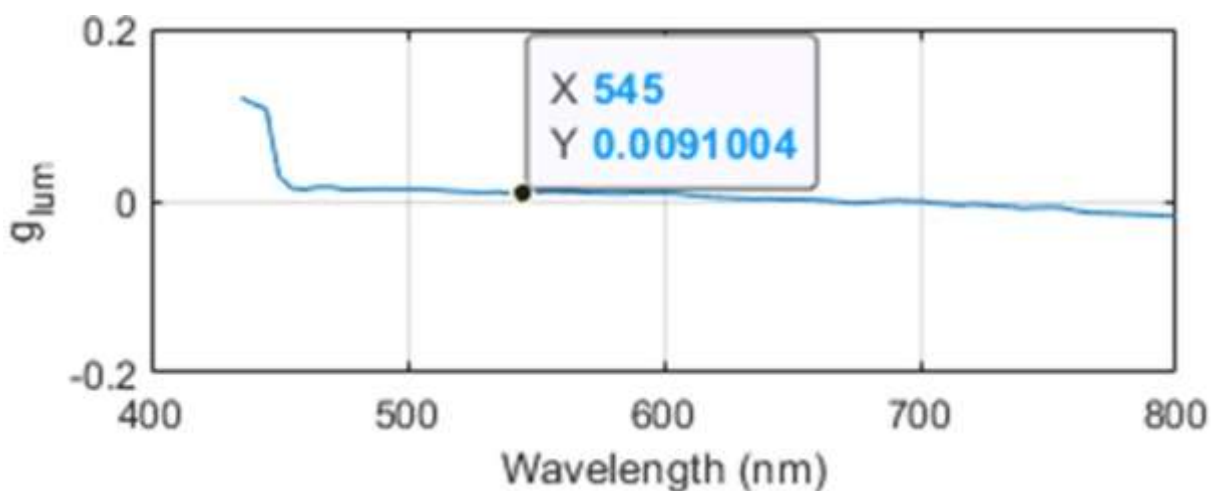


Figure A6. The luminescence dissymmetry factor (g_{lum}) data for [Ag(I)-6-thioguanosine]_n at 10 mM shows a value close to zero.

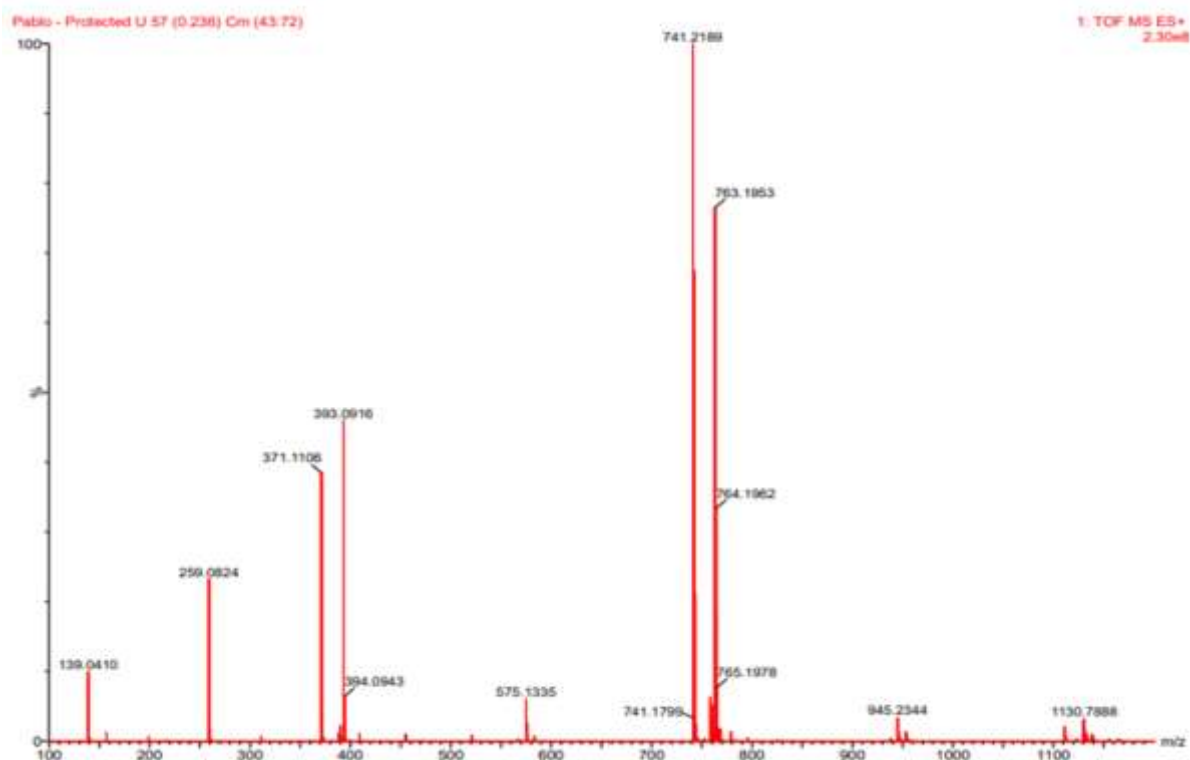
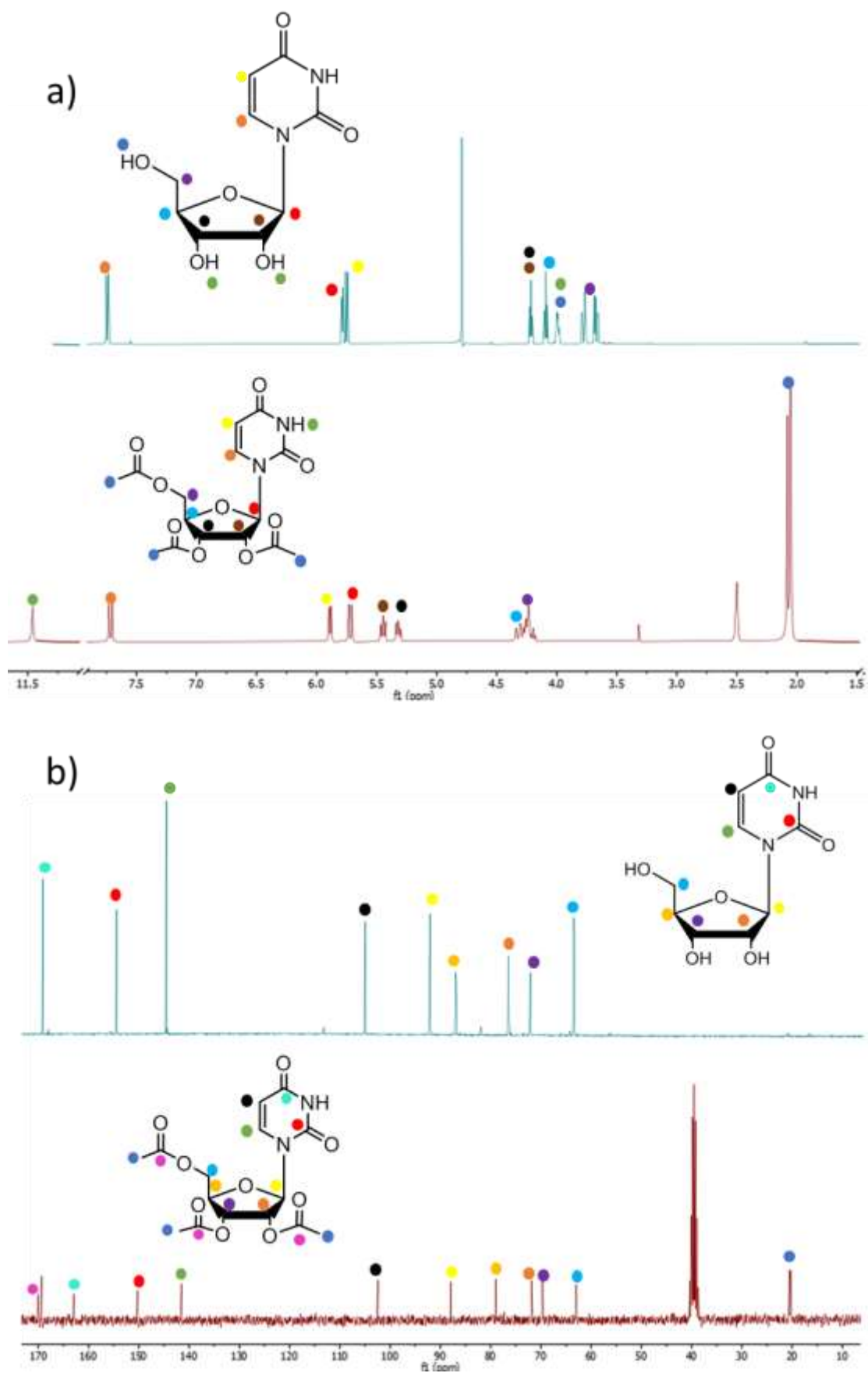


Figure A7. ESI data measured for uridine protected.



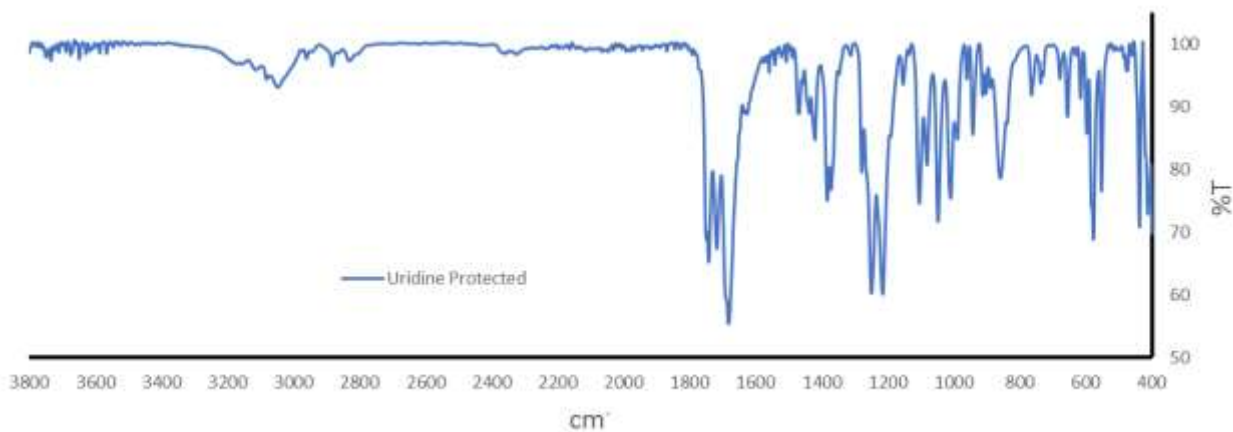


Figure A9. FTIR spectrum of uridine protected



Figure A10. ESI data measured for 4-thiouridine protected.

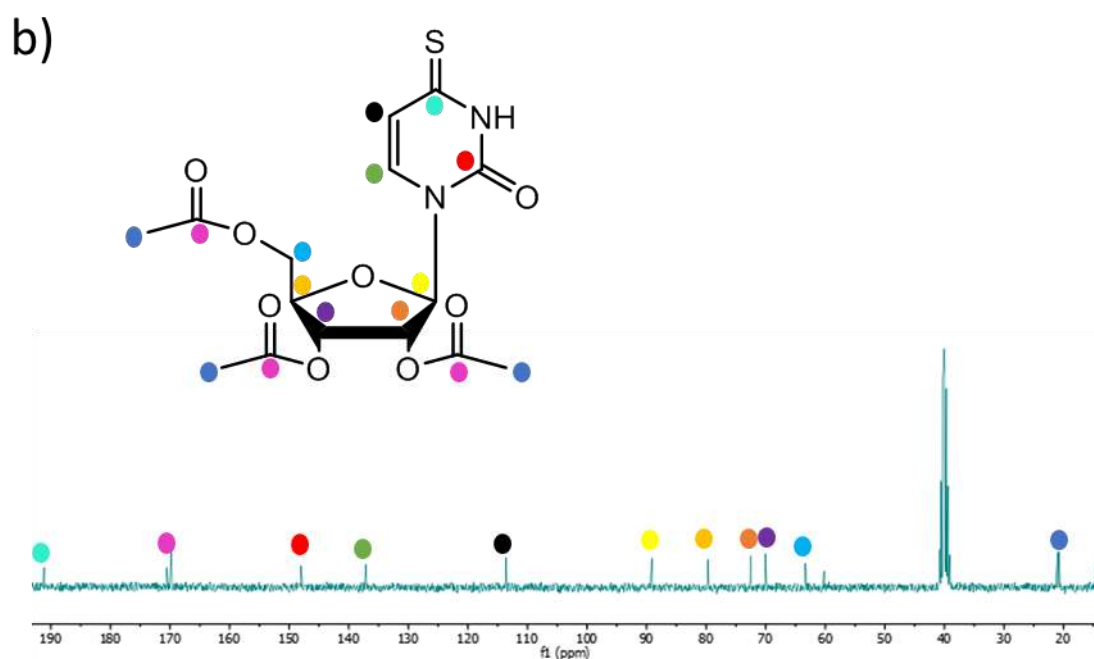
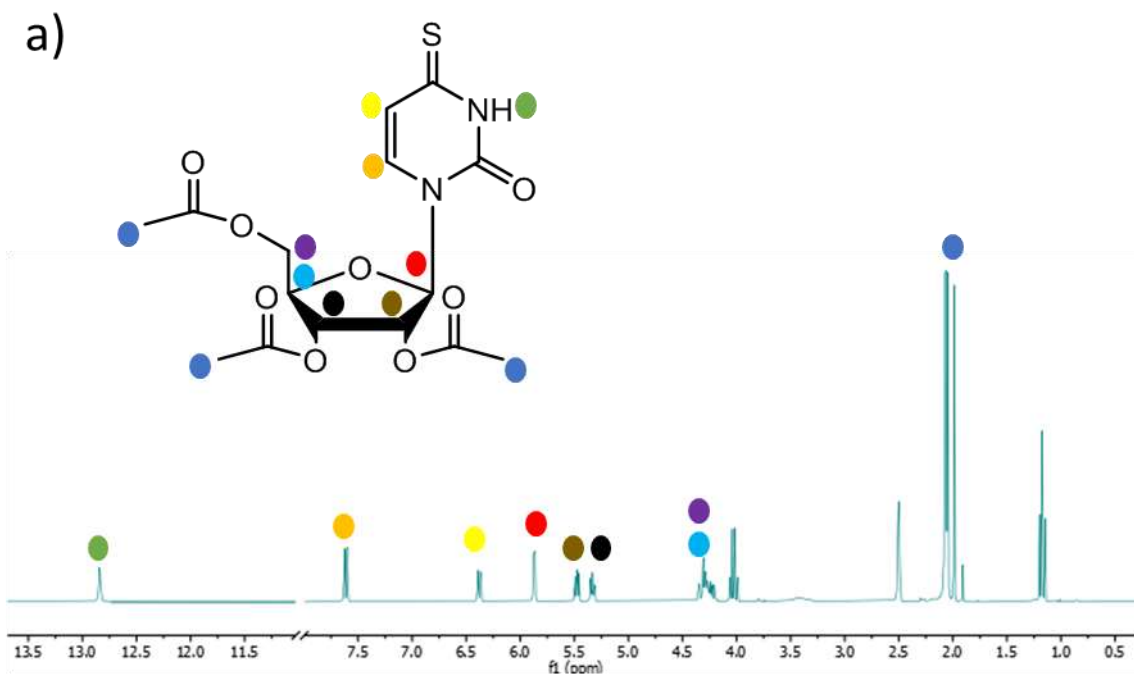


Figure A11. (a) ^1H NMR spectrum (300 MHz, $\text{DMSO-}d_6$) of 4-thiouridine protected b) ^{13}C NMR spectrum (75 MHz, $\text{DMSO-}d_6$) of 4-thiouridine protected.

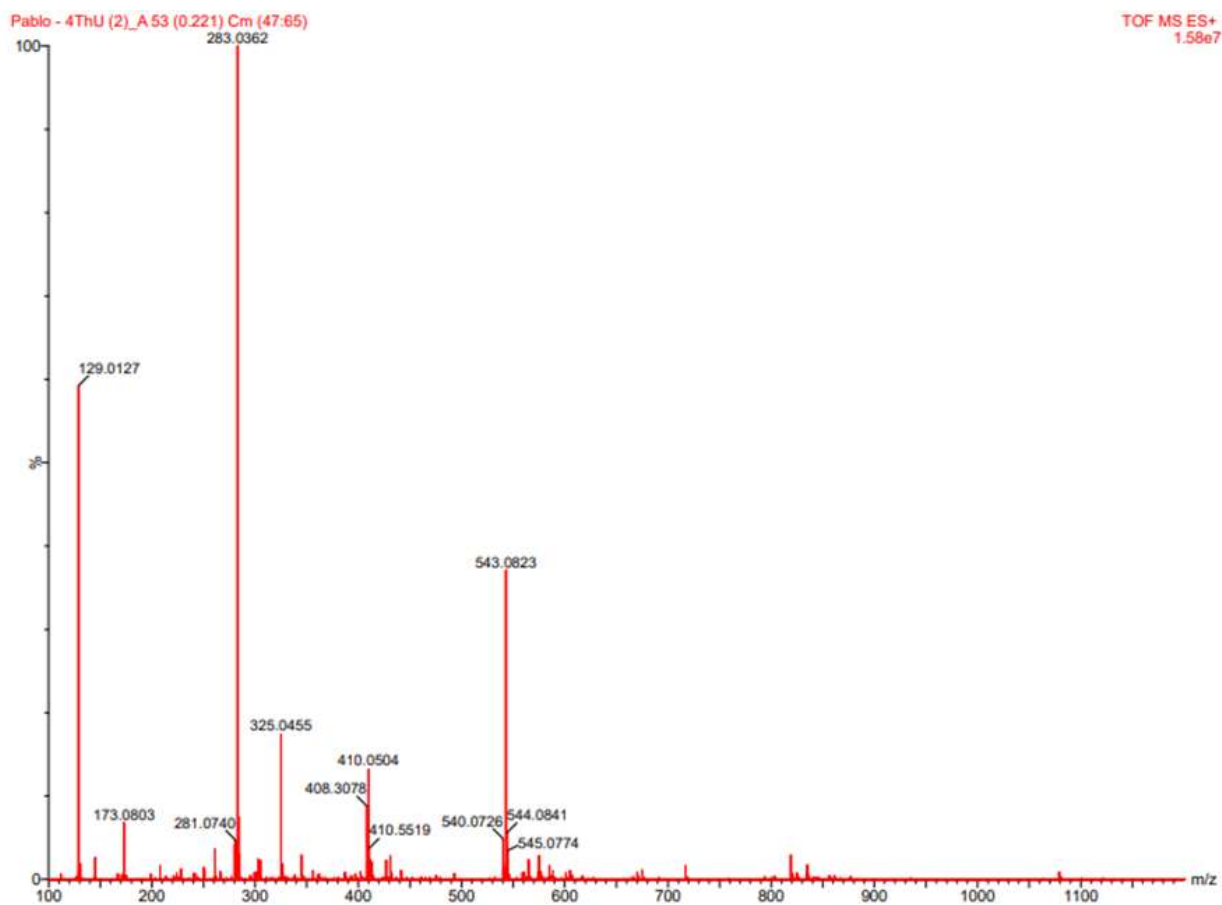


Figure A12. Figure A9. ESI data measured for 4-thiouridine.

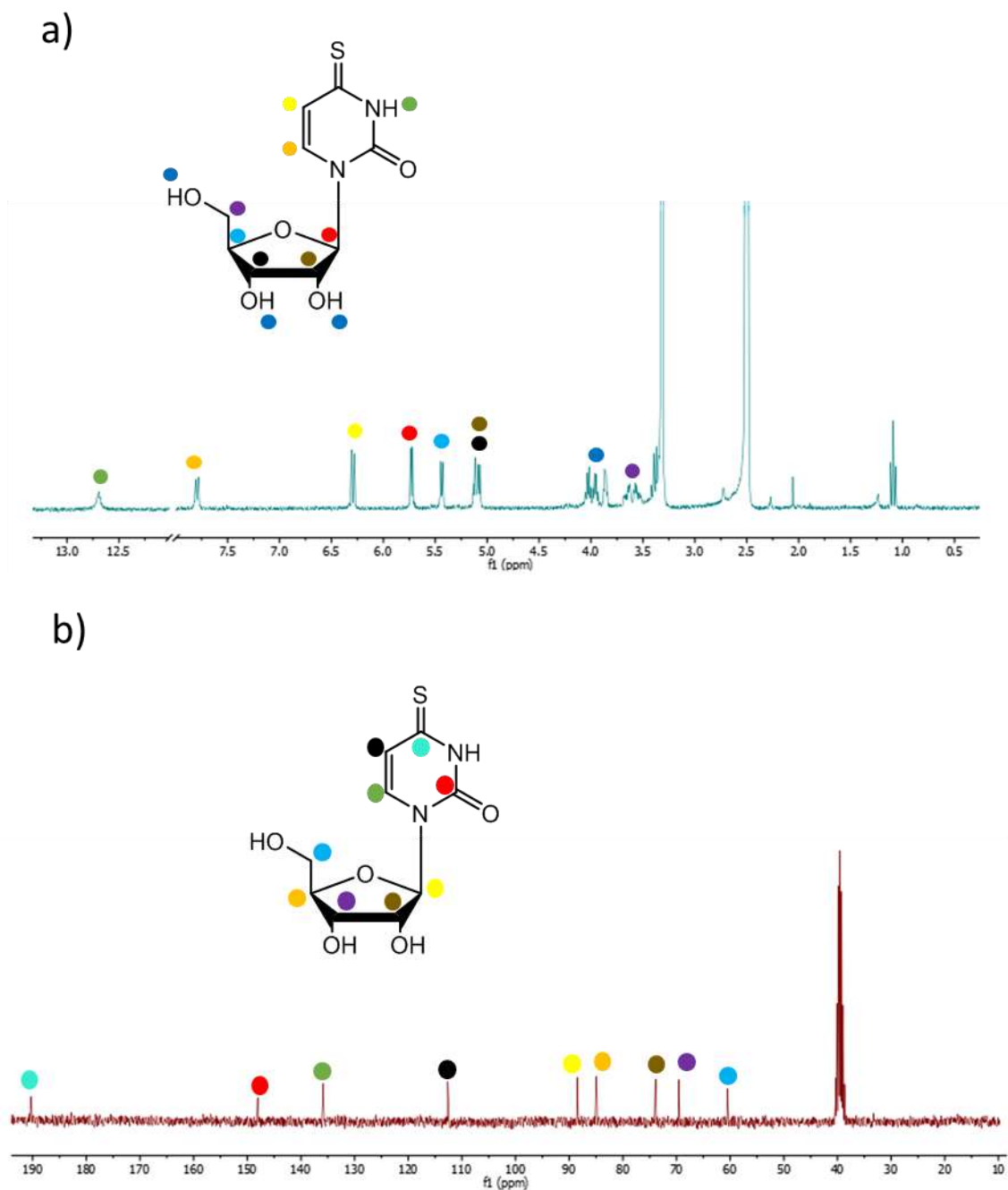


Figure A13. (a) ^1H NMR spectrum (300 MHz, $\text{DMSO-}d_6$) of 4-thiouridine b) ^{13}C NMR spectrum (75 MHz, $\text{DMSO-}d_6$) of 4-thiouridine.

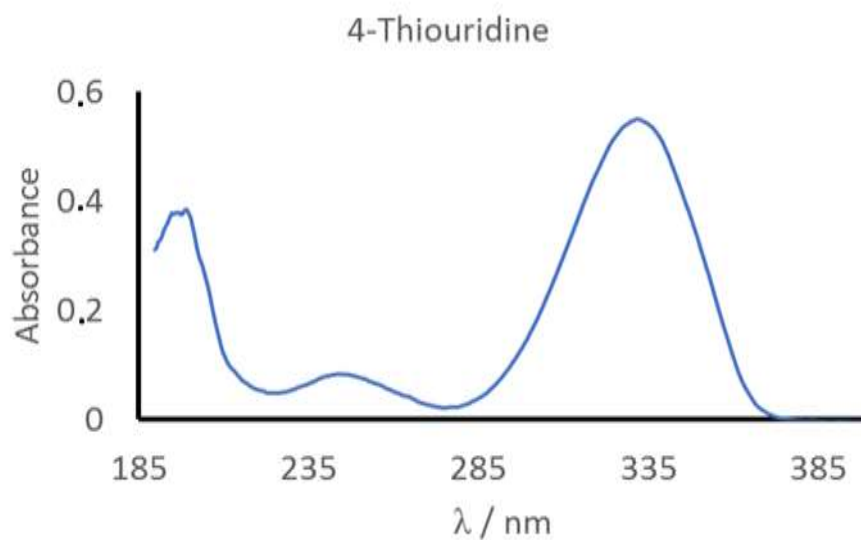


Figure A14. UV-Vis spectrum of 4-thiouridine.

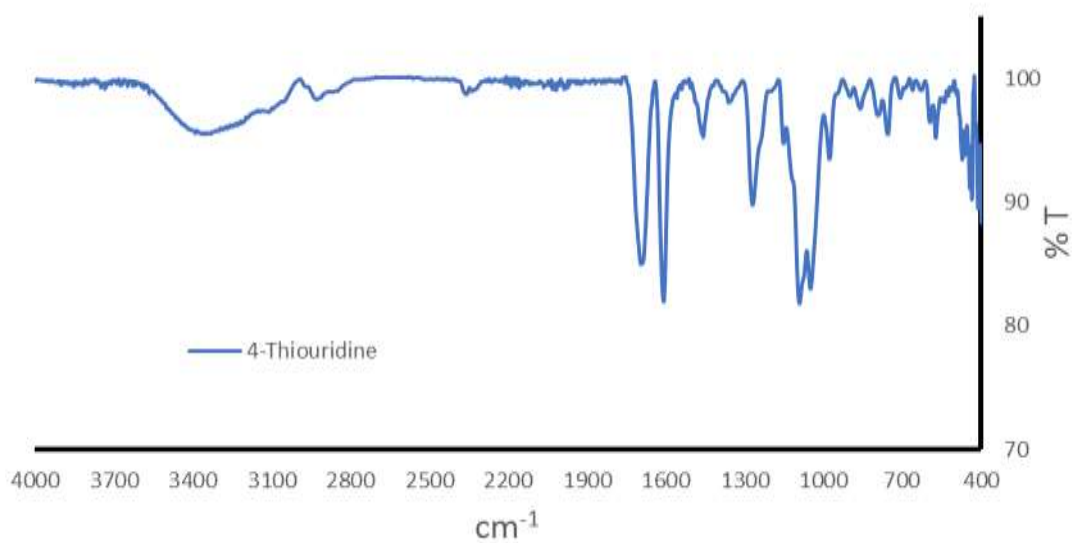


Figure A15. FTIR spectrum of 4-thiouridine.

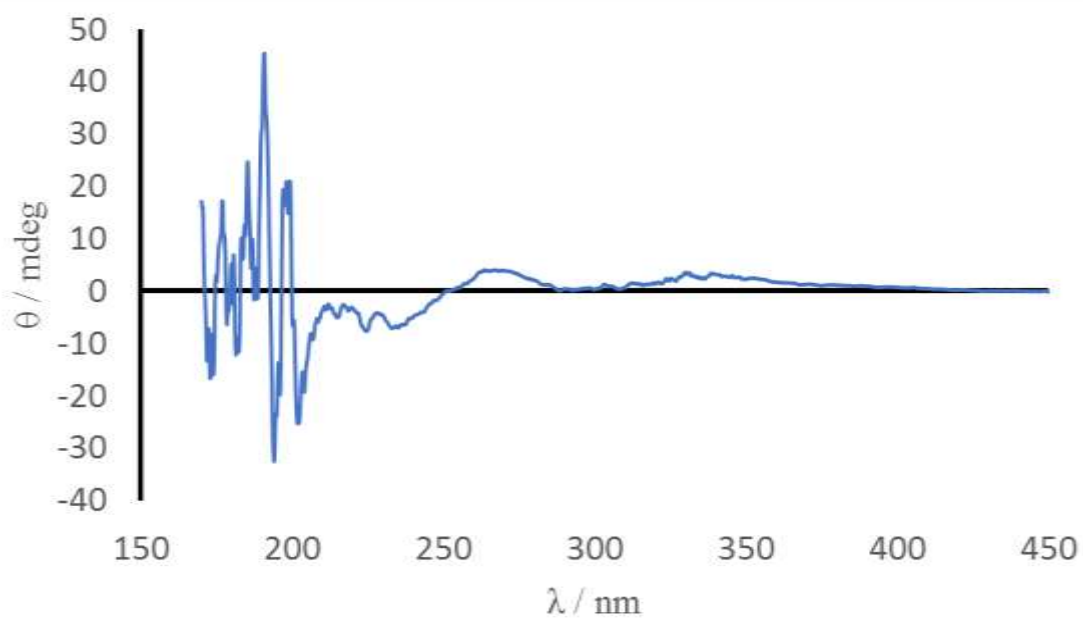


Figure A16. CD spectrum of 4-thiouridine.

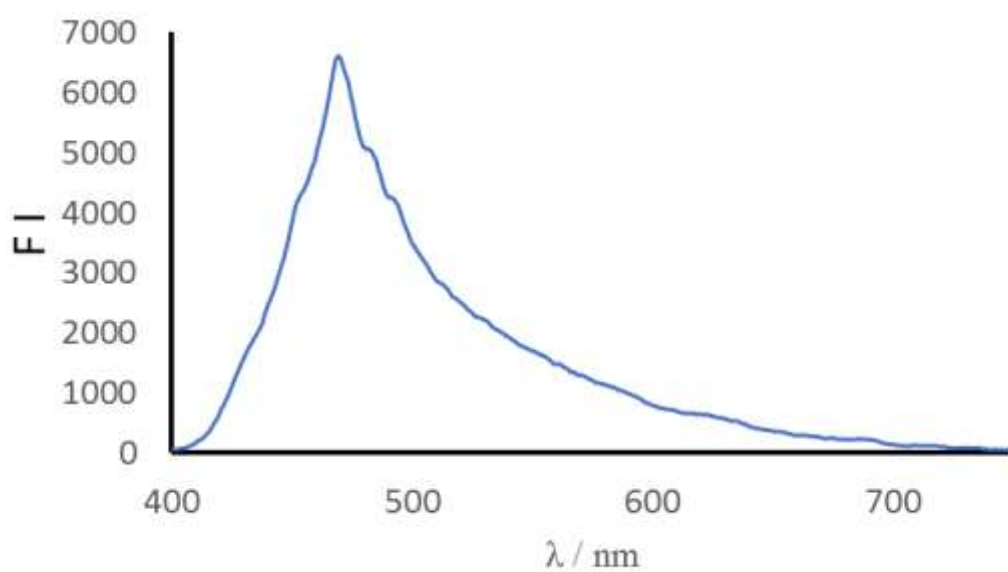


Figure A17. Luminescence spectrum of 4-thiouridine.

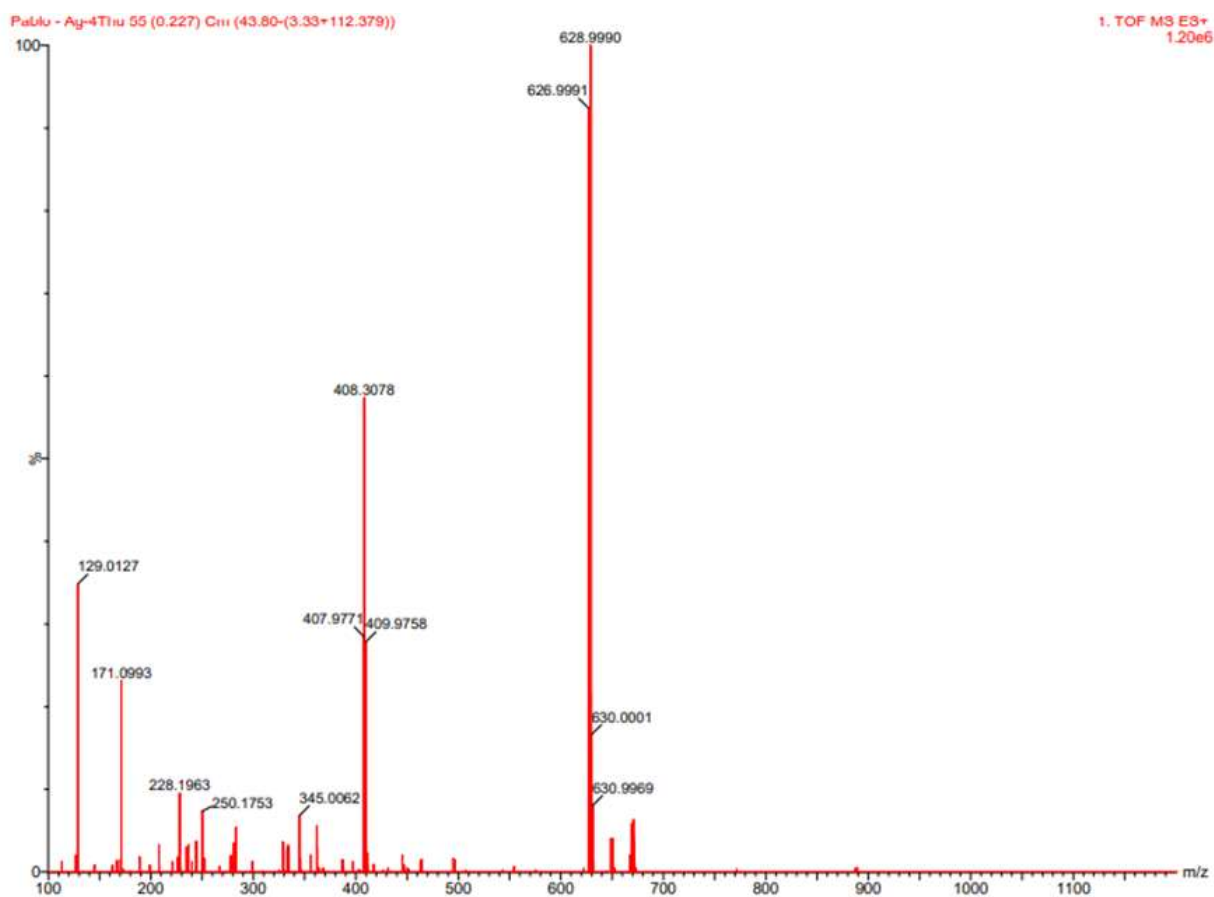


Figure A18. ESI data measured for $[\text{Ag}(\text{I})\text{-4-thiouridine}]_n$.



Figure A19. ESI data measured for $[\text{Au}(\text{I})\text{-4-thiouridine}]_n$.

Appendix references

1- Nurdillayeva, R., Oshido, A., Bamford, T., El-Zubir, O., Houlton, A., Hedley, J., Pike, A., Horrocks, B. R., *Nanotechnology* 2018, **29**, 135705.